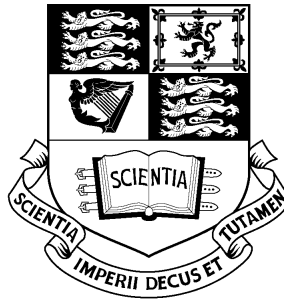# NON-LINEAR MODAL ANALYSIS METHODS FOR ENGINEERING STRUCTURES

by

Hugo Ramon Elizalde Siller

Department of Mechanical Engineering

Imperial College London / University of London

A thesis submitted for the degree of

Doctor of Philosophy

August, 2004

Abstract

This thesis presents two novel nonlinear modal analysis methods, aimed at the identification of representative engineering structures. The overall objective is to detect, localize, identify and quantify the nonlinearities in large systems, based on nonlinear frequency response functions (FRFs) as input data. The methods are first introduced in a direct-path, by analyzing a general theoretical system. Then, the concepts are extended to tackle a nonlinear identification via the reverse-path of the same methodologies.

The nonlinear formulation of this work is based in first-order describing functions, which represent the nonlinearities by amplitude-dependent coefficients. This formulation is the basic "engine" of the methods and techniques developed here. For the sake of clarity, the research has been restricted to deal with cubic stiffness and friction damping nonlinearities, although the inclusion of other types should be straightforward, given the generality of the developments.

The first direct-path method, the so-called "explicit formulation" (EF), is conducted entirely in the *physical domain*. This technique manipulates the physical coefficients stored in the system matrices, thus the term "explicit", yielding the nonlinear FRF at a selected DOF as a closed-form expression, regardless of the system's size. An optimized version of this method has been validated against real measurements taken from a test rig, and it was found that the nonlinear behaviour was predicted with reasonable accuracy.

A *reverse* path of the "explicit formulation", REF, was implemented as a nonlinear identification tool. In spite of successful results, it was concluded that the computational cost of this approach was too high

to gain acceptance in a practical analysis. Still, the method provides a much needed bridge between a full-size theoretical model and the relatively small number of experimental measurements that may be available.

The second main method, operating in a direct-path, is called the "hybrid modal technique" (HMT). It is based on a novel nonlinear modal expansion, which is analogous to existing nonlinear modal superposition techniques. The underlying linear system is expressed in generalized modal coordinates, while the nonlinearities are kept in the physical domain. The use of hybrid coordinates is a central feature, by which the localization of the nonlinearities is fully addressed.

A reverse-path of this method, R-HMT, incorporates the successive application of several "standalone" techniques, also developed here, which can be used independently to tackle different aspects of nonlinear modal analysis. When gathered together, the individual techniques provide a robust methodology, able to perform a nonlinear identification within the usual experimental restrictions, while exhibiting high computational efficiency.

The type of the nonlinearity can be identified by a newly introduced technique, based in the geometrical "footprint" of the extracted nonlinear component. The localization of the nonlinearities is then achieved by a linear least-squares calculation over a predefined *nonlinear region* of arbitrary size. This technique provides an unambiguous localization, provided that the analyzed frequency range is a fair representation of the system.

Although the nonlinear natural frequencies and modal damping are not explicitly needed for identifying the system or regenerating the responses at some other forcing level, a *fast approximation technique* (FAT) is introduced, allowing the *analytical* derivation of these parameters via newly-developed expressions. The FAT establishes links with other nonlinear methods and standard linear modal analysis techniques.

I would like to dedicate this thesis to:

My daughter, who is on her way right now[1]...

Rosca, for loving and supporting me no matter what...

My parents, J. Hugo & Delia, for absolutely everything else...

---

[1]Ana Sofia arrived on July 31_{st}, 2004.

Acknowledgements

Contents

Glossary

Subscripts

i, j Indexes representing: a) the (i, j) element of a matrix, e.g. K_{ij}, b) the i_{th} element of a vector, e.g. Y_i, or c) the spatial coordinates of a variable, e.g. $\tilde{g}_{ij}$.

M Index representing the theoretical number of modes of a system (infinity, for a continuous system), e.g. $\sum_{r=1}^{M} \phi_{ir}$, see equation (6.8), page 98. Not to be confounded with $[\mathbf{M}]$, the mass matrix, which always appears in **bold** style and between brackets, and never as an index.

r Index associated with a modal quantity of the r_{th} mode, e.g. λ_r.

s Index associated with a resonant modal quantity, e.g. λ_s.

Superscripts

$\tilde{}$ Acknowledges the nonlinear nature of a variable, e.g. $\tilde{G}$.

Roman letters (uppercase)

$A \ldots Z$ By convention in this thesis, **bold** Roman uppercase letters (plus a few standard Greek letters) represent matrices, while regular Roman uppercase letters represent vectors. Both are listed under the "**Matrices and vectors**" heading. The ones listed here are exceptions to this rule, due to their standardized use as variables.

N Total number of degrees of freedom (DOFs) of a system. Also used as a vector representing all the degrees of freedom.

$\tilde{Z}_{ij}$ $= |\tilde{Y}_i - \tilde{Y}_j|$, the magnitude of the relative amplitude of a nonlinear element linked to coordinates i and j.

Roman letters (lowercase)

f The forced degrees of freedom (DOFs) in a multi-excitation test. Also used as a vector representing these DOFs.

$\tilde{g}_{ij}$ Nonlinear restoring force between coordinates i and j.

$\tilde{gv}_i$ Total nonlinear restoring force at the coordinate i. It is also the i_{th} component of vector $\{\tilde{G}\}$, the nonlinear vector (NLV).

$\mathbf{i}$ $\sqrt{-1}$, the imaginary number, e.g. $cos\theta + \mathbf{i} \cdot sin\theta$. Not to be confounded with the spatial index i, which always appears in regular math mode. The latter is frequently used in this thesis.

k Linear stiffness coefficient. See equation (3.6), page 34.

m Number of modes in the analyzed frequency range.

m_{NL} Number of nonlinear modes as a subset of m.

n The degrees of freedom (DOFs) associated with nonlinear elements, abbreviated as *NL-DOFs*. Also used as a vector representing the *NL-DOFs*.

q The sampled frequency points in an FRF to be included in a nonlinear analysis.

y The system's response in the time domain.

Greek letters (uppercase)

Δ Not a variable by itself, but often used to express the nonlinear variation of an accompanying variable, e.g. $\boldsymbol{\Delta\tilde{\Phi}}$.

Γ The *nonlinear region*. Also used as a vector representing all the degrees of freedom inside this region.

Π Trust-region, a neighbourhood in which a simplified function $q(y)$ reasonably mimics the behaviour of the original, more complex function $f(y)$. Used during a nonlinear minimization, see equation 4.17, page 55.

$\Re$ The *measured region*. Also used as a vector representing all the degrees of freedom inside this region.

Greek letters (lowercase)

β Coefficient of a cubic stiffness element.

ϕ_{ir} Eigenvector corresponding to coordinate i, mode r. It is also the i, r component of matrix $[\mathbf{\Phi}]$.

γ Coefficient of a friction damping element.

η Linear hysteretic loss factor.

λ_r Eigenvalue corresponding to the r_{th} mode. It is also the r_{th} component of the diagonal matrix $\lceil \lambda \rfloor$.

π Pi.

θ Angle.

σ Fourier coefficient. See equation (3.4), page 33.

ω Frequency of excitation.

Matrices and vectors

$[\ ]$ Matrix.

$\lceil\ \rfloor$ Diagonal matrix.

$\{\ \}$ Column vector.

$[\ ]^T, \{\ \}^T$ Transpose of a matrix/vector.

$[\ ]^{-1}$ Inverse of a matrix.

$[\ ]^{+}$ Generalized (pseudo-inverse) of a matrix.

$[\alpha]$ Linear receptance.

$[\mathbf{C}]$ Linear viscous damping matrix.

$[\mathbf{D}]$ Linear hysteretic damping matrix.

$\lceil \mathbf{\Delta}\tilde{\lambda} \rfloor$ Nonlinear variation of the eigenvalues (diagonal matrix).

$[\mathbf{\Delta}\tilde{\mathbf{\Phi}}]$ Nonlinear variation of the eigenvectors.

$\{F\}$ Excitation vector.

$\{\tilde{\chi}\}$ The *extended* nonlinear modal vector (*extended* NLMV).

$\{\tilde{G}\}$ Nonlinear vector (NLV).

$[\mathbf{H}]$ Frequency response function (FRF).

$[\mathbf{I}]$ Identity matrix.

$[\mathbf{J}]$ Jacobi matrix.

$[\mathbf{K}]$ Linear stiffness matrix.

$[\mathbf{\Lambda}]$ Composite matrix. For the linear case, it's equivalent to the inverse of the linear receptance, $\mathbf{\Lambda} = \alpha^{-1}$.

$\lceil \lambda \rfloor$ Eigenvalue's diagonal matrix.

$[\mathbf{M}]$ Mass matrix.

$[\tilde{\nu}]$ The nonlinear matrix (NLM).

$\{P\}$ Modal amplitude (also known as "modal responses" or "generalized coordinates"). For the nonlinear case ($\tilde{P}$), it is often referred to as the "nonlinear normal modes" (NNMs).

$[\mathbf{\Phi}]$ Eigenvector's matrix.

$\{\mathbf{\Phi^T}\tilde{G}\}$ The nonlinear modal vector (NLMV). Although a function rather than a single variable, it is listed here because it is often referred to as an entity.

$\{\tilde{R}\}$ Modified excitation vector, used in the *optimized* EF method, see equation (4.13), page 52. Also used in the REF method with a slight modification, see equation (5.9), page 77.

$\{Res\}$ Residual of an FRF due to higher modes.

$[\tilde{\tau}]$ Matrix used during the localization of the nonlinear DOFs (*NL-DOFs*), those DOFs associated with nonlinear elements, see equation (8.35), page 171.

$\{Y\}$ System's response.

Abbreviations

DFM   Describing Function Method.

DOF(s)   Degree(s) Of Freedom.

EF   Explicit Formulation.

FAT   Fast Approximation Technique.

FE   Finite Element.

FEM   Finite Element Method.

FFT   Fast Fourier Transform.

FRF   Frequency Response Function.

HBM   Harmonic Balance Method.

HMT   Hybrid Modal Technique.

LMA   Linear Modal Analysis.

MDOF   Multi-Degree Of Freedom.

NL Nonlinear.

NL-FRF Nonlinear Frequency Response Function.

NLMA Nonlinear Modal Analysis.

NLMV Nonlinear Modal Vector, $\{\mathbf{\Phi^T}\tilde{G}\}$.

NNM(s) Nonlinear Normal Mode(s).

NLV Nonlinear Vector, $\{\tilde{G}\}$.

REF Reverse Explicit Formulation.

R-HMT Reverse Hybrid Modal Technique.

SDOF Single-Degree Of Freedom.

List of Figures

Chapter 1

Introduction

During the *structural dynamics 2000 forum*, published by Ewins & Inman (1), a list of questions was submitted by prominent researchers. The questions covered a variety of issues regarding the state of the art of structural dynamics and its future direction. Most of these acknowledged the failure of the current mathematical models to address real-life requirements. Some thought-provoking statements, listed below, were made:

- *"It is certainly a tribute to engineering savoir-faire (and a healthy dose of safety factors) that planes fly and nuclear reactors remain contained given the abiding inaccuracies in the mathematical models of complex technological structures"*, S. Cogan.

- *"Is it time to accept defeat and have a fundamental review of the modelling techniques?"*, M. Imregun.

- *"...or is a radically different methodology required to tackle the problems of detecting, quantifying and identifying non-linearities in real structures?"*, J. E. Cooper.

- *"The question is: How to make nonlinear analysis tools more accepted by and more user friendly to practical engineers?"*, B. Yang

Also in this forum, researchers were invited to submit ideas regarding *grand challenge problems in structural dynamics* (2), which would not be readily solved in the next few decades. Researchers such as D. Brown, I. Bucher, C. Farrar

and M. Imregun highlighted problems related to seismic activity, micro-electro-mechanical systems, vibration-based damage assessment and noise minimization.

All of them underlined the need of a better understanding of the nonlinear effects.

These arguments provide good grounds for conducting a research aimed to the development of mathematical models of engineering structures, fully accounting for nonlinearities. We are interested in developing the necessary theoretical background, but with an eye on its applicability to the practical identification of nonlinear structures.

1.1   Modal analysis

In the context of structural dynamics, *modal analysis* can be defined as the gathering of a variety of techniques, whose main aim is the dynamic characterization of engineering structures. Although useful as a theoretical tool to obtain the system's response by means of a root-finding procedure, its applications are mostly related to an experimental environment. In here, a system is identified (or characterized) by measuring its response under a known excitation, which is basically a reverse path of the theoretical approach.

Modal analysis as an engineering method has evolved considerably during the last 50 years, and this trend has been accelerated by computational leaps of recent decades and the development of robust measuring devices. Its success is mainly due to a simple engineering approach combined with a strong mathematical foundation, which relies on proved linear analytical theory.

In particular, the *modal superposition* theorem has become a cornerstone in the analysis of linear systems, allowing a relatively complex entity to be separated into smaller and manageable building blocks. In the field of linear modal analysis (LMA), this theorem is often applied to a multi-degree-of-freedom (MDOF) system to "break it" into several independent single-degree-of-freedom (SDOF) systems, each exclusively accounting for the behaviour of a given mode of the original system.

The aforementioned approach not only simplifies the analysis of large systems, but it also reduces the set of equations to be solved. Indeed, the physical

responses can be regenerated from the modal responses (or modal coordinates) of the equivalent SDOF systems.

Although, theoretically, a linear system will have as many modes as DOFs, the number of retained modes in practice is restricted to the measured frequency range. Only a few dominant modes may be enough to obtain an adequate regeneration of the physical responses, the rest having a smaller effect on them. This procedure is known as "modal truncation", and the essential parameters needed to describe a physical system in the modal space are called "modal parameters", namely, the eigenvalues and eigenvectors.

1.2 Nonlinear modal analysis (NLMA)

Methods such as the finite element method (FEM), LMA and other linear analysis techniques have established themselves as standard tools. They provide a reliable path to deal with a large variety of cases, even those exhibiting a certain degree of nonlinearity. Indeed, when the accuracy of the solution is not highly compromised, one is still better off treating the system as linear even if it is not (most probably it is not)[1].

Unfortunately, when the accuracy of the predicted response is of paramount importance, or the nonlinear effects are significant, a linear analysis will generally prove to be unreliable. Moreover, the recent quantum leaps in computational power have greatly raised the expectations on the analyst, who is under increasing pressure to provide highly accurate results. At the very least, he/she will face the situation of having to choose a suitable nonlinear method -from literally hundreds- which best matches his/her particular problem.

As pointed by Worden & Tomlinson (3), the last few decades have seen an explosion of methods aimed to tackle nonlinear issues, and we have ended up with a toolbox of powerful techniques capable of handling many particular situations. These techniques are, for the same reason, extremely case sensitive.

The sources of nonlinearities in a typical engineering structure are so diverse that it would be practically impossible to account for all of them, thus the eager-

---

[1] *"Trying to divide systems into linear and nonlinear, is like trying to divide the world into bananas and non-bananas"*. R. M. Rosenberg.

ness of engineers to neglect them whenever they are encountered. This attitude is partly caused by the lack of a unified theory that can handle general nonlinear cases while still providing a link with well-known, standardized linear tools documented by Ewins (4) and others.

Some of the issues that make a NLMA a puzzling task are listed below:

- A localized nonlinearity in a structure can have a significant global impact, while leaving some areas largely unaffected. Examples of local nonlinearities are: joints, shock absorbers, geometric discontinuities, regions undergoing large displacements, discrete spring/dampers, etc.

- The nonlinear effects are usually confined to just a few modes and coordinates, while the rest behave in a linear fashion.

- There is a lack of standardized parameters which can define, in an objective and sensible way, the "strength" of the nonlinearity.

- Finally, there is not an easy way to express a nonlinear response as a general closed-form algebraic function.

Because of the lack of a well-developed nonlinear theory, most efforts towards the establishment of a standard NLMA methodology have been done by incorporating nonlinear parameters into a linear frame. While this approach guarantees compatibility with LMA methods, it does not necessarily represent the best path.

Some authors (5) have raised serious questions about the validity of stretching linear concepts to analyze nonlinear systems, as there are some nonlinear phenomena that have no counter-part in linear systems. As an example, the "bifurcating nonlinear modes" are essentially nonlinear motions and cannot be regarded as analytic continuations of any linear modes. In such cases a *linearization* of the system either might not be possible, or might not provide all the possible resonances that can be realized.

In spite of this evidence, the development of nonlinear techniques analogous to the linear superposition would be of interest to express general transient responses as the algebraic addition of nonlinear modal responses, provided that a stable and periodic response dominates the nonlinear behaviour. Such an approach would

also provide an order reduction by possibly achieving decoupled equations of motion. These lines of research have gained momentum among specialists, often being revisited and expanded.

1.3 Nonlinear frequency response functions (NL-FRFs)

The frequency response function (or FRF) is, perhaps, the single most used tool in the field of modal analysis to describe the input-output relation of a system (Fig. 1.1).
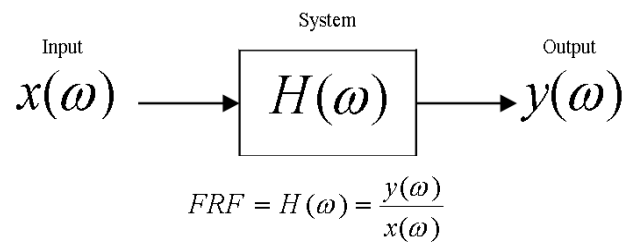
Figure 1.1: Simplified representation of a system, operating at frequency ω

Although its applications go far beyond the vibrations field, structural engineers use it almost invariably as a first step for assessing the dynamic features of a structure, as it offers highly condensed information at a glance:

- The resonances and anti-resonances, indicating the frequencies at which the highest and lowest amplitudes occur.

- The amount of damping, as a mechanism for absorbing energy.

- The phase-lag of the response relative to the input excitation.

These and other main characteristics can be visually observed in a single FRF plot (Fig. 1.2).

Further on, by obtaining several responses at different points of a structure, its predicted motion at any natural frequency can be animated in a computer;

Figure 1.2: A typical FRF of a mechanical structure

this provides an invaluable tool for visualizing the experimental mode-shapes, making it possible to compare them with the analytical ones (Fig. 1.3).

One of the central features that makes the FRF so appealing for analyzing linear systems is its invariantness to the input excitation, because of the assumption of linearity. This fact makes it possible to use a wide range of excitations (step sine, random noise, impulse, etc.) and still obtain the same function. Another desirable characteristic is the so-called "modal orthogonality", in which an FRF can be decomposed (or expanded) in several terms (or modal responses). Each term exclusively accounts for an individual mode, greatly simplifying the analysis by invoking modal superposition.

It would be very convenient if we could extend the definition of the FRF to describe nonlinear systems. Unfortunately, this is not so simple and the main single problem is that the coefficients contained in the mathematical model of a linear
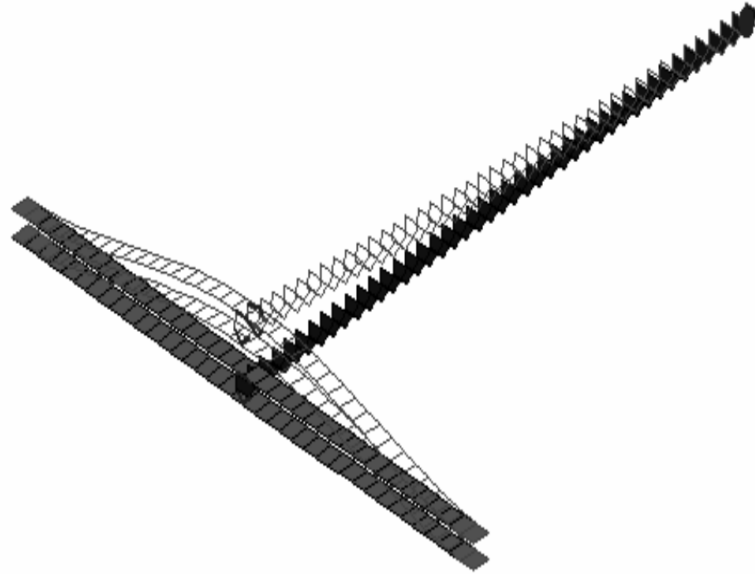
Figure 1.3: Visualization of an experimentally derived mode-shape

FRF (natural frequencies, damping factors and mode-shapes) are constant, as opposed to the nonlinear case in which such coefficients are amplitude-dependent.

Also, it can no longer be assumed that the nonlinear modes are orthogonal, but rather of a coupled nature, so the original concept of "normal modes" is somewhat lost. As a result of the nonlinearities, a plot of an FRF will appear distorted when compared to the linear case (Fig. 1.4).

In order to develop an effective NLMA method, a simple but general representation of a nonlinear FRF must be sought. Such expression would contain a mixture of linear and nonlinear coefficients. To this end, the describing function method (DFM) has demonstrated good results for obtaining amplitude-dependent coefficients of nonlinear elements, by averaging the nonlinear forces occurring in one load-cycle. These coefficients could be incorporated into a general formulation, allowing a nonlinear extension of the classical definition of the FRF.
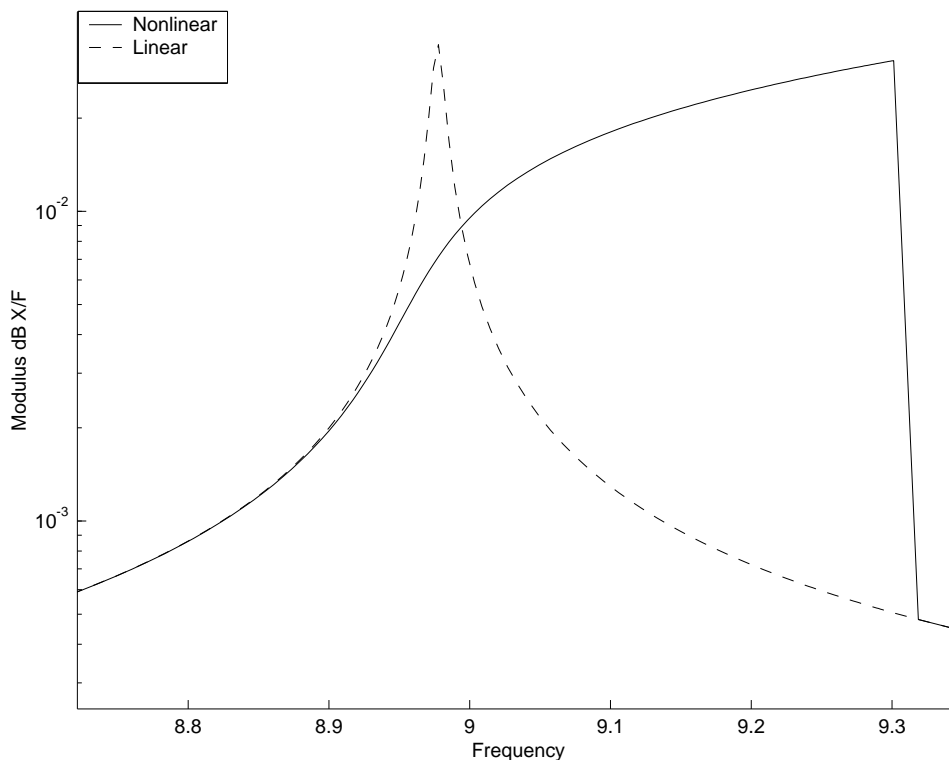
Figure 1.4: A distorted FRF due to a cubic stiffness nonlinearity

1.4   Identification of nonlinear systems

Benchmark nonlinear methods, such as the harmonic balance method (HBM), can handle general problems with a systematic approach, allowing an almost "one-size-fits-all" procedure, or at least, quite consistent guidelines for its solution. This happens because this class of methods are more suitable for a theoretical analysis (direct path) in which idealized models are already available (i.e., FEM), containing highly processed and organised input data, usually in the form of matrices.

Solving an identification problem is a much more blurred issue, mainly because it belongs to an experimental environment, in which the differences between a theoretical model and its experimental counterpart must be conciliated somehow (reverse path). Engineers know very well that most experimental models do not necessarily behave according to theory, sometimes providing more questions than

answers. A reliable identification method, therefore, must be able to get away with these uncertainties, still providing unambiguous results.

Any system can be fully described by the state $[x, y, H]$ (see Fig. 1.5). Actually, this set is over-determined, as by knowing two variables, it would be possible (at least in principle) to calculate the other one. This basic idea is the starting point for the vast majority of the identification problems.
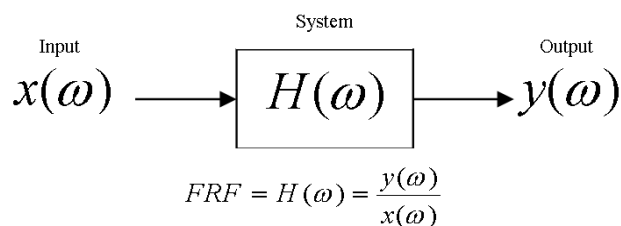
Figure 1.5: Simplified system

A linear system can be represented as an uncoupled transfer function (Fig. 1.5), in which the output y is fully characterized by the system's features H and the input excitation x. The identification of linear systems is a relatively established procedure, seeking to detect/quantify a set of linear coefficients which best describe H. This is done by measuring $[x, y]$ for several states, while observing the corresponding behaviour of H.

Problems start when the system is found to be amplitude dependent (Fig. 1.6). This condition is representative of most engineering structures containing nonlinearities. The introduced complexities can be represented by adding a closed loop with a feedback of the output, thus generating nonlinear effects in the response. The identification of this class of systems is the main subject of this thesis.

Specifically, we are faced with the problem of identifying the nonlinear component of H by knowing x, y and the linear component of H. In a NLMA context, the identification problem can be posed as follows: *Given some basic information of the system (its linear description) and the way it behaves under a known excitation (the measured responses), find the nonlinear elements inside the system which make it behave in a nonlinear fashion.*
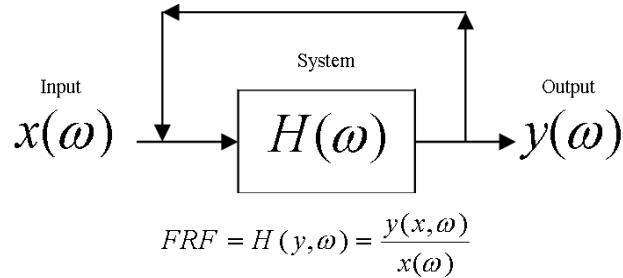
Figure 1.6: System with a closed loop

Typically, the location of nonlinear elements within the system is unknown, so before attempting an identification process it is a good idea to first detect where they are. This procedure is known as *nonlinear detection*. Also, the nature of the nonlinear elements (a physical description of the amplitude dependency) has to be assessed before establishing the parameters to be found.

Roughly speaking, the identification methods can be divided into parametric and nonparametric:

- Parametric methods assume a specific mathematical shape of the system (e.g., a SDOF oscillator) and aim to identify the parameters (m, c, k) included in the assumed model. The nonlinear mechanism is represented by a known analytical function and the measurements are used to generate a least-squares fitting to find its (usually constant) parameters. It is assumed that the nonlinearities are a-priori localized.

- Nonparametric methods are more general in nature, as the system is regarded as a black box. Both the type and location of the nonlinearities are unknown, thus creating favourable conditions for either an undetermined problem or an ill-posed one. An ideal nonparametric method has not been found but a number of techniques, such as the *Hilbert transform* or the *Volterra kernels*, are increasingly seen as feasible.

The technique introduced in this work can be regarded as parametric in a linear context, but nonparametric in the nonlinearity. In other words, it requires

some basic information about the underlying linear system, but assumes nothing about the nonlinearities (type and location).

When dealing with large systems, data incompleteness is invariably an issue. Usually, the experimental model is of a much reduced size than its theoretical counterpart, so the set of measured responses describes only a subset of the analytical responses. To further complicate things, it has been acknowledged that local nonlinearities can have a global effect, making nonlinear detection a very complex issue.

On the other hand, it is also known that some regions within the system are more likely to contain nonlinearities. Some of these were already identified as joints, shock absorbers, geometric discontinuities, etc. This feature can be exploited to manage a large identification problem much more efficiently, by approximately delimiting *nonlinear regions* prior to the analysis.

Depending on the degree of data incompleteness, a nonlinear identification can offer two types of solutions:

- For significantly incomplete data (e.g., few measurements), a *modal identification* is usually the best one can get, providing a solution in the form of identified modal coefficients. These are capable of explaining the nonlinear behaviour of the individual modes and even regenerate/predict the physical responses within a limited range, but the physical nonlinear components remain a black box.

- For fairly complete data (e.g., enough measurements), a *physical identification* should be possible, in principle. This solution would unveil the core of the nonlinear system, allowing the detection and quantification of the individual nonlinear elements. This would represent a full description of the nonlinear system, achieving unlimited prediction capabilities.

1.5 Frequency domain vs. time domain methods

The identification methods can be divided into two major groups, according to the nature of the input data they require:

1. **Time domain methods**. The input data is in the form of time signals, describing the motion of the structure as a function of time. This is advantageous, as these signals are directly provided by current measurement devices.

   These methods provide very accurate results, due to the explicit nature of the data. However, the solution is sought via direct integration of the system's equations, usually carried out by Montecarlo integration or similar. This requires a huge computational effort for lightly or moderately damped systems, representing the vast majority of engineering structures.

   Time domain methods were favoured in the early ages of modal analysis, due to its physical insight and direct interpretation of the results. Another decisive factor was the difficulty in performing a Fourier transform in real time, which is a requirement for the frequency domain methods.

2. **Frequency domain methods**. Recent developments in measuring devices such as frequency response analyzers (FRA) plus the advent of the fast Fourier transform (FFT) have led to a resurge in the frequency domain methods, which are increasingly seen as the most viable.

   This class of methods requires an FFT of the raw time signals, before they can be handled as input data. This process separates the time response into a number of harmonic components, each with a specific amplitude and frequency. Due to the periodic nature of this data, the computational effort is greatly reduced.

   The solution of these methods is regarded as approximate, as the events happening in one load-cycle are represented by average quantities. The accuracy will depend, among other issues, on the number of harmonics included in the analysis. For a large class of systems, including linear, a fundamental analysis (the first harmonic) provides workable results.

The methods developed in this research fall within the frequency domain group, chosen because of their good accuracy and computational capabilities. We will take advantage of the well-developed describing function theory (DFM) to formulate the nonlinear elements in the frequency domain.

1.6 Physical coordinates vs. modal coordinates

The identification methods can also be divided into two major categories, this time according to the type of coordinates in which the analysis takes place:

1. **Physical coordinates**. The analysis is based on the coefficients stored in the system's matrices, obtained by spatial discretization. The immediate advantage of this approach is its physical insight, due to the manipulation of mass, damping and stiffness coefficients. It follows that the solution will always be physically meaningful, this being a significant advantage.

   The disadvantages are also significant. Depending on the quality of the discretization, the amount of input data can be huge, easily in the order of tenths of thousand coefficients, which are inextricably tied by complex differential equations. Each one of these coefficients has a certain influence on every DOF of the system, resulting in a heavy algebraic manipulation and expensive computing requirements.

2. **Modal coordinates**. The analysis is carried out in the *modal space*, based on the so-called "generalized coordinates" and modal parameters (eigenvalues and eigenvectors). Usually, a relatively small number of modes are required to regenerate the system's response, and this feature greatly reduces the computational cost involved. In addition, the orthogonal property of the eigenvectors means that a given DOF is fully described by its own eigenvector, reducing even more the algebraic burden.

   If one disadvantage must be associated with such a powerful approach, is perhaps that the modal responses have little physical meaning; this is an issue during an updating or identification analysis, in which the differences between an experimental model and its theoretical counterpart must be conciliated. More often than not, implementing a modal correction leads to impossible physical arrangements, such as a new spring across previously unconnected internal nodes.

In this work, both approaches are analyzed, and their advantages and drawbacks are thoroughly reviewed.

1.7 Some remarks about higher-order harmonics

For a wide class of nonlinear systems subjected to a harmonic excitation, the response remains essentially harmonic, although there is a leakage of energy to frequencies other than the linear natural frequencies. This phenomena -called "higher order harmonics"- is a well known fact occurring in nearly all nonlinear systems and its existence can be mathematically proved by means of the Volterra-Weiner kernels (6). These functions predict resonances at certain multiples (depending on the type of nonlinearity) of the nonlinear natural frequency ω_n:

$$..., \frac{1}{3}\omega_n, \frac{1}{2}\omega_n, \omega_n, 2\omega_n, 3\omega_n, ...$$

By considering these extra-resonances, a worst-case scenario is given when one of these multiples coincides with the location of another natural frequency. This condition leads to an internal feedback phenomenon and higher-than-predicted amplitudes. However, there are currently some difficulties preventing the wide spreading of this theory in an engineering context, namely:

- Despite the amount of research in this field, so far there is little evidence suggesting that this is more than an academic issue in real structures. The author spent a significant amount of time searching for a representative engineering case where the aforementioned problem was relevant, without great success.

- The higher-order FRFs are not directly measurable using current measuring techniques, such FRFs being polluted by higher-order terms. Moreover, they are not directly comparable with each other -because of their different units-, making it difficult for the method to have a real impact.

Considering these arguments, the developments in this research neglect the effect of higher-order harmonics, this being one of the very few -but nevertheless main- assumptions. However, once the central issues developed here have been dealt with, accounting for higher-order harmonics will be just a natural, and possibly straightforward, extension.

1.8 Objectives of thesis

The three main objectives of this thesis can be listed as follows:

1. To develop an experimental method able to detect, characterize, localize and quantify the nonlinearities in an engineering structure.

2. To generate an explicit mathematical model of a nonlinear engineering structure, able to regenerate/predict its response under a different excitation.

3. The methods and models should handle general cases with a systematic approach. They should be compatible with established LMA and FE methods, as well as with existing nonlinear methods.

In order to comply with compatibility requirements, the input data should be based in measured nonlinear responses (NL-FRFs). Also, the method should deliver the nonlinear modal parameters (natural frequencies and modal damping) of the structure, as they are of standard use in other nonlinear methods.

In order to comply with the term "experimental", the method should deal effectively with the uncertainties arising from highly incomplete measurements, which is the rule under typical testing procedures.

1.9 Overview of thesis

The specific subjects addressed by this thesis can be visually observed in the flow chart of Fig. 1.7.

Chapter 2 presents a literature survey of the most recent developments in NLMA, specifically in those subjects related to this research.

Chapter 3 introduces the mathematical formulation of the nonlinear elements, based in the describing function method (DFM). It also presents essential concepts for subsequent developments, such as the nonlinear vector (NLV) and the nonlinear matrix (NLM). In addition, basic definitions such as the *nonlinear region* and the *measured region* are explained, needed to tackle large systems. This can be considered as the "reference" chapter of this thesis.

In Chapter 4, the "explicit formulation" (EF) is introduced. This is a direct-path method based in physical coordinates, which uses the linear coefficients stored in the system's matrices to represent the nonlinear FRF. An optimized version of the EF method is validated against nonlinear measurements taken from a test rig, successfully predicting the nonlinear behaviour.

Chapter 5 introduces a *reverse*-path of the explicit formulation, REF, to explore its suitability as an identification tool. The method is exemplified by solving a large virtual model of a thin plate containing cubic stiffness nonlinearities. The advantages and drawbacks of this *physical coordinates*-based method are thoroughly reviewed.

Chapter 6 presents a novel nonlinear modal expansion in the frequency domain called the "hybrid modal technique" (HMT), introduced here as a direct-path tool. This expansion expresses the linear part of the system in modal coordinates, while the nonlinearities are kept in the physical domain. This approach greatly reduces the computational requirements, by representing the nonlinear FRF in hybrid (modal/physical) coordinates.

Chapter 7 presents a novel technique for extracting nonlinear modal parameters (natural frequencies and modal damping) from measured responses, called "fast approximation technique" (FAT). The nonlinear parameters are *analytically* extracted via newly-developed equations, thus obviating the need of a nonlinear optimization[1]. In the author's opinion, the FAT is the most important theoretical contribution of this thesis.

In Chapter 8, the previously introduced techniques and methods are framed into a single identification method, called the "reverse-HMT" (R-HMT). By analyzing a large virtual model of a plate, the performance of this method is demonstrated, delivering both a modal *and* physical identification. The R-HMT is the single main contribution of this thesis to the field of NLMA.

Chapter 9 reviews the new developments and contributions made in this thesis, also suggesting avenues for future work.

Finally, three appendixes are included, containing information which is referred to throughout the thesis. These are:

---

[1]Currently the standard approach.

- Appendix A, containing the data of the Sample Cases #1 and #2. These small, virtual nonlinear systems are used recurrently to demonstrate, via numerical calculations, the performance of the introduced techniques. The nonlinearities considered in this research are restricted to cubic stiffness[1] and friction damping[2], although the developments are general enough to include most nonlinearities.

- Appendix B, containing the data of the Sample Case #3, a large virtual model of a plate. This model is used to demonstrate the performance of the REF and R-HMT methods as identification tools in a large-scale environment.

- Appendix C, describing the experimental validation of the EF method, which is the core of the nonlinear formulation in this thesis. Although restricted both in size and scope, this appendix represents a few months of work. It documents the design, construction, measurement and validation of a test rig containing cubic stiffness nonlinearities.

---

[1]Sample Case #1.
[2]Sample Case #2.
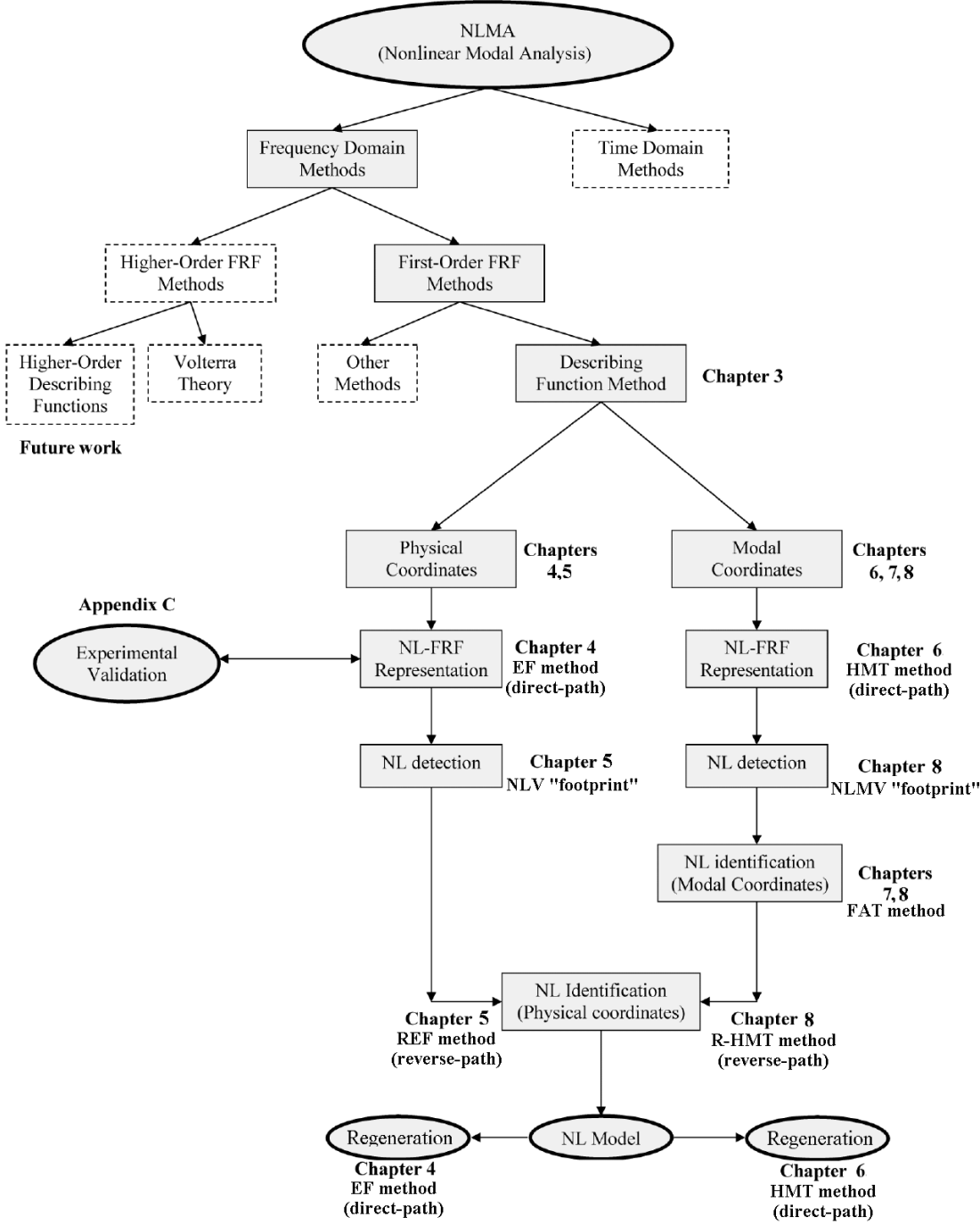
Figure 1.7: Overview of thesis

Chapter 2

Literature survey

Following is a brief review of the existing literature relevant to the topics covered in this thesis. The list is by no means exhaustive, but contains selected sources that either provided a starting point for this research or triggered ideas in a different direction.

2.1 The describing function method (DFM)

The main problem when dealing with nonlinear elements is their amplitude-dependence, which makes a traditional LMA a cumbersome task. This condition generates stiffness/damping coefficients which varies continuously with the level of the response. The DFM seeks to "describe" the relation between the fundamental harmonics of the response and the excitation, by calculating the average restoring force occurring in one cycle.

One of the first applications of the DFM for analyzing nonlinearities can be found in the work of Van der Pol (7), in his method of slowly-varying coefficients; he linearized a NL system by assuming certain parameters to remain constant when compared to the rate of change of the response. Bogoliubov & Mitropolsky (8) used a similar approach to find an equivalent linearization. Later on, Kul & Chen (9) developed a method for evaluating the describing functions of hysteretic-type nonlinearities, based on circular geometry shapes whose radius is a measure of the nonlinearities.

Watanabe & Sato (10) linearized the effects of nonlinear stiffness in a beam by the use of a first-order describing function. They used their results to develop

a nonlinear version of the "building block approach" (BBA), the NL BBA, for coupling NL structures.

Through their joint and independent work, Ozguven & Budak (11), (12), (13), (14), (15), (16), (17), were among the first to introduce describing functions in the context of a practical modal analysis. Working mainly in the *physical* domain, their approach to structural modification and non-proportional damping problems provided grounds for the development of a nonlinear matrix formulation, whose coefficients were amplitude dependent.

Kuran & Ozguven (18) developed a superposition approach for MDOF systems introducing describing functions for the cubic stiffness nonlinearity, which they called a "quasi-linearization". Tanrikulu et al (19) further developed this approach by including a wider range of first-order describing functions. More recently, Besancon-Voda & Blaha (20) presented a multi-input describing function for the friction damping nonlinearity by superimposing the effect of the excitations for two nonlinear electric components.

Also recently, Nassirharand & Karimib (21) introduced a software in the MAT-LAB environment for the input/output characterization of highly nonlinear multi-variable systems, aimed to obtain the sinusoidal-input describing function (SIDF) of a nonlinear liquid propellant engine.

There are a number of researchers who have expanded the concept of the describing function to account for higher-order harmonics, developing the so-called "multi-harmonic describing function". Kuran & Ozguven (18) extended their aforementioned method to account for higher-order terms. J. Vaqueiro (22) presented a detailed construction of first and third-order coefficients for the cubic stiffness nonlinearity, which better approximates the nonlinear response in the time domain.

Unfortunately, the addition of each higher harmonic results in doubling the set of NL equations to be solved, seriously questioning their impact. Although it is relatively straightforward to include them, there are many other important aspects worth analyzing that could be obscured by the added complexity.

2.2 Nonlinear normal modes (NNMs)

The development of nonlinear techniques analogous to the linear superposition has been the focus of much research in recent decades. Provided that the nonlinear response remains oscillatory and periodic, a nonlinear modal superposition would allow an order reduction by possibly achieving decoupled equations of motion. Following is a brief description of previous work in the field of NNMs:

Based in the concept of invariant manifolds, Shaw & Pierre (23), (24) presented a unique[1] and systematic approach to the definition and generation of NNMs for continuous systems. Using asymptotic series expansions, the method preserves the physical nature of the nonlinear mode-shapes and the associated modal dynamics. An interesting feature of this method is that scaled eigenvectors are calculated prior to the eigenvalues. However, the method provides accurate results only for weakly nonlinear systems, exhibiting growing divergence as the strength of the nonlinearities increased.

A year later, Boivin (25) complemented Shaw & Pierre's work by introducing some modifications enabling the same method to perform a "legitimate" modal analysis of the free response of nonlinear systems based on specific characteristics of such systems. Based on a geometric approach, he "recovered some desirable properties of the linear modal analysis of linear systems". In particular, this methodology leaves the modelled modes invariant from the non-modelled ones and vice versa, so that a reduced set of equations can be obtained. On the other hand, interactions between the modelled modes are accounted for, and for instance, internal resonances between them are treated without additional work.

Pesheck et al (26) also used the invariant manifold approach for the generation of reduced-order models for nonlinear vibrations of MDOF systems, extending the original concept to the so-called "multi-mode" manifolds. The dynamic models obtained from this technique allegedly capture the essential coupling between modes of interest, while avoiding coupling from other modes. Such an approach is useful for modelling complex system responses, and is essential when internal resonances exist between the modes. The results showed that the method is

---

[1]As claimed by the authors.

capable of accurately representing the nonlinear system dynamics with relatively few degrees of freedom over a range of vibration amplitudes.

The applicability of nonlinear modal parameters goes far beyond the field of modal analysis, as demonstrated by Shalev & Unger (27). He introduced a new method for solving nonlinear problems of structures subjected to buckling, in-plane and out-of-plane loads, using eigenfunctions as trial functions for solving a nonlinear FE problem; these were computed by a linear free vibration solution by using a standard FE code (MSC/NASTRAN). The system of equations was reduced dramatically and the governing equations, rendered by the Ritz method, represented the problem continuously by considering energy relations, thus not requiring an iterative or incremental solution.

Slaats et al (28) proposed three mode types for reducing nonlinear dynamical system equations resulting from finite element discretizations: tangent modes, modal derivatives and static modes. Tangent modes were obtained from an eigenvalue problem with a "momentary" tangent stiffness matrix, where the derivatives with respect to modal coordinates contained the reduction information. The approach taken in this time domain method could be compatible with the current research, in which modal increments are also analytically estimated[1]. This link represents a direction worth exploring in the future.

Pilipchuk & Ibrahim (29) examined different regimes of non-linear modal interactions of shallow suspended cables. Because of a high-energy level, the equations of motion in terms of in-plane and out-of-plane coordinates are strongly coupled and cannot be linearized. For this type of problem, a special coordinate transformation was introduced to reduce the number of strongly non-linear differential equations by one. The resulting equations of motion were written in terms of stretching, transverse (geometrical bending) and swinging coordinates, those equations being suitable for analysis using standard quantitative and qualitative techniques. Both free and forced vibrations of the cable were considered for in-plane and out-of-plane motions. The cable stretching free vibrations resulted in parametric excitation to the cable transverse motion. Under in-plane forced excitation the stretching motion was found to be directly excited while the transverse motion was parametrically excited.

---

[1]Although the expressions derived in this thesis are quite different.

Chong & Imregun ([30]) presented a general methodology for the coupling analysis of systems with relatively weak non-linearities, of the cubic stiffness type, by assuming that the response remains harmonic under harmonic excitation. The authors tackled the coupling problem by two different approaches: *profile constructing* (which uses the system's spatial data directly) and *parameter extracting*, which are based on their earlier method ([31]) for extracting nonlinear modal parameters from measured data. Both methods yielded virtually identical results and were able to predict the response of a coupled structure at various force levels, exhibiting good agreement with the standard harmonic balance method (HBM) and, most importantly, with measured data.

The current research has strong links with a method also introduced by Chong & Imregun ([31]), who explored the applicability of a superposition technique in which the NNMs are considered to behave nonlinearly at resonance and linearly elsewhere. The coupled nature of the nonlinear modal space was accounted for, by expressing the resonant nonlinear modal amplitude as a function of a few neighbouring modes. The nonlinear eigenvalues and eigenvectors were separately extracted from measured data and the physical response was expressed as an algebraic addition of the nonlinear modal coordinates. This method was able to successfully regenerate the response of the system at a different level of excitation (Fig. [2.1]).

2.3 Identification of nonlinear systems

This subject is most relevant to the present work, having a wide range of practical applications. Given its importance, there has been a vast amount of research in this field and huge advances have been made. Following is a brief description of some of the main methods currently in use:

Masry & Caughey ([32]) are among the pioneers in the field of modern system identification, for they laid the basis of one of the most used methods today, the RFS (Restoring Force-Surface). This time domain technique seeks to characterize the nonlinear component of a SDOF system by measuring different states $[y, \dot{y}, t]$ and plotting them in a 3D diagram. The resulting surface is then characterized by Chebyshev polynomials, representing the nonlinear force for each state; the

* : Measured responses
- : Regenerated from nonlinear modal analysis
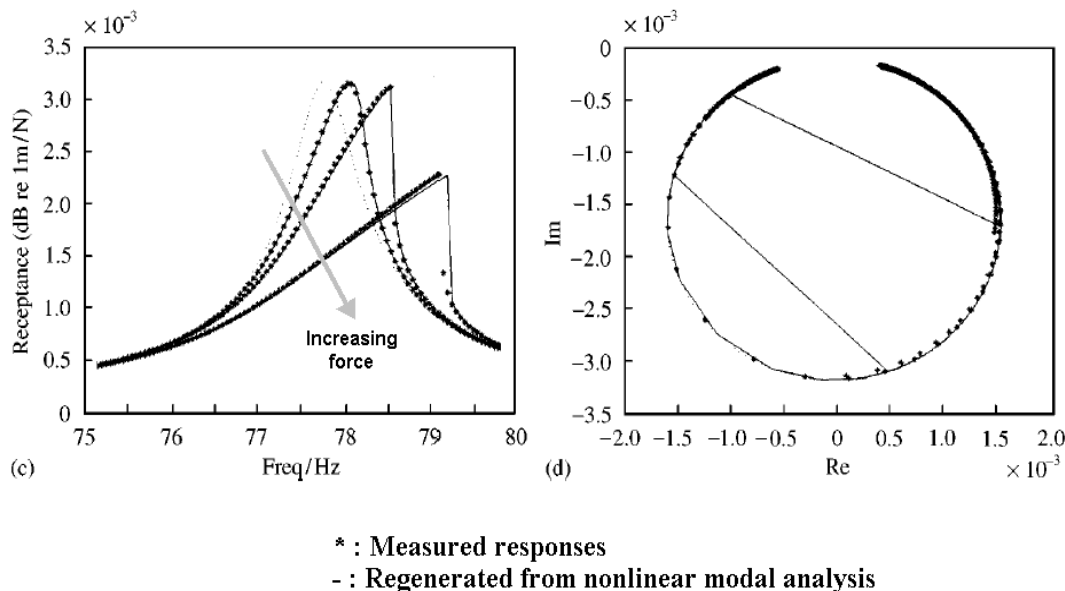
Figure 2.1: NL modal analysis and curve fit, by Chong & Imregun

shape of the diagram can shred some light about the type of nonlinearity in action. Crawley & Aubert (33) independently developed a similar approach by mapping the nonlinear force into complete polynomials, using a direct parametric identification approach.

The RFS method was also applied by Masry & Caughey to the identification of an MDOF system, by transforming the equations of motion into the space of modal coordinates; this approach can still build a surface and identify the nonlinear mechanism, but the identification and localization of the nonlinear elements becomes difficult because generally it is not possible going back to physical coordinates.

Dimitriadis & Cooper (34) also tackled the identification of MDOF systems, following a variant of the RFS method. By considering time responses at similar amplitudes, they achieved a constant nonlinear restoring force. This feature allowed the identification of small systems by means of a simple least-squares computation. However, the application of this method to large systems required a trial-and-error approach to spot the location of the nonlinearity, thus limiting

24

its generality.

Lin, Ewins & Lim (35) presented a method aimed to the identification of nonlinearity from analysis of complex modes. By considering two points of equal magnitude before and after resonance, 2 complex NL equations were constructed for a SDOF mode. The method can handle complex eigenvectors, which is the case for most practical structures. MDOF systems were also considered, and a numerical case for a 2 DOF system was successfully solved. The author of this thesis tried a similar approach, but concluded that the method only applies to systems with friction damping or weak stiffness nonlinearity. For strongly cubic stiffness systems, the jump condition destroys the symmetry of the resonance, thus being impossible two locate a point of similar magnitude after resonance.

Rice (36) used a first order describing function of a cubic stiffness nonlinearity for the identification of weakly nonlinear systems. This method received input-data in the time domain for several levels of excitations and constructed the variation of stiffness and damping ratios as an output.

Soize & Le Fur (37) described an identification technique based on equivalent stochastic linearization with constant coefficients. Although the model leads to a good identification of the total power of the stationary response, it can also give an incorrect identification of the matrix-valued spectral density functions. The authors improved the method by defining a multi-dimensional linear second-order dynamical system with random coefficients, which are found by an optimization procedure specifically developed to that end. A few numerical examples were successfully analyzed, although only weak nonlinearities were considered.

Richard & Singh (38) developed a spectral approach for identifying nonlinear systems when excited by a Gaussian random signal. The method obtains the underlying linear system without been contaminated by the nonlinearities. Once the conditioned FRFs have been estimated, the nonlinearities can be identified by estimating the coefficients of prescribed analytical functions which exist at or away from the excitation point.

Rosa et al (39) used an optimization technique to estimate the modal parameters of a nonlinear system. The estimation, performed in the frequency domain, seeks to minimize the total squared error between experimental and estimated

values of the nonlinear FRFs, its main purpose being to obtain greater accuracy than classical methods in complex cases such as highly damped systems, systems of high modal density and noisy experimental data. The results were compared with those obtained through a classical modal parameter estimation method, the orthogonal polynomials method. It was found that the introduced technique compares favourably to already established methods.

Al-Hadid & Wright (40) developed a force-state mapping technique for nonlinear systems and provided an extension to achieve the localization of nonlinear elements in a lumped-parameter system. The authors claimed that the use of Chebyshev polynomials for mapping the restoring surface is unnecessarily restrictive and that a simple approach, based on ordinary polynomials, provides a faster and more accurate identification for most nonlinearities. Moreover, it is mentioned that this improvement allows a simple methodology for localizing lumped nonlinear elements in MDOF system. Although no examples were shown, the authors used a matrix called the "possible locations of nonlinearities", resembling the concept of a *nonlinear region* developed in this thesis[1].

McEwan, Wright & Cooper (41) introduced a combined modal/finite element analysis technique for the dynamic response of a nonlinear beam subjected to harmonic excitation. A proprietary FEM code was used to construct static "nonlinear test cases" subjected to prescribed modal forces; the resultant modal displacements were used to construct a multi-dimensional surface, thus accounting for inter-modal coupling. The SVD decomposition was required to perform a backward elimination technique, finding an optimum series for a particular nonlinear modal restoring force. This approach is somewhat similar to the "polynomial" fitting developed in this thesis (R-HMT method, Chapter 8), although the reviewed method was restricted to a modal identification only.

Wright, Cooper & Desforges (42) presented a comprehensive review of several identification techniques using the normal-mode force appropriation. This method can measure the undamped natural frequencies and normal mode shapes of a structure, by applying a specific multi-excitation force, designed to neutralize the damping effects. Several approaches, such as the Square and Rectangular FRF matrix methods, were compared and the effect of a rank reduction was also

---

[1]The author reached this concept independently, and the approaches are still different.

explored. The authors concluded that the rectangular FRF matrix methods are superior to the square FRF ones, because the former considers all the responses simultaneously. It was found that the Multivariate Mode Indicator Function (MMIF) is the easiest to interpret for the identification of the undamped natural frequencies. The main drawback of this class of methods is the longer measurement time due to a multi-point excitation.

The classical force appropriation method was extended by Atkins, Wright & Worden (43) for the identification of nonlinear systems. The authors demonstrated that, given the right multi-excitation vector calculated in the *modal space*, it is possible to isolate a single nonlinear normal mode, for which a simple nonlinear SDOF method (such as the RFS) can be used. They illustrated the use of the Volterra kernels to identify the nonlinearity, although a number of optimization methods were considered to account for larger systems.

Wright et al (44) proposed an identification method for weakly nonlinear MDOF systems using a force appropriation approach. They extended the resonant decay method (RDM) to obtain the damping and nonlinear coupling during the response decay, allowing a large model to be identified approximately in a piecewise manner by curve-fitting a series of relatively small modal models. The authors demonstrated the method by analyzing a five DOF system. However, the identification was restricted to the modal space, while the physical nonlinear coefficients remained unknown.

Marchesiello et al (45) considered the conditioned reverse path method (CRP) to identify structures with different types of nonlinearities. One of the advantages of this particular method over similar ones is its ability to treat single-point excited systems with any kind of nonlinear topology. Also, the choice of a random noise excitation allowed a short measurement time. However, a major drawback is that the type of nonlinearity and its location is assumed to be known, which is a serious limitation in practice.

Platten, Wright & Cooper (46), presented a method for identifying nonlinearities in MDOF simulated and experimental systems, operating in the time domain. Interestingly enough, the authors mention that "...*the use of a model based upon modal (or possibly mixed physical / modal) space is arguably a powerful contender for being an identification algorithm with the potential of meeting*

the [ideal] *criteria set out above* [in this same paper] ...". The author of this thesis could not agree more[1], and this has been reflected in the development of the HMT and R-HMT methods, both presented in this thesis. However, these methods operate in the frequency domain.

One of the most popular identification methods working in the time domain is the so-called "Auto-Regressive with eXogenous inputs" (ARX), where the present output value is partly determined by or regressed on previous output values, as reviewed in (3). Billings et al (47) extended the ARX method to analyze nonlinear systems, the NARMAX, developing a wide range of applications to include any type of nonlinearity.

The Hilbert transform (48) has become a promising tool for identifying the presence and type of nonlinearity, because it considers the Fourier transform of a complex function (e.g., a nonlinear FRF) as a "Hilbert pair", where the real and imaginary part of the Fourier transform are intimately linked to the Hilbert transform of the same time signal. This feature allows the direct comparison of both transforms to spot the nonlinear function. However, it suffers from an expensive computational cost.

Lately, there has been an increasing research in the field of neural networks for nonlinear identification. The technique aims to identify the nonlinear restoring forces without any previous assumptions, thus classified as non-parametric. However, this approach requires a long "training" of the software before it can predict accurate results and offers little or no insight into the physics of the problem. Moreover, of all the available techniques, it is the less compatible with a standard LMA. Liang, Feng & Cooper (49) combined fuzzy theory with artificial neural network techniques, showing that such an approach is a feasible alternative for estimating nonlinear restoring forces. A good review of other methods in the field is shown in (3).

The main identification method introduced in this thesis took not a few ideas from the RFS method of Masry & Caughey (32), but it rather works in the frequency domain, thus making it more attractive from a computational point of view. Although the identification process of our method is carried out in the

---

[1]Although he was unaware of this paper at the time of developing the present research. Still, the reviewed paper and the developed methodologies follow different approaches.

modal space, the localization of the nonlinear elements is addressed by going back to physical coordinates. This is achieved by a newly-developed technique, which is applicable to general MDOF systems and most nonlinearities.

2.4 The harmonic balance method (HBM)

The HMB has become the closest to a standard methodology for analysing theoretical nonlinear systems. The main idea behind the method is to "balance" the different harmonics terms arising in the equations of motion due to nonlinearities. A common approach is to neglect higher-order terms, thus solving a fundamental (first harmonic) problem. Recently, there have been increasing developments towards a multi-harmonic approach, which renders more accurate results at the expense of a heavier computational cost.

Although the method is more suitable for a theoretical analysis, it is reviewed here due to its importance, and because some guidelines could be extended to an experimental methodology.

Ferri & Dowell (50) obtained frequency domain solutions to MDOF, dry friction damped systems. They used the so-called Galerkin/Newton-Raphson method, which is equivalent to the HBM when considering the fundamental term only. The set of NL equations was obtained by the "component mode synthesis" method, and solved by a Newton-Raphson scheme. The initial estimate was provided by a ramp function whose behaviour resembled that of the nonlinear friction element, thus improving the convergence rate.

Wang & Chen (51) investigated the vibration of a blade with friction damping by the HBM. In this formulation, a simplified FEM model was used, and further simplifications were made by considering the behaviour of a single mode. A micro-slip model was used to predict the response of the nonlinear element. The authors showed that, regardless of the number of harmonics considered, the problem was reduced to a set of two nonlinear equations plus a set of $2h$ linear equations, h being the number of harmonics.

Ren & Beards (52) presented a multi-harmonic version of the HBM. They used receptance-based information instead of spatial data, which reduces the size of the system to be solved and obviates the need of a FEM model. A perturbation

approach was implemented to achieve a close estimation of the response, which is an essential requirement of the Newton-Raphson algorithm used to solve the nonlinear set of equations. They showed that the nonlinear problem is completely defined by those DOFs associated with nonlinear elements, a claim independently confirmed by this research via a different path.

Hiamang & Mickens (53) considered a second-order nonlinear ODE, and obtained its solution by the HBM. A second approach was taken by solving the corresponding first-order energy relation. Although both problems are equivalent and were constrained by the same initial conditions, they led to different results. The authors concluded that this provides evidence of the ambiguities posed by a linearised problem.

Rice & Xu (54) improved a method originally presented by Budak, Ozguven et al (19), by including a technique which assured convergence in otherwise divergent nonlinear cases. The main improvement consisted in approximating the Jacobian by incorporating a "relaxation" matrix in the Newton-Raphson solver. The authors showed results for an experimental test-bed (an insulated plate), which compare well with time marching results.

Sanliturk, Imregun & Ewins (55) analysed the effect of friction dampers in turbine blades. The authors compared the results of the HBM and time marching methods, and found them to be in close agreement with experimental data. The nonlinear elements were modelled as a complex stiffness, using the linearised micro-slip and macro-slip models. The analysis indicated that both models achieve similar results, provided that the response surpasses the critical amplitude of the nonlinear elements.

Sanliturk & Ewins (56) developed a friction joint model exhibiting planar motion. Although both macro- and micro-slip elements were considered to demonstrate the proposed method, it can also consider experimental data in the form of a loading curve. The authors extended the HBM formulation to include a two-dimensional motion. Comparisons with the time marching method demonstrated a close agreement.

Chapter 3

The nonlinear formulation

3.1 Introduction

The spatial discretization of a linear system is a well-known procedure, and is the basis of standard methods such as FEM and LMA. This can be achieved by a number of techniques (e.g. Ritz, Galerkin, variational formulations), which provide a systematic approach for yielding the ordinary differential equations (ODE).

The main advantage of the aforementioned procedure is the compact representation of a large system in matrix format. The coefficients of the system's matrices represent local mass, damping or stiffness elements, and are all constant for a linear system. The spatial distribution of these elements is accounted for by their matrix indexes.

When considering nonlinear systems, it is just natural to attempt a matrix description of the nonlinearities. In this approach, the system is separated into linear and nonlinear components, where the last is based on a matrix containing a discrete representation of the nonlinearities. This nonlinear matrix is populated by local nonlinear coefficients (typically stiffness and/or damping related), which are amplitude-dependent.

The construction of a nonlinear matrix (NLM) has been addressed by some researchers, most notably by Ozguven & Budak (15), (16), (17), Kuran & Ozguven (18) and Tanrikulu & Imregun (19), who used the well-developed describing function theory (DFM) to obtain equivalent first-order coefficients of common

nonlinearities such as cubic stiffness and friction damping. These coefficients represent the basic "engine" of a nonlinear analysis, allowing the "merging" of linear and nonlinear components into a single matrix representation.

This chapter presents the formulation of nonlinear elements based on first-order describing functions, for cubic stiffness and friction damping types only. These are further used to construct a nonlinear matrix (NLM) and its associated nonlinear vector (NLV), representing the nonlinear component of an MDOF system. These concepts will provide the basic ingredients for the NLMA methods developed in this thesis.

The concepts introduced here are essential for subsequent derivations throughout this work. The reader is advised to revisit this chapter as often as needed, treating it as reference material.

3.2 Formulation of nonlinear coefficients via the describing function method (DFM)

The basic theory of the DFM relies on the fact that, when subjected to a harmonic excitation, a wide variety of nonlinear systems exhibit a periodic, oscillatory response that is sufficiently close to a pure sinusoidal. Although it is recognized that the response of a genuine nonlinear system will exhibit several harmonics of a given natural frequency, it is also true that the amplitudes of the sub/super harmonics are relatively small when compared with the fundamental.

The DFM then seeks to "describe" the relation between the fundamental harmonics of the response and the excitation, and calculates the average restoring force occurring in one cycle. It is clear that, because of a first-order assumption, the multi-harmonic behaviour will neither be captured, nor predicted, though extensions to such situations have been proposed by J. Vaqueiro (22), Kuran & Ozguven (18) and others.

Obtaining first-order coefficients for the cubic stiffness and friction damping nonlinearities is not novel, already being done by a variety of methods ranging from the HBM (57), (58) to the method of slowly-varying parameters (7), but it will be presented here for:

3.2 Formulation of nonlinear coefficients via the describing function method (DFM)

- the sake of completeness, and

- for elucidating some vague definitions in the current literature regarding non-grounded nonlinear elements (more on this later).

The analysis will be exemplified by considering the equation of motion of a simple oscillator subjected to a harmonic excitation:

$$m\ddot{y} + \tilde{g}\,(\dot{y}, y) = f \sin \omega t \qquad (3.1)$$

where $\tilde{g}\,(\dot{y}, y)$ encloses all the restoring forces, assumed to be a nonlinear function of the velocity and displacement $(\dot{y}, y)$ of the mass m. Its nonlinear nature is acknowledged by a " $\tilde{\ }$ " symbol on top.

If the response y is sufficiently close to a pure sinusoidal, and provided that little energy is leaked to frequencies other than the fundamental, then it is reasonable to assume that the nonlinear function $\tilde{g}\,(\dot{y}, y)$ is also of a periodically-oscillating nature. It is possible to find a linearized coefficient $\tilde{\nu}\,(\dot{y}, y)$ which provides the best average of the true restoring force. This coefficient acts on the fundamental harmonic of the nonlinear response $(\tilde{Y}^{1^{st}})$ for a single load-cycle, in such a way that:

$$\tilde{g}\,(\dot{y}, y) \approx \tilde{\nu}\,(\dot{y}, y) \cdot y, \qquad \text{for} \quad y \approx \tilde{Y}^{1^{st}} \sin(\omega t + \theta) = \tilde{Y}^{1^{st}} \sin \tau \qquad (3.2)$$

In order to find the NL coefficient $\tilde{\nu}\,(\dot{y}, y)$, the restoring force $\tilde{g}\,(\dot{y}, y)$ is expanded around y via a Fourier series, neglecting all the higher-order terms:

$$\tilde{g}\,(\dot{y}, y) \approx \tilde{\nu}\,(\dot{y}, y) \cdot y = \sigma_a^{1^{st}} y + \sigma_b^{1^{st}} y + \underbrace{\sigma_c^{2^{nd}} y + \sigma_d^{2^{nd}} y + ...}_{\text{Neglected terms}} \qquad (3.3)$$

where the σ functions are given by:

$$\sigma_a^{1^{st}} = \frac{1}{\pi \tilde{Y}^{1^{st}}} \int_0^{2\pi} \tilde{g}(\tilde{Y}^{1^{st}} \sin \tau, \omega \tilde{Y}^{1^{st}} \cos \tau) \sin \tau d\tau$$

$$\sigma_b^{1^{st}} = \frac{1}{\pi \tilde{Y}^{1^{st}}} \int_0^{2\pi} \tilde{g}(\tilde{Y}^{1^{st}} \sin \tau, \omega \tilde{Y}^{1^{st}} \cos \tau) \cos \tau d\tau \qquad (3.4)$$

so the NL coefficient $\tilde{\nu}\,(\dot{y}, y)$ is uniquely defined by

$$\tilde{\nu}\,(\dot{y}, y) = \sigma_a^{1^{st}} + \sigma_b^{1^{st}} \qquad (3.5)$$

3.2.1 Cubic stiffness describing function

The mathematical model of a cubic stiffness element can be expressed as:

$$\tilde{g}\left(\dot{y}, y\right) = ky + \beta y^3 \tag{3.6}$$

where the coefficient k represents the linear component of the spring, while the coefficient β accounts for the nonlinear effects due to the term y^3. Fig. 3.1 represents both the linear (dotted line) and the nonlinear (solid line) behaviour of a cubic stiffness element.
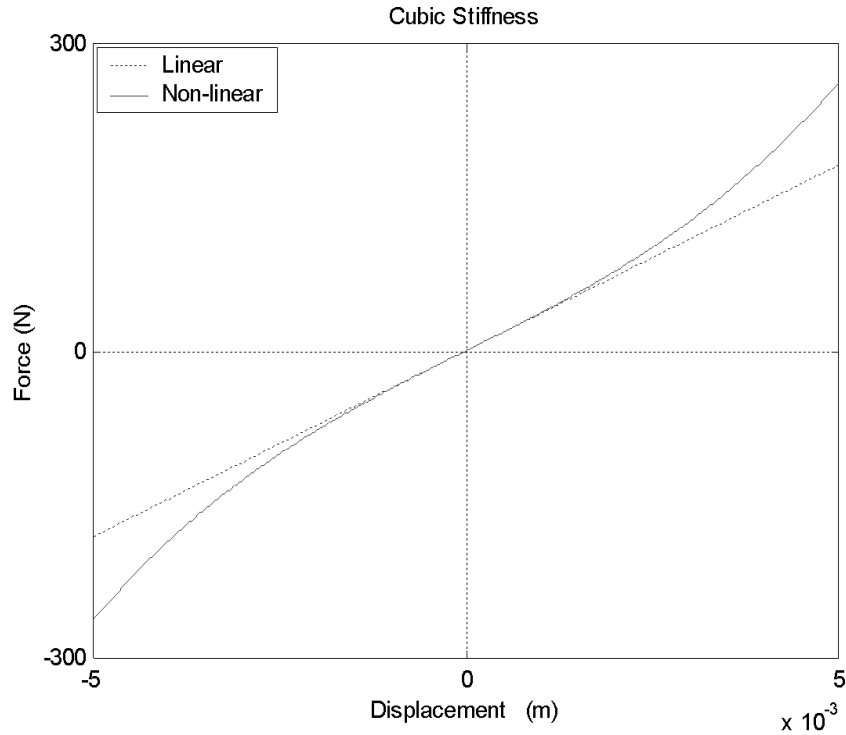
Figure 3.1: Behaviour of a cubic stiffness element

Notice that, while the overall stiffness of the spring indeed changes with the amplitude y, the stiffness coefficients k and β remain constant and are *not* frequency dependent. Otherwise, the differential equation (3.1) would be far more difficult to solve, this being of the type "time-varying coefficients". Introducing

3.2 Formulation of nonlinear coefficients via the describing function method (DFM)

(3.6) into (3.4), and dropping the superscript ^{1st} for the sake of clarity, we have:

$$\sigma_a = \frac{1}{\pi\tilde{Y}} \int_0^{2\pi} (ky + \beta y^3) \sin\tau d\tau$$

$$\sigma_b = 2\sin(\pi)\cos(\pi) = 0$$

(3.7)

Introducing these functions into (3.5) and developing further (the subscript $_k$ in $\tilde{\nu}_k$ meaning a stiffness-related coefficient):

$$\tilde{\nu}_k(\dot{y}, y) = \frac{1}{\pi\tilde{Y}} \int_0^{2\pi} (k\tilde{Y}\sin\tau + \beta\tilde{Y}^3\sin^3\tau)\sin\tau d\tau$$

$$\tilde{\nu}_k(\dot{y}, y) = \frac{1}{\pi\tilde{Y}} \int_0^{2\pi} k\tilde{Y}\sin^2\tau d\tau + \frac{1}{\pi\tilde{Y}} \int_0^{2\pi} \beta\tilde{Y}^3\sin^4\tau d\tau$$

$$\tilde{\nu}_k(\dot{y}, y) = \frac{k}{\pi} \int_0^{2\pi} \sin^2\tau d\tau + \frac{\beta\tilde{Y}^2}{\pi} \int_0^{2\pi} \sin^4\tau d\tau$$

$$\tilde{\nu}_k(\dot{y}, y) = \frac{k}{\pi}(\pi) + \frac{\beta\tilde{Y}^2}{\pi}\left(\frac{3}{4}\pi\right)$$

and we finally arrive to the first-order representation of a cubic stiffness element:

$$\tilde{\nu}_k(\dot{y}, y) = k + \frac{3}{4}\beta\tilde{Y}^2$$

(3.8)

where the nonlinear part of the coefficient is given by:

$$\boxed{\tilde{\nu}_k(\dot{y}, y) = \frac{3}{4}\beta\tilde{Y}^2}$$

(3.9)

The meaning of the NL coefficient $\tilde{\nu}_k(\dot{y}, y)$ can be better illustrated by observing that, according to (3.2), the restoring force has been approximated by the use of a linearized coefficient such as:

$$\tilde{g}(\dot{y}, y) \approx \tilde{\nu}_k(\dot{y}, y) \cdot y$$

(3.10)

$$\left(k \cdot \tilde{Y}\sin\tau + \beta \cdot \tilde{Y}^3\sin^3\tau\right) \approx \left(k + \frac{3}{4}\beta\tilde{Y}^2\right) \cdot \tilde{Y}\sin\tau$$

(3.11)

with the resulting fact that the true restoring function has both a $\sin\tau$ and a $\sin^3\tau$ terms while the linearized function has only a $\sin\tau$ term. Both functions are shown in Figure 3.2, where it can be seen that the linearized coefficient effectively averages the changes in the NL function.
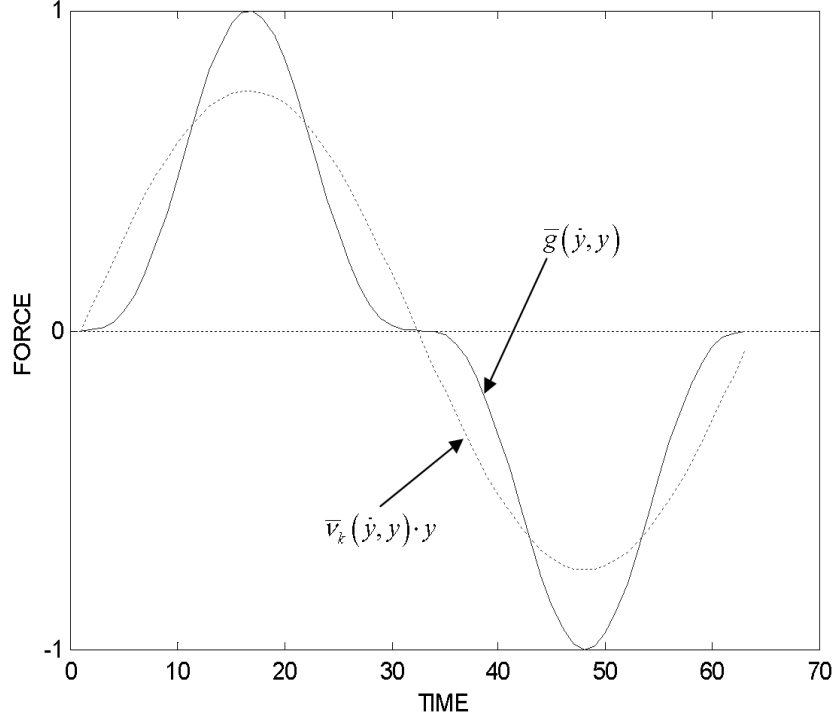
Figure 3.2: First-order describing function of a cubic stiffness element

3.2.1.1 Cubic stiffness non-grounded elements

Developments hitherto apply to a grounded element in which its only coordinate in motion is y. If the NL element is attached between two moving nodes y_1 and y_2 (meaning it is not grounded), a variable change is needed to apply the same procedure:

$$z = y_1 - y_2, \qquad \text{where} \quad y_1 = \tilde{Y}_1 \sin(\omega t + \theta_1), \quad y_2 = \tilde{Y}_2 \sin(\omega t + \theta_2)$$
and
$$z = \tilde{Z} \sin(\omega t + \theta_z) = \tilde{Z} \sin \tau, \qquad \text{where} \quad \tilde{Z} = |z| = |y_1 - y_2|, \quad \theta_z = \measuredangle (y_1, y_2) \tag{3.12}$$

and the NL restoring force becomes:

$$\tilde{g} (\dot{z}, z) \approx \tilde{\nu}_k (\dot{z}, z) \cdot z \tag{3.13}$$

Introducing this variable change and following a similar procedure, the following expression is readily available:

$$\tilde{\nu}_k\left(\dot{z}, z\right) = k + \frac{3}{4}\beta\tilde{Z}^2 \tag{3.14}$$

where the nonlinear part of the coefficient is given by:

$$\boxed{\tilde{\nu}_k\left(\dot{z}, z\right) = \frac{3}{4}\beta\tilde{Z}^2} \tag{3.15}$$

As before, the approximation is better understood when stated as a mathematical equality:

$$\left(k \cdot \tilde{Z}\sin\tau + \beta \cdot \tilde{Z}^3\sin^3\tau\right) \approx \left(k + \frac{3}{4}\beta\tilde{Z}^2\right) \cdot \tilde{Z}\sin\tau \tag{3.16}$$

There are some subtleties involved when dealing with non-grounded elements, but they will be explained in later sections, when the nonlinear matrix (NLM) is introduced.

3.2.2 Friction damping describing function

Obtaining the first-order describing function for the friction damping nonlinearity presents no significant additional difficulties. The restoring force is now given by the function:

$$\tilde{g}\left(\dot{y}, y\right) = c\dot{y} + \gamma\frac{\dot{y}}{|\dot{y}|}, \quad \text{for } y > \tilde{Y}_{limit} \text{ (slip condition)} \tag{3.17}$$

where the $|\dot{y}|$ term is used to ensure that the restoring force always opposes the direction of motion. This model is only valid during the "slip" stage, occurring at displacements over a certain limit $\tilde{Y}_{limit}$, which is related to the properties of the surfaces in contact. Barely below this threshold, a phenomenon known as "stick-slip" exists, characterized by intermittent motion and stationary behaviour. Such a condition invalidates (3.17).

For very small displacements, corresponding to the "stick-slip" stage, the nonlinear component $\gamma\frac{\dot{y}}{|\dot{y}|}$ in (3.17) is usually replaced by a linear elastic force proportional to the current amplitude of motion. The "stick" and "stick-slip" stages will not be included here, because the aim of the research is to focus
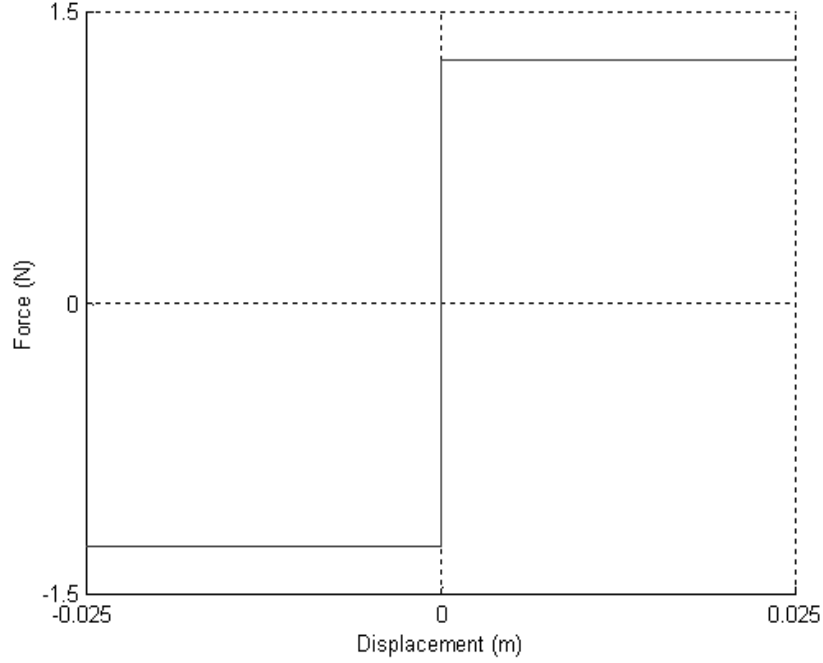
Figure 3.3: Behaviour of a friction damping element

in nonlinear descriptors. Fig. 3.3 illustrates the behaviour of a typical friction damping element.

The relation between the restoring force and its describing function is:

$$\tilde{g}\left(\dot{y}, y\right) \approx \tilde{\nu}_c\left(\dot{y}, y\right) \cdot y \tag{3.18}$$

where the subscript $_c$ in $\tilde{\nu}_c$ stands for a damping-related coefficient. The Fourier expansion produces:

$$\sigma_a = 0$$

$$\sigma_b = \frac{1}{\pi \tilde{Y}} \int_0^{2\pi} \left(c\dot{y} + \gamma \frac{\dot{y}}{|\dot{y}|}\right) \cos \tau d\tau \tag{3.19}$$

The non-zero integral must be solved by parts, to properly handle the $|\dot{y}|$ term. Further developing the algebra:

$$\tilde{\nu}_c\left(\dot{y}, y\right) = \frac{c}{\pi \tilde{Y}} \int_0^{2\pi} \left(\omega \tilde{Y} \cos \tau\right) \cos \tau d\tau + \frac{\gamma}{\pi \tilde{Y}} \int_0^{2\pi} \left(\frac{\omega \tilde{Y} \cos \tau}{\left|\omega \tilde{Y} \cos \tau\right|}\right) \cos \tau d\tau$$

$$\tilde{\nu}_c\left(\dot{y}, y\right) = \frac{\omega c}{\pi} \int_0^{2\pi} \cos^2\tau\, d\tau + \frac{\gamma}{\pi\tilde{Y}} \int_0^{2\pi} \left(\frac{\cos^2\tau}{|\cos\tau|}\right) d\tau$$

$$\tilde{\nu}_c\left(\dot{y}, y\right) = \frac{\omega c}{\pi} \int_0^{2\pi} \cos^2\tau\, d\tau + \frac{\gamma}{\pi\tilde{Y}} \left[2\int_0^{\frac{\pi}{2}} \cos\tau\, d\tau - \int_{\frac{\pi}{2}}^{3\frac{\pi}{2}} \cos\tau\, d\tau\right]$$

and we finally arrive to the first-order representation of a friction damping element:

$$\tilde{\nu}_c\left(\dot{y}, y\right) = \mathbf{i}\omega c + \mathbf{i}\frac{4\gamma}{\pi\tilde{Y}} \tag{3.20}$$

where the imaginary number "$\mathbf{i}$" has been added to account for the phase-shift introduced by the cosine term in (3.19). The nonlinear part of the coefficient is given only by:

$$\boxed{\tilde{\nu}_c\left(\dot{y}, y\right) = \mathbf{i}\frac{4\gamma}{\pi\tilde{Y}}} \tag{3.21}$$

The approximation involved is better understood when (3.20) is introduced in (3.18):

$$\left(c\cdot\omega\tilde{Y}\sin\tau + \gamma\cdot\frac{\omega\tilde{Y}\sin\tau}{\left|\omega\tilde{Y}\sin\tau\right|}\right) \approx \left(\mathbf{i}\omega c + \mathbf{i}\frac{4\gamma}{\pi\tilde{Y}}\right)\cdot\tilde{Y}\cos\tau \tag{3.22}$$

As seen in (3.22), the original restoring force -containing both a $\sin\tau$ and a $\frac{\sin\tau}{|\sin\tau|}$ terms- have been approximated by the use of a linearized coefficient which contains only the term $\cos\tau$. This is further exemplified in Fig. 3.4, showing that the describing function represents the best average of the varying restoring force.

3.2.2.1   Friction damping non-grounded elements

Following a similar approach to the cubic stiffness development, the variable change expressed in (3.12) is introduced. The NL restoring force becomes:

$$\tilde{g}\left(\dot{z}, z\right) \approx \tilde{\nu}_c\left(\dot{z}, z\right)\cdot z \tag{3.23}$$

After applying the describing function formulation, the linearized coefficient $\tilde{\nu}_c\left(\dot{z}, z\right)$ is found to be:

$$\tilde{\nu}_c\left(\dot{z}, z\right) = \mathbf{i}\omega c + \mathbf{i}\frac{4\gamma}{\pi\tilde{Z}} \tag{3.24}$$
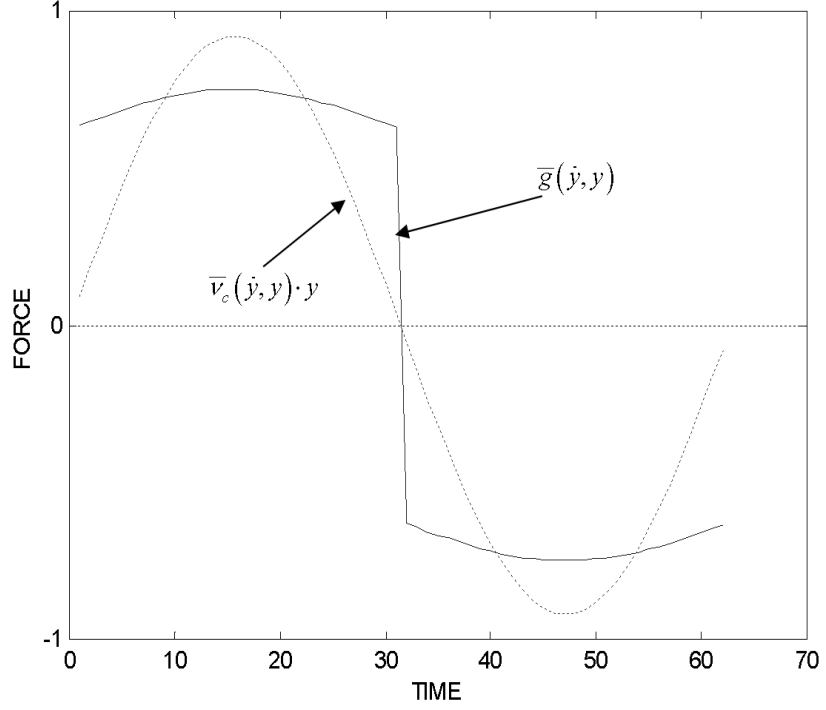
Figure 3.4: First-order describing function of a friction damping element

where the nonlinear part of the coefficient is given only by:

$$\tilde{\nu}_c\left(\dot{z}, z\right) = \mathbf{i}\frac{4\gamma}{\pi \tilde{Z}}$$

(3.25)

The approximation involved is:

$$\left(c \cdot \omega \tilde{Z}\sin\tau + \gamma \cdot \frac{\omega \tilde{Z}\sin\tau}{\left|\omega \tilde{Z}\sin\tau\right|}\right) \approx \left(\mathbf{i}\omega c + \mathbf{i}\frac{4\gamma}{\pi \tilde{Z}}\right) \cdot \tilde{Z}\cos\tau$$

(3.26)

3.3 The nonlinear vector (NLV) and the nonlinear matrix (NLM)

Expanding the idea of the simple oscillator introduced in (3.1) to an MDOF system, we have:

$$[\mathbf{M}]\{\ddot{y}\} + \{\tilde{G}(\dot{y}, y)\} = \{F\}e^{\mathbf{i}\omega t} \tag{3.27}$$

where $[\mathbf{M}]$ is the mass matrix, $\{\ddot{y}\}, \{\dot{y}\}$ and $\{y\}$ are the acceleration, velocity and displacement vectors (respectively), and $\{F\}$ is a harmonic excitation vector operating at frequency ω.

$\{\tilde{G}(\dot{y}, y)\}$ is a vector containing all the restoring forces in the system and, in general, being a function of all the displacements and velocities. We will abbreviate this nonlinear vector as the NLV.

For additive nonlinearities, $\tilde{g}(\dot{y}, y) = \tilde{g}_c(\dot{y}) + \tilde{g}_k(y)$, it is possible to expand the NLV into individual nonlinear restoring forces, as follows:

$$\{\tilde{G}(\dot{y}, y)\} = \left\{\begin{array}{c} \tilde{g}v_1(\dot{y}, y) \\ \tilde{g}v_2(\dot{y}, y) \\ \tilde{g}v_3(\dot{y}, y) \\ \vdots \\ \tilde{g}v_N(\dot{y}, y) \end{array}\right\}_N = \left\{\begin{array}{c} \tilde{g}_{11} + \tilde{g}_{12} + \tilde{g}_{13} + \cdots + \tilde{g}_{1N} \\ \tilde{g}_{21} + \tilde{g}_{22} + \tilde{g}_{23} + \cdots + \tilde{g}_{2N} \\ \tilde{g}_{31} + \tilde{g}_{32} + \tilde{g}_{33} + \cdots + \tilde{g}_{3N} \\ \vdots \\ \tilde{g}_{N1} + \tilde{g}_{N2} + \tilde{g}_{N3} + \cdots + \tilde{g}_{NN} \end{array}\right\}_N \tag{3.28}$$

where N is the size of the system (in DOFs). Each nonlinear function $\tilde{g}_{ij}$ represents a restoring force acting between DOFs i and j, while terms with repeated indexes $\tilde{g}_{ii}$ represent a restoring force between DOF i and ground. So, the i_{th} row of the NLV, containing the function $\tilde{g}v_i(\dot{y}, y)$, represents the combined effect of all the elements connected to DOF i ($\tilde{g}_{i1} + \tilde{g}_{i2} + \tilde{g}_{i3} + \cdots + \tilde{g}_{iN}$). By applying Newton's third law, we also recognize that $\tilde{g}_{ij} = -\tilde{g}_{ji}$.

At this stage, it is advantageous to replace each individual restoring function $\tilde{g}_{ij}$ with the linearized coefficients already developed in Section 3.2. If the system is assumed to have a harmonic response $\{y(t)\} = \{\tilde{Y}\}e^{\mathbf{i}\omega t}$, where $\{\tilde{Y}\} = \{|\tilde{Y}|e^{\mathbf{i}\theta}\}$ is a nonlinear complex vector allowing it to accommodate phase, then it is straightforward to re-define the describing coefficients for this condition.

For "grounded" NL elements, the re-definition is almost trivial:

$$\tilde{\nu}_{ii}(\dot{y}_i, y_i) \cdot y_i = \left(k_{ii} + \frac{3}{4}\beta_{ii}\left|\tilde{Y}\right|_i^2\right)\tilde{Y}_i \tag{3.29}$$

or[1]

$$\tilde{\nu}_{ii}\left(\dot{y}_i, y_i\right) \cdot y_i = \left(\mathbf{i}\omega c_{ii} + \mathbf{i}\frac{4\gamma_{ii}}{\pi\left|\tilde{Y}_i\right|}\right)\tilde{Y}_i \tag{3.30}$$

where the dependence of $\tilde{Y}$ on the harmonic term $e^{\mathbf{i}\omega t}$ has been obviated. For non-grounded NL elements, the NL coefficients can be redefined by "borrowing" from the FEM method the "direct stiffness" approach, in which the elements are formulated via a transformation matrix acting on all of its active coordinates (DOFs). For discrete nonlinear elements having only two active nodes (i and j) as local coordinates, the notation is as follows:

$$\tilde{g}_{ij} \approx \tilde{\nu}_{ij}(\dot{z}_{ij}, z_{ij}) \cdot z_{ij} = \tilde{\nu}_{ij}(\dot{y}_i, \dot{y}_j, y_i, y_j) \cdot (y_i - y_j) \tag{3.31}$$

which leads to:

$$\tilde{\nu}_{ij}\left(\dot{z}_{ij}, z_{ij}\right) \cdot z_{ij} = \left\{ \begin{matrix} k_{ij} & -k_{ij} \end{matrix} \right\}\left\{ \begin{matrix} \tilde{Y}_i \\ \tilde{Y}_j \end{matrix} \right\} + \left\{ \begin{matrix} \frac{3}{4}\beta_{ij}\left|\tilde{Z}_{ij}\right|^2 & -\frac{3}{4}\beta_{ij}\left|\tilde{Z}_{ij}\right|^2 \end{matrix} \right\}\left\{ \begin{matrix} \tilde{Y}_i \\ \tilde{Y}_j \end{matrix} \right\} \tag{3.32}$$

or

$$\tilde{\nu}_{ij}\left(\dot{z}_{ij}, z_{ij}\right) \cdot z_{ij} = \left\{ \begin{matrix} \mathbf{i}\omega c_{ij} & -\mathbf{i}\omega c_{ij} \end{matrix} \right\}\left\{ \begin{matrix} \tilde{Y}_i \\ \tilde{Y}_j \end{matrix} \right\} + \left\{ \begin{matrix} \mathbf{i}\frac{4\gamma_{ij}}{\pi\left|\tilde{Z}_{ij}\right|} & -\mathbf{i}\frac{4\gamma_{ij}}{\pi\left|\tilde{Z}_{ij}\right|} \end{matrix} \right\}\left\{ \begin{matrix} \tilde{Y}_i \\ \tilde{Y}_j \end{matrix} \right\} \tag{3.33}$$

where it can be seen that this formulation produces symmetrical coefficients, i.e. $\tilde{\nu}_{ij} = -\tilde{\nu}_{ji}$. Introducing the newly re-defined NL coefficients into (3.28), a matrix of NL coefficients is formed:

$$\{\tilde{G}\left(\dot{y}, y\right)\} = \begin{bmatrix} \sum\limits_{j=1}^{N}\tilde{\nu}_{1j} & \tilde{\nu}_{12} & \tilde{\nu}_{13} & \cdots & \tilde{\nu}_{1N} \\ \tilde{\nu}_{21} & \sum\limits_{j=1}^{N}\tilde{\nu}_{2j} & \tilde{\nu}_{23} & \cdots & \tilde{\nu}_{2N} \\ \tilde{\nu}_{31} & \tilde{\nu}_{32} & \sum\limits_{j=1}^{N}\tilde{\nu}_{3j} & \cdots & \tilde{\nu}_{3N} \\ \vdots & \vdots & \vdots & \ddots & \vdots \\ \tilde{\nu}_{N1} & \tilde{\nu}_{N2} & \tilde{\nu}_{N3} & \cdots & \sum\limits_{j=1}^{N}\tilde{\nu}_{Nj} \end{bmatrix}_{N,N} \left\{ \begin{matrix} \tilde{Y}_1 \\ \tilde{Y}_2 \\ \tilde{Y}_3 \\ \vdots \\ \tilde{Y}_N \end{matrix} \right\}_N \tag{3.34}$$

---

[1]Do not confound "$\mathbf{i}$" (the imaginary number) with "i" (an spatial index), both appearing for the first time together in (3.30).

The summation in the main diagonal of the matrix of coefficients is explained by the fact that, as seen in (3.32) and (3.33), each off-diagonal (non-grounded) coefficient $\tilde{\nu}_{ij}$ introduces an additive component (of equal magnitude but opposite sign) into the main diagonal (grounded) coefficient $\tilde{\nu}_{ii}$. Because of the assumption of additive nonlinearities, any NL coefficient $\tilde{\nu}_{ij}$ can be stiffness and/or damping related, both acting on the response vector $\left\{\tilde{Y}\right\}$. We will call the square and symmetrical matrix of nonlinear coefficients the NLM (nonlinear matrix), designated by the symbol $\tilde{\nu}$:

$$
\tilde{\nu} = \begin{bmatrix}
\sum_{j=1}^{N} \tilde{\nu}_{1j} & \tilde{\nu}_{12} & \tilde{\nu}_{13} & \cdots & \tilde{\nu}_{1N} \\
\tilde{\nu}_{21} & \sum_{j=1}^{N} \tilde{\nu}_{2j} & \tilde{\nu}_{23} & \cdots & \tilde{\nu}_{2N} \\
\tilde{\nu}_{31} & \tilde{\nu}_{32} & \sum_{j=1}^{N} \tilde{\nu}_{3j} & \cdots & \tilde{\nu}_{3N} \\
\vdots & \vdots & \vdots & \ddots & \vdots \\
\tilde{\nu}_{N1} & \tilde{\nu}_{N2} & \tilde{\nu}_{N3} & \cdots & \sum_{j=1}^{N} \tilde{\nu}_{Nj}
\end{bmatrix}_{N,N}
\tag{3.35}
$$

where the NLV $\tilde{G}$ and the NLM $\tilde{\nu}$ are linked by the following expression:

$$
\boxed{\{\tilde{G}\} = [\tilde{\nu}]\left\{\tilde{Y}\right\}}
\tag{3.36}
$$

An important remark:

- In order to maintain generality, the NLV $\{\tilde{G}\}$ and its associated NLM $[\tilde{\nu}]$ have been defined as containing all the restoring forces in the system, linear and nonlinear. In later developments, however, the linear component is usually explicitly written in the form of the well-known $[\mathbf{K}], [\mathbf{C}], [\mathbf{D}]$ (stiffness, viscous damping and hysteretic damping) matrices. In this case, the NLV and the NLM will represent nonlinear restoring forces *exclusively*.

3.4   The *NL-DOFs* (n), the *nonlinear region* (Γ) and the *measured region* ($\Re$)

One of the most difficult issues during a nonlinear analysis is the precise localization of the nonlinearities, this being recognized by most experts in the field.

3.4 The *NL-DOFs* (n), the *nonlinear region* (Γ) and the *measured region* ($\Re$)

Given that just a few nonlinear local agents can have a significant global impact, an uncompromised search would require measurements in nothing less than *all* the DOFs.

However, when dealing with large systems, relatively few measurements are available. In order to deal effectively with these uncertainties, the following main assumptions will be made throughout this work:

- The global nonlinear effects observed in the system's response are generated by relatively few nonlinear elements. Although their position is strictly unknown, they can be approximately delimited within a *nonlinear region* Γ prior to the analysis, where:

$$\Gamma \in N, \quad \text{typically } \Gamma \ll N \tag{3.37}$$

- The DOFs associated with nonlinear elements are defined as n, the nonlinear DOFs (*NL-DOFs*), where:

$$n \in \Gamma \in N, \quad \text{typically } n \ll \Gamma \ll N \tag{3.38}$$

Note that the exact position of n within Γ remains unknown.

- As demonstrated later[1], the *NL-DOFs* n need to be measured in order to be detected. Therefore, measurements in the whole *nonlinear region* Γ are mandatory for a successful localization.

Measurements outside Γ, while useless during a detection stage, are helpful to improve the quality of the nonlinear quantification, as well as to reduce the size of the analyzed system. All of the measured DOFs, both inside and outside Γ, will be represented by the *measured region* $\Re$, where:

$$n \in \Gamma \in \Re \in N \quad \text{typically } n \ll \Gamma \leq \Re \ll N \tag{3.39}$$

---

[1]But also dictated by common sense.

3.4 The *NL-DOFs* (n), the *nonlinear region* (Γ) and the *measured region* ($\Re$)

Experience shows that the assumption of a pre-defined *nonlinear region* is feasible in the context of an engineering structure. It has been observed that the nonlinearities are often caused by a few local agents[1], which can be approximately localized prior to the analysis. The areas associated with nonlinearities can be enclosed in a *nonlinear region* Γ of arbitrary size. Outside it, the system is assumed to be free of NL elements, although not free of NL effects!.

This assumption can be used to perform a dramatic size-reduction during a nonlinear analysis. Splitting the rows/columns of (3.36) into Γ and $(N - \Gamma)$ DOFs, we have:

$$\left\{ \begin{array}{c} \tilde{G}_{N-\Gamma} \\ \tilde{G}_{\Gamma} \end{array} \right\} = \left[\begin{array}{cc} 0_{(N-\Gamma),(N-\Gamma)} & 0_{(N-\Gamma),\Gamma} \\ 0_{\Gamma,(N-\Gamma)} & \tilde{\nu}_{\Gamma,\Gamma} \end{array} \right] \left\{ \begin{array}{c} \tilde{Y}_{N-\Gamma} \\ \tilde{Y}_{\Gamma} \end{array} \right\} \tag{3.40}$$

where the nonlinear coefficients $\tilde{\nu}_{i,j}$ outside the *nonlinear region* Γ are assumed to be zero. This leads to the reduced expression:

$$\boxed{\{\tilde{G}_{\Gamma}\} = [\tilde{\nu}_{\Gamma,\Gamma}]\{\tilde{Y}_{\Gamma}\}} \tag{3.41}$$

where:

$$\{\tilde{G}_{\Gamma}\} = \left\{ \begin{array}{c} \tilde{g}v_1(\dot{y}, y) \\ \tilde{g}v_2(\dot{y}, y) \\ \tilde{g}v_3(\dot{y}, y) \\ \vdots \\ \tilde{g}v_{\Gamma}(\dot{y}, y) \end{array} \right\}_{\Gamma} = \left\{ \begin{array}{c} \tilde{g}_{11} + \tilde{g}_{12} + \tilde{g}_{13} + \cdots + \tilde{g}_{1\Gamma} \\ \tilde{g}_{21} + \tilde{g}_{22} + \tilde{g}_{23} + \cdots + \tilde{g}_{2\Gamma} \\ \tilde{g}_{31} + \tilde{g}_{32} + \tilde{g}_{33} + \cdots + \tilde{g}_{3\Gamma} \\ \vdots \\ \tilde{g}_{\Gamma 1} + \tilde{g}_{\Gamma 2} + \tilde{g}_{\Gamma 3} + \cdots + \tilde{g}_{\Gamma\Gamma} \end{array} \right\}_{\Gamma} \tag{3.42}$$

and:

$$\tilde{\nu}_{\Gamma,\Gamma} = \left[\begin{array}{ccccc} \sum\limits_{j=1}^{\Gamma} \tilde{\nu}_{1j} & \tilde{\nu}_{12} & \tilde{\nu}_{13} & \cdots & \tilde{\nu}_{1\Gamma} \\ \tilde{\nu}_{21} & \sum\limits_{j=1}^{\Gamma} \tilde{\nu}_{2j} & \tilde{\nu}_{23} & \cdots & \tilde{\nu}_{2\Gamma} \\ \tilde{\nu}_{31} & \tilde{\nu}_{32} & \sum\limits_{j=1}^{\Gamma} \tilde{\nu}_{3j} & \cdots & \tilde{\nu}_{3\Gamma} \\ \vdots & \vdots & \vdots & \ddots & \vdots \\ \tilde{\nu}_{\Gamma 1} & \tilde{\nu}_{\Gamma 2} & \tilde{\nu}_{\Gamma 3} & \cdots & \sum\limits_{j=1}^{\Gamma} \tilde{\nu}_{\Gamma j} \end{array} \right]_{\Gamma,\Gamma} \tag{3.43}$$

In expressions (3.42) and (3.43), $\tilde{g}_{ij}$ and $\tilde{\nu}_{ij}$ are now the restoring force and NL coefficient corresponding to DOFs Γ_i and Γ_j.

---

[1]See Chapter 1.

3.5 Concluding remarks

The nonlinear elements have been formulated based in an already proven "engine", the describing function method (DFM). The formulation introduced in this work neglects the existence of sub/super harmonics, this being one of our main assumptions, otherwise recognizing the amplitude-dependency of the coefficients. This assumption, while inaccurate for a time domain representation, works very well in the frequency domain, which considers average quantities in a single load-cycle.

This nonlinear formulation allows the construction of a nonlinear vector (NLV) and a nonlinear matrix (NLM), which in turn will achieve the "merging" of linear and nonlinear components into a single matrix representation. Special techniques will be developed in coming chapters to take advantage of such representation.

Finally, the definition of the *NL-DOFs* n within a *nonlinear region* Γ (both included in the *measured region* $\Re$) allowed a size-reduction in the nonlinear formulation. This feature will be exploited to achieve an efficient identification when dealing with large systems.

Chapter 4

The explicit formulation (EF) of nonlinear FRFs for MDOF systems (a direct-path approach)

4.1   Introduction

The basic ingredient of any modal analysis method is a set of FRF measurements for the system under study. Currently, the derivation of mathematical models based on linear FRFs is a well-established procedure, and linear modal analysis (LMA) is recognized as a robust and effective identification tool (4),(59). However, a general nonlinear model from available FRFs of a nonlinear system has yet to be found, this being a main obstacle towards the establishment of a general nonlinear methodology. Many of the existing methods can only deal with specific cases.

A severe problem for experimental nonlinear identification is that the relatively few measurements available must be compared to FRFs from large theoretical formulations. However, due to the coupled nature of a nonlinear problem, a theoretical approach, such as the harmonic balance method (HBM), must compute *all* responses at once. For large systems, this results in a nonlinear optimization problem with a large number of unknowns, a major computational challenge even by today's standards.

It makes more sense, at least when dealing with experimentally derived data, to be able to formulate the theoretical responses at the measured coordinates

only. This approach will yield a reduced number of nonlinear equations to be solved, simplifying the process of nonlinear identification. The method described in this chapter tackles this issue by deriving the nonlinear response at selected coordinates, given a fully described theoretical system (a direct-path approach).

The introduced technique, called "explicit formulation" (EF), provides a discrete representation of a nonlinear FRF as a closed-form algebraic expression, for a selected DOF. This is done in a systematic way regardless of the system's size.

The term "explicit" arises from the fact that the proposed model is based on the physical coefficients stored in the $[\mathbf{M}], [\mathbf{K}], [\mathbf{C}]$ (mass, stiffness and damping) matrices, thus classified as a *physical-coordinates* method. The nonlinearities are represented by a nonlinear matrix (NLM) and its associated nonlinear vector (NLV)[1], allowing the seamlessly merging of the linear and nonlinear components into a single matrix formulation.

A matrix inversion, commonly associated with a standard modal analysis, is avoided by defining the nonlinear FRF as the ratio of two determinants instead. Although not particularly efficient in computational terms, the technique offers an unparalleled degree of robustness. An *optimized* EF method will also be developed, aimed to maintain computational economy when dealing with large systems.

The *optimized* EF will be validated against real measurements taken from a test rig containing cubic stiffness nonlinearities, whose design, construction and testing are detailed in Appendix C. The nonlinear formulation of this research is fully contained in the EF method; therefore, its experimental validation will support subsequent developments, which are all based in the same nonlinear "engine".

The proposed methodology shares a common philosophy found in other NL methods: first, the equations of motion are derived by model discretization via FEM, Galerkin or Ritz methods; then the NL ordinary differential equations (ODE) are converted into a set of NL algebraic equations, which is usually solved by a Newton-Raphson scheme, or more specialized algorithms. The current technique was programmed in MATLAB (60) and a modified Newton-Raphson approach was used to deal with a large set of nonlinear equations, incorporating the

---

[1]Both introduced in Chapter 3.

so-called "trust-regions" and "pre-conditioned gradients" (PCG) (61), (62), (63) to find a global solution.

However, it must be said that the emphasis of this chapter is not related to the optimum solution of a NL set of equations, a major subject by itself, but rather to a new approach for the inclusion of nonlinearities into a general formulation.

The EF method can be summarized in the flow chart shown in Fig. 4.1.

4.2   The explicit formulation of nonlinear FRFs

The equation of motion of a general nonlinear system subjected to harmonic excitation can be described by the following nonlinear ordinary differential equation:

$$[\mathbf{M}]\{\ddot{y}\} + [\mathbf{C}]\{\dot{y}\} + \mathbf{i}\,[\mathbf{D}]\{y\} + [\mathbf{K}]\{y\} + \{\tilde{G}\,(\dot{y}, y)\} = \{F\}\,e^{\mathbf{i}\omega t} \qquad (4.1)$$

where $[\mathbf{M}],[\mathbf{C}]$, $[\mathbf{D}]$ and $[\mathbf{K}]$ are the mass, viscous damping, hysteretic damping and stiffness matrices -respectively- of the underlying linear system; $\{\ddot{y}\}, \{\dot{y}\}$ and $\{y\}$ are the acceleration, velocity and displacement vectors, and $\{F\}$ is a harmonic excitation vector operating at frequency ω.

The nonlinear component of the system is represented by the nonlinear vector (NLV) $\{\tilde{G}\}$[1], which is a function of all displacements and velocities in the general case.

Considering a harmonic response $\{y(t)\} = \{\tilde{Y}\}e^{\mathbf{i}\omega t}$, where $\{\tilde{Y}\} = \{|\tilde{Y}|e^{\mathbf{i}\theta}\}$ is a nonlinear complex vector allowing it to accommodate phase, the equation of motion is further reduced to:

$$\left(-\omega^2\,[\mathbf{M}] + \mathbf{i}\omega\,[\mathbf{C}] + \mathbf{i}\,[\mathbf{D}] + [\mathbf{K}]\right)\left\{\tilde{Y}\right\} + \{\tilde{G}(\omega, \tilde{Y})\} = \{F\} \qquad (4.2)$$

The *linear receptance* can be defined as (4):

$$[\alpha] = \left(-\omega^2\,[\mathbf{M}] + \mathbf{i}\omega\,[\mathbf{C}] + \mathbf{i}\,[\mathbf{D}] + [\mathbf{K}]\right)^{-1} \qquad (4.3)$$

and its inverse, $[\mathbf{\Lambda}] = [\alpha]^{-1}$, as:

$$[\mathbf{\Lambda}] = -\omega^2\,[\mathbf{M}] + \mathbf{i}\omega\,[\mathbf{C}] + \mathbf{i}\,[\mathbf{D}] + [\mathbf{K}] \qquad (4.4)$$

---

[1]Introduced in Chapter 3

Figure 4.1: Flow diagram of the EF method (a direct-path approach)

According to (3.36), the nonlinear vector (NLV) $\{\tilde{G}\}$ can be expressed in terms of the nonlinear matrix (NLM) $[\tilde{\nu}]$ and the response vector:

$$\{\tilde{G}\} = [\tilde{\nu}]\left\{\tilde{Y}\right\} \tag{4.5}$$

Introducing (4.4) and (4.5) into (4.2), we have:

$$([\mathbf{\Lambda}] + [\tilde{\nu}])\left\{\tilde{Y}\right\} = \{F\} \tag{4.6}$$

leading to the final compact representation of the NL system:

$$\left[\tilde{\mathbf{\Lambda}}\right]\left\{\tilde{Y}\right\} = \{F\}, \qquad \text{where} \qquad \left[\tilde{\mathbf{\Lambda}}\right] = [\mathbf{\Lambda}] + [\tilde{\nu}] \tag{4.7}$$

$\left[\tilde{\mathbf{\Lambda}}\right]$ is a composite matrix, enclosing linear and nonlinear coefficients, and it is formulated for the current state $[\dot{y}, y, \omega]$. It can be considered to be the system matrix. Obtaining the roots of the determinant of $\left[\tilde{\mathbf{\Lambda}}\right]$ yields the frequency-dependent nonlinear natural frequencies and damping ratios.

Using (4.7), it can be shown that the response at any given DOF i can be described by the ratio of two determinants (64):

$$\tilde{Y}_i = \frac{\det\begin{pmatrix} \tilde{\Lambda}_{1,1} & \cdots & \vdots & \cdots & \tilde{\Lambda}_{1,N} \\ \vdots & \ddots & \vdots & \cdot\cdot\cdot & \vdots \\ \vdots & \cdots & F & \cdots & \vdots \\ \vdots & \cdot\cdot\cdot & \vdots & \ddots & \vdots \\ \tilde{\Lambda}_{N,1} & \cdots & \vdots & \cdots & \tilde{\Lambda}_{N,N} \end{pmatrix}_{N,N}}{\det(\tilde{\mathbf{\Lambda}})} \overset{\downarrow\ i_{th}\ \text{column}}{} \tag{4.8}$$

where N is the size of the system and the matrix in the numerator is formed by replacing the force vector $\{F\}$ in the i_{th} column of the composite matrix $\left[\tilde{\mathbf{\Lambda}}\right]$. Equation 4.8 is the core expression of the EF method.

For a typical engineering structure containing localized nonlinearities (joints, geometric discontinuities, shock absorbers, etc.), the nonlinear matrix $[\tilde{\nu}]$ is highly sparse, with just a few nonzero entries. The notation:

$$\begin{aligned} \Lambda_{ij} &= (-\omega^2 m_{ij} + \mathbf{i}\omega c_{ij} + \mathbf{i}d_{ij} + k_{ij}) \\ \tilde{\Lambda}_{ij} &= (-\omega^2 m_{ij} + \mathbf{i}\omega c_{ij} + \mathbf{i}d_{ij} + k_{ij} + \tilde{\nu}_{ij}) \end{aligned} \tag{4.9}$$

distinguishes between linear (Λ_{ij}) and nonlinear ($\tilde{\Lambda}_{ij}$) coefficients, both contained in $[\tilde{\mathbf{\Lambda}}]$.

4.3 Extension of the EF method to large systems: the *optimized* EF

Equation (4.8) is both suitable and instructive for the analysis of small-sized systems because it maintains the physical connectivities. In other words, a nonlinear coefficient $\tilde{\Lambda}_{ij}$ represents a physical link (linear and nonlinear) acting between DOFs i and j. However, for large systems, the fact that the nonlinearities are scattered throughout $[\tilde{\mathbf{\Lambda}}]$ makes a nonlinear analysis cumbersome and computationally expensive. This can be overcome by further manipulation of (4.7), as follows:

Defining n as those DOFs associated with nonlinear elements[1], (4.7) can be split into n and $(N-n)$ components:

$$\begin{bmatrix} \mathbf{\Lambda}_{(N-n),(N-n)} & \mathbf{\Lambda}_{(N-n),n} \\ \mathbf{\Lambda}_{n,(N-n)} & \tilde{\mathbf{\Lambda}}_{n,n} \end{bmatrix} \left\{ \begin{array}{c} \tilde{Y}_{N-n} \\ \tilde{Y}_n \end{array} \right\} = \left\{ \begin{array}{c} F_{N-n} \\ F_n \end{array} \right\} \tag{4.10}$$

where the nonlinearities have been concentrated in sub-matrix $[\tilde{\mathbf{\Lambda}}_{n,n}]$, the remaining terms being linear. Splitting (4.5) in the same fashion, we obtain:

$$\left\{ \begin{array}{c} \tilde{G}_{N-n} \\ \tilde{G}_n \end{array} \right\} = \begin{bmatrix} 0_{(N-n),(N-n)} & 0_{(N-n),n} \\ 0_{n,(N-n)} & \tilde{\nu}_{n,n} \end{bmatrix} \left\{ \begin{array}{c} \tilde{Y}_{N-n} \\ \tilde{Y}_n \end{array} \right\} \tag{4.11}$$

where the scattered nonlinear coefficients have been concentrated in sub-matrix $[\tilde{\nu}_{n,n}]$. Inserting (4.11) to (4.10) and transferring the nonlinear terms to the RHS, we finally arrive at:

$$\tilde{Y}_i = \frac{\det\left(\begin{array}{ccccc} \Lambda_{1,1} & \cdots & & \cdots & \Lambda_{1,N} \\ \vdots & \ddots & & \ddots & \vdots \\ \vdots & \cdots & \tilde{R} & \cdots & \vdots \\ \vdots & \ddots & & \ddots & \vdots \\ \Lambda_{N,1} & \cdots & & \cdots & \Lambda_{N,N} \end{array} \right)_{N,N}}{\det(\mathbf{\Lambda})} \tag{4.12}$$

$\downarrow i_{th}$ column

where:

$$\tilde{R} = \left\{ \begin{array}{c} F_{N-n} \\ F_n - \tilde{\nu}_{n,n}\tilde{Y}_n \end{array} \right\} \tag{4.13}$$

---

[1] The *NL-DOFs*, see Chapter 3.

4.3 Extension of the EF method to large systems: the *optimized* EF

Equations (4.12) and (4.13) represent the enhanced method (called here the "*optimized* EF") which allows a more efficient calculation of the nonlinear responses when dealing with large systems. Although the size of the matrix $[\boldsymbol{\Lambda}]$ is still N, the solution technique has been greatly simplified because of the following reasons:

1. Expressions (4.12) and (4.13) represent a reduced system of n nonlinear equations ($\tilde{Y}_i$, defined for the DOFs $i \in n$) with n unknowns, the nonlinear responses at the same n DOFs $\{\tilde{Y}_n\}$ being contained in $\{\tilde{R}\}$, where typically $n \ll N$. This demonstrates that a nonlinear system can be fully described by first calculating the nonlinear responses at the n DOFs only.

2. The fact that the unknowns $\{\tilde{Y}_n\}$ are concentrated in the numerator of (4.12), in vector $\{\tilde{R}\}$, is very convenient during a nonlinear optimization. This greatly reduces the computational cost of the solution by updating a local region of the numerator's matrix in (4.12). The matrix in the denominator ($[\boldsymbol{\Lambda}]$) remains unchanged for a given frequency ω.

3. Once the nonlinear responses $\{\tilde{Y}_n\}$ are calculated, the problem has been reduced to a *linear* one. The remaining responses $\{\tilde{Y}_{N-n}\}$ can be found all at once by solving the top equation of (4.10), or by employing (4.12) on an individual basis, for $i \in (N - n)$.

4. Despite the relatively high computational effort in obtaining a determinant, the ability to calculate just a few discrete analytical responses to match their experimental counterparts is well worth the cost. Professor J. R. Wright has pointed out that the determinant of a large matrix can be calculated from the trace of its eigenvalues, an approach which is likely to improve the method dramatically. This issue is well worth exploring as an avenue of future work.

5. This technique allows the inclusion of any kind of damping (viscous and/or hysteretic, proportional or not) without any special consideration.

4.4 Minimization of a large set of nonlinear equations

The Newton-Raphson method is among the most popular for solving nonlinear functions, providing a simple mechanism for iteratively converging to the solution from a sufficiently close initial guess. Currently, there are no methods which can guarantee global convergence in a nonlinear problem, so the importance of estimating a proper initial guess can not be over-stressed (62).

If the algebraic set is equated to zero by transferring the RHS to the LHS, the solution vector is also called the *roots* of the system; in the context of a numerical problem, a residual term is often found instead of an exact solution (zero). By comparing different residuals in several local minima, the global solution can be assigned to that point containing the minimum residual; the advantage in doing so is that convergence is achieved, even if the algorithm is unable to find an exact solution (because of noisy data or because the system simply does not have a zero).

The Newton-Raphson problem can be mathematically stated as finding the vector $\{y\}$ which is the best solution (minimum residual) for the function $\{f(y)\}$,

$$\{f(y)\} \approx \{0\} \tag{4.14}$$

The iterative scheme is based in the equation

$$\{y^{(k+1)}\} = \{y^k\} - \epsilon \, [J]^{-1} \, \{f(y^k)\}, \qquad 0 < \epsilon < 1 \tag{4.15}$$

where the updated vector $\{y^{(k+1)}\}$ corresponding to the $(k + 1)$ iteration is produced from the actual vector $\{y^k\}$ and the Jacobian $[J]$. The problem is reduced to find the value of ϵ which minimizes the residual (4.14).

For a multi-variable problem, the Jacobian is defined by:

$$[J] = \frac{\partial \{f(y^k)\}}{\partial \{y^k\}} = \begin{bmatrix} \frac{\partial f_1}{\partial y_1} & \frac{\partial f_1}{\partial y_2} & \cdots & \frac{\partial f_1}{\partial y_n} \\ \frac{\partial f_2}{\partial y_1} & \frac{\partial f_2}{\partial y_2} & \cdots & \frac{\partial f_2}{\partial y_n} \\ \vdots & \vdots & \ddots & \vdots \\ \frac{\partial f_n}{\partial y_1} & \frac{\partial f_n}{\partial y_2} & \cdots & \frac{\partial f_n}{\partial y_n} \end{bmatrix} \tag{4.16}$$

When dealing with a large number of equations, say more than 50, the rate of convergence can be improved by adopting a "trust-region" approach (61), (63), in which the function to minimize $\{f(y)\}$ -usually of a higher order- is approximated with a simpler function $\{q(y)\}$ which reasonably mimics the behaviour of the original function in a neighbourhood $\prod$ around the point $\{y\}$. This neighbourhood is called a "trust region" and the trial step $\{s\}$ is computed by minimizing the function over $\prod$. The problem is then transformed such as:

$$\min\{\{f(y)\}, \{y\} \in \prod\} \rightarrow \min\{\{q(s)\}, \{s\} \in \prod\} \tag{4.17}$$

Typically, $\{q(y)\}$ is taken to be a quadratic approximation defined by the first two terms of a Taylor expansion of $\{f(y)\}$, and the neighbourhood $\prod$ is usually spherical or ellipsoidal in shape. Mathematically, the "trust-region" sub-problem is defined as:

$$\min\left\{\frac{1}{2}\{s\}^T[\mathbf{T}]\{s\} + \{s\}^T\{g\}, \text{ such that } \|\mathbf{A}s\| \leq \Delta\right\} \tag{4.18}$$

where $\{g\}$ is the gradient of $\{f(y)\}$ at the current point $\{y\}$, $[\mathbf{T}]$ is the Hessian matrix (the symmetric matrix of second derivatives), $[\mathbf{A}]$ is a diagonal scaling matrix, Δ is a positive scalar and $\| \quad \|$ is the 2-norm. A successful iteration is achieved if the following condition is met:

$$\text{if } \{f(y+s)\} \leq \{f(y)\}, \quad \{y\} = \{y\} + \{s\} \tag{4.19}$$

Because the computational cost of solving even the reduced problem is still proportional to several factorizations of $[\mathbf{T}]$, the subspace S is usually restricted to be two-dimensional and being determined with the aid of a preconditioned conjugate gradient (PCG), described in (61), (62) and (63).

Applying the aforementioned scheme for solving the analytical responses $\left\{\tilde{Y}\right\}$ leads to the following procedure:

1. **Establish a vector of unknown variables.** In this case, given by the nonlinear responses $\{\tilde{Y}_n\}$

2. **Construct the set of nonlinear algebraic equations.** These are based in (4.12), forming the vector $\{\tilde{Y}_n\}^{analytical}$. The objective function is $\{f(y)\} = \{f(\tilde{Y}_1, \tilde{Y}_2, \tilde{Y}_3, ... \tilde{Y}_n)\}$.

3. **Provide an initial guess $\{\tilde{Y}_n\}^{trial}$ for the first iteration.** The linear response are chosen to this end.

4. **Real-imaginary splitting.** The standard minimization scheme used in this work[1] cannot handle complex variables, so the problem must be split into real and imaginary parts before proceeding. This can be mathematically stated as:

$$\{f(y)\} = \left\{ \begin{array}{c} f_{\mathrm{Re}}(y) \\ \cdots\cdots\cdots \\ f_{\mathrm{Im}}(y) \end{array} \right\}_{2n} = \left\{ \begin{array}{c} \mathrm{Re}(\tilde{Y}_n^{trial} - \tilde{Y}_n^{analytical}) \\ \cdots\cdots\cdots\cdots\cdots \\ \mathrm{Im}(\tilde{Y}_n^{trial} - \tilde{Y}_n^{analytical}) \end{array} \right\}_{2n} \approx \left\{ \begin{array}{c} 0 \\ \cdots \\ 0 \end{array} \right\}_{2n} \tag{4.20}$$

5. **Iterative procedure.** The iterative procedure will conclude when the objective function $\{f(y)\}$ is less than a pre-defined tolerance (say, between 1-2%) away from the previous iteration. It will deliver the $\{\tilde{Y}_n\}$ responses for the actual excitation frequency only, so a new minimization must be applied for the next step-frequency. This time, the calculated responses serve very well as an initial guess for the algorithm -instead of the linear solution.

6. **Linear solver.** After the responses for all the frequency range have been calculated, the n nonlinear FRFs are now available, and most importantly, the problem has been transformed into a *linear* one. The remaining responses $\{\tilde{Y}_{N-n}\}$ can be found all at once by solving the top equation of (4.10), or by employing (4.12) on an individual basis, for $i \in (N-n)$.

4.5 Sample Case #1: a cubic stiffness example

The EF method will be exemplified with its application to a small sample case. Although in principle there is no restriction at all -other than the computational cost- on the size of the system it can handle, having a small system is visually instructive. Based on this same argument, the case will be restricted to include

---

[1]Provided by MATLAB (60).

cubic stiffness nonlinearities while observing that mixed nonlinearities should not represent a significant obstacle.

The Sample Case #1 is thoroughly described in Appendix A, and shown here in Fig. 4.2 for convenience.
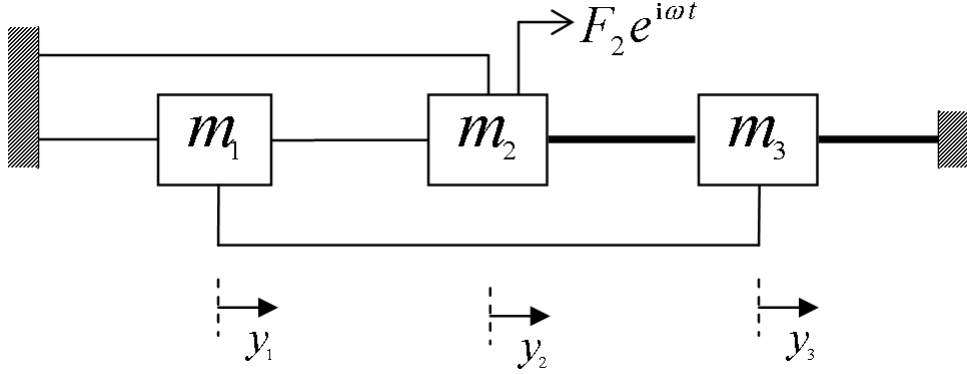
Figure 4.2: Sample Case #1

Our aim is to obtain the nonlinear FRFs, and we start by calculating the nonlinear vector (NLV); given that the nonlinear springs (represented by the two thick lines in Fig. 4.2) are located one at mass m_3 and another between masses m_2 and m_3, it follows that the only non-zero restoring forces in (3.28) are $\tilde{g}_{23}$, $\tilde{g}_{32}$ and $\tilde{g}_{33}$:

$$\{\tilde{G}\left(\dot{y}, y\right)\} = \left\{ \begin{array}{c} \tilde{g}v_1(\dot{y}, y) \\ \tilde{g}v_2(\dot{y}, y) \\ \tilde{g}v_3(\dot{y}, y) \end{array} \right\} = \left\{ \begin{array}{c} \tilde{g}_{11} + \tilde{g}_{12} + \tilde{g}_{13} \\ \tilde{g}_{21} + \tilde{g}_{22} + \tilde{g}_{23} \\ \tilde{g}_{31} + \tilde{g}_{32} + \tilde{g}_{33} \end{array} \right\} = \left\{ \begin{array}{c} 0 \\ \tilde{g}_{23} \\ \tilde{g}_{32} + \tilde{g}_{33} \end{array} \right\}$$

Next, we use (3.29) to express the nonlinear coefficient for the grounded element represented by the restoring force $\tilde{g}_{33}$:

$$\tilde{g}_{33} = \tilde{\nu}_{33}\left(\dot{y}_3, y_3\right) \cdot y_3 = \left(\frac{3}{4}\beta_{33}\left|\tilde{Y}_3\right|^2\right)\tilde{Y}_3$$

The restoring forces $\tilde{g}_{23}$ and $\tilde{g}_{32}$ due to the non-grounded spring are both obtained by using (3.32):

$$\tilde{g}_{23} = \tilde{\nu}_{23}\left(\dot{z}_{23}, z_{23}\right) \cdot z_{23} = \left\{ \begin{array}{cc} \frac{3}{4}\beta_{23}\left|\tilde{Z}_{23}\right|^2 & -\frac{3}{4}\beta_{23}\left|\tilde{Z}_{23}\right|^2 \end{array} \right\}\left\{ \begin{array}{c} \tilde{Y}_2 \\ \tilde{Y}_3 \end{array} \right\}$$

57

and

$$\tilde{g}_{32} = \tilde{\nu}_{32}\left(\dot{z}_{32}, z_{32}\right) \cdot z_{32} = \left\{ \begin{array}{cc} \frac{3}{4}\beta_{32}\left|\tilde{Z}_{32}\right|^2 & -\frac{3}{4}\beta_{32}\left|\tilde{Z}_{32}\right|^2 \end{array} \right\} \left\{ \begin{array}{c} \tilde{Y}_3 \\ \tilde{Y}_2 \end{array} \right\}$$

where $\left|\tilde{Z}_{ij}\right| = \left|\tilde{Y}_i - \tilde{Y}_j\right|$; we observe that, because $\beta_{32} = \beta_{23}$ and $\left|\tilde{Z}_{32}\right| = \left|\tilde{Z}_{23}\right|$, Newton's third law remains true such as $\tilde{g}_{32} = -\tilde{g}_{23}$. Introducing all these expressions into the NLV (3.28), we obtain

$$\left\{ \begin{array}{c} \tilde{g}v_1(\dot{y}, y) \\ \tilde{g}v_2(\dot{y}, y) \\ \tilde{g}v_3(\dot{y}, y) \end{array} \right\} = \frac{3}{4} \cdot \left[\begin{array}{ccc} 0 & 0 & 0 \\ 0 & \beta_{23}\left|\tilde{Z}_{23}\right|^2 & -\beta_{23}\left|\tilde{Z}_{23}\right|^2 \\ 0 & -\beta_{23}\left|\tilde{Z}_{23}\right|^2 & \left(\beta_{33}\left|\tilde{Y}_3\right|^2 + \beta_{23}\left|\tilde{Z}_{23}\right|^2\right) \end{array} \right] \left\{ \begin{array}{c} \tilde{Y}_1 \\ \tilde{Y}_2 \\ \tilde{Y}_3 \end{array} \right\}$$

$$(4.21)$$

where the matrix containing the nonlinear coefficients is the NLM $[\tilde{\nu}]$, defined in (3.35).

Given that we are dealing with a small system, we will use the non-optimized EF (4.8), as it offers a more physical insight than its optimized counterpart (4.12). By (4.8), the nonlinear FRFs are readily determined as:

$$\tilde{Y}_1 = \frac{\det\left(\begin{array}{ccc} 0 & \Lambda_{12} & \Lambda_{13} \\ F_2 & \tilde{\Lambda}_{22} & \tilde{\Lambda}_{23} \\ 0 & \tilde{\Lambda}_{32} & \tilde{\Lambda}_{33} \end{array} \right)}{\det(\tilde{\boldsymbol{\Lambda}})}, \quad \tilde{Y}_2 = \frac{\det\left(\begin{array}{ccc} \Lambda_{11} & 0 & \Lambda_{13} \\ \Lambda_{21} & F_2 & \tilde{\Lambda}_{23} \\ \Lambda_{31} & 0 & \tilde{\Lambda}_{33} \end{array} \right)}{\det(\tilde{\boldsymbol{\Lambda}})},$$

$$\tilde{Y}_3 = \frac{\det\left(\begin{array}{ccc} \Lambda_{11} & \Lambda_{12} & 0 \\ \Lambda_{21} & \tilde{\Lambda}_{22} & F_2 \\ \Lambda_{31} & \tilde{\Lambda}_{32} & 0 \end{array} \right)}{\det(\tilde{\boldsymbol{\Lambda}})}$$

or simply

$$\frac{\tilde{Y}_1}{F_2} = \frac{\Lambda_{13}\tilde{\Lambda}_{32} - \Lambda_{12}\tilde{\Lambda}_{33}}{\det(\tilde{\boldsymbol{\Lambda}})}, \qquad \frac{\tilde{Y}_2}{F_2} = \frac{\Lambda_{11}\tilde{\Lambda}_{33} - \Lambda_{31}\Lambda_{13}}{\det(\tilde{\boldsymbol{\Lambda}})}, \qquad \frac{\tilde{Y}_3}{F_2} = \frac{\Lambda_{12}\Lambda_{31} - \Lambda_{11}\tilde{\Lambda}_{32}}{\det(\tilde{\boldsymbol{\Lambda}})}$$

where

$$\det(\tilde{\boldsymbol{\Lambda}}) = \Lambda_{11}\tilde{\Lambda}_{22}\tilde{\Lambda}_{33} - \Lambda_{11}\tilde{\Lambda}_{23}\tilde{\Lambda}_{32} - \Lambda_{21}\Lambda_{12}\tilde{\Lambda}_{33} + \Lambda_{21}\Lambda_{13}\tilde{\Lambda}_{32} + \Lambda_{31}\Lambda_{12}\tilde{\Lambda}_{23} - \Lambda_{31}\Lambda_{13}\tilde{\Lambda}_{22}$$

$$(4.22)$$

From (4.9) and (4.21), we observe that:

$$
\begin{aligned}
\tilde{\Lambda}_{22} &= \tilde{\Lambda}_{22}(\Lambda_{22}, \tilde{Y}_2, \tilde{Y}_3, \beta_{23}), \\
\tilde{\Lambda}_{23} &= \tilde{\Lambda}_{23}(\Lambda_{23}, \tilde{Y}_2, \tilde{Y}_3, \beta_{23}), \\
\tilde{\Lambda}_{32} &= \tilde{\Lambda}_{23}, \\
\tilde{\Lambda}_{33} &= \tilde{\Lambda}_{33}(\Lambda_{33}, \tilde{Y}_2, \tilde{Y}_3, \beta_{23}, \beta_{33})
\end{aligned}
\tag{4.23}
$$

Equation (4.23) shows that the determinant of $[\tilde{\boldsymbol{\Lambda}}]$ is a square function of β_{23}, due to the determinant's 1_{st} and 2_{nd} terms. However, β_{33}, only shows up in a linear fashion (e.g., determinant's $3_{rd.}$ term contains a single nonlinear element, $\tilde{\nu}_{33}$). Such a feature suggests that the system will be, overall, much more sensitive to variations in the non-grounded nonlinearity β_{23}.

Another useful conclusion can be drawn from (4.23): the determinant of $[\tilde{\boldsymbol{\Lambda}}]$ contains all the nonlinear coefficients in the system. Because it is a common denominator, it follows that any change in any of the nonlinear elements will influence all the responses at once, which is an expected result. However, the extent at which each individual response will be influenced also depends on the numerator, though this is a more subtle issue:

- $\frac{\tilde{Y}_3}{F_2}$ will be much more sensitive to variations in β_{23} than in β_{33}, because $\tilde{\Lambda}_{33}$ does not appear in its numerator.

- $\frac{\tilde{Y}_2}{F_2}$ will be much more sensitive to changes in β_{33} than in β_{23}, because $\tilde{\Lambda}_{23}$ does not appear in its numerator. This is *not* an obvious conclusion, since mass m_2 is not physically linked to element β_{33}.

  However, it could well be that smaller variations in the square variable β_{23} (occurring in the denominator) override large variations in the linear variable β_{33} (occurring in the numerator). Still, the first argument holds true, when comparing the behaviour of the different nonlinear FRFs.

- When considering the nonlinear FRF $\frac{\tilde{Y}_1}{F_2}$ we can only say that it will exhibit the highest sensitivity to the nonlinearities, as judged by the presence of both β_{23} and β_{33} in the numerator (both contained in $\tilde{\Lambda}_{23}$ and $\tilde{\Lambda}_{33}$). Intuition has proved completely wrong in this case, since $\tilde{Y}_1$ would be expected to be the least affected DOF in the system, given that it is the furthest away from the "nonlinear region".

The nonlinear FRFs $\frac{\tilde{Y}_1}{F_2}$, $\frac{\tilde{Y}_2}{F_2}$ and $\frac{\tilde{Y}_3}{F_2}$ together form a set of 3 complex nonlinear equations with 3 complex unknowns (the responses $\tilde{Y}_1$, $\tilde{Y}_2$ and $\tilde{Y}_3$), valid for a single frequency ω; the responses can be solved by using a standard Newton-Raphson algorithm at the resonant regions only, where the nonlinearities are expected to become active, everywhere else being replaced by the linear responses.

The performance of the EF method will be compared with the "harmonic balance method" which is a recognized benchmark for nonlinear problems. The particular HBM code used in this work was written by Dr. Evgeny Petrov (65) under a long term research program at Imperial College London for the vibration analysis of nonlinear structures with different types of nonlinearities, such as friction damping and cubic stiffness.

After applying the minimization process for every step frequency $\Delta\omega$ in the vicinity of resonance, the nonlinear response is obtained and shown in Figs. 4.3 and 4.4.

The dotted line represents the linear response, while the solid line represents the results obtained from the benchmark method, labelled as "HBM". Finally, the "■" marks around the resonances are the results from the EF method, which are in excellent agreement with the benchmark. The calculations took about 8 seconds per resonance, with a 1.5GHz Pentium computer equipped with 500MB of RAM.

4.6 Sample Case #2: a friction damping example

The EF method will now be exemplified in a system containing friction damping nonlinearities. Sample Case #2 is identical to #1, except that the two NL elements are of the friction damping type, as described in Appendix A.

Following a similar approach to the Sample Case #1, the nonlinear matrix
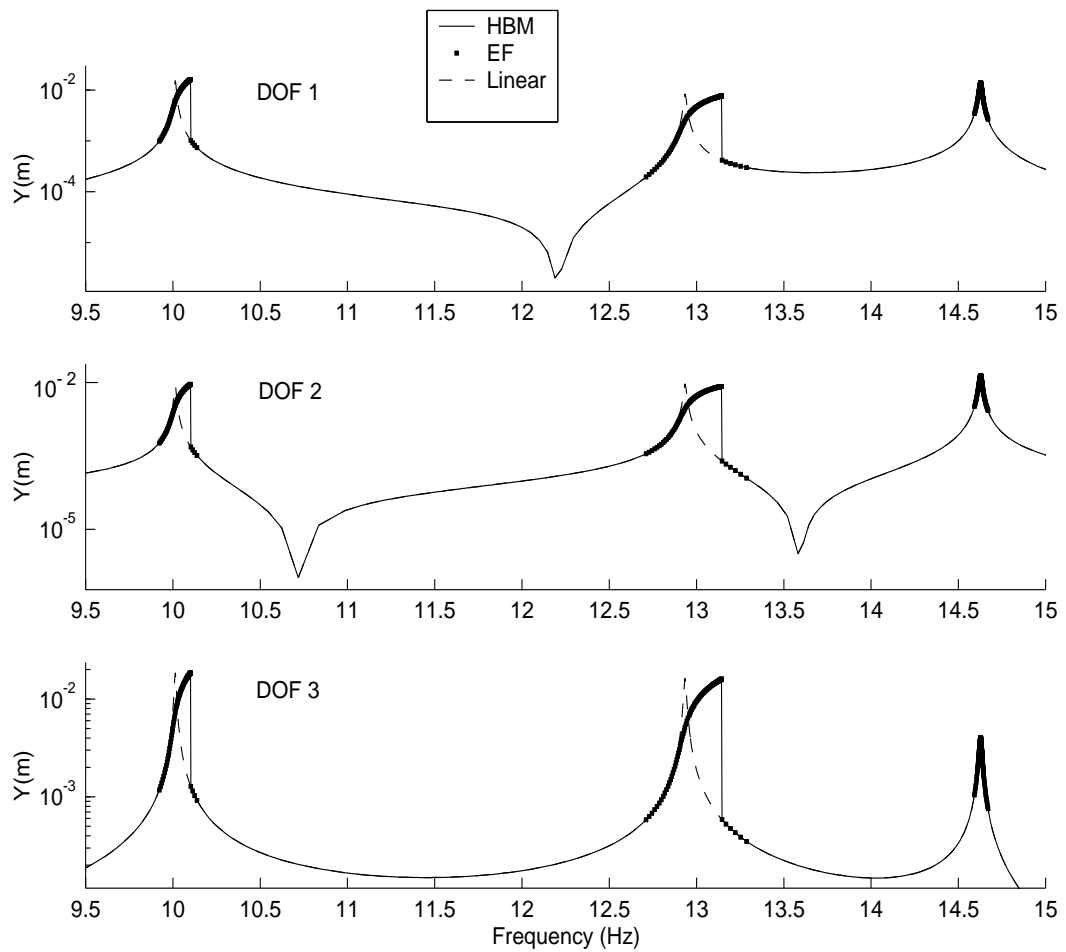
Figure 4.3: Sample Case #1, calculated nonlinear response. A Zoom-In of the individual resonances is shown in Fig. 4.4

Figure 4.4: Sample Case #1, Zoom-In of the individual resonances of Fig. 4.3

(NLM) is built as:

$$[\tilde{\nu}] = \mathbf{i}\frac{4}{\pi} \cdot \begin{bmatrix} 0 & 0 & 0 \\[1em] 0 & \frac{\gamma_{23}}{|\tilde{Z}_{23}|} & -\frac{\gamma_{23}}{|\tilde{Z}_{23}|} \\[1em] 0 & -\frac{\gamma_{23}}{|\tilde{Z}_{23}|} & \left(\frac{\gamma_{33}}{|\tilde{Y}_3|} + \frac{\gamma_{23}}{|\tilde{Z}_{23}|}\right) \end{bmatrix}$$

After applying (4.8), the nonlinear response is calculated and shown in Figs. 4.5 and 4.6. It can be seen that the EF method ("+" marks) is in complete agreement with the benchmark HBM (solid line), both exhibiting NL distortions when compared to the linear case (dotted line).

The effect of the nonlinearity is an overall reduction in the amplitudes, being more noticeable in the first and second modes. This explains why this nonlinear mechanism is so welcome (and even induced) in turbine bladed disks, where higher amplitudes are a risk for the structure stability.

The third mode is less affected because, at higher frequencies, the NL damping force is overwhelmed by the linear restoring forces; the more pronounced effect in the second mode can be explained by the fact that two masses are in opposite motion, generating an additive effect of the friction forces.

All the discussed issues for the Sample Case #1 (Section 4.5), regarding the sensitivity of the nonlinear FRFs to the nonlinearities, remain valid.

4.7 Experimental validation of the *optimized* EF method

The *optimized* EF method was experimentally validated against real measurements taken from a test rig. The experiment is thoroughly described in Appendix C, so in this section only the final results are shown.

Nonlinear FRFs were measured for several points on the structure, for different force levels within the range $0.5 - 1.5N$. The same FRFs were numerically calculated by the *optimized* EF (4.12).

Fig. 4.7 shows the results for the point-FRF in the vicinity of the first mode, for four increasing levels of excitation. The linear FRFs are shown for each

Figure 4.5: Sample Case #2, calculated nonlinear response. A Zoom-In of the individual resonances is shown in Fig. 4.6

Figure 4.6: Sample Case #2, calculated nonlinear response (Zoom-In)

Figure 4.7: Experimental and EF-predicted nonlinear point-FRFs (dB), for four increasing levels of excitation, covering the first mode of the test rig

case, both numerical (dashed line) and measured ("+" marks). Overlying are the nonlinear counterparts, showing the numerical (solid line) and measured ("x" marks) results. A reasonable agreement can be seen for the first bending mode of the structure (the fundamental response).

Observe that the numerical excitation level F_{th} needed to match a measurement taken at a level F_{exp} is, in general, lower. This is probably due to a pre-load effect because of a defective assembly, as deduced from the increasing trend. Also, the effect of a slow force control is more evident at higher levels of excitation, as we move closer to resonance. The scattered points in this region are believed to be caused by force-dropouts, rather than a true nonlinear behaviour.

In spite of these discrepancies, it can be concluded that the *optimized* EF method can reasonably characterize the behaviour of a large engineering structure.

4.8   Concluding remarks

This chapter was devoted to the introduction of the EF method in a direct-path approach, that is, analyzing a fully described theoretical model. The main feature of this method is its ability to express a discrete nonlinear FRF in closed-form. This allows a systematic and consistent approach to calculate selected theoretical responses of a general NL system. The term "explicit" suggests that the formulation is based on the physical parameters stored in the system's matrices, making it compatible with a standard FEM code.

Among the most important developments of this chapter, we can highlight:

- The performance of the EF method was successfully tested in two small sample cases (Sample Cases #1 and #2), containing cubic stiffness and friction damping nonlinearities. The calculated responses showed excellent agreement with the benchmark multi-harmonic balance method.

- The *optimized* EF was experimentally validated against real measurements taken from a test rig. These results show that the method can reasonably characterize the real behaviour of a large structure.

- Finally, it should be pointed out that expanding the method to account for a multi-harmonic behaviour will be straightforward, as the required describing functions are already available for most nonlinearities.

The main drawback of the EF method is the high computational effort involved in the calculations. This is due to the large amount of information stored in the system's matrices, and the heavy algebraic manipulation incurred. This drawback is shared by the vast majority of methods based in physical coordinates, but the EF improves this condition by calculating a reduced set of coordinates only.

Chapter 5

The reverse explicit formulation (REF): an identification method

5.1   Introduction

In this chapter, a reverse-path of the EF method[1] will be explored to determine its suitability as a NL identification tool. This problem is more representative of an experimental case, in which the nonlinear coefficients of the system are attempted to be identified, based in the input-output information. The underlying linear system is also assumed to be known.

Unlike a theoretical analysis, based on differential equations with well defined boundary conditions, the solution of an identification problem is generally non-unique. This is due to the under-determined nature of the problem, because of the impossibility of measuring *all* of the DOFs of the system. Consequently, more than one set of parameters can emulate the observed responses. The mathematical proof of the solution non-uniqueness will be given in subsequent chapters, where a modal approach will easily expose this condition.

The main advantage of a *physical coordinates*-based identification method is that the results are physically meaningful, since the parameters to be identified are stiffness, damping and mass coefficients. As a drawback, it can be mentioned the high computational effort due to the algebraic manipulation of a large amount of data, namely *all* of the parameters in the system's matrices.

---

[1]Introduced in Chapter 4.

The "reverse explicit formulation" (REF) method can be divided in five major stages, according to Fig. 5.1.
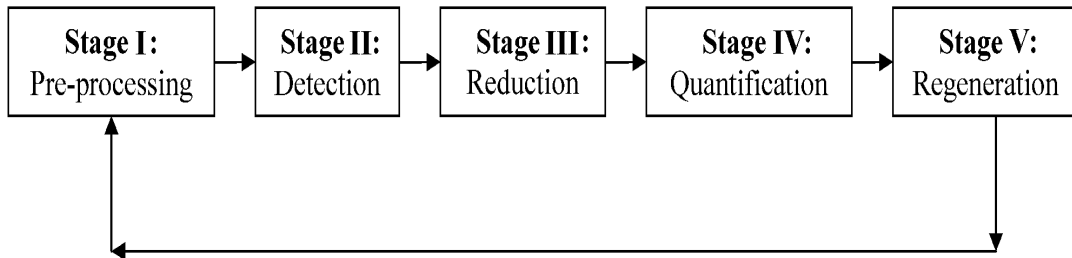
Figure 5.1: The five major stages of the REF method

This process can be implemented iteratively, until the regenerated responses closely match the measured responses. Even then, there is no guarantee that the genuine nonlinearities have been faithfully identified because, as already explained, the solution of an identification problem is generally non-unique. This just means that the obtained solution generates the same observed behaviour *at the measured coordinates*.

The following sections are organized sequentially according to Fig. 5.1, describing the successive stages for the application of the REF method. Then, a sample case of a large structure[1] will be solved, applying the same procedure.

A more detailed flow chart of the REF method is shown in Fig. 5.2.

5.2   Stage I: pre-processing

The following regions must be defined in advance, according to the guidelines given in Section 3.4:

- The *system's DOFs N*: a vector gathering all the DOFs in the system, according to a previous discretization. Its number must suffice to accurately describe the behaviour of the system within the analyzed frequency range.

---

[1]Sample Case #3, described in Appendix B.
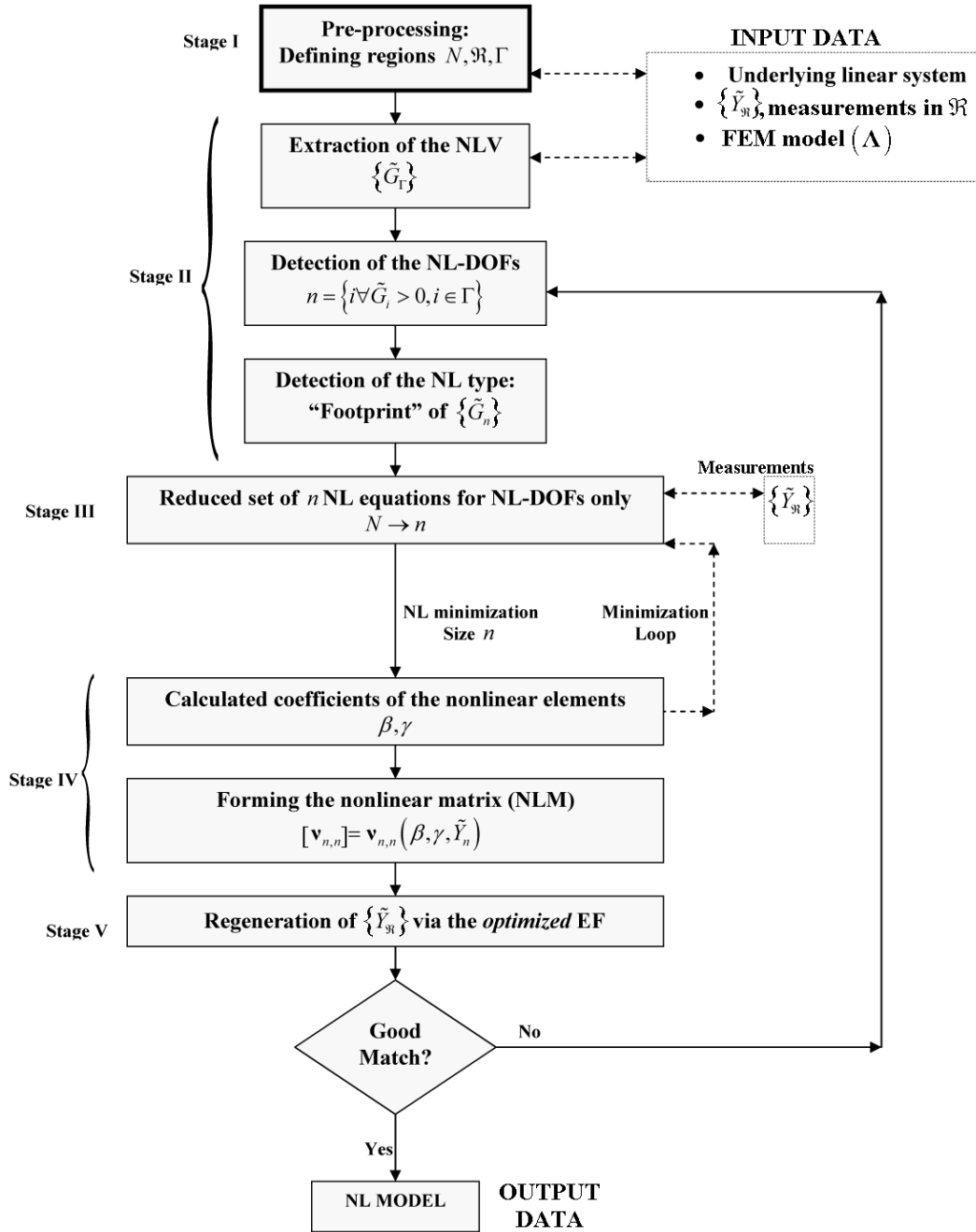
Figure 5.2: Flow diagram of the REF method (a reverse-path approach)

- The *nonlinear region* Γ: a vector gathering all the DOFs which are possibly associated with NL elements (the *NL-DOFs)*.

- The *measured region* $\Re$: a vector gathering all the DOFs which have been measured, both inside and outside Γ.

- The forced DOFs f: a vector gathering all the DOFs which provide excitation to the system[1].

The following relation must hold:

$$\Gamma \in \Re \in N, \quad \text{typically} \quad \Gamma \leq \Re \ll N \tag{5.1}$$

5.3 Stage II: detection of the *NL-DOFs*

This step focuses in the detection of the n *NL-DOFs*[2], contained in the *nonlinear region* Γ. The nonlinear vector (NLV) was defined in (3.28), as:

$$\{\tilde{G}(\dot{y}, y)\} = \left\{ \begin{array}{c} \tilde{g}v_1(\dot{y}, y) \\ \tilde{g}v_2(\dot{y}, y) \\ \tilde{g}v_3(\dot{y}, y) \\ \vdots \\ \tilde{g}v_N(\dot{y}, y) \end{array} \right\}_N = \left\{ \begin{array}{c} \tilde{g}_{11} + \tilde{g}_{12} + \tilde{g}_{13} + \cdots + \tilde{g}_{1N} \\ \tilde{g}_{21} + \tilde{g}_{22} + \tilde{g}_{23} + \cdots + \tilde{g}_{2N} \\ \tilde{g}_{31} + \tilde{g}_{32} + \tilde{g}_{33} + \cdots + \tilde{g}_{3N} \\ \vdots \\ \tilde{g}_{N1} + \tilde{g}_{N2} + \tilde{g}_{N3} + \cdots + \tilde{g}_{NN} \end{array} \right\}_N \tag{5.2}$$

where $\tilde{g}_{ij}$ represents the nonlinear restoring force between DOFs i and j, and $\tilde{g}_{ii}$ represents a grounded NL element at DOF i. It follows that $\tilde{g}v_i$ gives the total restoring force of all the nonlinear elements associated with DOF i, and we can use this feature to detect nonlinearities at this DOF (at least, in principle).

From (4.5) and (4.6), we can obtain another useful representation of the NLV, in terms of the nonlinear responses and the linear system's matrices:

$$\boxed{\{\tilde{G}\} = \{F\} - [\mathbf{\Lambda}]\left\{\tilde{Y}\right\}} \tag{5.3}$$

---

[1]The developments in this research account for a multi-excitation test, unless the opposite is highlighted.

[2]Those DOFs associated with nonlinear elements.

Theoretically, the non-zero entries in the $\{\tilde{G}\}$ would indicate the presence of nonlinear activity at the correspondent DOFs, thus allowing the detection of the *NL-DOFs*. However, this requires that the full vector of nonlinear responses $\{\tilde{Y}\}$ is known (measured), which is clearly unrealistic even for small sizes, as the rotational DOFs are commonly unmeasured. Nonetheless, further manipulation can relax this restriction.

Recalling the concept of a *nonlinear region*[1] Γ, we can partition (5.3) into those DOFs inside (Γ) and outside ($N - \Gamma$) this region:

$$\left\{ \begin{array}{c} 0 \\ \tilde{G}_\Gamma \end{array} \right\} = \left\{ \begin{array}{c} F_{N-\Gamma} \\ F_\Gamma \end{array} \right\} - \left[\begin{array}{cc} \mathbf{\Lambda}_{(N-\Gamma),(N-\Gamma)} & \mathbf{\Lambda}_{(N-\Gamma),\Gamma} \\ \mathbf{\Lambda}_{\Gamma,(N-\Gamma)} & \mathbf{\Lambda}_{\Gamma,\Gamma} \end{array} \right] \left\{ \begin{array}{c} \tilde{Y}_{N-\Gamma} \\ \tilde{Y}_\Gamma \end{array} \right\} \qquad (5.4)$$

where it has been assumed that $\{\tilde{G}_{N-\Gamma}\}$ is zero, as all the nonlinear elements are contained within Γ. Thus, the bottom equation of (5.4) can be written as:

$$\{\tilde{G}_\Gamma\} = \{F_\Gamma\} - [\mathbf{\Lambda}_{\Gamma,(N-\Gamma)}] \underbrace{\{\tilde{Y}_{N-\Gamma}\}}_{Unknown} - [\mathbf{\Lambda}_{\Gamma,\Gamma}]\{\tilde{Y}_\Gamma\} \qquad (5.5)$$

which is, sadly, undetermined, since $\{\tilde{Y}_{N-\Gamma}\}$ are mostly unmeasured responses. However, the theoretical counterpart of $\{\tilde{Y}_{N-\Gamma}\}$ can be recovered from the top equation of (5.4), as follows:

$$\{\tilde{Y}_{N-\Gamma}\} = [\mathbf{\Lambda}_{(N-\Gamma),(N-\Gamma)}]^{-1} \left(\{F_{N-\Gamma}\} - [\mathbf{\Lambda}_{(N-\Gamma),\Gamma}]\{\tilde{Y}_\Gamma\} \right) \qquad (5.6)$$

It has to be recognized that (5.6) represents a huge computational effort for a large system, as the inversion $[\mathbf{\Lambda}_{(N-\Gamma),(N-\Gamma)}]^{-1}$ must be performed for *every analyzed frequency*. This is a severe drawback of the REF method, only avoided if the nonlinearities are localized in advance.

Continuing with the main developments, the NLV for the *nonlinear region* Γ can be finally written as:

$$\boxed{\{\tilde{G}_\Gamma\} = \{F_\Gamma\} - [\mathbf{\Lambda}_{\Gamma,(N-\Gamma)}][\mathbf{\Lambda}_{(N-\Gamma),(N-\Gamma)}]^{-1} \left(F_{N-\Gamma} - \mathbf{\Lambda}_{(N-\Gamma),\Gamma}\tilde{Y}_\Gamma \right) - [\mathbf{\Lambda}_{\Gamma,\Gamma}]\{\tilde{Y}_\Gamma\}}$$
$$(5.7)$$

where the non-zero[2] entries of $\{\tilde{G}_\Gamma\}$ will define the n *NL-DOFs*.

---

[1]See Chapter 3.

[2]Or above certain threshold.

5.4 Stage II: detection of the nonlinear mechanism

This stage deals with the detection of the nonlinear mechanism (cubic stiffness, friction damping, etc.), allowing a full parametrization of the nonlinearities and greatly simplifying the analysis afterwards.

We define $\{\tilde{G}_n\}$ as a sub-NLV containing the n non-zero entries of $\{\tilde{G}_\Gamma\}$, therefore reducing the nonlinear component of the system to a minimum size. Our aim is to characterize the type of nonlinearity based on this information.

Because $\{\tilde{G}_n\}$ contains the nonlinear activity at each *NL-DOF*, it follows that the geometric shape, or "footprint", of this nonlinear function can suggest the type of nonlinearity involved. This research has focused on the cubic stiffness and friction damping types, so only these will be analyzed.

Perhaps the best way to describe this procedure is by considering a numerical case, and draw conclusions from there. Fig. 5.3 shows two different types of NLVs, extracted from the Sample Cases #1 and #2[1]. Which figure corresponds to which NL type, we will not tell just yet, as doing so could deprive us from an interesting discussion.

Let us first consider the NLV shown in Fig. 5.3(a). We observe that:

- The function is significant in the vicinity of the resonances only, just where the FRF-distortions are evident. This observation suggests that the distortions are well explained by the presence of nonlinearities.

- The NLV's magnitude remains constant within these regions. This observation agrees with a friction damping model (Eq. 3.21), which predicts a constant restoring force.

- The slightly curved shape seen in the 9-10 Hz. range (Fig. 5.4) could be well explained by the existence of non-grounded NL elements, whose restoring force is simultaneously dependent on two different responses (Eq. 3.25).

---

[1]See Appendix A.
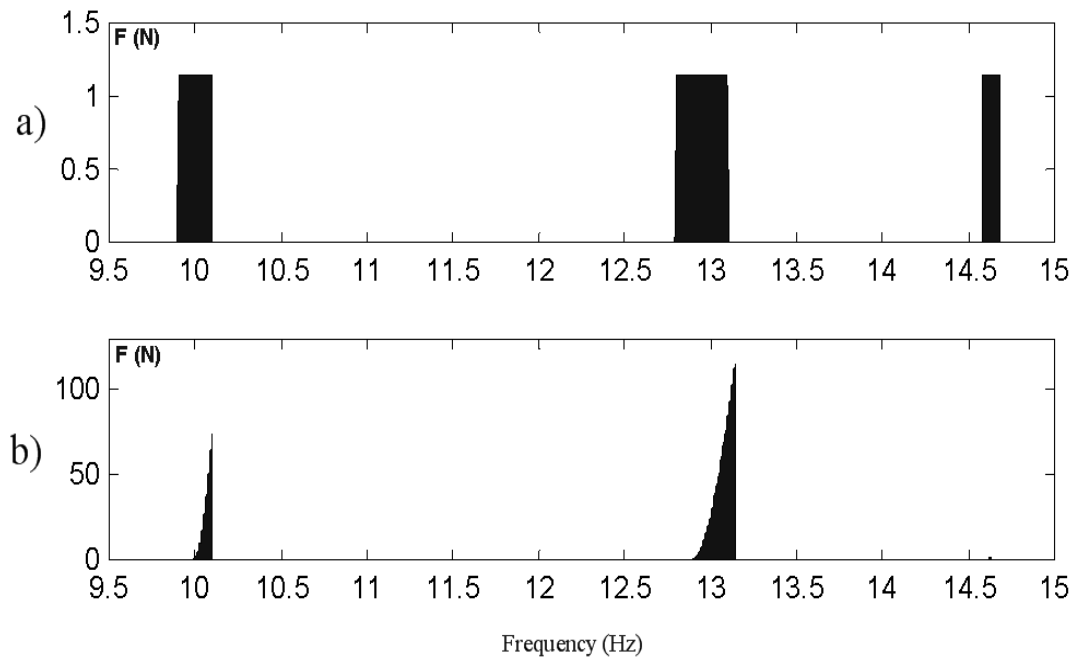
Figure 5.3: Magnitude of two different types of NLVs
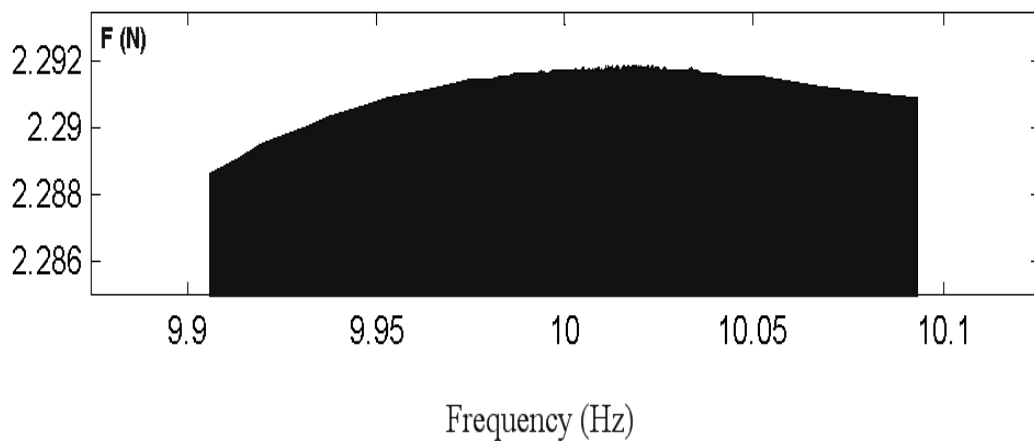
Figure 5.4: Zoom-In of the NLV shown in 5.3(a)

- A quick glance at the imaginary component of the NLV's magnitude (Fig. 5.5a) will provide more solid evidence of a friction damping mechanism. It can be confirmed that the NL restoring force changes sign just after resonance, in agreement with (3.17).
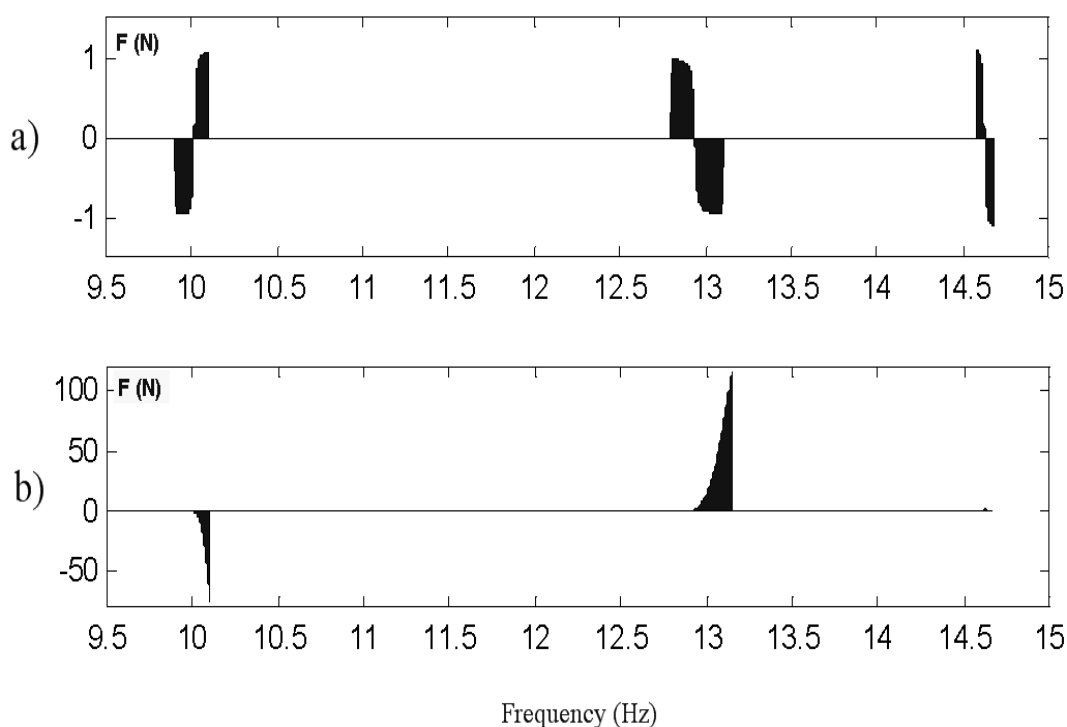
Figure 5.5: Imaginary part of the NLV of Fig. 5.3

Now, we turn our attention to Fig. 5.3(b). The immediate good news is that this NLV exhibits a strikingly different "footprint", also noticing that:

- The NLV's magnitude reaches a maximum at frequencies higher than the linear natural frequencies[1]. This suggests an increase in the stiffness of the system.

- The NLV's magnitude appears to increase monotonically with the overall level of the response, with a higher-than-linear proportionality.

---

[1]See Sample Case #1 in Appendix A.

76

- These observations agree well with a cubic stiffness mechanism, expressed in (3.9).

Indeed, the NL mechanisms of Figs. 5.3(a) and (b) are friction damping and cubic stiffness, respectively.

These guidelines provide a reliable tool to distinguish the NL mechanism prior to a quantification stage. This research has also found evidence that other nonlinearities (such as velocity-squared, softening stiffness, bilinear stiffness, etc.) exhibit a unique footprint, easily incorporating them into this technique.

5.5   Stage III: reduction

Once the nonlinearities have been fully parametrized, a reduced set of NL equations can be posed. We can also take advantage of the measured responses, $\{\tilde{Y}_{\Re}\}$, to reduce the size of the analyzed system by treating them as prescribed boundary conditions.

By an analogous procedure in which the *optimized* EF (4.12) was developed (Section 4.2), the following expression can be derived:

$$\tilde{Y}_i = \cfrac{\det\begin{pmatrix} \Lambda_{1,1} & \cdots & \left\{ \begin{matrix} \vdots \\ \vdots \\ \tilde{R}_S \\ \vdots \\ \vdots \end{matrix} \right. & \cdots & \Lambda_{1,S} \\ \vdots & \ddots & \vdots & \ddots & \vdots \\ \vdots & \cdots & & \cdots & \vdots \\ \vdots & \ddots & \vdots & \ddots & \vdots \\ \Lambda_{S,1} & \cdots & & \cdots & \Lambda_{S,S} \end{pmatrix}}{\det(\mathbf{\Lambda_S})}, \; i \in n \qquad \overset{\downarrow \, i_{th} \text{ column}}{} \tag{5.8}$$

where:

$$
\begin{aligned}
&S = N - \Re + n, \\[2mm]
&\left\{ \tilde{R} \right\}_S = \{F\}_S - [\mathbf{\Lambda}]_{S,(\Re-n)} \left\{ \tilde{Y} \right\}_{(\Re-n)} - [\tilde{\nu}]_{S,S} \left\{ \tilde{Y} \right\}_S, \quad \text{and} \\[2mm]
&[\tilde{\nu}]_{S,S} = \begin{bmatrix} 0_{(N-\Re),(N-\Re)} & 0_{(N-\Re),n} \\ 0_{n,(N-\Re)} & \tilde{\nu}_{n,n} \end{bmatrix}_{S,S}
\end{aligned}
\tag{5.9}
$$

where the size of the analyzed system has been reduced to S. Equations (5.8) and (5.9) represent the *optimized* REF, a reduced set of n NL equations which can be solved via a nonlinear minimization.

5.6 Stage IV: quantification

The quantification of the unknown coefficients in (5.8) and (5.9) can be sought by a nonlinear minimization, similar to the one already described in Section 4.4. The input data must be organized into a set of NL equations and a vector of unknowns, taking care that the resulting problem is neither undetermined, nor ill-posed.

The procedure can be organized as follows:

1. **Define the vector of unknowns.** This is directly taken from the submatrix $[\tilde{\nu}_{n,n}]$ in (5.9), containing the unknown nonlinear coefficients β, γ. This assumes that the nonlinear mechanism has already been identified, otherwise $[\tilde{\nu}_{n,n}]$ will contain nonlinear functions of an unknown nature, and the solution is far more complex. The number of unknown coefficients within $[\tilde{\nu}_{n,n}]$ is:

$$\frac{n^2 + n}{2} \tag{5.10}$$

2. **Constrain the vector of unknowns.** In order to avoid local convergence, sensible upper and lower boundaries must be set for the vector of unknowns, and this step can be carried out by replacing the variable x with a constrained one, say $x\_bounded$, governed by the equation:

$$x\_bounded = Lower + (Upper - Lower) * \sin^2 x \tag{5.11}$$

where $Lower$ and $Upper$ are the lower and upper limit values, respectively, of the variable x, which is only allowed to vary between zero and one. Although this step greatly improves the global convergence characteristics of the algorithm by supplying a starting point assumedly close to the solution, it can also cause no convergence at all if the boundaries are inaccurate.

In the case of a real and positive valued variable x (such as β or γ), the boundaries are easily set between zero (lower limit) and an upper limit high enough to allow the NL element to behave nonlinearly at the observed level of response. To this end, the force-displacement curve of a typical linear element in the location of interest can be used as a basis.

3. **Define the set of nonlinear equations.** This is done by applying (5.8) for the set of n *NL-DOFs*, where the LHS can be equated to the measured responses at the same n DOFs.

   By splitting (5.8) into real and imaginary parts, the number of available equations-per-frequency point is equal to $2n$, which is much smaller than the number of unknowns $(\frac{n^2+n}{2})$. Provided that a nonlinear mechanism has already been detected or assumed, the number of NL equations can be expanded as follows:

   Because the unknown coefficients β, γ are real and positive-valued, we can consider multiple frequency points at once, say q sample points, which are all valid for the same coefficients. Thus, the number of NL equations grows to $2nq$, while the number of unknowns remains at $\frac{n^2+n}{2}$. The q frequency points must be selected from those regions where the effect of the nonlinearities is stronger, typically in the vicinity of the resonances.

   In order to avoid an underdetermined problem, the following relation must hold:

   $$q \geq \text{round}\left(\frac{n+1}{4}\right) \tag{5.12}$$

4. **Iterative procedure.** The analysis will conclude when the objective function $\{f(y)\}$,

   $$\{f(y)\} = \left\{ \begin{array}{c} \text{Re}(\tilde{Y}_n^{analytical} - \tilde{Y}_n^{measured}) \\ \cdots\cdots\cdots\cdots\cdots \\ \text{Im}(\tilde{Y}_n^{analytical} - \tilde{Y}_n^{measured}) \end{array} \right\}_{2nq} \approx 0 \tag{5.13}$$

   is less than a pre-defined tolerance (say, between 1-2%) away from the previous iteration.

5.7 Stage V: regeneration

The *optimized* EF in a direct path, (4.12), can be used to regenerate the measured responses. Any mismatch will indicate that either the set of *n NL DOFs* is not genuine, or that the nonlinear mechanism in action does not correspond to the mathematical model being fitted. In this case, the analysis must be performed again, this time choosing a different set of *n* NL-DOFs or considering a different type of nonlinearity.

Be aware that, due to the solution non-uniqueness of the analysis, a close match does not guarantee that the genuine nonlinearities have been faithfully identified. It just means that the obtained solution generates the same observed behaviour *at the measured coordinates.*

5.8 Sample Case #3: the REF method exemplified

The performance of the REF method will be exemplified in the identification of a large system, given by the Sample Case #3. The system is thoroughly described in Appendix B, so only the main results will be presented here. For convenience, the Sample Case #3 is re-displayed in Fig. 5.6.
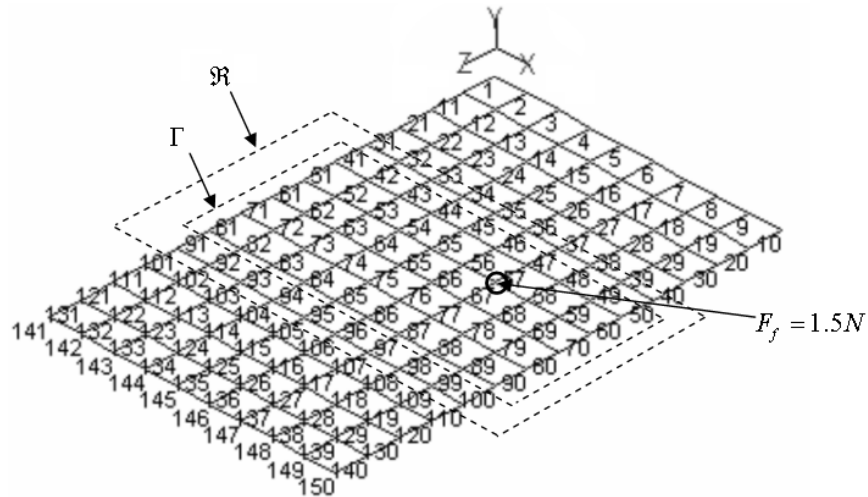
Figure 5.6: The Sample Case #3

5.9 Sample Case #3: pre-processing (stage I)

The pre-defined regions for the Sample Case #3, given both in *DOF* and *nodal* notation, are:

$$
\begin{aligned}
N &= \left\{ \underbrace{(1,2,3,4,5,6)}_{11(x,y,z,\theta_x,\theta_y,\theta_z)}, \underbrace{(7,8,9,10,11,12)}_{12(x,y,z,\theta_x,\theta_y,\theta_z)}, \ldots, \underbrace{(775,\ldots,780)}_{140(x,y,z,\theta_x,\theta_y,\theta_z)} \right\} \text{ (DOF notation)} \\
&\qquad\qquad\qquad\qquad\qquad\qquad\qquad\qquad\qquad\qquad\qquad\qquad\quad \text{(node notation)} \\
\Re &= \left\{ \underbrace{182}_{41Y}, \underbrace{188}_{42Y}, \underbrace{194}_{43Y}, \ldots, \underbrace{596}_{110Y} \right\} \text{ (DOF notation)} \\
&\qquad\qquad\qquad\qquad\qquad\qquad\qquad\quad \text{(node notation)} \\
\Gamma &= \left\{ \underbrace{236}_{51Y}, \underbrace{242}_{52Y}, \underbrace{248}_{53Y}, \ldots, \underbrace{536}_{100Y} \right\} \text{ (DOF notation)} \\
&\qquad\qquad\qquad\qquad\qquad\qquad\qquad\quad \text{(node notation)} \\
f &= \left\{ \underbrace{338}_{67Y} \right\} \text{ (DOF notation)} \\
&\qquad\qquad\quad \text{(node notation)}
\end{aligned}
$$

where $N, \Re, \Gamma$ and f are a-priori defined by the analyst. These regions are shown in Fig. 5.6.

5.10 Sample Case #3: detection of the *NL-DOFs* (stage II)

A nonlinear detection was performed by employing (5.7),

$$
\boxed{\{\tilde{G}_\Gamma\} = \{F_\Gamma\} - [\mathbf{\Lambda}_{\Gamma,(N-\Gamma)}][\mathbf{\Lambda}_{(N-\Gamma),(N-\Gamma)}]^{-1}\left(F_{N-\Gamma} - \mathbf{\Lambda}_{(N-\Gamma),\Gamma}\tilde{Y}_\Gamma\right) - [\mathbf{\Lambda}_{\Gamma,\Gamma}]\{\tilde{Y}_\Gamma\}}
$$

(5.14)

The results are shown in Fig. 5.7, showing the accumulated magnitude of the NLV for a frequency range 8-35 Hz. Three localized nonlinearities can be easily spotted at DOFs 51Y, 62Y and 92Y, sharing a common order of magnitude. A fourth possible *NL-DOF* at DOF 67Y was discarded, due to its comparatively low magnitude[1]. Thus, it was decided to represent the *NL-DOFs* by $n = \{51Y, 62Y, 92Y\}$ (which is the right answer).

As already mentioned, this detection approach conveys a huge computational effort, equivalent to solving a linear problem for each analyzed frequency, and

---

[1]DOF 67Y is, curiously enough, the forced DOF.
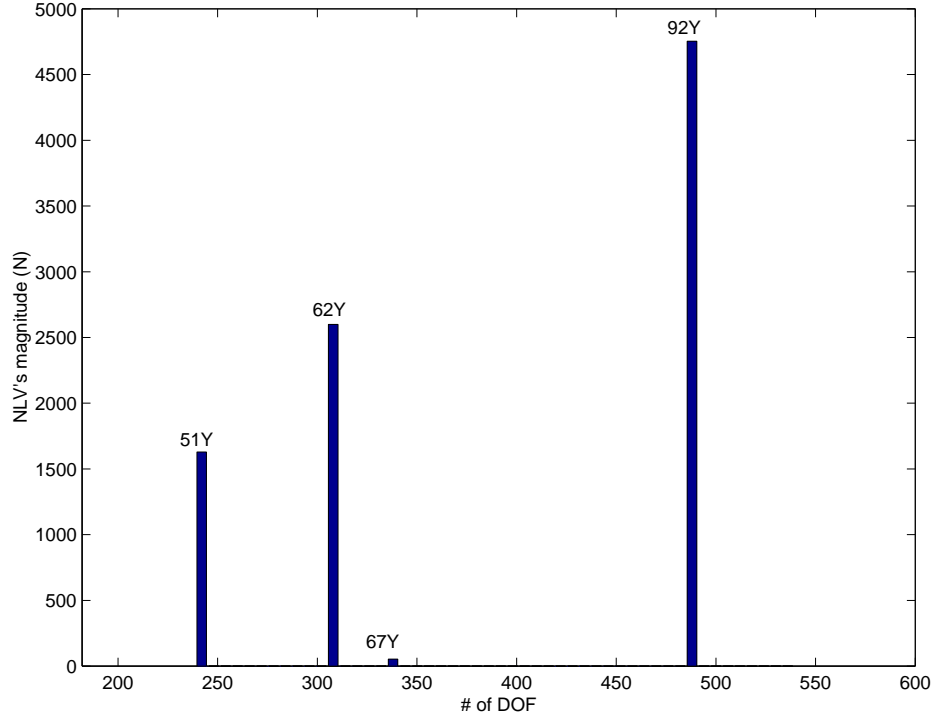
Figure 5.7: Extracted NLV (accumulated magnitude) for the Sample Case #3, detecting 3 localized NL elements at DOFs 51Y,62Y and 92Y. The DOF 67Y, which corresponds to the forced DOF, was discarded due to its comparatively low magnitude

it should be considered as a main drawback of the REF method. On the other hand, Fig. 5.7 proves that it provides reliable answers.

5.11 Sample Case #3: detection of the nonlinear mechanism (stage II)

In Section 5.4, it was introduced a visual technique for assessing the type of nonlinear mechanism acting on a system. The technique is based on the geometric shape of the extracted NLV, whose "footprint" can be associated with the type of nonlinearity.

The NLV for the three detected *NL-DOFs* is shown in Fig. 5.8(a),(b) and (c), for a frequency range encompassing the first resonance, as the strongest nonlinear

Figure 5.8: NLV for the detected *NL-DOFs* of the Sample Case #3

effects are observed there. Recalling the given guidelines, we observe that the NLV is significant only in the vicinity of this resonance, that a maximum is found at the resonant frequency and that the NLV's magnitude appear to increase monotonically with the overall level of the responses.

These observations suggest a cubic stiffness type, which is correct.

5.12   Sample Case #3: reduction (stage III)

Because the Sample Case #3 includes only grounded nonlinearities only[1], the connectivity pattern of the nonlinear elements in the sub-matrix $[\tilde{\nu}_{n,n}]$ is reduced

---

[1]For simplicity. This is not a restriction of the REF method.

to:

$$[\tilde{\nu}_{n,n}] = \begin{bmatrix} \beta_{51Y} \left| \tilde{Y}_{51Y} \right|^2 & 0 & 0 \\ 0 & \beta_{62Y} \left| \tilde{Y}_{62Y} \right|^2 & 0 \\ 0 & 0 & \beta_{92Y} \left| \tilde{Y}_{92Y} \right|^2 \end{bmatrix} \tag{5.15}$$

$[\tilde{\nu}_{n,n}]$ is enlarged into $[\tilde{\nu}]_{S,S}$ as follows:

$$[\tilde{\nu}]_{S,S} = \begin{bmatrix} 0_{(N-\Re),(N-\Re)} & 0_{(N-\Re),n} \\ 0_{n,(N-\Re)} & \tilde{\nu}_{n,n} \end{bmatrix}_{S,S} \tag{5.16}$$

and further included in $\left\{ \tilde{R} \right\}_S$:

$$\left\{ \tilde{R} \right\}_S = \{F\}_S - [\boldsymbol{\Lambda}]_{S,(\Re-n)} \left\{ \tilde{Y} \right\}_{(\Re-n)} - [\tilde{\nu}]_{S,S} \left\{ \tilde{Y} \right\}_S \tag{5.17}$$

so we finally arrive to the *optimized* REF representation:

$$\tilde{Y}_i = \frac{\det \begin{pmatrix} \Lambda_{1,1} & \cdots & \vdots & \cdots & \Lambda_{1,S} \\ \vdots & \ddots & \vdots & \iddots & \vdots \\ \vdots & \cdots & \tilde{R}_S & \cdots & \vdots \\ \vdots & \iddots & \vdots & \ddots & \vdots \\ \Lambda_{S,1} & \cdots & \vdots & \cdots & \Lambda_{S,S} \end{pmatrix}}{\det(\boldsymbol{\Lambda_S})}, \; i \in \{n\} \tag{5.18}$$

$$\downarrow i_{th} \text{ column}$$

(5.18) represents a set of $2n$ (6) sets of NL equations, by splitting it into real and imaginary components. The vector of unknowns is conformed by the unknown coefficients $\{\beta_{51Y}, \beta_{62Y}, \beta_{92Y}\}$. For this particular problem, the reduced size of the analyzed system is $S = 713$, representing a reduction of 8.58%. However, the main reduction has been achieved by the *optimized* REF, which reduces the system of NL equations from N down to n.

5.13 Sample Case #3: quantification (stage IV)

Before applying the nonlinear minimization, two tasks must be completed:

- **Expanding the set of NL equations.** The set of $2n$ NL equations can be expanded by considering a total of $q = 15$ sample frequencies, evenly distributed within the vicinity of all the observable resonances. This increases the number of equations to $2nq = 90$, while the number of unknowns remains 3.

- **Constraining the vector of unknowns.** Suitable upper and lower limits for the unknown coefficients can be defined as follows:

According to the ideas exposed in Section 5.6, it is observed that a typical stiffness value among the n diagonal entries of the stiffness matrix of the system is around $k = 1.11e5 \, N/m$. As shown in Fig 5.9, an upper limit of β of $1.5e8 \, N/m^3$ combined with an observed response of $0.026m$, would account for even unrealistic levels of nonlinearity.

On the other hand, a plausible lower limit appears to be $1e5 \, N/m^3$, as this coefficient generates no discernible nonlinear effects. However, we must take into account the possibility that one or more DOFs within n are not genuine *NL-DOFs*, but rather the result of a wrong detection. We would expect, in this case, a null identified coefficient.

Considering the aforementioned arguments we will constrain the identified coefficients to lie within the range:

$$0 \le \beta \le 1.5e8 \, N/m^3 \tag{5.19}$$

After applying an iterative nonlinear minimization, the coefficients β for the *NL-DOFs* n are found. This results are shown in Table 5.1, exhibiting good accuracy.

DOF	True $\beta(x10^6)$	Identified $\beta(x10^6)$	error (%)
51Y	1.6	1.5204	4.96%
62Y	1.5	1.5178	1.19%
92Y	7.82	7.4360	4.91%

Table 5.1: Identified coefficients for the Sample Case #3

Figure 5.9: Force-displacement curves for different values of β

5.14   Sample Case #3: regeneration (stage V)

Figures 5.10 and 5.11 show the original linear and nonlinear responses (dashed and solid line, respectively) for the *NL-DOFs*. Superimposed in "■", the regenerated responses by the *optimized* EF (4.12) are shown. It can be seen that the quality of the regeneration is very good.
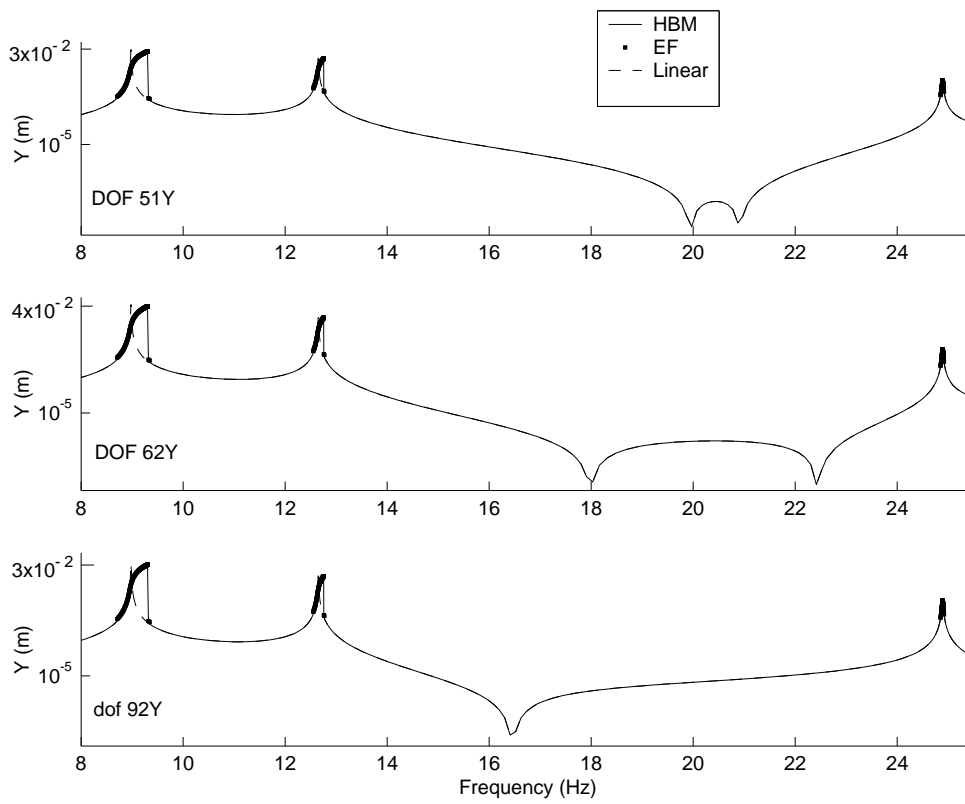
Figure 5.10: Regenerated response for the Sample Case #3. A Zoom-In of the individual resonances is shown in Fig. 5.11

Figure 5.11: Regenerated response for the Sample Case #3 (Zoom-In)

5.15 Concluding remarks

Initially developed as a theoretical method, the explicit formulation (EF) has been investigated in a *reverse* path, thus called the REF method, to asses its suitability as an identification technique. Being a *physical coordinates*-based method, the results from an identification analysis are always physically meaningful, in the form of stiffness, damping or mass coefficients. This is a major advantage over a modal technique.

The REF method was framed in a sequence of five major stages, thus providing a systematic methodology for tackling general systems. It was shown that the analysis of large systems can be reduced in size by using the measured responses as prescribed boundary conditions. Moreover, the set of NL equations to be solved can be reduced from N down to n (typically $n \ll N$), by a similar approach in which the *optimized* EF was developed, leading to the *optimized* REF.

A nonlinear minimization, required to calculate the coefficients of the nonlinear elements, can be properly constrained by the judicious use of a typical force-displacement diagram in the vicinity of the NL-DOFs. This feature greatly improves the convergence capabilities of the algorithm.

A virtual model of a large plate[1] was solved by the REF method. In spite of successful results, it was found that the computational effort is too high to gain acceptance in a practical modal analysis. Specifically, the precise localization of the n NL-DOFs conveys very expensive calculations, which can lead to noisy results. This problem is likely to be exacerbated when dealing with experimental data.

Some other highlights of this chapter are:

- A qualitative method was presented, allowing the detection of the nonlinear mechanism. The technique is based in the geometric "footprint" of the extracted NLV, able to discriminate between cubic stiffness and friction damping types.

- Some important issues can be suggested for future work, such as the detection of the nonlinear mechanism based on a statistical analysis of the

---

[1]Sample Case #3, described in Appendix B.

extracted NLV, rather than in a simple visual inspection. Also, it was mentioned that other nonlinear mechanisms could be tested to find their unique "footprint", building a library for on-line detection from measured signals.

- Finally, it should be pointed out that expanding the method to account for a multi-harmonic behaviour will be straightforward, as the required describing functions are already available for most nonlinearities. However, the practical advantages in doing so are not clear, as the current measuring techniques of higher harmonics are extremely difficult to implement.

Chapter 6

A hybrid modal technique (HMT) for the formulation of nonlinear FRFs of MDOF systems (a direct-path approach)

6.1 Introduction

It has been shown that *physical coordinates*-based methods can successfully predict the nonlinear behaviour of real structures. This approach provides a deep insight into the physics of the problem, due to the direct manipulation of mass, damping and stiffness coefficients.

However, such advantage is not so attractive if one considers the heavy computational burden incurred. This is largely due to the large amount of data included in the formulation, namely *all* of the parameters stored in the system's physical matrices. A modal approach would, theoretically, improve this condition by expressing the response as a function of eigenvalues and eigenvectors, thus greatly reducing the amount of input data.

Sadly, the development of a nonlinear *modal coordinates*-based method is a cumbersome task because of the amplitude-dependence of the modal parameters. This introduces significant ambiguity when applying main concepts such as the *modal superposition* theorem. Strictly speaking, linear theorems can not be employed in the analysis of nonlinear systems, but that should not stop us from

exploring analogous relations which can elucidate the behaviour of such systems.

In the last few decades, a growing amount of research has focused on nonlinear systems, and it is only natural that the idea of "normal modes" has been put to test in a nonlinear environment. The concept of nonlinear normal modes (or NNMs) was introduced in 1966 by Rosenberg et al (66) in relation to conservative lumped parameter systems, and formed the basis of works that followed.

An accepted definition of the NNMs of an undamped (discrete or continuous) system is (5) "a synchronous periodic oscillation where all material points of the system reach their extreme values or pass through zero simultaneously". Clearly, when a discrete system vibrates in a NNM, the corresponding oscillation is represented by a line in its configuration space, which is termed modal line. A modal line represents the synchronous oscillation of the system in the configuration space during a NNM motion. Linear systems possess straight modal lines since their coordinates are related linearly during a normal mode oscillation. In nonlinear systems, the modal lines can be either straight or curved. The latter cases are generic in nonlinear discrete systems, since straight nonlinear modal lines reflect symmetries of the system

The theory of NNMs has evolved considerably in the last two decades (67), (66), (24), (5), to the stage in which they are usually represented by invariant manifolds in the phase space (Fig. 6.1). One of the striking conclusions of the analysis of invariant manifolds is the fact that nonlinear systems can exhibit a *higher* number of modes than DOFs, a feature with no parallel in linear systems. Also, the NNM can exhibit bifurcations, instabilities or even chaotic behaviour for well-defined conditions.

Although the aforementioned arguments raise serious questions about the validity of stretching linear concepts to analyze nonlinear systems, the development of nonlinear techniques equivalent to the linear superposition is still of great interest. In cases where a stable and periodic response dominates the nonlinear behaviour, a nonlinear modal superposition would allow an order reduction by possibly achieving decoupled equations of motion. These lines of research have acquired much interest recently.

This chapter introduces a novel nonlinear modal technique which attempts to simulate a nonlinear superposition of NNMs, as suggested by Chong & Imregun
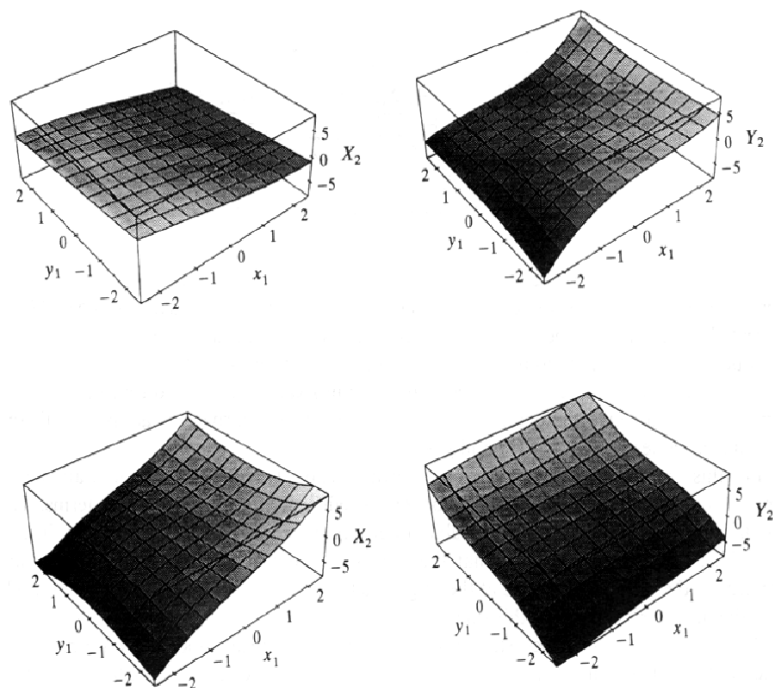
Figure 6.1: Examples of nonlinear invariant modal surfaces, as developed by S. W. Shaw & C. Pierre. x_1, y_1 are the physical displacement and velocity (respectively)of a given DOF. X_2, Y_2 are generalized (modal) displacements and velocities

(31), still recognizing the coupled nature of the nonlinear modal space. One of the limiting assumptions of the NNM theory is that the nonlinearities are confined to the resonant region, anywhere else being replaced by a linear fashion. The validity of this assumption will be explored in the light of newly developed expressions relating the NNM with the physical responses.

The traditional nonlinear modal expansion (based on nonlinear eigenvectors and eigenvalues) will be put to test against a newly introduced "hybrid" expansion. The term "hybrid" arises from the fact that the underlying linear system is reduced and expressed by its *modal* parameters (linear eigenvectors and eigenvalues), while the nonlinearities are still formulated in the *physical* domain.

It is believed that the new technique performs better in an experimental environment, because the extracted nonlinearities are concentrated in a single, thus

stronger, nonlinear modal term. The extracted nonlinear term has a very explicit *physical* meaning, being analytically related to the nonlinear coefficients of the system.

The approach developed here considers the nonlinearities as part of the external excitation while the system itself remains linear. Although the method recognizes the existence of nonlinear eigenvectors and eigenvalues, the physical responses are determined without explicitly calculating these modal quantities.

This chapter presents a theoretical discussion of the "hybrid modal technique" (HMT) method, introducing its main concepts from a direct-path point of view. Although the method has no restriction, other than the computational cost, regarding the size of the system, small systems are better suited to illustrate concepts, and they will be used for this end.

The HMT can also be implemented in a reverse path, serving this time as an identification tool. However, the additional complexities arising from this analysis are heavily subjected to the degree of data incompleteness, thus the surrounding issues are more related to the realm of large systems. The identification of large systems through the HMT will be tackled in later chapters.

The introduced methodology is summarized in the flow chart of Fig. 6.2.

6.2 Traditional linear and nonlinear modal analysis

In this section, we will briefly summarize the procedure which is known as "linear modal analysis" (LMA), also explaining how, for good or bad, these concepts are stretched to handle nonlinear systems. Although the technique is more often associated with an experimental environment in which a mathematical model must be fitted to raw measured data (a reverse path), the method is also useful as a theoretical tool (direct path).

The latter approach allows the calculation of the physical response of a system by means of a root-finding procedure, as well as determining some important modal parameters (natural frequencies and damping ratios). The theoretical linear background presented here is no more than the essential information needed

Figure 6.2: Flow diagram of the HMT method (direct-path approach)

to start a nonlinear analysis; the reader is referred to a wealth of excellent material in the field -such as (4) and (59)- for a deeper insight.

The general representation of a linear system with hysteretic proportional damping and subjected to a harmonic excitation is given by the ordinary differential equation:

$$[\mathbf{M}]\{\ddot{y}\} + [\mathbf{K}]\{y\} + \mathbf{i}[\mathbf{D}]\{y\} = \{F\}e^{\mathbf{i}\omega t} \tag{6.1}$$

where $[\mathbf{M}], [\mathbf{K}]$ and $[\mathbf{D}]$ are the mass, stiffness and hysteretic damping matrices, respectively, $\{y\}, \{\dot{y}\}, \{\ddot{y}\}$ are the vectors of displacements, velocities and accelerations, and $\{F\}$ is the harmonic excitation vector operating at frequency ω. Assuming a harmonic response $\{y\} = \{Y\}e^{\mathbf{i}\omega t}$, where $\{Y\} = \{|Y|e^{\mathbf{i}\theta}\}$ is a complex magnitude allowing it to accommodate phase, the problem is transformed to the frequency domain:

$$\left(-\omega^2 \mathbf{M} + \mathbf{K} + \mathbf{i}\mathbf{D}\right)\{Y\} = \{F\} \tag{6.2}$$

The eigensolution of the homogeneous part of (6.2) brings out the diagonal matrix of eigenvalues $\lceil \lambda^2 \rfloor$ (where the brackets "$\lceil \ \rfloor$" denotes a diagonal matrix) and the mass-normalized matrix of eigenvectors $[\boldsymbol{\Phi}]$. Both matrices are related by the so-called orthogonal properties, which are stated as:

$$\begin{aligned} [\boldsymbol{\Phi}]^{\mathbf{T}}[\mathbf{M}][\boldsymbol{\Phi}] &= [\mathbf{I}] \\ [\boldsymbol{\Phi}]^{\mathbf{T}}[\mathbf{K} + \mathbf{i}\mathbf{D}][\boldsymbol{\Phi}] &= \lceil \lambda^2 \rfloor \end{aligned} \tag{6.3}$$

where $[\mathbf{I}]$ is the Identity matrix. Relations 6.3 are the key to transform a linear MDOF system into several SDOF components, each one of them exclusively accounting for the behaviour of a single mode. This property is closely related to another important property of linear systems, the *modal superposition*, by which the physical responses $\{Y\}$ are expressed as a linear combination of its modal responses $\{P\}$:

$$\{Y\} = [\boldsymbol{\Phi}]\{P\} \tag{6.4}$$

where $\{P\}$ is an orthogonal vector. Fig. 6.3 shows an FRF comprised of 3 modes (solid line, labelled "FRF") and the corresponding modal responses (labelled "P1", "P2" and "P3") for each individual mode. At resonance, the physical
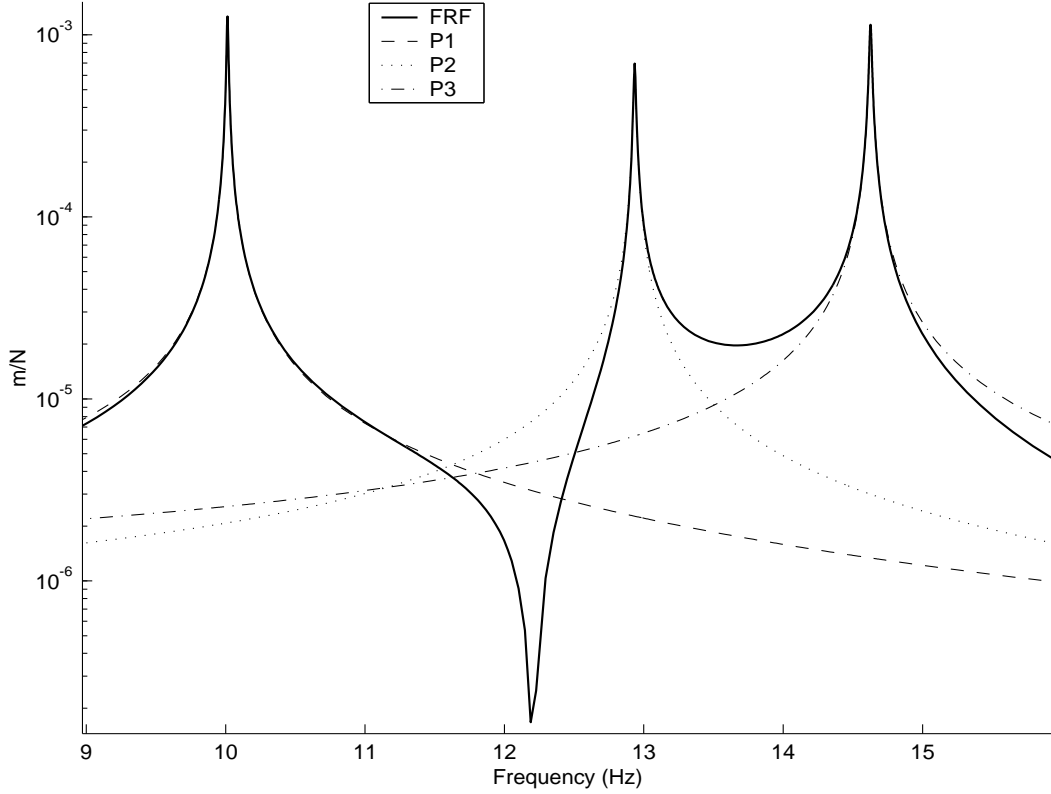
Figure 6.3: Modal responses of a linear FRF

response is dominated by a single modal response, while the contribution of the other two is very small[1]. According to the principle of *modal superposition*, the algebraic summation of the three modal responses results in the physical FRF.

Substituting (6.4) into (6.2), and pre-multiplying by $[\mathbf{\Phi}]^{\mathbf{T}}$, we have:

$$[\mathbf{\Phi}]^{\mathbf{T}} \left(-\omega^2 \mathbf{M} + \mathbf{K} + \mathbf{iD} \right) [\mathbf{\Phi}]\{P\} = [\mathbf{\Phi}]^{\mathbf{T}} \{F\} \tag{6.5}$$

and further introducing the orthogonal relationships (6.3), we arrive at:

$$\lceil \lambda^2 - \omega^2 \rfloor \{P\} = \{\mathbf{\Phi^T} F\} \tag{6.6}$$

where $\lceil \lambda^2 - \omega^2 \rfloor$ is a diagonal matrix containing the natural frequencies and the damping ratios for each mode, $\{P\}$ is the vector of modal responses and $\{\mathbf{\Phi^T} F\}$

---

[1]This statement is true only for well separated modes like these. This simple example is used to illustrate some basic concepts.

can be seen as a vector of modal forces for the equivalent SDOF systems. As $\lceil \lambda^2 - \omega^2 \rfloor$ is a diagonal matrix, the uncoupled nature of the linear modal space is guaranteed as a direct consequence of the orthogonal relations (6.3).

The response of the linear system $\{Y\}$ can be easily drawn from (6.6), pre-multiplying both sides by $[\mathbf{\Phi}]\lceil \lambda^2 - \omega^2 \rfloor^{-1}$,

$$\{Y\} = [\mathbf{\Phi}]\lceil \lambda^2 - \omega^2 \rfloor^{-1}\{\mathbf{\Phi^T} F\} \tag{6.7}$$

The i_{th} component of (6.7) can also be expressed as a summation of individual terms, as shown:

$$Y_i = \sum_{r=1}^{M} \frac{\phi_{ir}\Im_r}{\lambda_r^2 - \omega^2} \tag{6.8}$$

where M is the total number of modes of the system and $\Im_r = \left(\mathbf{\Phi^T} F\right)_r$ is the modal excitation force corresponding to the r_{th} mode. For the classical definition of the frequency response function (FRF) in which only a single node j is being excited at a time, we have:

$$\frac{Y_i}{F_j} = H_{ij} = \sum_{r=1}^{M} \frac{\phi_{ir}\phi_{jr}}{\lambda_r^2 - \omega^2} \tag{6.9}$$

where H_{ij} is the FRF of node i when the system is being excited at node j. The principle of reciprocity of linear systems guarantees that $H_{ij} = H_{ji}$, thus generating a symmetric FRF matrix. Observing (6.9), it can be recognized that the MDOF system of (6.1) has been transformed to M SDOF systems, where the response of the r_{th} component is given by

$$\frac{\phi_{ir}\phi_{jr}}{\lambda_r^2 - \omega^2} \tag{6.10}$$

(6.10) is the very same expression representing each one of the SDOF curves already shown in Fig. 6.3.

6.2.1 Linear modal analysis (LMA) extended for nonlinear systems

The existing tools for performing a LMA are so powerful and of widespread use, that one is always tempted to use them for analyzing nonlinear systems. At the

very least, an unsuccessful attempt may indicate the presence (and maybe the type) of a nonlinear mechanism, which is not a bad start in itself.

The main problem of using a LMA approach for modeling nonlinear systems is the fact that the modal parameters contained in the linear formulation of the FRF (6.9) are constant coefficients, as opposed to the nonlinear case, where these are amplitude-dependent. Nevertheless, the departure point for expanding the concepts of LMA to account for nonlinear systems is a nonlinear version of (6.9):

$$\tilde{H}_{ij}(\omega, \tilde{Y}) = \sum_{r=1}^{M} \frac{\tilde{\phi}_{ir}(\omega, \tilde{Y})\tilde{\phi}_{jr}(\omega, \tilde{Y})}{\tilde{\lambda}_r^2(\omega, \tilde{Y}) - \omega^2} \tag{6.11}$$

where the amplitude-dependency of the modal parameters has been acknowledged by expressing them as functions of the frequency and/or amplitude. For simplicity, the " ˜ " symbol will be used to denote a nonlinear variable, obviating such dependency.

As a consequence of the nonlinearities, the FRF matrix is no longer invariant to changes in the excitation vector; the characteristic known as "reciprocity" is lost ($\tilde{H}_{ij} \neq \tilde{H}_{ji}$), modal superposition does not hold anymore and, in general, every parameter that used to be a constant *property* of the system is now a variable. The easiest way to spot nonlinearities in an FRF plot is to look for distortions at the resonances, where the amplitude-dependency of the modal parameters generates noticeable deviations from the linear shape.

By an analogous procedure in which (6.11) was defined, the nonlinear version of (6.4) can also be written for any particular state $[\omega, \tilde{Y}]$ resulting in:

$$\{\tilde{Y}(\omega, \tilde{Y})\} = [\tilde{\boldsymbol{\Phi}}(\omega, \tilde{Y})]\{\tilde{P}(\omega, \tilde{Y})\} \tag{6.12}$$

as well as the nonlinear version of (6.6), drawn by replacing the constant modal coefficients with amplitude-dependent parameters:

$$\lceil \tilde{\lambda}^{\mathbf{2}}(\omega, \tilde{Y}) - \omega^{\mathbf{2}} \rfloor \{\tilde{P}(\omega, \tilde{Y})\} = \{\tilde{\boldsymbol{\Phi}}^{\mathbf{T}}(\omega, \tilde{Y})F\} \tag{6.13}$$

Equations 6.12 and 6.13 represent the modal space of a nonlinear system, characterized by being coupled. Although this is not immediately obvious in (6.13) due to the still diagonal matrix $\lceil \tilde{\lambda}^{\mathbf{2}}(\omega, \tilde{Y}) - \omega^{\mathbf{2}} \rfloor$, the amplitude-dependency

of the nonlinear modal coefficients dissolves the appealing *modal superposition* property found in the linear modal space.

Fig. 6.4 shows a nonlinear FRF comprised of 3 modes and exhibiting strong nonlinearities at modes 1 and 2 (solid line). Also shown (in dashed lines) are the correspondent nonlinear modal responses. Unlike the linear ones -which exhibit a single peak at the correspondent resonance- these contain peaks at every resonance, these being more pronounced where the nonlinearities are stronger. Thus, it cannot longer be safely assumed that the response at resonance is dominated by a single modal response, nor that away from resonance the nonlinear mode behaves linearly.
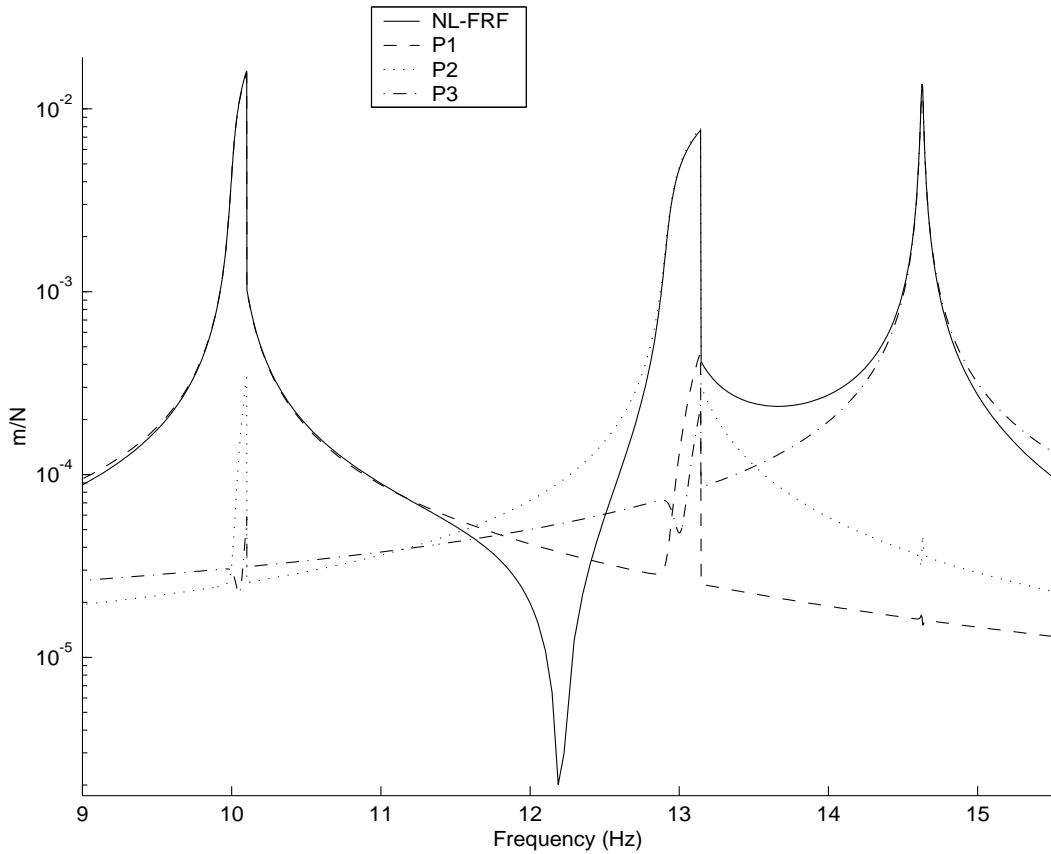
Figure 6.4: Modal responses of a nonlinear FRF

6.3 The nonlinear modal space

A general nonlinear dynamic system with proportional hysteretic damping can be mathematically defined by the nonlinear ordinary differential equation,

$$[\mathbf{M}]\{\ddot{y}\} + [\mathbf{K}]\{y\} + \mathbf{i}[\mathbf{D}]\{y\} + \{\tilde{G}(\dot{y}, y)\} = \{F\}e^{\mathbf{i}\omega t} \qquad (6.14)$$

where $\{\tilde{G}(\dot{y}, y)\}$ is the nonlinear vector (NLV) already introduced in Chapter 3, containing all the nonlinearities in the system.

Assuming an oscillatory, periodic and essentially harmonic response, the problem is transformed to the frequency domain:

$$\left(-\omega^2\mathbf{M} + \mathbf{K} + \mathbf{i}\mathbf{D}\right)\left\{\tilde{Y}\right\} + \{\tilde{G}(\omega, \tilde{Y})\} = \{F\} \qquad (6.15)$$

Pre-multiplying this equation by the transpose of the *linear* matrix of eigenvectors $[\mathbf{\Phi}]^{\mathbf{T}}$, we have:

$$[\mathbf{\Phi}]^{\mathbf{T}}\left(-\omega^2\mathbf{M} + \mathbf{K} + \mathbf{i}\mathbf{D}\right)\left\{\tilde{Y}\right\} + \{\mathbf{\Phi}^{\mathbf{T}}\tilde{G}(\omega, \tilde{Y})\} = \{\mathbf{\Phi}^{\mathbf{T}}F\} \qquad (6.16)$$

As argued before, at any particular state $[\omega, \tilde{Y}]$ the system's physical response can be expanded in, or transformed to, its nonlinear modal responses $\{\tilde{P}\}$,

$$\{\tilde{Y}(\omega, \tilde{Y})\} = [\tilde{\mathbf{\Phi}}(\omega, \tilde{Y})]\{\tilde{P}(\omega, \tilde{Y})\} \qquad (6.17)$$

where $[\tilde{\mathbf{\Phi}}]$ is the nonlinear matrix of eigenvectors, which is dependent on both amplitude and frequency. This matrix can be decomposed[1] into a linear component $[\mathbf{\Phi}]$ -the linear "mass normalized" eigenvector matrix- and a varying nonlinear component $[\mathbf{\Delta}\tilde{\mathbf{\Phi}}(\omega, \tilde{Y})]$:

$$\{\tilde{Y}\} = \left[\mathbf{\Phi} + \mathbf{\Delta}\tilde{\mathbf{\Phi}}\right]\{\tilde{P}\} \qquad (6.18)$$

where the $[\omega, \tilde{Y}]$ dependence has been obviated by the use of the " ~ " symbol. Inserting (6.18) into (6.16):

$$[\mathbf{\Phi}]^{\mathbf{T}}\left(-\omega^2\mathbf{M} + \mathbf{K} + \mathbf{i}\mathbf{D}\right) \cdot [\mathbf{\Phi} + \mathbf{\Delta}\tilde{\mathbf{\Phi}}]\{\tilde{P}\} + \{\mathbf{\Phi}^{\mathbf{T}}\tilde{G}\} = \{\mathbf{\Phi}^{\mathbf{T}}F\}$$

---

[1]This decomposition is a central development of the HMT method, also essential in forthcoming chapters.

and further developing the algebra:

$$[\mathbf{\Phi}]^{\mathbf{T}} \left(-\omega^2 \mathbf{M} + \mathbf{K} + \mathbf{iD}\right) \cdot [\mathbf{\Phi}]\{\tilde{P}\}+$$
$$[\mathbf{\Phi}]^{\mathbf{T}} \left(-\omega^2 \mathbf{M} + \mathbf{K} + \mathbf{iD}\right) \cdot [\mathbf{\Delta \tilde{\Phi}}]\{\tilde{P}\}+$$
$$\{\mathbf{\Phi^T} \tilde{G}\} = \{\mathbf{\Phi^T} F\} \quad (6.19)$$

$$[\mathbf{\Phi}]^{\mathbf{T}} \left(-\omega^2 \mathbf{M} + \mathbf{K} + \mathbf{iD}\right) \cdot [\mathbf{\Phi}]\{\tilde{P}\}+$$
$$[\mathbf{\Phi}]^{\mathbf{T}} \left(-\omega^2 \mathbf{M} + \mathbf{K} + \mathbf{iD}\right) \cdot \underbrace{\left(\mathbf{\Phi \Phi^{-1}}\right)}_{\substack{\text{Introduced} \\ \text{term} = [\mathbf{I}]}} \cdot [\mathbf{\Delta \tilde{\Phi}}]\{\tilde{P}\}+$$
$$\{\mathbf{\Phi^T} \tilde{G}\} = \{\mathbf{\Phi^T} F\} \quad (6.20)$$

$$[\mathbf{\Phi}]^{\mathbf{T}} \left(-\omega^2 \mathbf{M} + \mathbf{K} + \mathbf{iD}\right) [\mathbf{\Phi}] \cdot \left(\mathbf{I} + \mathbf{\Phi^{-1} \Delta \tilde{\Phi}}\right)\{\tilde{P}\} + \{\mathbf{\Phi^T} \tilde{G}\} = \{\mathbf{\Phi^T} F\} \quad (6.21)$$

The linear term $[\mathbf{\Phi}]^{T} \left(-\omega^2 \mathbf{M} + \mathbf{K} + \mathbf{iD}\right) [\mathbf{\Phi}]$ can be reduced by the orthogonal properties (6.3). Introducing (6.3) into (6.21), we finally obtain:

$$\boxed{\lceil \mathbf{\lambda^2} - \mathbf{\omega^2} \rfloor \left(\mathbf{I} + \mathbf{\Phi^{-1} \Delta \tilde{\Phi}}\right)\{\tilde{P}\} + \{\mathbf{\Phi^T} \tilde{G}\} = \{\mathbf{\Phi^T} F\}} \quad (6.22)$$

which is the mathematical representation of an MDOF nonlinear system in the modal space. Observe that there are no approximations in obtaining this expression[1].

(6.22) represents the modal equivalent of the so-called *normal nonlinear modes* (NNMs), which has been the subject of much research and re-definitions over the last decades. The NNMs are usually considered as orthogonal -that is, independent from each other- where the mode is affected by the nonlinearities at resonance only, otherwise behaving linearly. In other words, a modal superposition is invoked to partition an MDOF nonlinear system into several SDOF components, each one of them exclusively accounting for a single nonlinear mode.

By comparing (6.22) to its linear counterpart, given by (6.6), we find that the nonlinear formulation contains all of the linear terms plus two new nonlinear

---

[1]The variation in the eigenvectors, often neglected, have been considered. The first-order assumption does not invalidate this equation, provided that $\{\tilde{G}\}$ is a multi-harmonic descriptor.

terms, $(\boldsymbol{\Phi}^{-1}\boldsymbol{\Delta}\tilde{\boldsymbol{\Phi}})$ and $\{\boldsymbol{\Phi}^{\mathbf{T}}\tilde{G}\}$. These must be the ones responsible for the non-linear modal behaviour, directly related to the assumption of orthogonality made by the NNMs theory. The question is, in the light of (6.22), just how valid this assumption is?

To better answer this question, let us analyze each of the nonlinear terms separately:

1. It is clear from (6.22) that the r_{th} modal coordinate $(\tilde{P}_r)$ contains components belonging to all other modes, caused by the nonlinear term $(\boldsymbol{\Phi}^{-1}\boldsymbol{\Delta}\tilde{\boldsymbol{\Phi}})$. This term seems to be directly responsible for modal coupling effects by introducing non-diagonal entries in the eigenvalue matrix. This further invalidates the assumption of *modal superposition* stating that modes are independent from each other (or orthogonal). However, before rushing to conclusions, we should first find out how significant this term is, and how it behaves at resonant condition.

   It has been observed -both in this research and in published articles- that the nonlinear variation of the eigenvectors $[\boldsymbol{\Delta}\tilde{\boldsymbol{\Phi}}]$ usually falls within the range of 1-20%, thus being fairly small. In the vicinity of the resonant mode r_{th}, $(\boldsymbol{\Phi}^{-1}\boldsymbol{\Delta}\tilde{\boldsymbol{\Phi}})$ becomes negligible compared to the magnitude of the modal coordinate $\tilde{P}_r$, severely attenuating its influence. Away from resonance, however, $\tilde{P}_r$ decays to small values (sometimes being neglected!) and the influence of $(\boldsymbol{\Phi}^{-1}\boldsymbol{\Delta}\tilde{\boldsymbol{\Phi}})$ becomes dominant.

   The last statement directly relates this nonlinear term to the coupled nature of the nonlinear modal space, in which a modal coordinate exhibits distortions at every other resonance. For this reason, $(\boldsymbol{\Phi}^{-1}\boldsymbol{\Delta}\tilde{\boldsymbol{\Phi}})$ will be referred to as the "nonlinear coupling term". The strength of the coupling effect will depend on specific characteristics of the system under analysis.

2. $\{\boldsymbol{\Phi}^{\mathbf{T}}\tilde{G}\}$ is the other nonlinear term appearing in (6.22). It is, as it will be soon demonstrated, the main source of nonlinearities in the resonant modal amplitude. Indeed, it is such the importance of this nonlinear function that an entire section will be devoted to it.

Because of its main role as generator of nonlinearities in the resonant mode, and because it contains the already introduced nonlinear vector (NLV) $\{\tilde{G}\}$, this term will be referred to as the "nonlinear modal vector" (NLMV).

6.4 The nonlinear modal vector (NLMV)

Recalling (3.28), the NLMV $\{\mathbf{\Phi^T}\tilde{G}\}$ can be expanded as:

$$\{\mathbf{\Phi^T}\tilde{G}\} = \left\{ \begin{array}{c} \phi_{11}\tilde{g}v_1 + \phi_{21}\tilde{g}v_2 + \cdots + \phi_{\mathrm{N}1}\tilde{g}v_N \\ \vdots \\ \phi_{1\mathrm{r}}\tilde{g}v_1 + \phi_{2\mathrm{r}}\tilde{g}v_2 + \cdots + \phi_{\mathrm{Nr}}\tilde{g}v_N \\ \vdots \\ \phi_{1\mathrm{M}}\tilde{g}v_1 + \phi_{2\mathrm{M}}\tilde{g}v_2 + \cdots + \phi_{\mathrm{NM}}\tilde{g}v_N \end{array} \right\}_M \tag{6.23}$$

where $\tilde{g}v_i$ represents the combined effect of all the nonlinear elements associated with the i_{th} DOF. The r_{th} row of (6.23) represents the nonlinearity acting at the r_{th} modal coordinate $\tilde{P}_r$, given by:

$$\left(\mathbf{\Phi}^T\tilde{G}\right)_r = (\phi_{1\mathrm{r}}\tilde{g}v_1 + \phi_{2\mathrm{r}}\tilde{g}v_2 + \cdots + \phi_{\mathrm{Nr}}\tilde{g}v_N) \tag{6.24}$$

(6.24) shows that the r_{th} component of the NLMV, $\left(\mathbf{\Phi}^T\tilde{G}\right)_r$, contains every single restoring force in the system (embedded in the functions $\tilde{g}v_1, \tilde{g}v_2, \cdots, \tilde{g}v_N$). This clearly explains why any NL element, in any position within the system, is certain to have a global influence, affecting all the resonances. However, the extent at which a given NL element $\tilde{g}_{ii}$ (contained in the function $\tilde{g}v_i$) influences mode r_{th}, also depends on the "weight" factor ϕ_{ir}. This is also true for "non-grounded" elements $\tilde{g}_{ij}$, but things get less clear here because its behaviour is influenced by more than one eigenvector at a time -more on this later.

(6.24) also explains another well-known odd fact: higher modes are expected to behave linearly, due to the occurrence of small amplitudes. However, occasionally a higher mode will also exhibit strong nonlinear effects. This behaviour can be explained by the presence of a "non-grounded" NL element acting between two DOFs i, j with eigenvectors of equal magnitude but opposite sign[1]. This

---

[1]This feature is often found in symmetric structures.

could create an additive effect and induce a noticeable nonlinear behaviour, as exemplified in (6.25):

$$\phi_{ir}\tilde{g}_{ij} + \phi_{jr}\tilde{g}_{ji} \;=\; \phi_{ir}\tilde{g}_{ij} + (-\phi_{ir})(-\tilde{g}_{ij}) \;=\; 2\phi_{ir}\tilde{g}_{ij} \tag{6.25}$$

where it can be seen that such a feature doubles the nonlinear restoring force of a similar grounded nonlinearity.

Finally, (6.24) proves that the NLMV will exhibit significant peaks whenever the functions $\tilde{g}v_1, \tilde{g}v_2, \cdots, \tilde{g}v_N$ (which are amplitude-dependent) are significant. This will invariably occur at every resonance, being more noticeable if the mode under analysis has eigenvectors of considerable magnitude.

Fig. 6.5a shows a nonlinear FRF comprising 3 modes and exhibiting strong nonlinearities in the first and second modes, while Fig. 6.5b displays the 3 functions of the NLMV for the same system. It is clear that the NLMV contains significant activity at every resonance, rather than only at their own modal coordinate. Moreover, the third component of the NLMV exhibits even stronger peaks at other resonances. Such a finding represents evidence regarding the coupling effects of the nonlinearities.

Although the NLMV has been defined in this section as $\{\mathbf{\Phi^T}\tilde{G}\}$, in later sections it will emerge with a slightly different form, also containing the external linear forces acting in the system; the extended definition of the NLMV containing external forces is:

$$\boxed{\{\tilde{\chi}\} = \{\mathbf{\Phi}^T F\} - \{\mathbf{\Phi}^T \tilde{G}\}} \tag{6.26}$$

where the first term in the RHS of (6.26) represents the external linear modal forces. We will call $\{\tilde{\chi}\}$ the *extended* NLMV.

6.5   The hybrid modal technique (HMT)

One of the drawbacks of expressing a NL system in the modal space is the fact that the formulation of the nonlinear elements in the NLV $\{\tilde{G}\}$ is based in the *physical* -instead of *modal*- coordinates of the system, the very unknowns we are looking for. A fully modal approach would have to express the nonlinear restoring forces in $\{\tilde{G}\}$ as functions of the modal responses $\{\tilde{P}\}$, as in[1] (32), (33), (3) and

---

[1]The cited works considered systems with 1 or 2 DOFs.
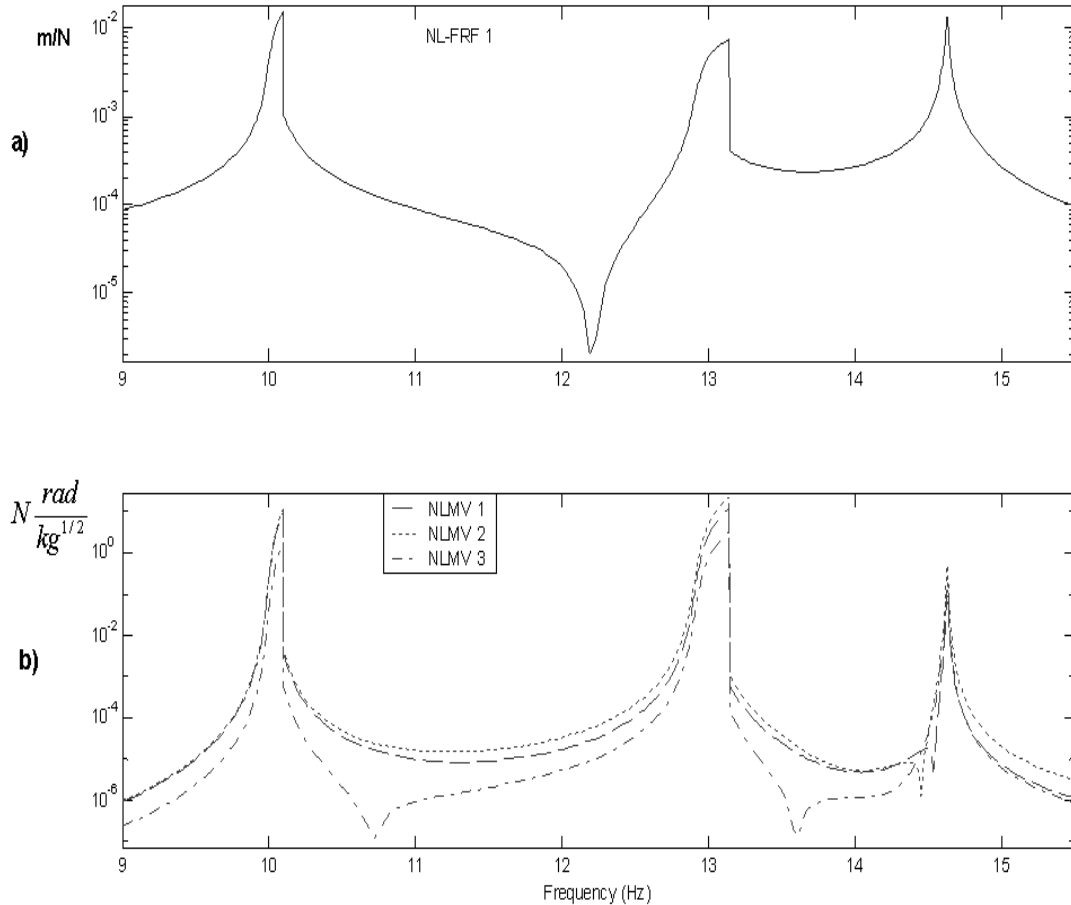
Figure 6.5: NLMV of a 3-DOF system

(43). Considering that the modal space is coupled, the mathematics involved (already complicated) start looking prohibitive for general MDOF systems.

A further drawback of a nonlinear modal analysis formulation when used as an identification tool is the fact that the physical location of the nonlinearities cannot be identified, since this information is not explicitly contained in a typical modal formulation.

As significant as these disadvantages may appear, modal analysis is still an invaluable tool for reducing a linear system to a manageable size. This section introduces a "hybrid" modal technique (HMT) that uses a standard modal anal-

ysis to express the behaviour of the underlying linear system, while keeping the formulation of the nonlinearities in the physical domain, thus the name "hybrid".

The starting point of the analysis is Equation (6.22), which describes the nonlinear modal space:

$$\lceil \lambda^2 - \omega^2 \rfloor \left(\mathbf{I} + \boldsymbol{\Phi}^{-1} \boldsymbol{\Delta} \tilde{\boldsymbol{\Phi}} \right) \{\tilde{P}\} + \{\boldsymbol{\Phi}^{\mathbf{T}} \tilde{G}\} = \{\boldsymbol{\Phi}^{\mathbf{T}} F\}$$

Pre-multiplying by $[\boldsymbol{\Phi}] \lceil \lambda^2 - \omega^2 \rfloor^{-1}$ and extending the algebra further:

$$[\boldsymbol{\Phi}] \left(\mathbf{I} + \boldsymbol{\Phi}^{-1} \boldsymbol{\Delta} \tilde{\boldsymbol{\Phi}} \right) \{\tilde{P}\} = [\boldsymbol{\Phi}] \lceil \lambda^2 - \omega^2 \rfloor^{-1} \left(\{\boldsymbol{\Phi}^{\mathbf{T}} F\} - \{\boldsymbol{\Phi}^{\mathbf{T}} \tilde{G}\} \right)$$

$$\underbrace{\left(\boldsymbol{\Phi} + \boldsymbol{\Delta} \tilde{\boldsymbol{\Phi}} \right)}_{[\tilde{\boldsymbol{\Phi}}]} \{\tilde{P}\} = [\boldsymbol{\Phi}] \lceil \lambda^2 - \omega^2 \rfloor^{-1} \left(\{\boldsymbol{\Phi}^{\mathbf{T}} F\} - \{\boldsymbol{\Phi}^{\mathbf{T}} \tilde{G}\} \right)$$

$$[\tilde{\boldsymbol{\Phi}}] \{\tilde{P}\} = [\boldsymbol{\Phi}] \lceil \lambda^2 - \omega^2 \rfloor^{-1} \left(\{\boldsymbol{\Phi}^{\mathbf{T}} F\} - \{\boldsymbol{\Phi}^{\mathbf{T}} \tilde{G}\} \right)$$

$$\{\tilde{Y}\} = [\boldsymbol{\Phi}] \lceil \lambda^2 - \omega^2 \rfloor^{-1} \left(\{\boldsymbol{\Phi}^{\mathbf{T}} F\} - \{\boldsymbol{\Phi}^{\mathbf{T}} \tilde{G}\} \right)$$

Recalling (6.26), we finally arrive to an equation expressing the nonlinear physical responses:

$$\boxed{\{\tilde{Y}\} = [\boldsymbol{\Phi}] \lceil \lambda^2 - \omega^2 \rfloor^{-1} \{\tilde{\chi}\}} \tag{6.27}$$

Note that, in (6.27), the *only* nonlinear variable is the *extended* NLMV $\{\tilde{\chi}\}$, while the rest are purely linear parameters. This remarkable feature achieves a long-sought issue of most nonlinear modal methods: the neat separation of the system into linear and nonlinear components.

The i_{th} component of (6.27) can be also expressed as a modal expansion in the *linear* modal space:

$$\boxed{\tilde{Y}_i = \sum_{r=1}^{M} \frac{\phi_{ir} \tilde{\chi}_r}{\lambda_r^2 - \omega^2}} \tag{6.28}$$

The similarities between (6.28) and its linear version, (6.8), are enlightening as well as appealing. Indeed, the original problem of a NL system being excited by a constant force has been transformed to one in which the underlying linear system is being excited by a nonlinear force. Although this may misrepresent the physics of the problem, the series expressed in (6.28) is much more effective[1]

---

[1]In the author's opinion.

for analyzing NL systems in an experimental environment than the traditional nonlinear series, already introduced in (6.11) and rewritten here:

$$\tilde{H}_{ij}(\omega, \tilde{Y}) = \sum_{r=1}^{M} \frac{\tilde{\phi}_{ir}(\omega, \tilde{Y})\tilde{\phi}_{jr}(\omega, \tilde{Y})}{\tilde{\lambda}_r^2(\omega, \tilde{Y}) - \omega^2}$$

This is due to the very small individual variations happening both in the eigenvectors and eigenvalues which nevertheless causes significant effects when combined. These small variations are much more difficult to extract individually than identifying a single, combined and strong nonlinear component $\{\tilde{\chi}\}$.

Considering the N physical responses of an MDOF system, (6.27) can be expressed in matrix form, as following:

$$\left\{ \begin{array}{c} \tilde{Y}_1 \\ \tilde{Y}_2 \\ \vdots \\ \tilde{Y}_N \end{array} \right\}_N = \left[\begin{array}{cccc} \frac{\phi_{11}}{\lambda_1^2 - \omega^2} & \frac{\phi_{12}}{\lambda_2^2 - \omega^2} & \cdots & \frac{\phi_{1M}}{\lambda_M^2 - \omega^2} \\ \frac{\phi_{21}}{\lambda_1^2 - \omega^2} & \frac{\phi_{22}}{\lambda_2^2 - \omega^2} & \cdots & \frac{\phi_{2M}}{\lambda_M^2 - \omega^2} \\ \vdots & \vdots & \ddots & \vdots \\ \frac{\phi_{N1}}{\lambda_1^2 - \omega^2} & \frac{\phi_{N2}}{\lambda_2^2 - \omega^2} & \cdots & \frac{\phi_{NM}}{\lambda_M^2 - \omega^2} \end{array} \right]_{N,M} \left\{ \begin{array}{c} \tilde{\chi}_1 \\ \tilde{\chi}_2 \\ \vdots \\ \tilde{\chi}_M \end{array} \right\}_M \qquad (6.29)$$

(6.29) represents a nonlinear system of equations which can be solved by a Newton-Raphson scheme to find the nonlinear responses $\{\tilde{Y}\}$. Observe that the coefficients contained in the matrix to be inverted (or manipulated) are all linear, therefore not prone to ill-conditioning.

The system (6.29) can be dramatically reduced to a minimum size if only the n *NL-DOFs* are included in the analysis ($n \ll N$). This is possible because $\{\tilde{\chi}\}$ depends exclusively on variables associated with the n *NL-DOFs*:

$$\{\tilde{\chi}\} = \{\tilde{\chi}(\tilde{\nu}_{n,n}, \tilde{Y}_n)\} \qquad (6.30)$$

The modal nature of (6.29) also means that a modal truncation is possible. This is achieved by focusing the analysis in the vicinity of a few selected m resonances ($m \ll M$), equivalent to selecting a few columns in (6.29). Care should be taken about including all modes with significant nonlinearities, as well as those behaving linearly but likely to introduce strong residual effects within the measured frequency range.

Although a modal truncation allows the analyst to neglect non-essential data (weak modes), it is, strictly speaking, an unsafe procedure. As already shown in Fig. 6.5, even weakly nonlinear modes can introduce significant nonlinear effects in nearby modes. This issue can be overcome by extending the frequency range well above the last observed nonlinear mode.

After both a spatial and modal reduction, (6.29) is transformed to:

$$
\left\{
\begin{array}{c}
\tilde{Y}_1 \\
\tilde{Y}_2 \\
\vdots \\
\tilde{Y}_n
\end{array}
\right\}_n
= [\mathbf{\Phi}]_{n,m} \cdot \lceil \lambda^2 - \omega^2 \rceil^{-1}_{m,m} \cdot
\left\{
\begin{array}{c}
\tilde{\chi}_1 \left(\tilde{\nu}_{n,n}, \tilde{Y}_n \right) \\
\tilde{\chi}_2 \left(\tilde{\nu}_{n,n}, \tilde{Y}_n \right) \\
\vdots \\
\tilde{\chi}_m \left(\tilde{\nu}_{n,n}, \tilde{Y}_n \right)
\end{array}
\right\}_m
\tag{6.31}
$$

which represents a set of n NL equations with n unknowns, $\{\tilde{Y}_n\}$, contained in $\{\tilde{\chi}_m\}$. This can be solved through a Newton-Raphson algorithm, similar to the already introduced in Section 4.4.

After the n nonlinear responses have been obtained, (6.29) is transformed into a *linear* set of equations, this time including only those terms associated with *Linear-DOFs* (DOFs free of NL elements):

$$
\left\{
\begin{array}{c}
\tilde{Y}_1 \\
\tilde{Y}_2 \\
\vdots \\
\tilde{Y}_{N-n}
\end{array}
\right\}_{N-n}
= [\mathbf{\Phi}]_{(N-n),m} \cdot \lceil \lambda^2 - \omega^2 \rceil^{-1}_{m,m} \cdot
\left\{
\begin{array}{c}
\tilde{\chi}_1 \left(\tilde{\nu}_{n,n}, \tilde{Y}_n \right) \\
\tilde{\chi}_2 \left(\tilde{\nu}_{n,n}, \tilde{Y}_n \right) \\
\vdots \\
\tilde{\chi}_m \left(\tilde{\nu}_{n,n}, \tilde{Y}_n \right)
\end{array}
\right\}_m
\tag{6.32}
$$

where $\{\tilde{\chi}_m\}$ is now a known vector.

6.6 Nonlinear minimization scheme

The nonlinear minimization presented here is based in the Newton-Raphson scheme already introduced in Section 4.4, with some minor adaptations:

1. **Establish the size of the system to be solved.** Only the n *NL-DOFs* and the m selected modes should be considered, constructing a reduced system $[n, m]$.

2. **Establish the vector of unknowns.** This corresponds to the unknown responses associated with the n NL-DOFs, $\{\tilde{Y}_n\}$.

3. **Establish the set of NL equations.** This is expressed by (6.31), where the LHS vector is considered to be the "analytical" solution, $\{\tilde{Y}_n\}^{analytical}$.

4. **Provide an initial guess $\{\tilde{Y}_n\}^{trial}$ for the first iteration.** For the present work, the linear solution $\{\tilde{Y}_n\}^{trial} = \{Y_n\}^{linear}$ was chosen.

5. **Construct the *extended* NLMV.** First construct the NLV $\{\tilde{G}_n\}$ for the n NL-DOFs. Then calculate the NLMV $\{\boldsymbol{\Phi}_{m,n}^{\mathbf{T}} \tilde{G}_n\}$. Finally, obtain the *extended* NLMV $\{\tilde{\chi}_m\}$:

$$\{\tilde{\chi}_m\} = \{\boldsymbol{\Phi}_{m,n}^{\mathbf{T}} F_n\} - \{\boldsymbol{\Phi}_{m,n}^{\mathbf{T}} \tilde{G}_n\}$$

6. **Real-imaginary split.** The standard minimization routine available in MATLAB (60) cannot handle complex variables, so the NL equations must be split into their real and imaginary parts before proceeding. This can be mathematically stated as:

$$\{f(y)\} = \left\{ \begin{array}{c} \mathrm{Re}(\tilde{Y}^{trial} - \tilde{Y}^{analytical}) \\ \dots\dots\dots\dots\dots \\ \mathrm{Im}(\tilde{Y}^{trial} - \tilde{Y}^{analytical}) \end{array} \right\}_{2n} \approx \left\{ \begin{array}{c} 0 \\ \cdots \\ 0 \end{array} \right\}_{2n} \tag{6.33}$$

7. **Calculate $\{\tilde{Y}_n\}$.** The iterative procedure will terminate when the updated solution vector $\{f(y)\}$ is less than a pre-defined tolerance (say, between 1-2%) away from the previous iteration. It will contain the required responses for the actual excitation frequency only, so the whole procedure must be re-applied for the next step-frequency, with the added contribution that now the calculated responses serve very well as an initial guess for the algorithm.

8. **Calculate $\{\tilde{Y}_{N-n}\}$.** Once the $\{\tilde{Y}_n\}$ responses have been calculated, the problem has been transformed to a *linear* one. The remaining responses $\{\tilde{Y}_{N-n}\}$ (typically $n \ll N$) can be obtained by using (6.28) on an individual basis, or using (6.32) for the whole set of $(N-n)$ unknowns.

6.7 Sample Case #1: a cubic stiffness modal example

The HMT method will be exemplified with its application to a small sample case. Although in principle there is no restriction at all -other than the computational cost- on the size of the system it can handle, having a small enough system is visually instructive. Based on this same argument, the case will be restricted to include cubic stiffness nonlinearities while observing that mixed nonlinearities should not represent a significant obstacle.

The Sample Case #1 is thoroughly described in Appendix A, and shown here in Fig. 6.6 for convenience.
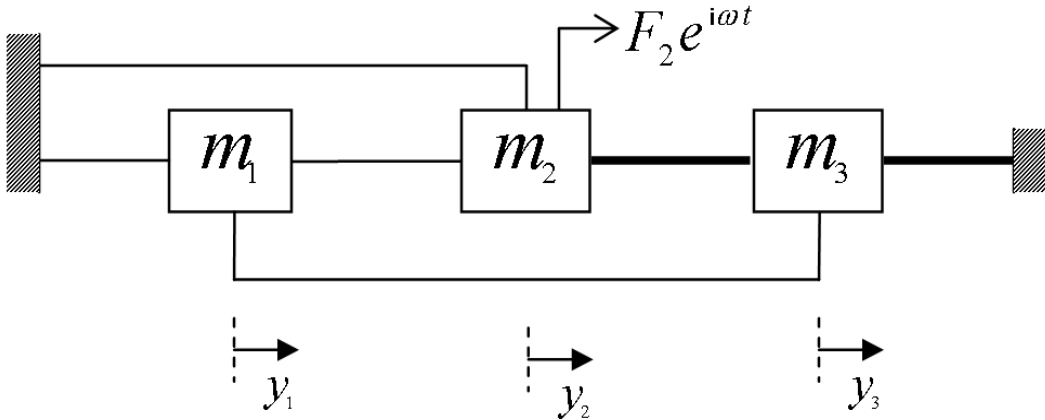
Figure 6.6: Sample Case #1

Our aim is to obtain the nonlinear FRFs, and we start by recalling the NLV for this problem, already obtained in Section 4.5:

$$\{\tilde{G}\} = \left\{ \begin{array}{c} \tilde{g}v_1 \\ \tilde{g}v_2 \\ \tilde{g}v_3 \end{array} \right\} = \frac{3}{4} \begin{bmatrix} 0 & 0 & 0 \\ 0 & \beta_{23}\left|\tilde{Z}_{23}\right|^2 & -\beta_{23}\left|\tilde{Z}_{23}\right|^2 \\ 0 & -\beta_{23}\left|\tilde{Z}_{23}\right|^2 & \left(\beta_{33}\left|\tilde{Y}_3\right|^2 + \beta_{23}\left|\tilde{Z}_{23}\right|^2\right) \end{bmatrix} \left\{ \begin{array}{c} \tilde{Y}_1 \\ \tilde{Y}_2 \\ \tilde{Y}_3 \end{array} \right\}$$

where $\left|\tilde{Z}_{ij}\right| = \left|\tilde{Y}_i - \tilde{Y}_j\right|$. The NLV vector can also be expressed in a more compact

form:

$$\{\tilde{G}\} = \left\{ \begin{array}{c} \tilde{g}v_1 \\ \tilde{g}v_2 \\ \tilde{g}v_3 \end{array} \right\} = \frac{3}{4} \left\{ \begin{array}{c} 0 \\ \beta_{23} \left|\tilde{Z}_{23}\right|^3 e^{\mathbf{i}\theta_{23}} \\ \beta_{23} \left|\tilde{Z}_{23}\right|^3 e^{\mathbf{i}\theta_{23}} + \beta_{33} \left|\tilde{Y}_3\right|^3 e^{\mathbf{i}\theta_3} \end{array} \right\}$$

where $\theta_{ij} = \measuredangle(\tilde{Y}_i, \tilde{Y}_j)$ and $\tilde{g}v_1 = 0$ simply because there are not NL elements attached to DOF 1. Next we calculate the NLMV by using (6.23):

$$\{\mathbf{\Phi}^\mathbf{T} \tilde{G}\} = \frac{3}{4} \left\{ \begin{array}{c} (\phi_{21} + \phi_{31}) \left(\beta_{23} \left|\tilde{Z}_{23}\right|^3 e^{\mathbf{i}\theta_{23}} \right) + \phi_{31} \left(\beta_{33} \left|\tilde{Y}_3\right|^3 e^{\mathbf{i}\theta_3} \right) \\ (\phi_{22} + \phi_{32}) \left(\beta_{23} \left|\tilde{Z}_{23}\right|^3 e^{\mathbf{i}\theta_{23}} \right) + \phi_{32} \left(\beta_{33} \left|\tilde{Y}_3\right|^3 e^{\mathbf{i}\theta_3} \right) \\ (\phi_{23} + \phi_{33}) \left(\beta_{23} \left|\tilde{Z}_{23}\right|^3 e^{\mathbf{i}\theta_{23}} \right) + \phi_{33} \left(\beta_{33} \left|\tilde{Y}_3\right|^3 e^{\mathbf{i}\theta_3} \right) \end{array} \right\} \quad (6.34)$$

where each row represents the nonlinearity affecting the correspondent modal coordinate.

In the interest of clarity, Fig. 6.7a previews the (soon to be calculated!) nonlinear response at coordinate 1 and Fig. 6.7b shows its three associated NLMV defined in (6.34); it can be observed that each function of the NLMV exhibits strong components at every resonance and, in the case of NLMV 3, its components at the first and second resonances are even stronger than the observed in its own modal coordinate.

(6.34) also allows the following interesting observation: the extent to which a given NL element, say β_{33}, will exert influence in mode s is determined by its numerical value as well as by its "weight" factor ϕ_{3s}. For "non-grounded" elements such as β_{23} the situation is less well-defined because of the simultaneous dependency on two eigenvectors, ϕ_{2s} and ϕ_{3s}. For the extreme case in which these two eigenvectors are identical but of opposite sign (quite common for symmetrical structures), the nonlinearity disappears completely. *This is the mathematical proof for the solution non-uniqueness of an identification problem.*
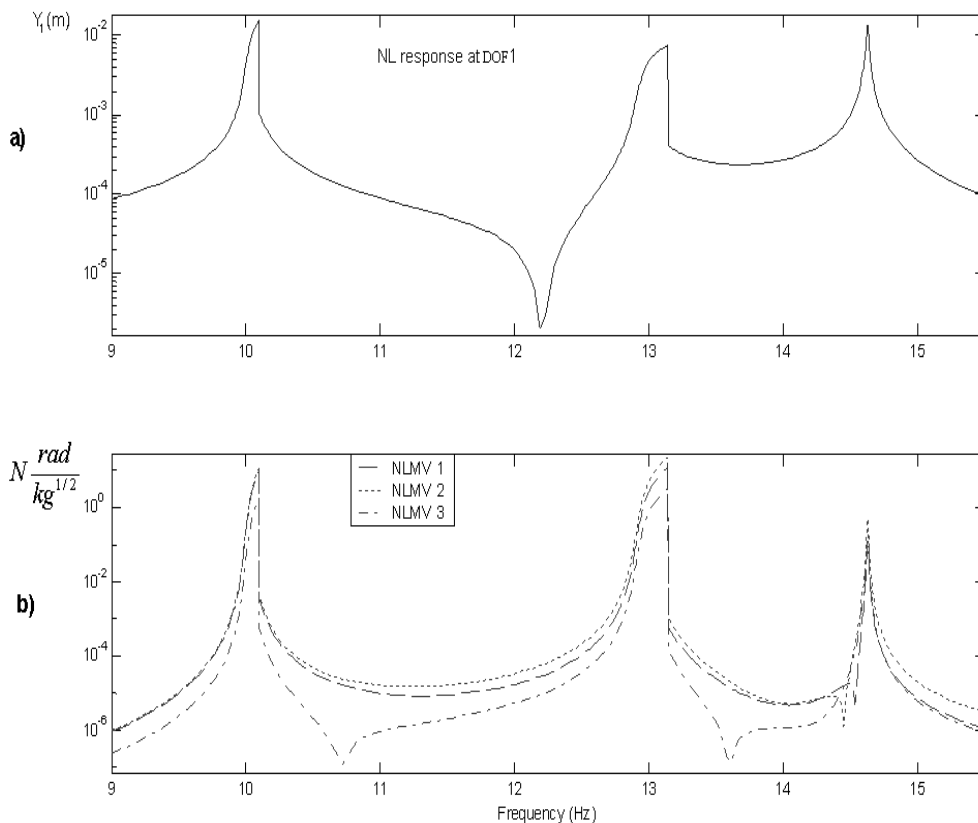
Figure 6.7: Sample Case #1, NLMV

The *extended* NLMV is derived straightforwardly:

$$\{\tilde{\chi}\} = -\frac{3}{4} \left\{ \begin{array}{c} (\phi_{21} + \phi_{31}) \left(\beta_{23} \left| \tilde{Z}_{23} \right|^3 e^{\mathbf{i}\theta_{23}} - F_2 \right) + \phi_{31} \left(\beta_{33} \left| \tilde{Y}_3 \right|^3 e^{\mathbf{i}\theta_3} \right) \\ (\phi_{22} + \phi_{32}) \left(\beta_{23} \left| \tilde{Z}_{23} \right|^3 e^{\mathbf{i}\theta_{23}} - F_2 \right) + \phi_{32} \left(\beta_{33} \left| \tilde{Y}_3 \right|^3 e^{\mathbf{i}\theta_3} \right) \\ (\phi_{23} + \phi_{33}) \left(\beta_{23} \left| \tilde{Z}_{23} \right|^3 e^{\mathbf{i}\theta_{23}} - F_2 \right) + \phi_{33} \left(\beta_{33} \left| \tilde{Y}_3 \right|^3 e^{\mathbf{i}\theta_3} \right) \end{array} \right\}$$

Finally we invoke the nonlinear modal expansion stated in (6.29) to generate

a system of nonlinear equations,

$$
\left\{
\begin{array}{c}
\tilde{Y}_1 \\
\tilde{Y}_2 \\
\tilde{Y}_3
\end{array}
\right\} =
\left[
\begin{array}{ccc}
\dfrac{\phi_{11}}{\lambda_1^2-\omega^2} & \dfrac{\phi_{12}}{\lambda_2^2-\omega^2} & \dfrac{\phi_{13}}{\lambda_3^2-\omega^2} \\[2ex]
\dfrac{\phi_{21}}{\lambda_1^2-\omega^2} & \dfrac{\phi_{22}}{\lambda_2^2-\omega^2} & \dfrac{\phi_{23}}{\lambda_3^2-\omega^2} \\[2ex]
\dfrac{\phi_{31}}{\lambda_1^2-\omega^2} & \dfrac{\phi_{32}}{\lambda_2^2-\omega^2} & \dfrac{\phi_{33}}{\lambda_3^2-\omega^2}
\end{array}
\right]
\left\{
\begin{array}{c}
\tilde{\chi}_1 \\
\tilde{\chi}_2 \\
\tilde{\chi}_3
\end{array}
\right\}
$$

The nonlinear expressions are valid for a single frequency ω; in order to decrease the computational burden, the responses can be solved just around resonance, where the nonlinearities are expected to become active, everywhere else being replaced by the linear responses. This procedure is valid because sub/super harmonics are not considered in this work.

The performance of the HMT method will be compared with the "harmonic balance method" which is a recognized benchmark for nonlinear problems. The particular HBM code used in this work was written by Dr. Evgeny Petrov (65) under a long term research program at Imperial College London for the vibration analysis of nonlinear structures with different types of nonlinearities, such as friction damping and cubic stiffness.

The nonlinear response shown in Figs. 6.8 and 6.9 was obtained by applying the minimization scheme presented in Section 6.6.

The dashed line represents the linear response, while the solid line represents the results obtained from the benchmark method (labelled as "HBM"). Finally, the "■" marks around the resonances are the results from the HMT, which are in excellent agreement with the benchmark. The HMT calculations took about 4 seconds per resonance, in a 1.5GHz Pentium computer equipped with 500MB of RAM.

This compares very favourably with the computation time of the EF method, which took 8 seconds per resonance for the same problem. The regenerated responses of Fig. 6.8 (HMT) and Fig. 4.3, page 61 (EF), are virtually identical.
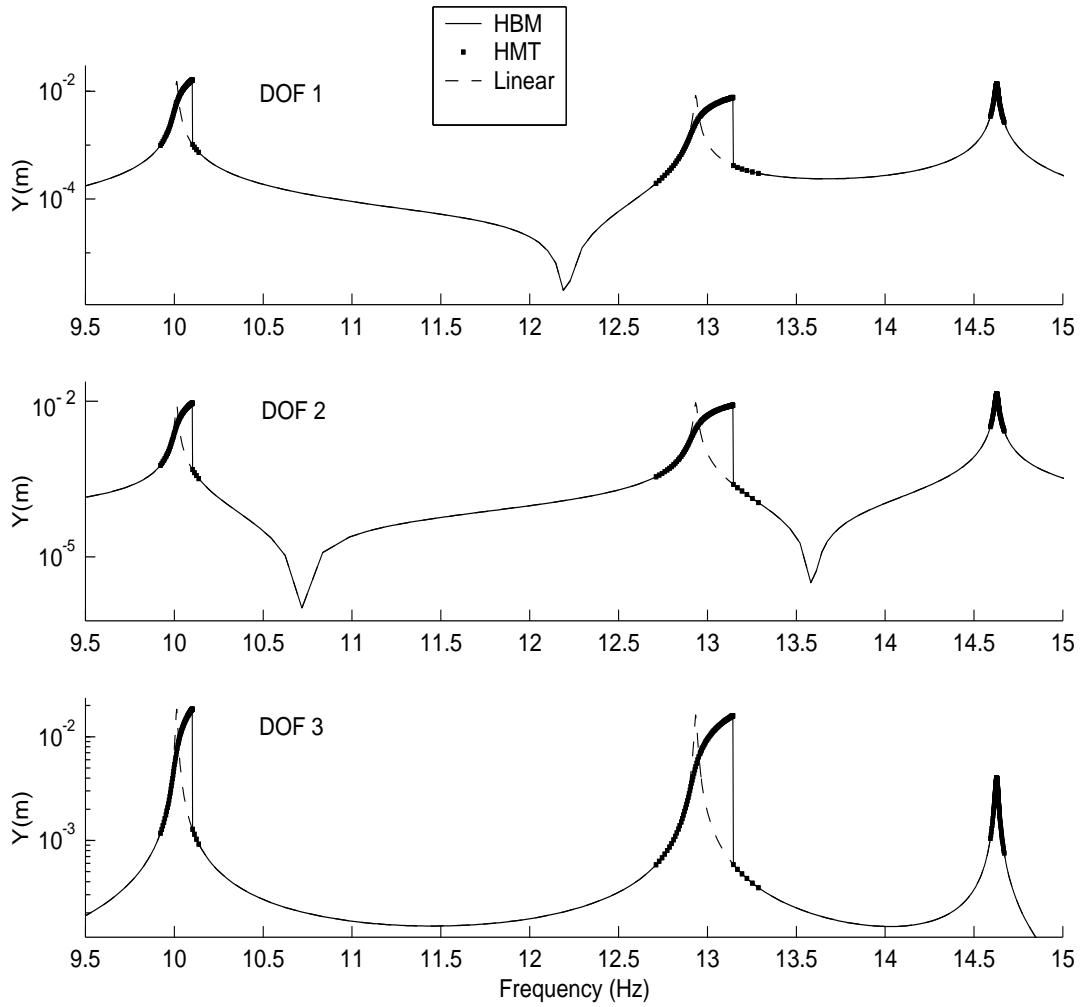
Figure 6.8: Sample Case #1, calculated nonlinear response. A Zoom-In of the individual resonances is shown in Fig. 6.9
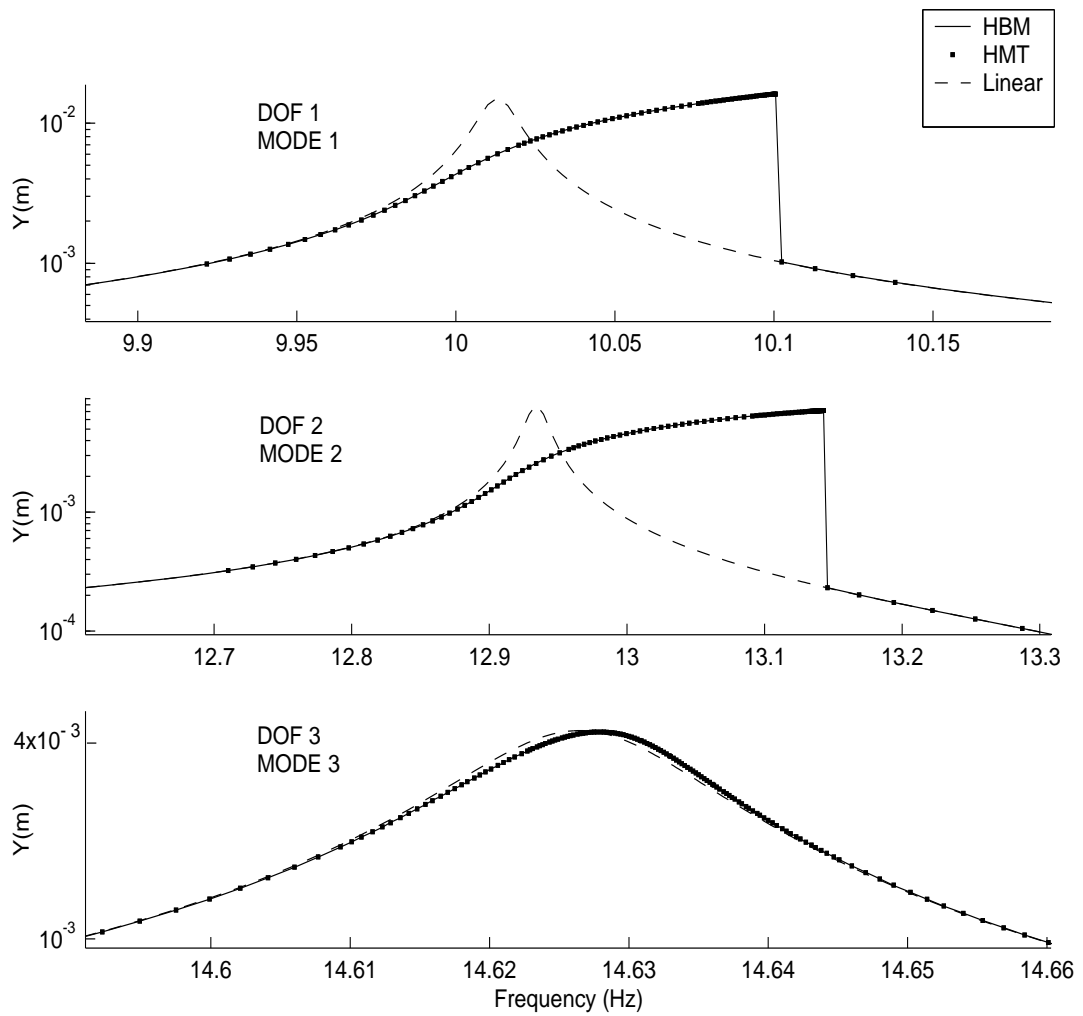
Figure 6.9: Sample Case #1, Zoom-In at the individual resonances of Fig. 6.8

6.8 Sample Case #2: a friction damping modal example

The HMT method will now be exemplified in a system containing friction damping nonlinearities. Sample Case #2 is identical to #1, except that the two NL elements are of the friction damping type, as described in Appendix A.

The NLV for this problem was already obtained in Section 4.6, expressed as:

$$
\{\tilde{G}\} = \left\{ \begin{array}{c} \tilde{g}v_1 \\ \tilde{g}v_2 \\ \tilde{g}v_3 \end{array} \right\} = \mathbf{i}\frac{4}{\pi} \begin{bmatrix} 0 & 0 & 0 \\ 0 & \frac{\gamma_{23}}{|\tilde{Z}_{23}|} & -\frac{\gamma_{23}}{|\tilde{Z}_{23}|} \\ 0 & -\frac{\gamma_{23}}{|\tilde{Z}_{23}|} & \left(\frac{\gamma_{33}}{|\tilde{Y}_3|} + \frac{\gamma_{23}}{|\tilde{Z}_{23}|} \right) \end{bmatrix} \left\{ \begin{array}{c} \tilde{Y}_1 \\ \tilde{Y}_2 \\ \tilde{Y}_3 \end{array} \right\}
$$

where $\left| \tilde{Z}_{ij} \right| = \left| \tilde{Y}_i - \tilde{Y}_j \right|$. The NLV vector can also be expressed in a more compact form:

$$
\{\tilde{G}\} = \left\{ \begin{array}{c} \tilde{g}v_1 \\ \tilde{g}v_2 \\ \tilde{g}v_3 \end{array} \right\} = \mathbf{i}\frac{4}{\pi} \left\{ \begin{array}{c} 0 \\ \gamma_{23}\frac{\tilde{Z}_{23}}{|\tilde{Z}_{23}|}e^{\mathbf{i}\theta_{23}} \\ \gamma_{23}\frac{\tilde{Z}_{23}}{|\tilde{Z}_{23}|}e^{\mathbf{i}\theta_{23}} + \gamma_{33}\frac{\tilde{Y}_3}{|\tilde{Y}_3|}e^{\mathbf{i}\theta_3} \end{array} \right\}
$$

where $\theta_{ij} = \measuredangle(\tilde{Y}_i, \tilde{Y}_j)$ and $\tilde{g}v_1 = 0$ simply because there are not NL elements attached to coordinate 1. Next we calculate the NLMV as follows:

$$
\{\mathbf{\Phi^T}\tilde{G}\} = \mathbf{i}\frac{4}{\pi} \left\{ \begin{array}{c} (\phi_{21} + \phi_{31}) \left(\gamma_{23}\frac{\tilde{Z}_{23}}{|\tilde{Z}_{23}|}e^{\mathbf{i}\theta_{23}} \right) + \phi_{31} \left(\gamma_{33}\frac{\tilde{Y}_3}{|\tilde{Y}_3|}e^{\mathbf{i}\theta_3} \right) \\ (\phi_{22} + \phi_{32}) \left(\gamma_{23}\frac{\tilde{Z}_{23}}{|\tilde{Z}_{23}|}e^{\mathbf{i}\theta_{23}} \right) + \phi_{32} \left(\gamma_{33}\frac{\tilde{Y}_3}{|\tilde{Y}_3|}e^{\mathbf{i}\theta_3} \right) \\ (\phi_{23} + \phi_{33}) \left(\gamma_{23}\frac{\tilde{Z}_{23}}{|\tilde{Z}_{23}|}e^{\mathbf{i}\theta_{23}} \right) + \phi_{33} \left(\gamma_{33}\frac{\tilde{Y}_3}{|\tilde{Y}_3|}e^{\mathbf{i}\theta_3} \right) \end{array} \right\} \tag{6.35}
$$

where each row now represents the nonlinearity affecting the correspondent modal coordinate.

In the interest of clearness, Fig. 6.10a shows the (soon to be calculated!) nonlinear response at coordinate 1 and Fig. 6.10b shows the three NLMV's defined in (6.35); as expected for this nonlinear mechanism, the nonlinear modal forces

jump between constant values according to the direction of the relative motion. It can be seen that each function of the NLMV exhibits non-zero components at every resonance and, in the case of NLMV 3, its components at the 1st and 2nd resonances are even stronger than the observed at its own 3rd mode.
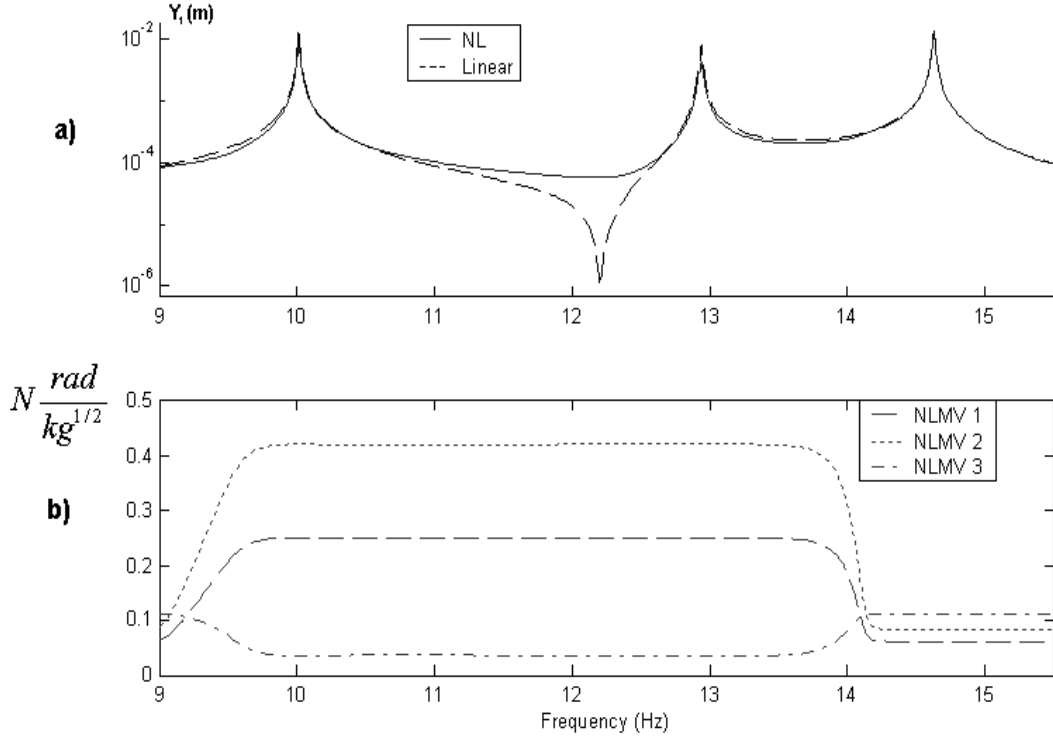
Figure 6.10: Sample Case #2, NLMV

All the remarks given in Section 6.7, regarding the coupling behaviour of the NLMV, are still valid. The *extended* NLMV is:

$$
\{\tilde{\chi}\} = -\mathbf{i}\frac{4}{\pi}
\left\{
\begin{array}{l}
(\phi_{21} + \phi_{31})\left(\gamma_{23}\frac{\tilde{Z}_{23}}{|\tilde{Z}_{23}|}e^{\mathbf{i}\theta_{23}} - F_2\right) + \phi_{31}\left(\gamma_{33}\frac{\tilde{Y}_3}{|\tilde{Y}_3|}e^{\mathbf{i}\theta_3}\right) \\[2mm]
(\phi_{22} + \phi_{32})\left(\gamma_{23}\frac{\tilde{Z}_{23}}{|\tilde{Z}_{23}|}e^{\mathbf{i}\theta_{23}} - F_2\right) + \phi_{32}\left(\gamma_{33}\frac{\tilde{Y}_3}{|\tilde{Y}_3|}e^{\mathbf{i}\theta_3}\right) \\[2mm]
(\phi_{23} + \phi_{33})\left(\gamma_{23}\frac{\tilde{Z}_{23}}{|\tilde{Z}_{23}|}e^{\mathbf{i}\theta_{23}} - F_2\right) + \phi_{33}\left(\gamma_{33}\frac{\tilde{Y}_3}{|\tilde{Y}_3|}e^{\mathbf{i}\theta_3}\right)
\end{array}
\right\}
$$

Finally we use (6.29) to generate a system of nonlinear equations,

$$
\left\{ \begin{array}{c} \tilde{Y}_1 \\ \tilde{Y}_2 \\ \tilde{Y}_3 \end{array} \right\} = \left[\begin{array}{ccc} \frac{\phi_{11}}{\lambda_1^2 - \omega^2} & \frac{\phi_{12}}{\lambda_2^2 - \omega^2} & \frac{\phi_{13}}{\lambda_3^2 - \omega^2} \\[2mm] \frac{\phi_{21}}{\lambda_1^2 - \omega^2} & \frac{\phi_{22}}{\lambda_2^2 - \omega^2} & \frac{\phi_{23}}{\lambda_3^2 - \omega^2} \\[2mm] \frac{\phi_{31}}{\lambda_1^2 - \omega^2} & \frac{\phi_{32}}{\lambda_2^2 - \omega^2} & \frac{\phi_{33}}{\lambda_3^2 - \omega^2} \end{array} \right] \left\{ \begin{array}{c} \tilde{\chi}_1 \\ \tilde{\chi}_2 \\ \tilde{\chi}_3 \end{array} \right\}
$$

The nonlinear responses shown in Fig. 6.11 and 6.12 were obtained by applying the minimization scheme presented in Section 6.6. It can be seen that the HMT ("■" marks) is in complete agreement with the benchmark (solid line), both exhibiting lower amplitudes at resonance when compared to the linear case (dashed line).

The effect of the nonlinearity is an overall reduction of the amplitudes, this being more noticeable in the first and second modes. This reduction explains why this nonlinear mechanism is so welcome (and even induced) in turbine bladed disks, where higher amplitudes are a risk for the structural integrity.

The third mode is less affected because, at higher frequencies, the NL damping force is overwhelmed by the linear restoring forces; the more pronounced effect in the second mode can be explained by the fact that two masses are in opposite motion, generating an additive effect of the friction forces.
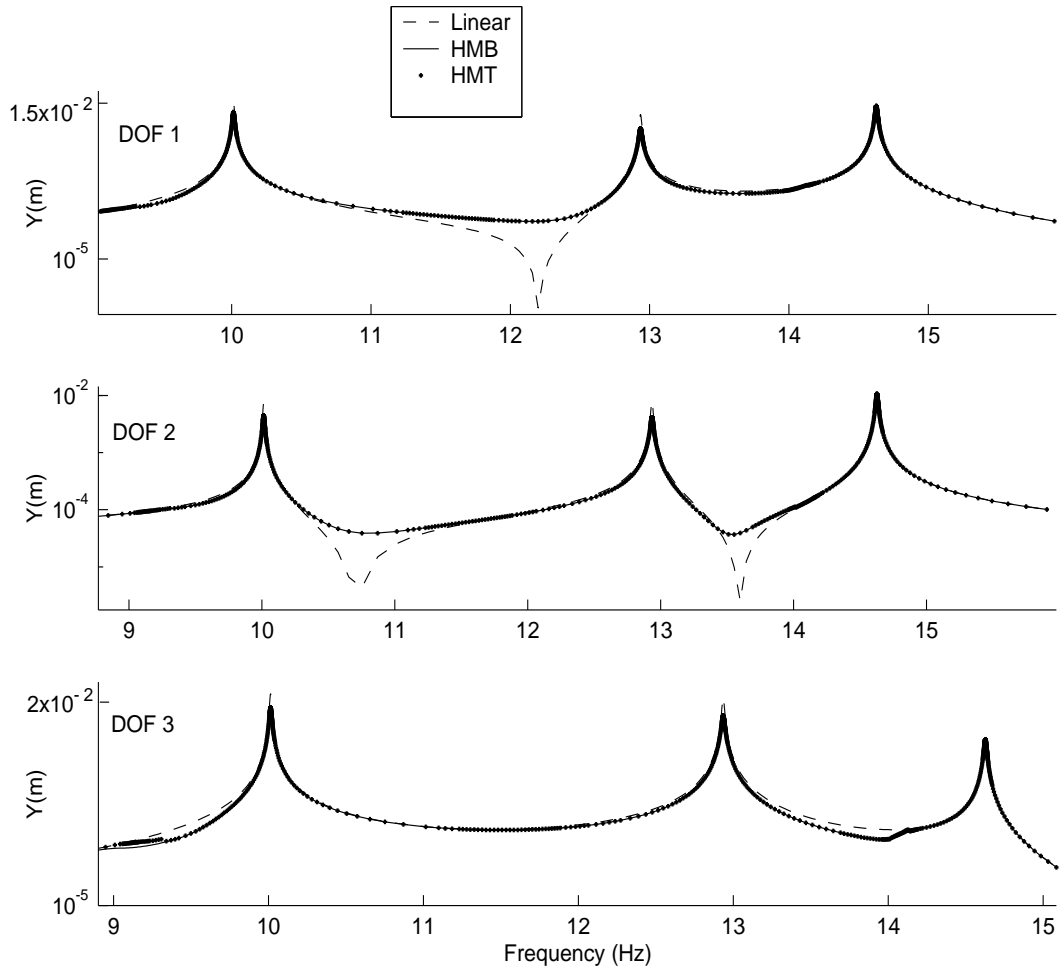
Figure 6.11: Sample Case #2, calculated nonlinear response. The nonlinear effects at resonance are better exposed in Fig. 6.12, showing a Zoom-In of each mode
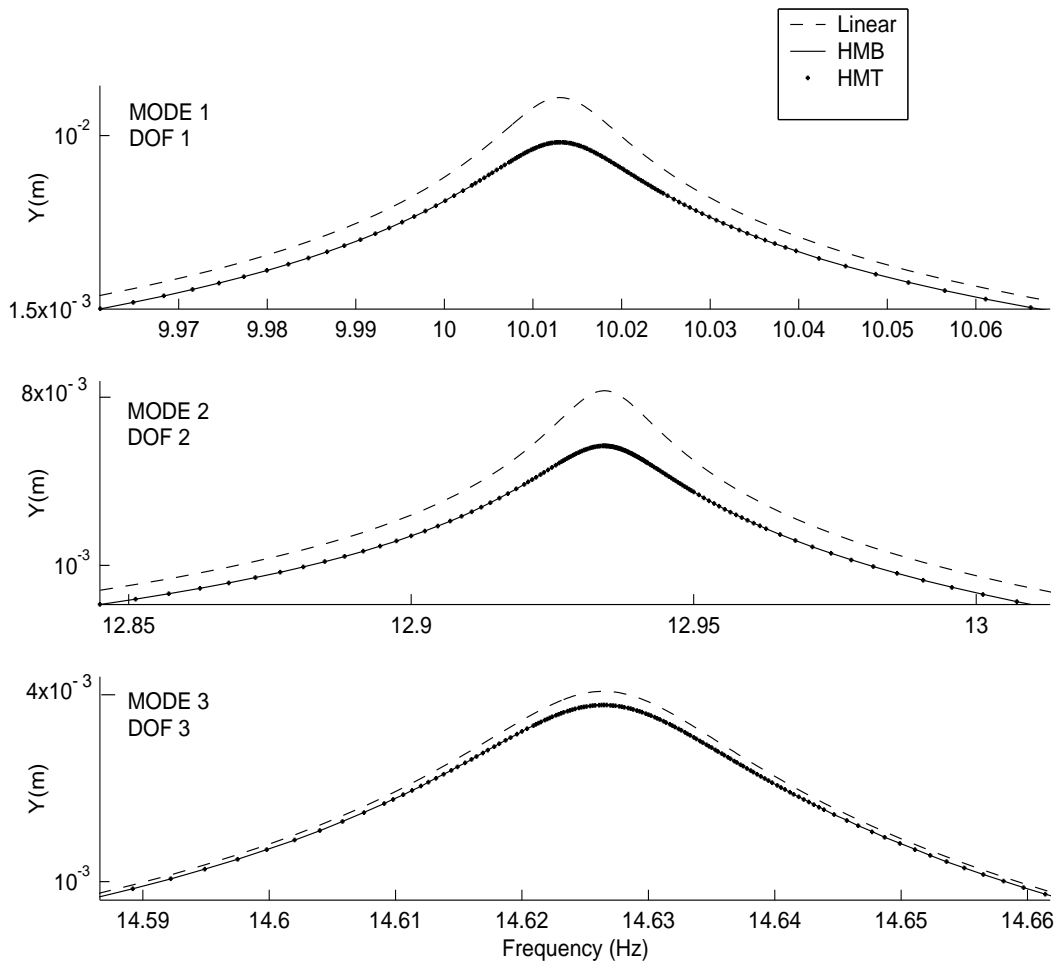
Figure 6.12: Sample Case #2, calculated nonlinear response (Zoom-In)

6.9   Concluding remarks

The most important development of this chapter has been the HMT method in
a direct-path approach, this is, by analyzing a fully described theoretical system.
The main features of the method can be summarized as follows:

- The HMT represents, basically, a nonlinear modal superposition. How-
  ever, it is mathematically exact[1]. In other words, no approximations have
  been involved in its derivation, fully accounting for the intermodal coupling
  effects.

- The term "hybrid" arises from the fact that the underlying linear system has
  been reduced by expressing it in the modal space, while the nonlinearities
  are kept in the physical domain (in the form of describing functions). Due
  to this feature, the location of the NL elements is fully achieved by the
  HMT, when used as an identification tool.

- This method is quite effective in an experimental environment, concentrat-
  ing all the nonlinearities in one single term per mode, the NLMV. This has
  an explicit physical meaning, being analytically linked to the coefficients of
  the physical NL elements.

- The set of NL equations to be solved can be dramatically reduced, both
  in spatial and modal coordinates, by including only the n *NL-DOFs* and a
  few m selected modes.

- Although the method recognizes the existence of amplitude-dependant (non-
  linear) eigenvalues and eigenvectors, the responses are obtained without
  explicitly calculating them.

- The method was successfully tested against simulated data for two small
  systems containing cubic stiffness and friction damping nonlinearities. In
  computational terms, it proved highly efficient when compared to the EF
  method, introduced in Chapter 4.

---

[1]Under the assumptions of a first-order formulation. However, even this restriction can be
relaxed if the NLV $\{\tilde{G}\}$ is a multi-harmonic descriptor.

Other achievements of this chapter are:

- A new mathematical expression (6.22), describing the nonlinear modal space, have been obtained. This is the theoretical basis not only for the HMT method, but also for main developments in subsequent chapters.

- The main assumption of the *nonlinear normal modes* method, that the nonlinearities are confined to the resonant region, has shown to be unduly restrictive, but probably valid in practical situations. Indeed, it was proved that the nonlinear space is coupled, but in the context of a traditional expansion, the *nonlinear normal modes* assumption offers acceptable results.

Chapter 7

Analytical derivation of NL modal parameters via a fast approximation technique (FAT)

7.1   Introduction

The standard modal expansion for linear systems was given by (6.9),

$$\frac{Y_i}{F_j} = H_{ij} = \sum_{r=1}^{M} \frac{\phi_{ir}\phi_{jr}}{\lambda_r^2 - \omega^2}$$

which is the basis for the traditional nonlinear modal expansion, given by (6.11),

$$\tilde{H}_{ij}(\omega, \tilde{Y}) = \sum_{r=1}^{M} \frac{\tilde{\phi}_{ir}(\omega, \tilde{Y})\tilde{\phi}_{jr}(\omega, \tilde{Y})}{\tilde{\lambda}_r^2(\omega, \tilde{Y}) - \omega^2}$$

On the other hand, the newly developed HMT expansion for nonlinear systems was given by (6.28),

$$\tilde{Y}_i = \sum_{r=1}^{M} \frac{\phi_{ir}\tilde{\chi}_r}{\lambda_r^2 - \omega^2}$$

Comparing these expressions, it is clear that one of the main advantages of the HMT expansion (6.28) is that it avoids the explicit calculation of nonlinear eigenvectors and eigenvalues. Consequently, one of its main disadvantages may be a lack of methodology for determining these parameters.

Indeed, such is the importance of these nonlinear modal parameters that one is left wishing to know them, even if they're not explicitly needed to calculate the response. Here are a few reasons why:

- The concept of varying eigenvalues and eigenvectors in (6.11) has physical grounds. Indeed, it can be proven (3) that the nonlinearities arising, for example, from a cubic stiffness mechanism are dependent on some material properties with a cubic power. This leads to an increase in the overall stiffness and, in the end, to an increase in the natural frequencies of vibration.

- On the other hand, the HMT represents, basically, the underlying linear structure being subjected to a nonlinear force, which does not describe the true physics of the problem.

- Translating the HMT results to standard NL modal parameters will provide links with other nonlinear methods, such as (30).

In this chapter, the nonlinear information contained in the NLMV $\{\mathbf{\Phi^T}\tilde{G}\}$ will be transformed to more standardized parameters, namely, nonlinear eigenvalues ($\tilde{\lambda}^2$) and eigenvectors ($\tilde{\mathbf{\Phi}}$). This transformation will be carried out by newly-developed analytical expressions, providing a fast -albeit approximated- derivation. The introduced technique is thus called the "fast approximation technique" (FAT).

There is another compelling reason for realizing this transformation, much more important than for purely comparative purposes:

The nonlinear information contained in the NLMV of any given mode is usually highly coupled, exhibiting strong nonlinear components at every other resonance[1]. If we wish to use this information within a modal superposition context, it is necessary to decompose the NLMV into individual modal components, effectively decoupling the problem. The derivation of nonlinear eigenvalues and eigenvectors achieves this task by extracting information related to a single mode only, as illustrated in Fig. 7.1.

It must be remarked that the FAT does not represent, per se, a final identification, because the obtained results are still amplitude- or frequency-dependent,

---

[1]See Fig. 6.5, page 106.

i.e. $\tilde{\lambda}_r(\omega), \tilde{\boldsymbol{\Phi}}_r(\omega)$. A further transformation, represented in Fig. 7.1 as a "polynomial fitting", must be applied in order to provide an invariant model, valid for any level of excitation[1].

Nevertheless, the FAT provides a straightforward, *analytical* approach for calculating the nonlinear eigenvalues and eigenvectors, thus obviating more complex procedures. The current approach for this task is based on a nonlinear optimization from measured data, a calculation which suffers from well-known problems such as ill-conditioning and divergence.

The FAT method is graphically represented in the flow chart of Fig. 7.2.
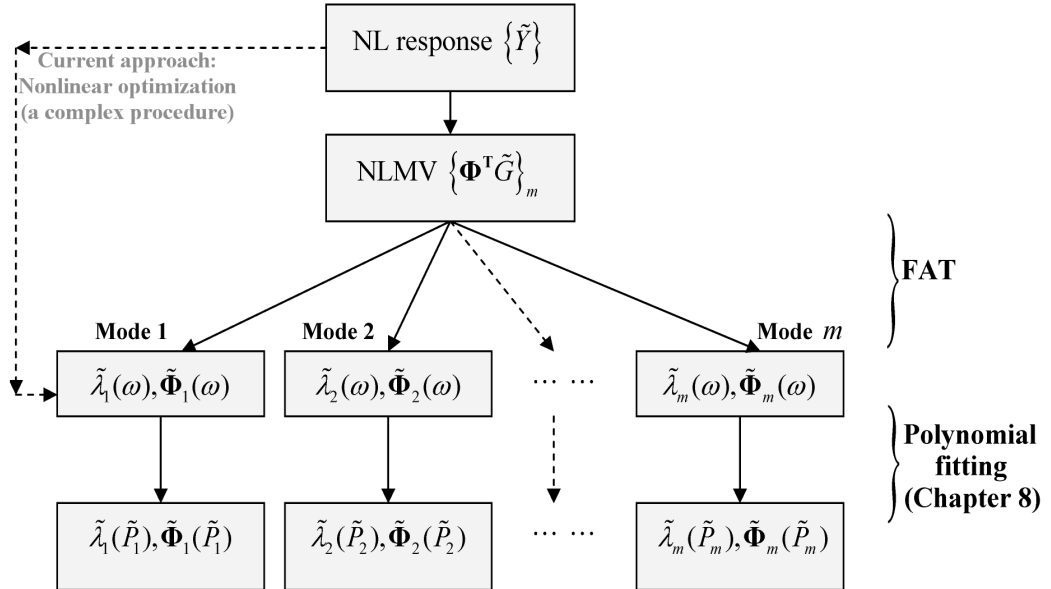
Figure 7.1: Transforming/decoupling the NLMV

---

[1]Within a restricted range. This second transformation will be introduced in Chapter 8, but it can be said in advance that it requires only a simple data manipulation.

INPUT DATA

NLMV $\left\{ \boldsymbol{\Phi}^{\mathbf{T}}\tilde{G} \right\}$

The NLMV can be calculated from $\tilde{Y}$ and $\tilde{G}$. Note that $\boldsymbol{\Phi}$ is the *linear* matrix of eigenvectors.

Initial guess: $\Delta\tilde{\boldsymbol{\Phi}} = 0$

$\tilde{\boldsymbol{\Phi}} = \boldsymbol{\Phi} + \Delta\tilde{\boldsymbol{\Phi}}$

The nonlinear eigenvector is expressed as the addition of a linear ($\boldsymbol{\Phi}$) and a nonlinear ($\Delta\tilde{\boldsymbol{\Phi}}$) component (central assumption of the FAT).

$\tilde{P} = \tilde{\boldsymbol{\Phi}}^{-1}\tilde{Y}$

The nonlinear normal modes $\left(\tilde{P}\right)$ are calculated as functions of the responses.

Core expression of the FAT.

$$\Delta\tilde{\lambda}_s^2 \approx \frac{\left(\boldsymbol{\Phi}^{\mathbf{T}}\tilde{G}\right)_s + \left(\Delta\tilde{\boldsymbol{\Phi}}^{\mathbf{T}}F\right)_s}{\tilde{P}_s}$$

The variation of the s_{th} nonlinear eigenvalue $\left(\Delta\tilde{\lambda}_s^2\right)$ is obtained via FAT.

Point-FRF $\left(\tilde{H}_{jj}\right)$:

$$\tilde{\Phi}_{js} = \sqrt{\left(\lambda_s^2 + \Delta\tilde{\lambda}_s^2 - \omega^2\right)\left(\tilde{H}_{jj} - \sum_{r=1, r\neq s}^{m}\frac{\Phi_{jr}^2}{\lambda_r^2 - \omega^2}\right)}$$

Knowing $\Delta\tilde{\lambda}_s^2$, the nonlinear eigenvector at the forced dof, $\tilde{\Phi}_{js}$, is calculated.

$$\tilde{\Phi}_{is} = \frac{\left(\lambda_s^2 + \Delta\tilde{\lambda}_s^2 - \omega^2\right)\left(\tilde{H}_{ij} - \sum_{r=1, r\neq s}^{m}\frac{\Phi_{ir}\Phi_{jr}}{\lambda_r^2 - \omega^2}\right)}{\tilde{\Phi}_{js}}$$
for $i \in N$, $i \neq j$

By knowing $\tilde{\Phi}_{js}$, the nonlinear eigenvectors at the remaining coordinates, $\tilde{\Phi}_{is}$, for $i \in N$, are calculated.

Iterative loop

$\Delta\tilde{\boldsymbol{\Phi}} = \tilde{\boldsymbol{\Phi}} - \boldsymbol{\Phi}$

$$\tilde{\boldsymbol{\Phi}} = \begin{pmatrix} \Phi_{1,1} & \cdots & \begin{matrix}\vdots\end{matrix} & \cdots & \Phi_{1,M} \\ \vdots & \ddots & \vdots & \iddots & \vdots \\ \vdots & \cdots & \tilde{\boldsymbol{\Phi}}_{\mathbf{s}} & \cdots & \vdots \\ \vdots & \iddots & \vdots & \ddots & \vdots \\ \Phi_{N,1} & \cdots & \begin{matrix}\vdots\end{matrix} & \cdots & \Phi_{N,M} \end{pmatrix}_{N,M}$$

The full matrix of nonlinear eigenvectors, $\tilde{\boldsymbol{\Phi}}$, is completed by filling up the remaining columns with linear information.

Next mode s

Figure 7.2: Flow diagram for the FAT calculation of nonlinear eigenvalues and eigenvectors

7.2   FAT calculation of the nonlinear eigenvalues

The modal space of a linear system was expressed by (6.6):

$$\lceil \lambda^2 - \omega^2 \rfloor \{P\} = \{\mathbf{\Phi}^{\mathbf{T}} F\}$$

A similar expression for a nonlinear system, (6.13), was written for a particular state $[\omega, \tilde{Y}]$:

$$\lceil \tilde{\lambda}^2(\omega, \tilde{Y}) - \omega^2 \rfloor \{\tilde{P}(\omega, \tilde{Y})\} = \{\tilde{\mathbf{\Phi}}^{\mathbf{T}}(\omega, \tilde{Y}) F\}$$

The nonlinear eigenvalues and eigenvectors can be decomposed into linear ($\lceil \lambda \rfloor, [\mathbf{\Phi}]$) and nonlinear components ($\lceil \mathbf{\Delta}\tilde{\lambda}(\omega, \tilde{Y}) \rfloor, [\mathbf{\Delta}\tilde{\mathbf{\Phi}}(\omega, \tilde{Y})]$), accounting for the variations due to nonlinearities:
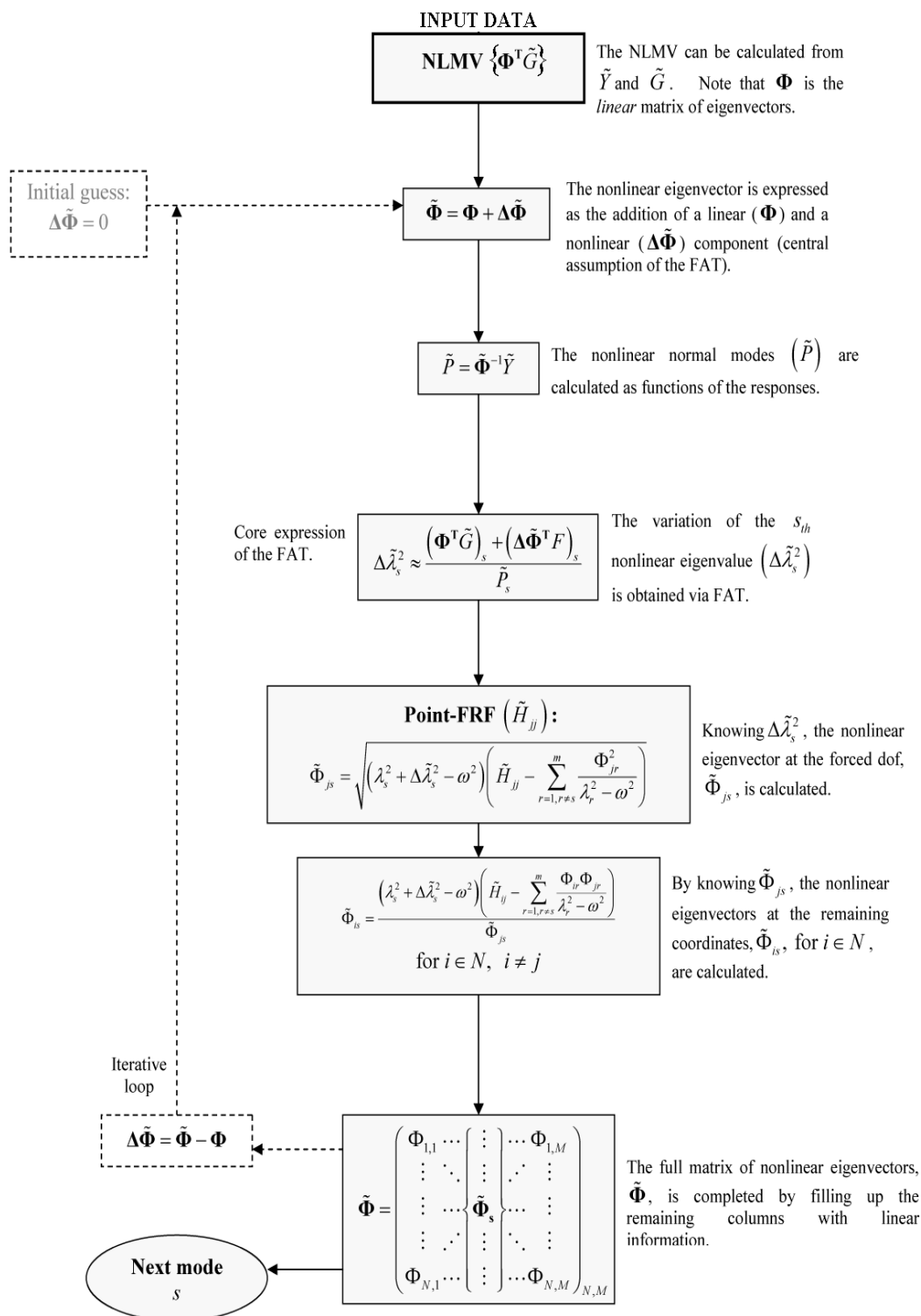
$$\lceil (\lambda^2 + \mathbf{\Delta}\tilde{\lambda}^2) - \omega^2 \rfloor \{\tilde{P}\} = \{(\mathbf{\Phi} + \Delta\tilde{\mathbf{\Phi}})^{\mathbf{T}} F\} \tag{7.1}$$

Comparing (7.1) with the recently developed (6.22), which describes the nonlinear modal space:

$$\lceil \lambda^2 - \omega^2 \rfloor \left(\mathbf{I} + \mathbf{\Phi}^{-1}\mathbf{\Delta}\tilde{\mathbf{\Phi}} \right) \{\tilde{P}\} + \{\mathbf{\Phi}^{\mathbf{T}}\tilde{G}\} = \{\mathbf{\Phi}^{\mathbf{T}} F\}$$

we conclude that the nonlinear variation of the r_{th} eigenvalue, $\Delta\tilde{\lambda}_r^2$, is given by:

$$\boxed{\Delta\tilde{\lambda}_r^2 = \frac{\left(\mathbf{\Phi}^{\mathbf{T}}\tilde{G} \right)_r + \left((\lambda_r^2 - \omega^2)\,(\mathbf{\Phi}^{-1}\mathbf{\Delta}\tilde{\mathbf{\Phi}})\{\tilde{P}\} \right)_r + \left(\mathbf{\Delta}\tilde{\mathbf{\Phi}}^{\mathbf{T}} F \right)_r}{\tilde{P}_r}} \tag{7.2}$$

where the sub-index "$_r$" refers to the r_{th} modal coordinate.

Equation (7.2) establishes, for the first time, an analytic relationship explaining the increment in natural frequencies and damping values caused by the addition of a nonlinear physical component $\{\tilde{G}\}$, the nonlinear vector (NLV), in the system.

Another interesting characteristic of this equation is that it links together the variation of the two modal parameters of a nonlinear system, namely the eigenvalues $\lceil \Delta\tilde{\lambda}_r^2 \rfloor$ and eigenvectors $[\mathbf{\Delta}\tilde{\mathbf{\Phi}}]$. Although mutually dependent from a theoretical point of view, a traditional experimental NLMA procedure extracts these parameters independently, thus increasing the complexity of the nonlinear fitting algorithms used to construct the mathematical model of the system.

Unfortunately, (7.2) cannot be solved as it is, mainly because the term $[\mathbf{\Phi}]^{-1}$ is virtually impossible to calculate from experimental data. Still, it offers a deep insight into the physics of a NL modal system and, by introducing some sensible simplifications, it will prove a highly valuable tool for a practical NLMA.

Having said this, let us analyze in more detail each one of the three main terms in the numerator of (7.2), as a better understanding will allow a better judgment regarding the simplifications needed:

1. The first of them, $\left(\mathbf{\Phi^T}\tilde{G}\right)_r$, is already a familiar term, the "nonlinear modal vector" (NLMV). It was exhaustively discussed in Section 6.4, being recognized as the main source of nonlinearity in the resonant mode. Not much can, and should not, be done to simplify this already linearised term.

2. The second term, $\left((\lambda_r^2 - \omega^2)(\mathbf{\Phi}^{-1}\mathbf{\Delta\tilde{\Phi}})\{\tilde{P}\}\right)_r$, the "nonlinear coupling term", has also been discussed. It has a relatively low contribution to the resonant mode but plays a significant role as a coupling agent. Although its strength can be significant away from resonance, we are mainly interested in how the eigenvalue varies in the vicinity of a resonant mode, so this term can be neglected within this region without major concerns[1].

3. The third term, $\left(\mathbf{\Delta\tilde{\Phi}^T}F\right)_r$, can be seen as the increase in the modal force due to the correspondent increment in the local eigenvectors. Although it has been said that $[\mathbf{\Delta\tilde{\Phi}}]$ is fairly small for a wide variety of NL systems, it will introduce a small error whenever it is neglected. This can be easily remedied by implementing an iterative procedure that estimates $[\mathbf{\Delta\tilde{\Phi}}]$, soon to be described.

   Note that:
   $$\left(\mathbf{\Delta\tilde{\Phi}^T}F\right)_r = \left\{\mathbf{\Delta\tilde{\Phi}}_r\right\}_f^{\mathbf{T}}\{F\}_f \tag{7.3}$$
   where f represents the forced DOFs. In other words, only the f entries of $\left\{\mathbf{\Delta\tilde{\Phi}}_r\right\}$ need to be estimated to accurately calculate $\Delta\tilde{\lambda}_r$.

---

[1] This simplification is the main cause of the approximation incurred in a traditional modal expansion, Eq. (6.11).

Having made the best possible case for neglecting the two "troublemaker" terms from (7.2), the following simplified expression is derived:

$$\Delta \tilde{\lambda}_r^2 \approx \frac{\left(\mathbf{\Phi}^{\mathbf{T}} \tilde{G} \right)_r}{\tilde{P}_r} \tag{7.4}$$

This is a rather elegant result, as it explicitly links the NLV $\{\tilde{G}\}$ (defined in the physical domain) with the nonlinear natural frequencies and damping ratios (modal parameters). A most interesting observation is that the nonlinear normal mode $\tilde{P}_r$ also appears in the equation.

In the past, researchers like Chong & Imregun (31), (30), Setio (68), Shaw (24) and others have suggested the existence of an invariant relationship between the nonlinear mode $\tilde{P}_r$ and its associated nonlinear natural frequency, by extracting experimental curves; these curves were successfully used to predict a nonlinear modal behaviour (Fig. 7.3), but the nature of the relation remained unknown. Equation (7.4) explicitly confirms such relation and establishes it analytically.
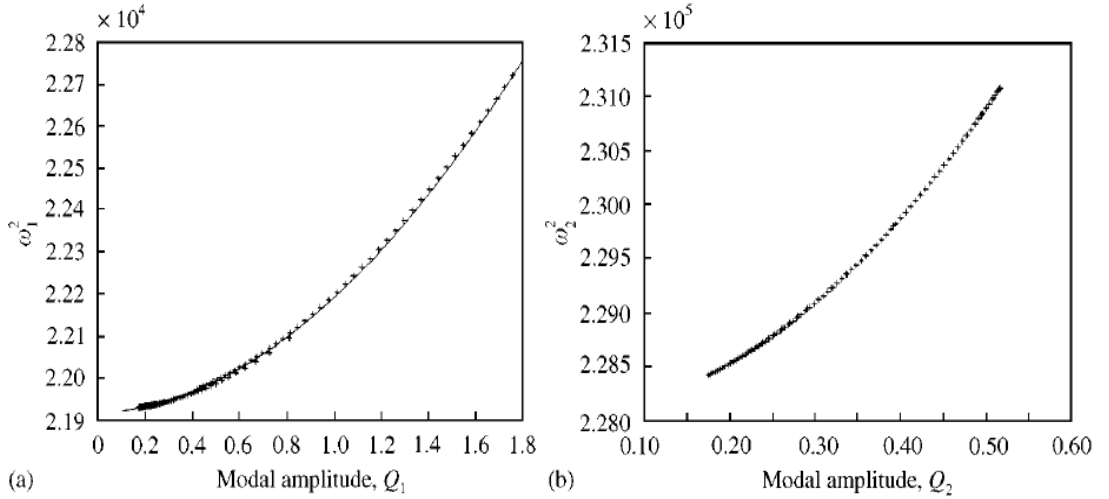

Figure 7.3: Experimental results of Chong & Imregun suggesting a relation between the modal amplitude and the nonlinear natural frequencies

7.3 FAT calculation of the nonlinear eigenvectors

With the aid of the calculated NL eigenvalues, it is now possible to calculate associated nonlinear eigenvectors. The eigenvectors' accuracy will depend on the eigenvalues' accuracy, and an iterative procedure can be established to simultaneously improve both.

We are still faced with the problem of translating the HMT results of (6.28),

$$\tilde{Y}_i = \sum_{r=1}^{M} \frac{\phi_{ir} \tilde{\chi}_r}{\lambda_r^2 - \omega^2}$$

into equivalent variables of the traditional nonlinear modal expansion (6.11),

$$\tilde{H}_{ij}(\omega, \tilde{Y}) = \sum_{r=1}^{M} \frac{\tilde{\phi}_{ir}(\omega, \tilde{Y}) \tilde{\phi}_{jr}(\omega, \tilde{Y})}{\tilde{\lambda}_r^2(\omega, \tilde{Y}) - \omega^2}$$

In the vicinity of the s_{th} resonant mode, (6.11) can be rewritten as follows:

$$\tilde{H}_{ij} = \frac{\tilde{\phi}_{is} \tilde{\phi}_{js}}{\tilde{\lambda}_s^2 - \omega^2} + \sum_{r=1, r \neq s}^{M} \frac{\tilde{\phi}_{ir} \tilde{\phi}_{jr}}{\tilde{\lambda}_r^2 - \omega^2} \tag{7.5}$$

where the resonant mode s has been taken out of the series, and the nonlinear variables have been represented by a " ~ " symbol on top. According to the *nonlinear normal modes* assumption, the residual term $\sum$ in (7.5) can be considered to behave linearly, therefore being replaced by the linear counterpart:

$$\tilde{H}_{ij} = \frac{\tilde{\phi}_{is} \tilde{\phi}_{js}}{\tilde{\lambda}_s^2 - \omega^2} + \sum_{r=1, r \neq s}^{M} \frac{\phi_{ir} \phi_{jr}}{\lambda_r^2 - \omega^2} \tag{7.6}$$

where the resonant mode s remains the only nonlinear mode. Focusing on the point-FRF $\tilde{H}_{jj}$, we obtain:

$$\tilde{H}_{jj} = \frac{\tilde{\phi}_{js}^2}{\tilde{\lambda}_s^2 - \omega^2} + \sum_{r=1, r \neq s}^{M} \frac{\phi_{jr}^2}{\lambda_r^2 - \omega^2} \tag{7.7}$$

At this point, we recall (7.4), expressing the variation of the resonant eigenvalue s:

$$\Delta\tilde{\lambda}_s^2 \approx \frac{\left(\mathbf{\Phi^T}\tilde{G}\right)_s}{\tilde{P}_s}$$

so the point-FRF can be rewritten as:

$$\tilde{H}_{jj} = \frac{\tilde{\phi}_{js}^2}{\left(\lambda_s^2 + \Delta\tilde{\lambda}_s^2\right) - \omega^2} + \sum_{r=1,r\neq s}^{M} \frac{\phi_{jr}^2}{\lambda_r^2 - \omega^2} \tag{7.8}$$

$\tilde{H}_{jj}$ is the measured nonlinear FRF at node j, simply given by:

$$\tilde{H}_{jj} = \frac{\tilde{Y}_j}{F_j} \tag{7.9}$$

Finally, the nonlinear eigenvector of the resonant mode s at the excitation point j -$\tilde{\phi}_{js}$- is directly calculated as:

$$\boxed{\tilde{\phi}_{js} = \sqrt{\left(\lambda_s^2 + \Delta\tilde{\lambda}_s^2 - \omega^2\right)\left(\tilde{H}_{jj} - \sum_{r=1,r\neq s}^{M} \frac{\phi_{jr}^2}{\lambda_r^2 - \omega^2}\right)}} \tag{7.10}$$

and the nonlinear eigenvectors for the rest of the coordinates ($i = 1 \ldots N$, $i \neq j$) are easily found by:

$$\boxed{\tilde{\phi}_{is} = \frac{\left(\lambda_s^2 + \Delta\tilde{\lambda}_s^2 - \omega^2\right)\left(\tilde{H}_{ij} - \sum_{r=1,r\neq s}^{M} \frac{\phi_{ir}\phi_{jr}}{\lambda_r^2 - \omega^2}\right)}{\tilde{\phi}_{js}}, \quad i = 1 \ldots N,\ i \neq j} \tag{7.11}$$

Once the s_{th} eigenvalue and its associated eigenvectors $\{\tilde{\mathbf{\Phi}}\}_\mathbf{s}$ (a single-row column) are known, the nonlinear description for this mode is completed by filling-up the rest of the eigenvector's matrix with linear information, as follows:

$$\tilde{\mathbf{\Phi}}_{N,M} = \begin{pmatrix} \phi_{1,1} & \cdots & \vdots & \cdots & \phi_{1,M} \\ \vdots & \ddots & \vdots & \iddots & \vdots \\ \vdots & \cdots & \left\{\tilde{\mathbf{\Phi}}_\mathbf{s}\right\} & \cdots & \vdots \\ \vdots & \iddots & \vdots & \ddots & \vdots \\ \phi_{N,1} & \cdots & \vdots & \cdots & \phi_{N,M} \end{pmatrix} \tag{7.12}$$

This last step is strictly invalid, since a theoretical eigenvalue problem predicts a full matrix of nonlinear eigenvectors at any frequency. However, the incurred error is small in the vicinity of the s_{th} resonance, for fairly separated modes[1].

Once the nonlinear eigenvectors $\{\tilde{\boldsymbol{\Phi}}\}_s$ for all the coordinates in the vicinity of resonance s have been found, the global nonlinear eigenvalue can be updated by revisiting (6.18) and (7.4), as follows:

$$\left\{\boldsymbol{\Delta}\tilde{\boldsymbol{\Phi}}\right\}_s = \left\{\tilde{\boldsymbol{\Phi}}\right\}_s - \{\boldsymbol{\Phi}\}_s$$

$$\{\tilde{P}\} = \left[\boldsymbol{\Phi} + \boldsymbol{\Delta}\tilde{\boldsymbol{\Phi}}\right]^{-1}\{\tilde{Y}\}$$

$$\Delta\tilde{\lambda}_s^2 \approx \frac{\left(\boldsymbol{\Phi}^{\mathbf{T}}\tilde{G}\right)_s + \left(\boldsymbol{\Delta}\boldsymbol{\Phi}_{\mathbf{s}}^{\mathbf{T}}F\right)_s}{\tilde{P}_s}$$

where the -initially neglected- term $[\boldsymbol{\Delta}\tilde{\boldsymbol{\Phi}}]$ is now included, as a first estimation has already been achieved.

The aforementioned procedure can be iteratively implemented, improving the accuracy of the calculated nonlinear eigenvalues and eigenvectors. The flow chart was already shown in Fig. 7.2, page 127.

7.4 The FAT exemplified

The FAT will be exemplified by obtaining the nonlinear modal parameters of the Sample Cases #1 and #2, described in Appendix A. We will compare our results with the theoretical values obtained from solving the eigenvalue problem for every frequency, considered the exact solution. The NLMV, input data of the FAT, can be calculated straightforwardly from the nonlinear responses already obtained in Chapters 4 and 6.

---

[1]This issue is a drawback of the traditional nonlinear modal expansion 6.11, successfully avoided by the HMT expansion.

7.4.1 NL modal parameters for the Sample Case #1

The following results were obtained by performing a FAT calculation for the Sample Case #1:

- Fig. 7.4 shows the FAT results ("■") for the NL natural frequencies at the end of the 1st iteration, exhibiting remarkable agreement with the theoretical values (solid line).

  As expected for a cubic stiffness mechanism, the natural frequencies increase continuously as the excitation approaches resonance, suddenly dropping when the modal amplitude drops too.

  These results show that the FAT is an excellent choice for obtaining the variation of the natural frequencies when the NL mechanism is stiffness-related, without the need of an iterative procedure.

- Fig. 7.5 shows the FAT results ("■") for the NL modal damping, at the end of the 5th iteration, exhibiting remarkable agreement with the theoretical values (solid line). As expected for this class of systems, the variation is very small.

- Fig. 7.6 shows the nonlinear variation of the natural frequencies for the entire frequency range. This result was already shown in Fig. 7.4, but only for the region encompassing resonance. This time, the analyzed range is enlarged to show the effects of the neglected "nonlinear coupling term" in (7.2).

- Fig. 7.7 shows the real part of the matrix of nonlinear eigenvectors in the vicinity of resonance; the results are satisfactory, considering the small variations exhibited.

- Regarding the imaginary part of the nonlinear eigenvectors, the calculation is rather noisy, as shown in Fig. 7.8. Given that the theoretical predictions deviate very little from zero, this does not come as a surprise; actually, by considering them zero, a smoother regeneration is achieved.

- Fig. 7.9 shows the regenerated nonlinear response by the traditional nonlinear expansion, using the eigen-parameters calculated by the FAT. A close agreement with the theoretical prediction can be appreciated.
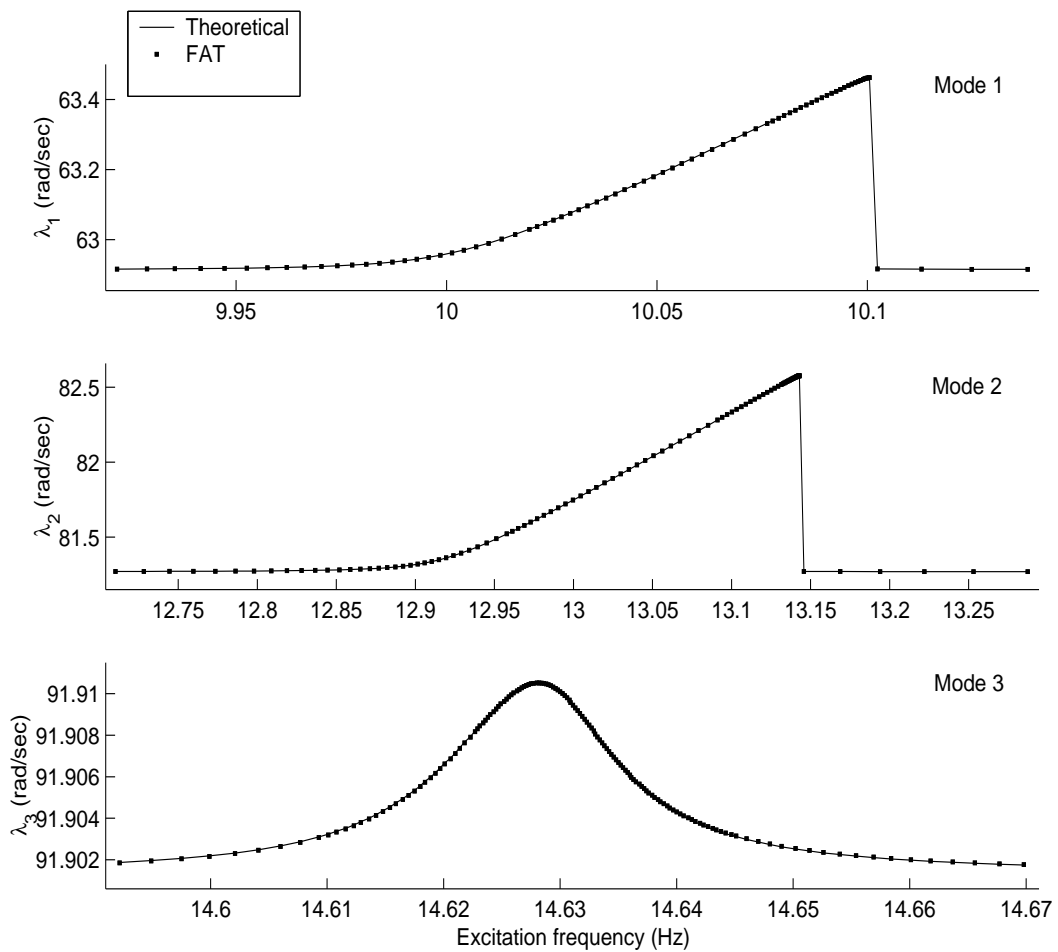

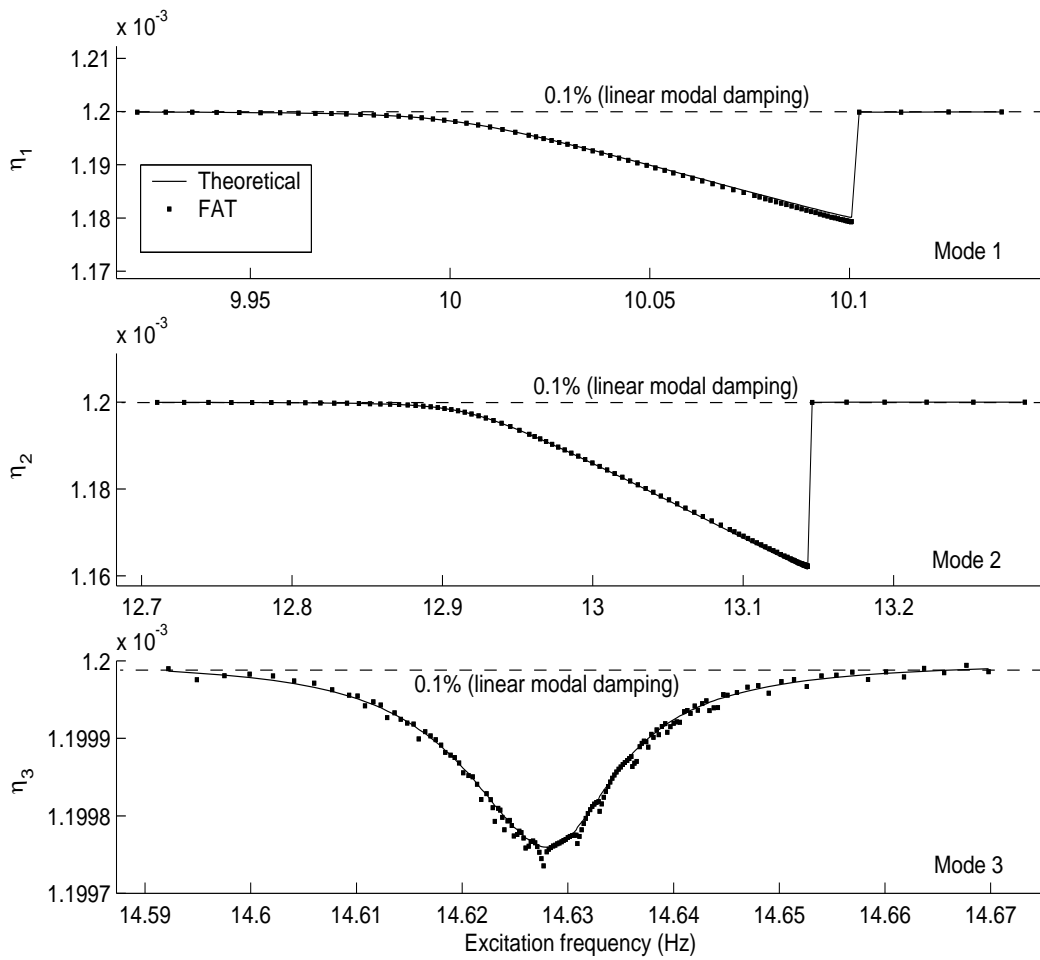Figure 7.4: Sample Case #1, nonlinear natural frequencies $(\tilde{\lambda}_r)$ at the end of the first iteration

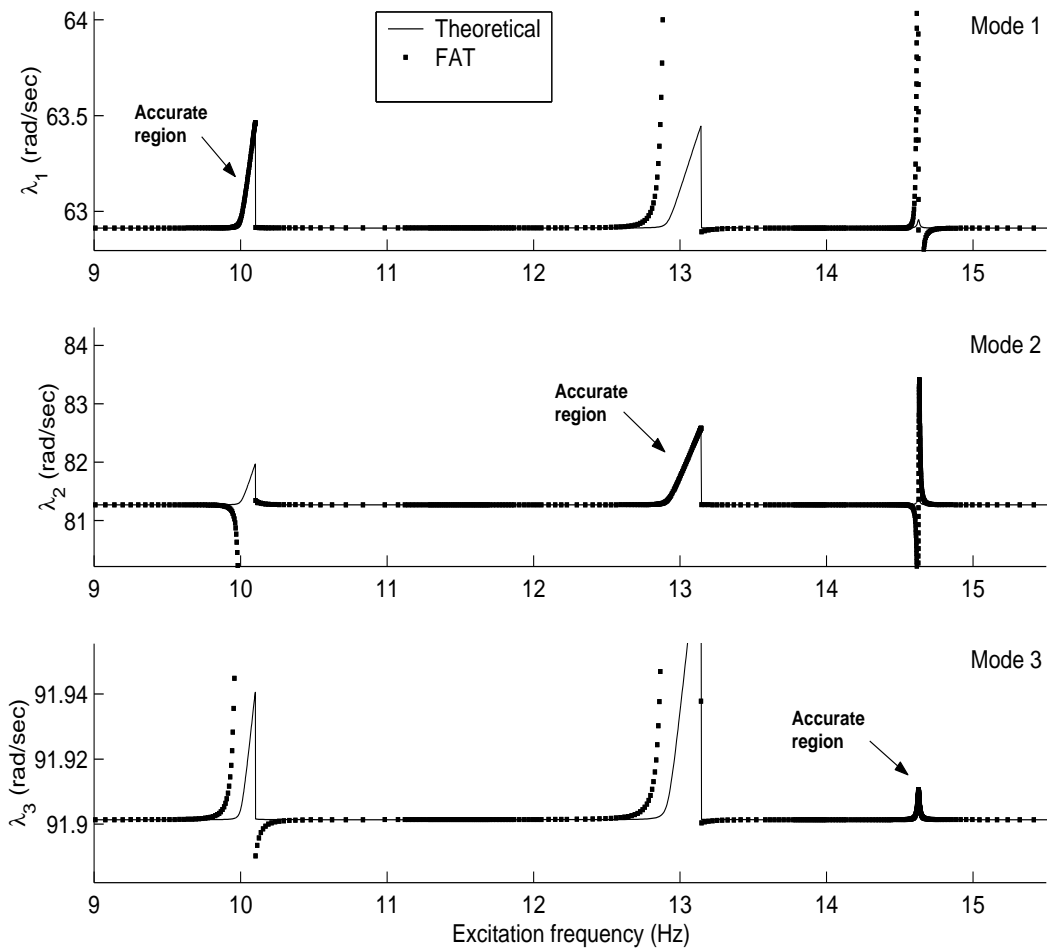Figure 7.5: Sample Case #1, nonlinear damping $(\tilde{\eta}_r)$ at the end of the fifth iteration

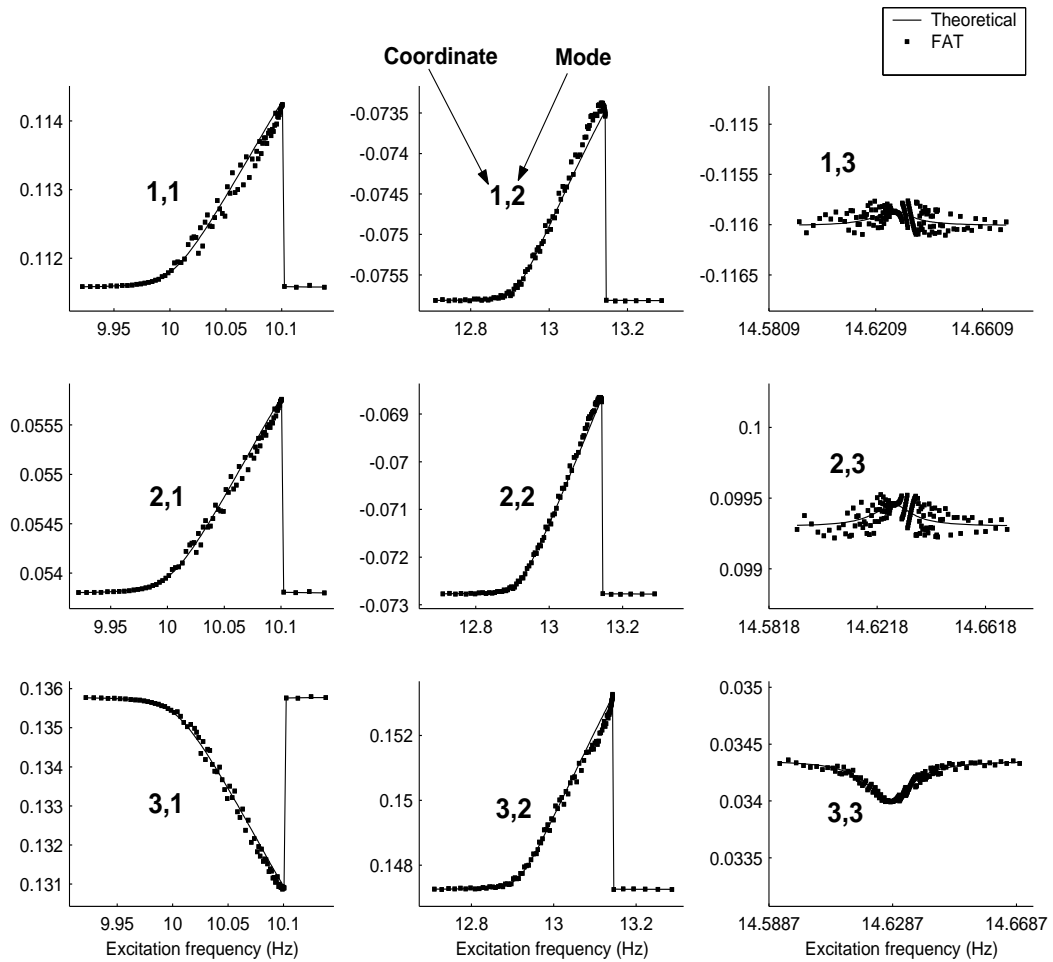Figure 7.6: Sample Case #1, inaccuracies of the FAT outside the resonant region

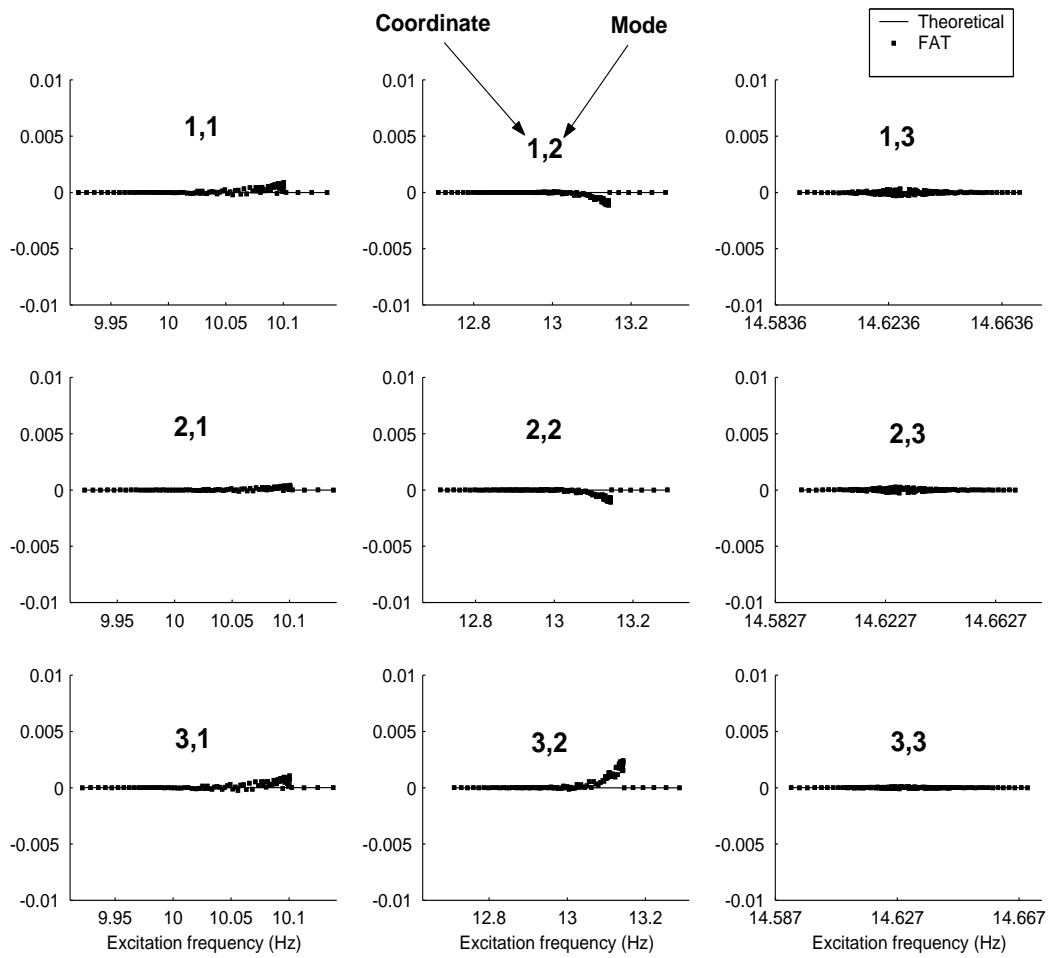Figure 7.7: Sample Case #1, real part of the nonlinear eigenvectors (in $rad/kg^{1/2}$) at the end of the fifth iteration

Figure 7.8: Sample Case #1, imaginary part of the nonlinear eigenvectors (in $rad/kg^{1/2}$) at the end of the fifth iteration
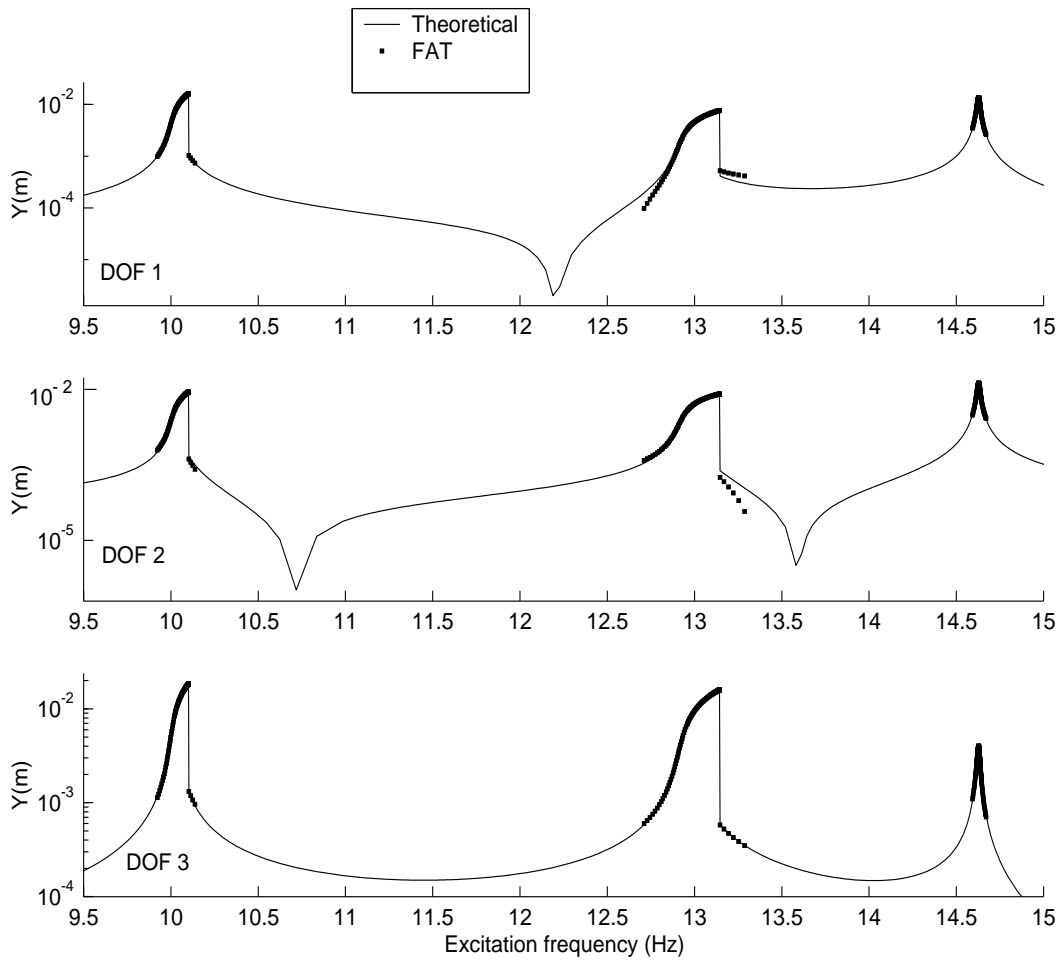
Figure 7.9: Sample Case #1, regeneration of the nonlinear response by the traditional nonlinear expansion, using the eigen-parameters calculated by the FAT

7.4.2 NL modal parameters for the Sample Case #2

The following results were obtained by performing a FAT calculation for the Sample Case #2:

- Fig. 7.10 shows the FAT results ("■") for the NL modal damping at the end of the 1st iteration, exhibiting remarkable agreement with the theoretical values (solid line).

  As expected for a friction damping mechanism, the overall modal damping changes continuously as the excitation approaches resonance, exhibiting a minimum/maximum exactly at resonance.

  These results show that the FAT is an excellent choice for obtaining the variation of modal damping when the NL mechanism is velocity-dependant (such as in friction damping), without the need of an iterative procedure.

- Fig. 7.11 shows the FAT results ("■") for the nonlinear natural frequencies, at the end of the 5th iteration, exhibiting remarkable agreement with the theoretical values (solid line). As expected for this class of systems, the variation is very small.

- Fig. 7.12 shows the nonlinear variation of the modal damping for the entire frequency range. This result was already shown in Fig. 7.10, but only for the region encompassing resonance. This time, the analyzed range is enlarged to show the effects of the neglected "nonlinear coupling term" in (7.2).

- Fig. 7.13 shows the imaginary part of the matrix of nonlinear eigenvectors in the vicinity of resonance; the results are satisfactory, considering the small variations exhibited.

- Regarding the real part of the nonlinear eigenvectors, the calculation is rather noisy, as shown in Fig. 7.14. Given that the theoretical predictions deviate very little from the linear values, this doesn't come as a surprise; actually, by considering them to remain linear, a smoother regeneration is achieved.

- Fig. 7.15 shows the regenerated nonlinear response by the traditional non-linear expansion, using the eigen-parameters calculated by the FAT. A close agreement with the theoretical prediction can be appreciated.
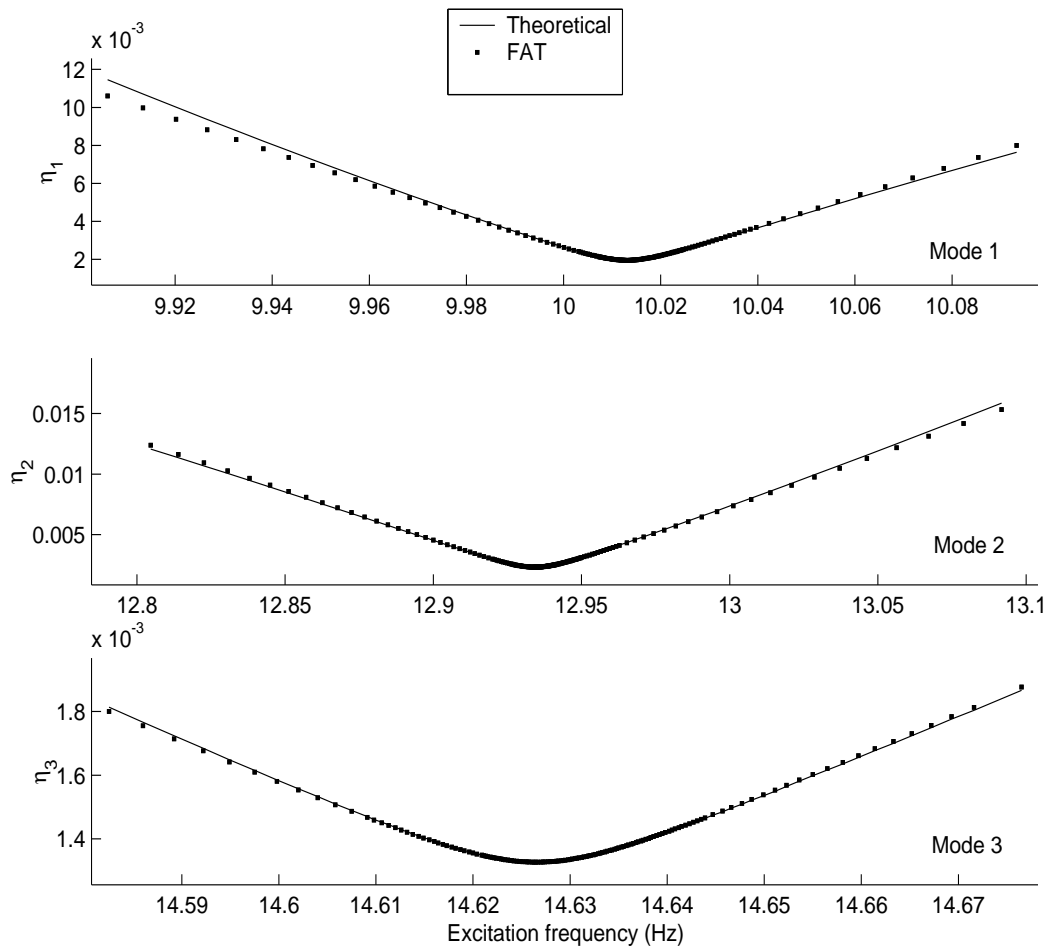
Figure 7.10: Sample Case #2, nonlinear modal damping $(\tilde{\eta}_r)$ at the end of the first iteration
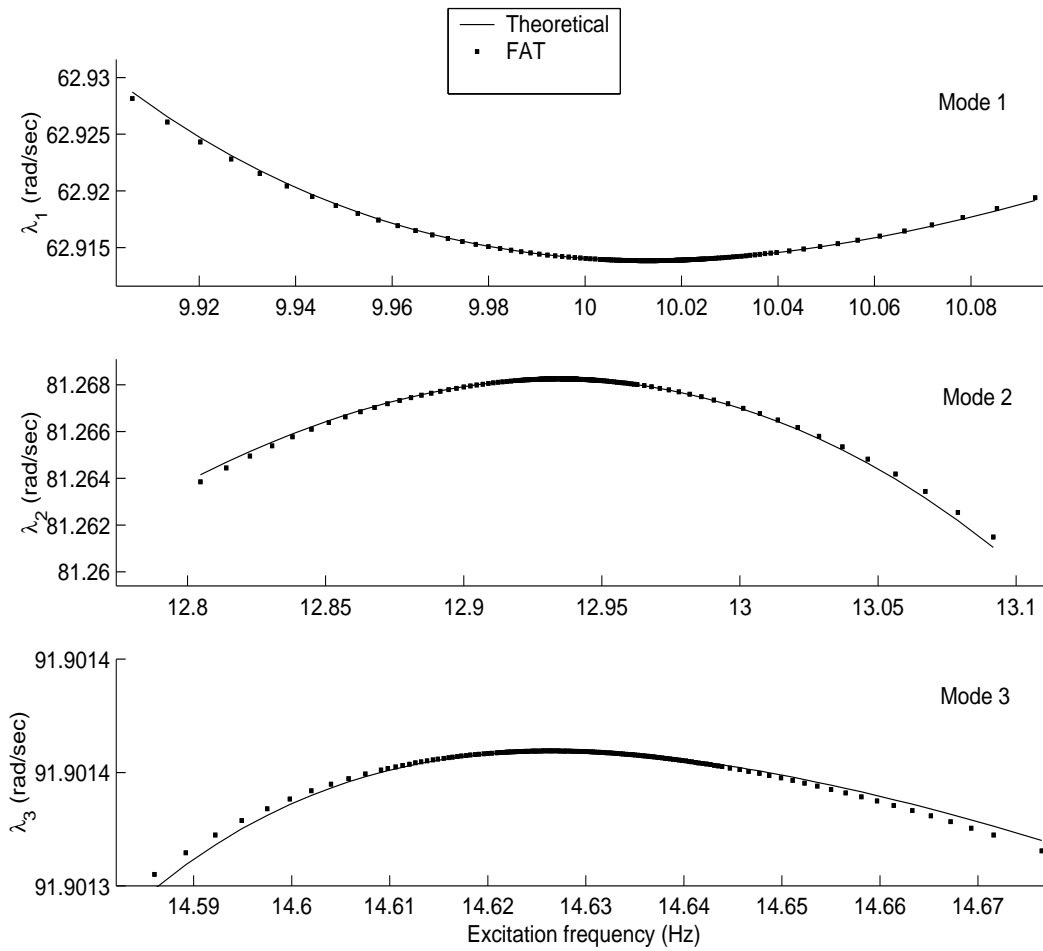
Figure 7.11: Sample Case #2, nonlinear natural frequencies $(\tilde{\lambda}_r)$ at the end of the fifth iteration
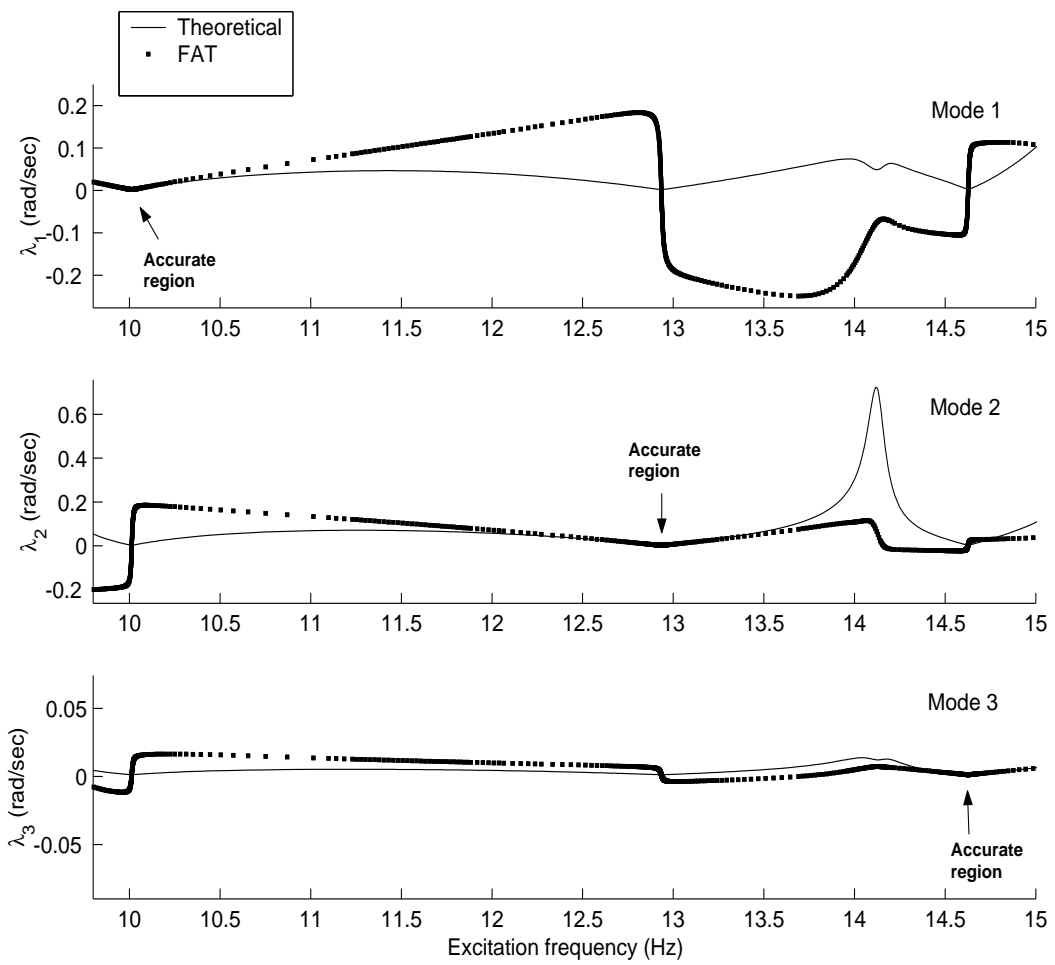
Figure 7.12: Sample Case #2, inaccuracies of the FAT outside the resonant region

Figure 7.13: Sample Case #2, imaginary part of the nonlinear eigenvectors (in $rad/kg^{1/2}$) at the end of the fifth iteration

Figure 7.14: Sample Case #2, real part of the nonlinear eigenvectors (in $rad/kg^{1/2}$) at the end of the fifth iteration

Figure 7.15: Sample Case #2, regeneration by the traditional nonlinear expansion, using the eigen-parameters calculated by the FAT

7.5 Concluding remarks

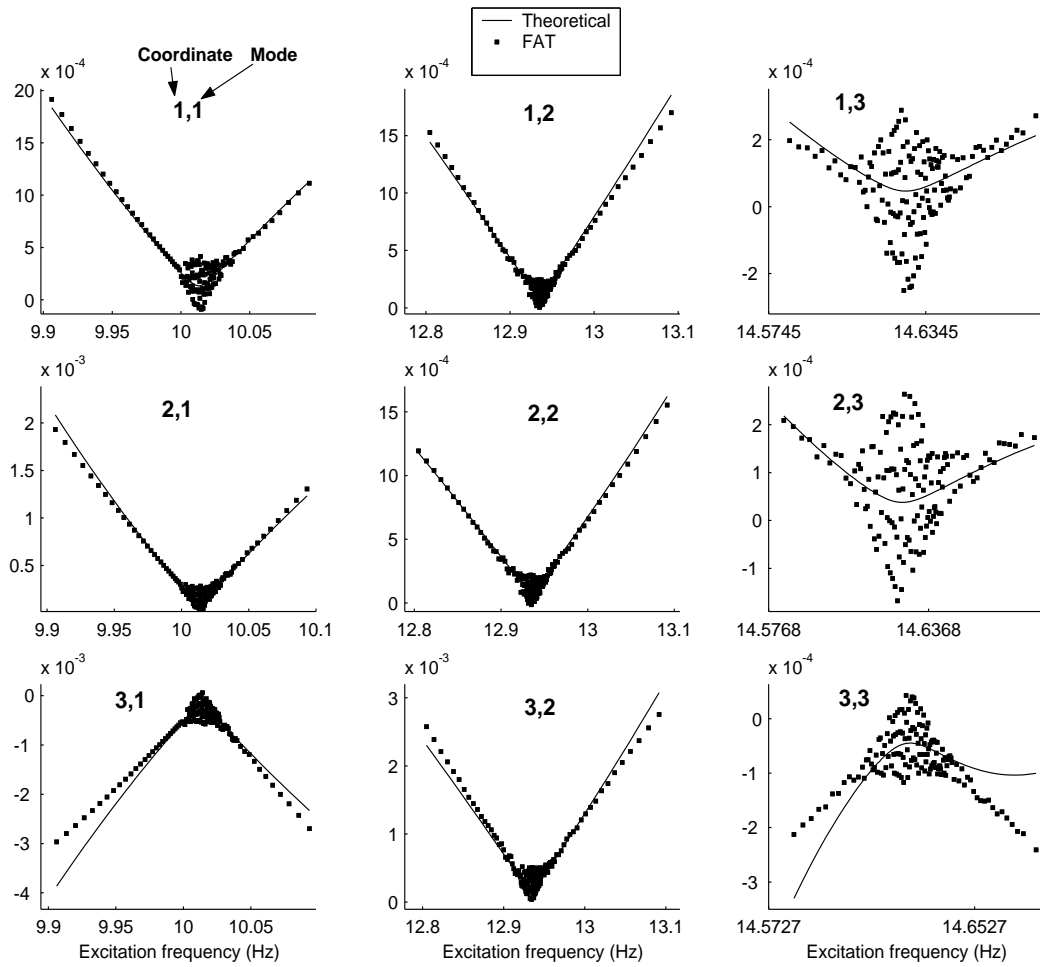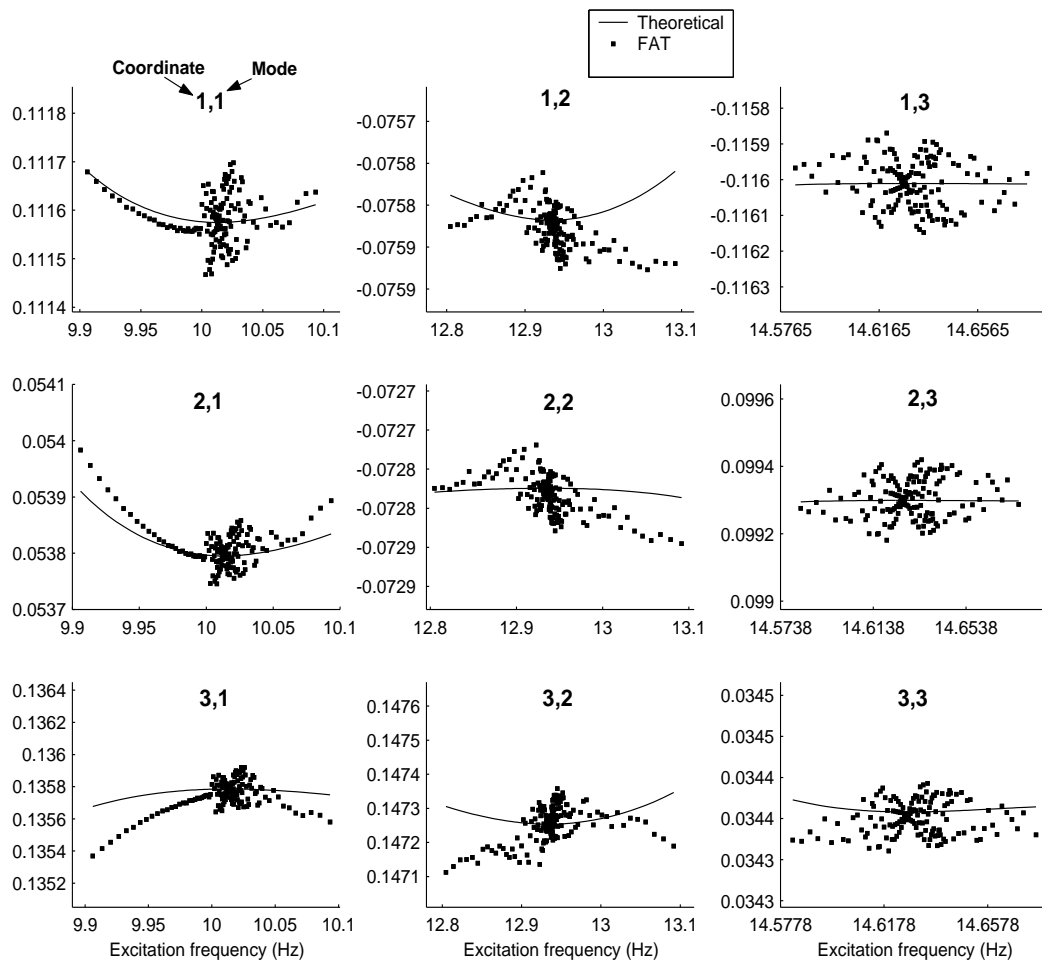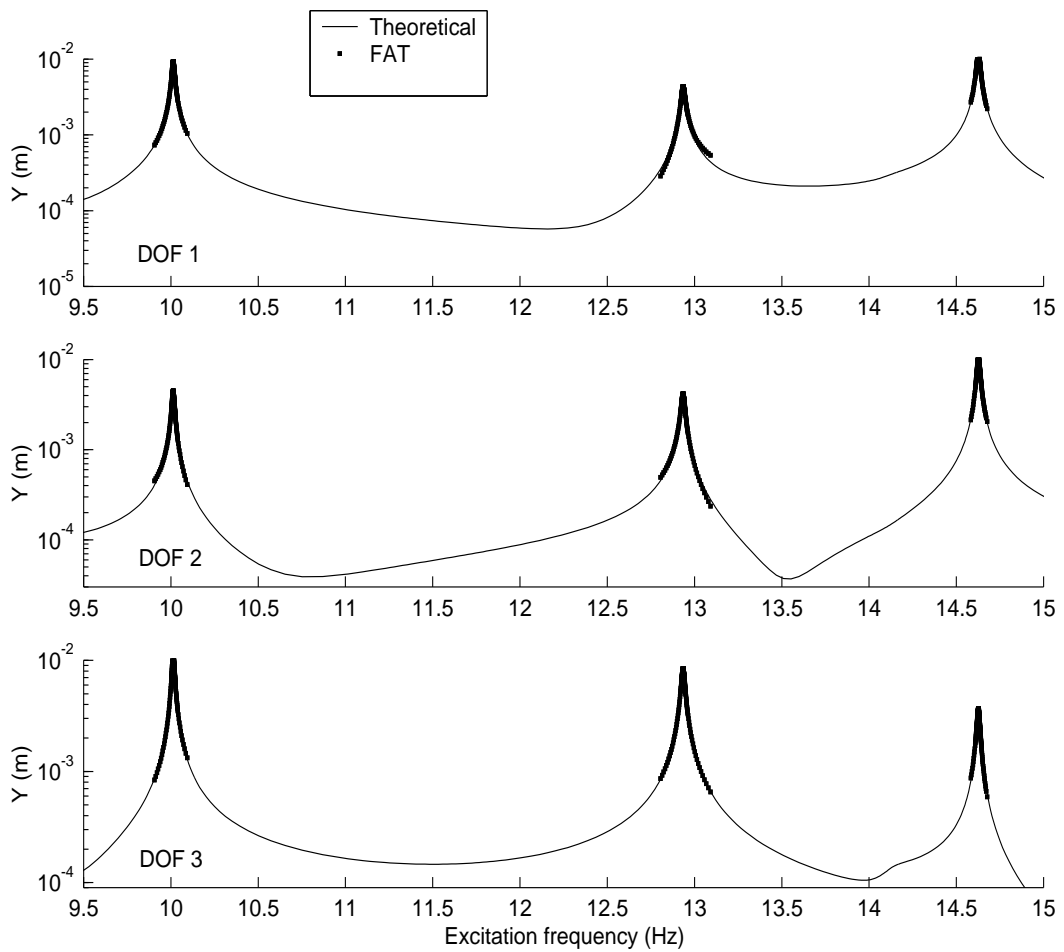The aim of this chapter has been the introduction of the "fast approximation technique" (FAT) as a tool for decoupling the nonlinear information contained in the NLMV, into single-modal parameters. The latter are the well-known nonlinear eigenvalues ($\tilde{\lambda}^2$) and eigenvectors ($\tilde{\boldsymbol{\Phi}}$), which are of standardized use in other NLMA methods. On a minor point, the FAT offers a comparative tool between the traditional (6.11) and the HMT (6.28) nonlinear modal expansions.

Although the NLMV -basic input data of the FAT- can be calculated based on the NL response $\{\tilde{Y}\}$ and a full description of the nonlinear component $\{\tilde{G}\}$[1], forthcoming developments will show that it can also be *extracted* straightforwardly from experimental measurements. This will reveal the FAT as a highly valuable tool, allowing the *analytical* derivation of nonlinear eigenvalues and eigenvectors, based exclusively on these same measurements. No previous knowledge about the position or type of the nonlinearities will be required to accomplish this.

Currently, the standard approach for the extraction of NL modal parameters is based on nonlinear solvers. They are prone to ill-conditioning, due to the small variations happening both in the eigenvectors and eigenvalues, which are, nevertheless, significant when combined. The FAT greatly simplifies this extraction.

On a more general remark, the FAT provides analytical grounds for previous works (31), (30), (68). Based on numerical/experimental observations, they suggested an invariant relationship between the nonlinear modal eigenvalues and their correspondent modal amplitudes. This relationship is analytically confirmed by the FAT.

In the author's opinion, the FAT is the single most important theoretical contribution of this research, as well as an essential ingredient of the main NLMA method produced in this thesis (R-HMT, Chapter 8).

---

[1]An improbable situation in an experimental testing.

Chapter 8

The reverse-HMT (R-HMT) method for the identification of large structures

8.1 Introduction

In spite of earlier efforts and the review of several approaches, a fundamental problem for analysing nonlinear systems still persists: there is a lack of a unified method which can seamlessly handle general nonlinear systems, including large engineering structures. There is a need for a method that can provide, without gross simplifications, a full and unambiguous identification every time, using data acquired within the common restrictions of an experimental environment.

If we were asked to produce a list of attributes we would expect from such a method, we would probably end up with something like this:

- Simple to use, so engineers will embrace it.

- Compatible with LMA and standard FE techniques, but does not require a FEM model.

- Relies as little as possible on expert input.

- Size of the model does not matter, within the usual computational restrictions.

- Works with measured data acquired *anywhere* in the system. The availability of more measurements would simply yield higher-quality results.

- Allows a neat separation of the system into linear and nonlinear components, previous to any quantification stage.

- Automatic detection of the nonlinear modes and the type of nonlinearity.

- Automatic and unambiguous localization of the nonlinear elements, provided there are associated measurements.

- If there are no such measurements, the method should still provide a valid mathematical model within a useful range. It should allow, at least, the regeneration/prediction of the response at selected DOFs for different levels of excitation. This is one of the main aims of any method of this kind.

- The method should be numerically stable, relying on proven linear solvers or linear least-squares algorithms. If nonlinear solvers are required, the number of variables should be as small as possible. A good initial guess should be available in such cases.

- The method should not be case sensitive.

We intend to introduce a method that represents a step forward towards this ideal. This will be achieved by gathering the previously developed techniques into a general methodology.

The method that will be presented here is, basically, a *reverse-path* version of the HMT method, thus called the R-HMT. This technique allows the extraction of the NLMV from just a few measurements, made *anywhere* in the system. The NLMV contains all the information needed to characterize both the type and position of the nonlinear elements, provided that they are included in the measurements.

The FAT, introduced earlier as a comparative tool, now stands as an essential ingredient of this method, decoupling the extracted NLMV into single-modal NL parameters. These are further converted to polynomials, providing an invariant

NL model valid for any excitation level[1]. This path provides a "black box" model, capable of regenerating/predicting responses within a useful range, even with scarce data.

An interesting tool, the "nonlinear modal grade", is developed to quantify, in an objective way, the strength of the nonlinearity in a given mode. This allows the automatic selection of those modes to be included in a nonlinear analysis, the rest taken as linear. In a *modal superposition* context, this approach greatly improves the computational efficiency.

Finally, the precise localization of the NL elements in a large system is achieved by a simple linear least-squares operation over a *nonlinear region* of arbitrary size. The results of this technique are unambiguous provided that the analyzed frequency range is a fair representation of the system.

The reader is strongly advised to read Chapters 3 to 7 before attempting to read this, as they contain essential information for the derivations presented here. A brief look to reference (30) is also recommended.

The following sections are organized sequentially, simulating successive stages for the application of the R-HMT method. Then, a sample case of a large structure[2] will be solved, applying the same procedure.

A flow chart of the R-HMT method is shown in Fig. 8.1.

8.2 Stage I: pre-processing data

The input data must be organized in a few regions, which are defined next:

- N: total number of DOFs of the nonlinear system, according to a discretization previously made by the analyst.

- $\Re$: the *measured region*, a vector containing all the measured DOFs. The measurements can be made anywhere in the system.

- f: the forced DOFs at which the system is being excited[3]. These must be also measured ($f \in \Re$), in order to provide the mass-normalization. It is

---

[1] Within a range.

[2] Sample Case #3, described in Appendix B.

[3] The developments in this research account for a multi-excitation test, except when the opposite is highlighted.
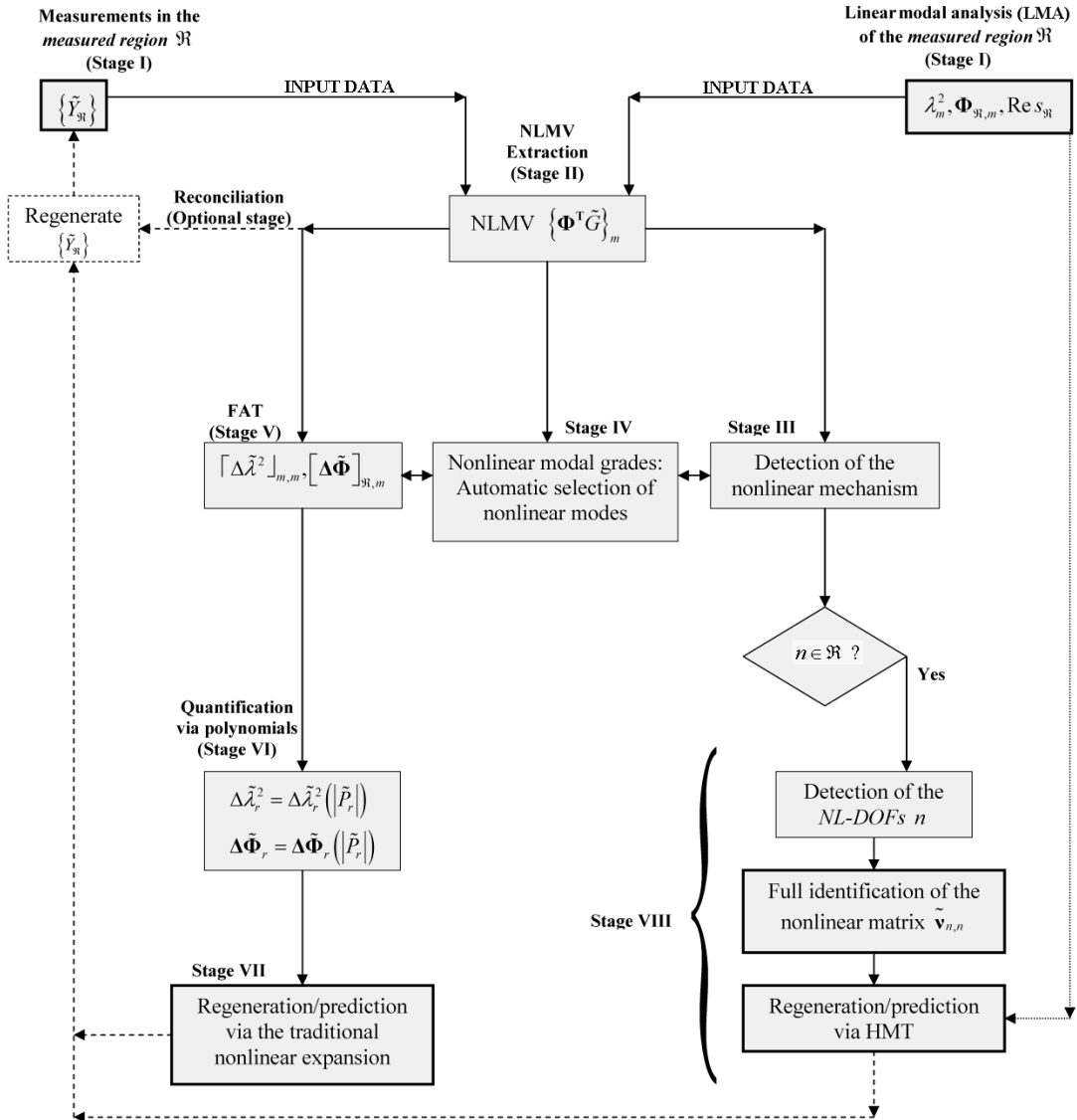
Figure 8.1: Flow diagram of the reverse-HMT (R-HMT) method

assumed that all excitation is applied at a single frequency, although the phases between individual forces can be different.

- m: the number of identified modes within the analyzed frequency range, typically the first few ones.

- m_{NL}: the number of nonlinear modes, as a subset of m. This definition is required to select the modes to be included in a nonlinear analysis, the rest being assumed as linear. This task is usually performed by the analyst, although an automated procedure will be developed here to tackle the issue.

The following definitions, although not part of the input data, will be useful for the derivation of the method:

- M: the total number of modes of the system under analysis (infinity, for a continuous system).

- n: the *NL-DOFs*, those DOFs associated with discrete NL elements.

The following relations must hold:

$$\begin{aligned} f \in \Re \in N, \quad &\text{typically} \quad f \ll \Re \ll N \\ m_{NL} \in m \in M, \quad &\text{typically} \ m_{NL} < m \ll M \end{aligned} \tag{8.1}$$

The following relation is optional, but essential for the localization of the *NL-DOFs*:

$$n \in \Re, \quad \text{typically } n \ll \Re \tag{8.2}$$

Completing the input data, a linear modal analysis (LMA) of the *measured region* $\Re$ for the m modes must be performed. This will provide the linear eigenvalues and eigenvectors $\lceil \lambda \rfloor, [\boldsymbol{\Phi}]$, as well as the linear residuals due to higher-modes, $\{Res\}$.

8.3   Stage II: NLMV extraction

The aim of this section is to separate the system into its linear and nonlinear components, prior to any quantification stage. This can be achieved by extracting

the NLMV $\{\boldsymbol{\Phi}^{\mathbf{T}}\tilde{G}\}$, expressed in (6.23), which contains all the nonlinearities in the system.

The HMT expansion, defined in (6.27), is rewritten here:

$$\left\{\tilde{Y}\right\}_N = [\boldsymbol{\Phi}]_{N,M}\,\lceil\lambda^2 - \omega^2\rfloor^{-1}_{M,M}\,\{\tilde{\chi}\}_M \tag{8.3}$$

where $\{\tilde{Y}\}$ is the vector of nonlinear responses, $[\boldsymbol{\Phi}]$ is the *linear* matrix of mass normalized eigenvectors, $\lceil\lambda^2 - \omega^2\rfloor$ is the diagonal (symbolized by the brackets "$\lceil\ \rfloor$") matrix of *linear* eigenvalues, ω is the excitation frequency and $\{\tilde{\chi}\}$ is the *extended* NLMV of (6.26).

Equation 8.3 can be subdivided, row-wise, in the measured ($\Re$) and unmeasured ($N-\Re$) responses. Column-wise, it can also be subdivided in those modes inside (m) and outside ($M-m$) the analyzed frequency range, as follows:

$$\left\{\begin{array}{c}\tilde{Y}_{N-\Re}\\\tilde{Y}_{\Re}\end{array}\right\}_N =$$

$$\left[\begin{array}{cc}\boldsymbol{\Phi}_{(N-\Re),m} & \boldsymbol{\Phi}_{(N-\Re),(M-m)}\\\boldsymbol{\Phi}_{\Re,m} & \boldsymbol{\Phi}_{\Re,(M-m)}\end{array}\right]_{N,M}\left[\begin{array}{cc}(\lambda^2-\omega^2)_m & 0\\0 & (\lambda^2-\omega^2)_{M-m}\end{array}\right]^{-1}_{M,M}\left\{\begin{array}{c}\tilde{\chi}_m\\\tilde{\chi}_{M-m}\end{array}\right\}_M \tag{8.4}$$

Separating (8.4) into m and $(M-m)$ components, we have:

$$\left\{\begin{array}{c}\tilde{Y}_{N-\Re}\\\tilde{Y}_{\Re}\end{array}\right\}_N =$$

$$\left[\begin{array}{c}\boldsymbol{\Phi}_{(N-\Re),m}\\\boldsymbol{\Phi}_{\Re,m}\end{array}\right]_{N,m}\qquad\lceil\lambda^2-\omega^2\rfloor^{-1}_{m,m}\quad\{\tilde{\chi}_m\}\qquad + \tag{8.5}$$

$$\left[\begin{array}{c}\boldsymbol{\Phi}_{(N-\Re),(M-m)}\\\boldsymbol{\Phi}_{\Re,(M-m)}\end{array}\right]_{N,(M-m)}\lceil\lambda^2-\omega^2\rfloor^{-1}_{\substack{M-m,\\M-m}}\{\tilde{\chi}_{M-m}\}$$

where the second term of the RHS can be seen as the nonlinear residual ($\tilde{Res}$) component of the higher modes in the measured frequency range:

$$\left\{\begin{array}{c}\tilde{Y}_{N-\Re}\\\tilde{Y}_{\Re}\end{array}\right\}_N = \left[\begin{array}{c}\boldsymbol{\Phi}_{(N-\Re),m}\\\boldsymbol{\Phi}_{\Re,m}\end{array}\right]_{N,m}\lceil\lambda^2-\omega^2\rfloor^{-1}_{m,m}\{\tilde{\chi}_m\} + \left\{\begin{array}{c}\tilde{Res}_{N-\Re}\\\tilde{Res}_{\Re}\end{array}\right\}_N \tag{8.6}$$

$\{\tilde{Y}_{N-\Re}\}$ represents the unmeasured responses, so we discard the corresponding rows and further develop the measured component $\{\tilde{Y}_\Re\}$:

$$\left\{\tilde{Y}_\Re\right\} = [\boldsymbol{\Phi}_{\Re,m}] \lceil\lambda^2 - \omega^2\rfloor^{-1}_{m,m} \{\tilde{\chi}_m\} + \left\{\tilde{R}es_\Re\right\} \tag{8.7}$$

where $\{\tilde{R}es_\Re\}$ is the nonlinear residual of the (higher) modes outside the analyzed frequency range, for the measured ($\Re$) coordinates only:

$$\left\{\tilde{R}es_\Re\right\} = \left[\boldsymbol{\Phi}_{\Re,(M-m)}\right] \lceil\lambda^2 - \omega^2\rfloor^{-1}_{\substack{M-m,\\M-m}} \{\tilde{\chi}\}_{M-m} \tag{8.8}$$

Its linear counterpart, on the other hand, is given by:

$$\{\mathrm{Res}_\Re\} = \left[\boldsymbol{\Phi}_{\Re,(M-m)}\right] \lceil\lambda^2 - \omega^2\rfloor^{-1}_{\substack{M-m,\\M-m}} \left\{\boldsymbol{\Phi}^T F\right\}_{M-m} \tag{8.9}$$

which can be found by performing a LMA in the *measured region* $\Re$ (4).

If the analyzed frequency range is extended well beyond those modes exhibiting strong nonlinearities (typically the few first ones), then the nonlinear effects of $\{\tilde{\chi}_{M-m}\}$ are severely attenuated for these modes, and it can be assumed that:

$$\left\{\tilde{R}es_\Re\right\} \approx \{\mathrm{Res}_\Re\} \tag{8.10}$$

Introducing (8.10) in (8.7), we have:

$$\left\{\tilde{Y}_\Re\right\} = [\boldsymbol{\Phi}_{\Re,m}] \lceil\lambda^2 - \omega^2\rfloor^{-1}_{m,m} \{\tilde{\chi}_m\} + \{\mathrm{Res}_\Re\} \tag{8.11}$$

Our aim is to extract the *extended* NLMV $\{\tilde{\chi}_m\}$. Solving for this variable, it follows that:

$$\{\tilde{\chi}_m\} = \left([\boldsymbol{\Phi}_{\Re,m}] \lceil\lambda^2 - \omega^2\rfloor^{-1}_{m,m}\right)^{-1} \left\{\tilde{Y}_\Re - \mathrm{Res}_\Re\right\} \tag{8.12}$$

and we finally arrive at:

$$\boxed{\{\tilde{\chi}_m\} = \lceil\lambda^2 - \omega^2\rfloor_{m,m} [\boldsymbol{\Phi}_{\Re,m}]^+ \left\{\tilde{Y}_\Re - \mathrm{Res}_\Re\right\}} \tag{8.13}$$

where:

$$[\boldsymbol{\Phi}_{\Re,m}]^+ = \left([\boldsymbol{\Phi}_{\Re,m}]^T [\boldsymbol{\Phi}_{\Re,m}]\right)^{-1} [\boldsymbol{\Phi}_{\Re,m}]^T \tag{8.14}$$

is the Moore-Penrose pseudo-inverse (69), as the direct inversion $[\boldsymbol{\Phi}_{\Re,m}]^{-1}$ does not strictly exist. The pseudo-inverse minimizes the sum of the squares of all entries, providing a best-fit solution, in a least-squares sense. The SVD (4) decomposition can also be used for this end, probably being a more robust alternative.

Once $\{\tilde{\chi}_m\}$ has been extracted, the *standard* NLMV can be recovered by simply applying (6.26):

$$\left\{\boldsymbol{\Phi}^{\mathbf{T}}\tilde{G}\right\}_m = \left\{\boldsymbol{\Phi}^{\mathbf{T}}F\right\}_m - \{\tilde{\chi}\}_m \tag{8.15}$$

where

$$\left\{\boldsymbol{\Phi}^{\mathbf{T}}F\right\}_m = [\boldsymbol{\Phi}_{f,m}]^T \{F\}_f \tag{8.16}$$

is the linear modal force, depending exclusively on the f excited DOFs and the m measured modes.

Equation (8.13) deserves some important remarks:

- It represents a straightforward calculation, since all the terms in the RHS are known, a feature which makes the extraction process a very robust procedure. Although $\{\tilde{\chi}_m\}$ does not, per se, represents a final identification, it does allow a neat separation of the linear and nonlinear components of the system prior to a quantification stage. This is an important achievement in itself.

- The posed problem is well over-determined, because typically $\Re \gg m$. This feature allows small inconsistencies in the data to be averaged out, in a least-squares sense (4). Observe that the minimum number of measurements required to extract $\{\tilde{\chi}_m\}$ is $\Re = m$. This condition should be attainable in any experiment.

- $[\boldsymbol{\Phi}_{\Re,m}]^+$ needs to be evaluated just once, since it contains pure *linear* parameters only. Thus, the extraction does not involve costly matrix inversions. Note that the eigenvalues λ^2 are also linear, and that the only nonlinear variable in the RHS is $\{\tilde{Y}_{\Re}\}$, which is known for all the frequency range.

- $\{\text{Re}s_{\Re}\}$ typically emerges from a previous LMA of the measured linear modes. D. J. Ewins (4) describes several ways in which the residuals can

be handled. They range from rough approximations as mass and spring elements, to more sophisticated approaches treating the residual as a "pseudomode", lying outside the measured frequency range. Any of these is compatible with the present formulation.

For this work, the residual is simply treated as a vector containing the necessary corrections that allow a successful regeneration of the linear FRFs.

- The NLMV $\{\mathbf{\Phi^T}\tilde{G}\}_m$ is the main result of the extraction process. It represents the nonlinear component of the system, although not explicitly localized or quantified yet.

  Note that the only approximation incurred in extracting $\{\mathbf{\Phi^T}\tilde{G}\}_m$ is the linearized residual $\{\text{Res}_\Re\}$. For an extended frequency range well beyond the nonlinear modes, the error should be very small.

  A rule of thumb for the practicing engineer is as follows: *during a NLMA, the measured frequency range should be extended as far as possible from the highest nonlinear mode.*

8.4 Optional stage: reconciliation

The extraction process introduced in Section 8.3 allows the implementation of an *optional* modal procedure known as "reconciliation", in which the responses are regenerated by distinct sets of redundant data. The degree of matching among the regenerated responses is related to the overall quality of the measurements, where the non-matching sets may indicate poor data.

We are in the favourable position of performing a reconciliation with the information hitherto obtained, before committing to a lengthy quantification stage.

This is achieved by taking several subsets of $\Re$ of size equal to m, thus generating various square sub-matrices $[\mathbf{\Phi}_{m,m}]$ and associated sub-vectors $\{\tilde{Y}_m\}$. Each square subsystem (8.13) is solved, and the extracted $\{\tilde{\chi}_m\}$ is further used to regenerate *all* the measured responses $\Re$ at once, by using the direct path of the HMT (8.11). The regenerated responses should be nearly identical for all subsets, also matching the experimental measurements $\{\tilde{Y}_\Re\}$.

The non-matching subsets can be spotted and either re-measured or simply removed. Then, a consistent group of subsets can be used all at once in (8.13), thus providing an improved least-square extraction of the NLMV.

8.5 Stage III: detection of the nonlinear mechanism

A qualitative technique to determine the nonlinear mechanism acting in a system was introduced in Section 5.4. This was based on the visual assessment of the geometric "footprint" of the NLV $\{\tilde{G}\}$, and it was proved to be effective to discriminate between cubic stiffness and friction damping nonlinearities. General guidelines were provided to allow a consistent detection and it was mentioned that the identification of other nonlinear types could be easily incorporated to this technique.

In this section, we will explore the extension of this idea to the modal equivalent of the NLV, namely the NLMV $\{\mathbf{\Phi^T}\tilde{G}\}$. Perhaps the best way to provide useful guidelines is to perform a nonlinearity detection by means of a numerical example.

Fig. 8.2 shows the extracted NLMV, for the first three modes only, of a system with different nonlinearities. Following is a brief discussion of these results.

- Fig. 8.2(a) displays the magnitude of the NLMV for purely cubic stiffness-type nonlinearities. It can be seen that these functions resemble the geometry of the nonlinear FRFs, exhibiting peaks at all resonances, with the characteristic "jump" found in the nonlinear modes. It can also be verified that the NLMV increases monotonically with the overall level of the responses, as expected from the relationship (3.9).

- Fig. 8.2(b) displays the magnitude of the NLMV for purely friction damping nonlinearities. A distinctive feature is that these functions exhibit well-defined regions at a constant value, with sudden jumps at some frequencies. The nonlinear force also remains constant in the vicinity of resonance, in agreement with the friction damping model (3.21). A glance at the imaginary part of this NLMV (not shown) would confirm that this force changes
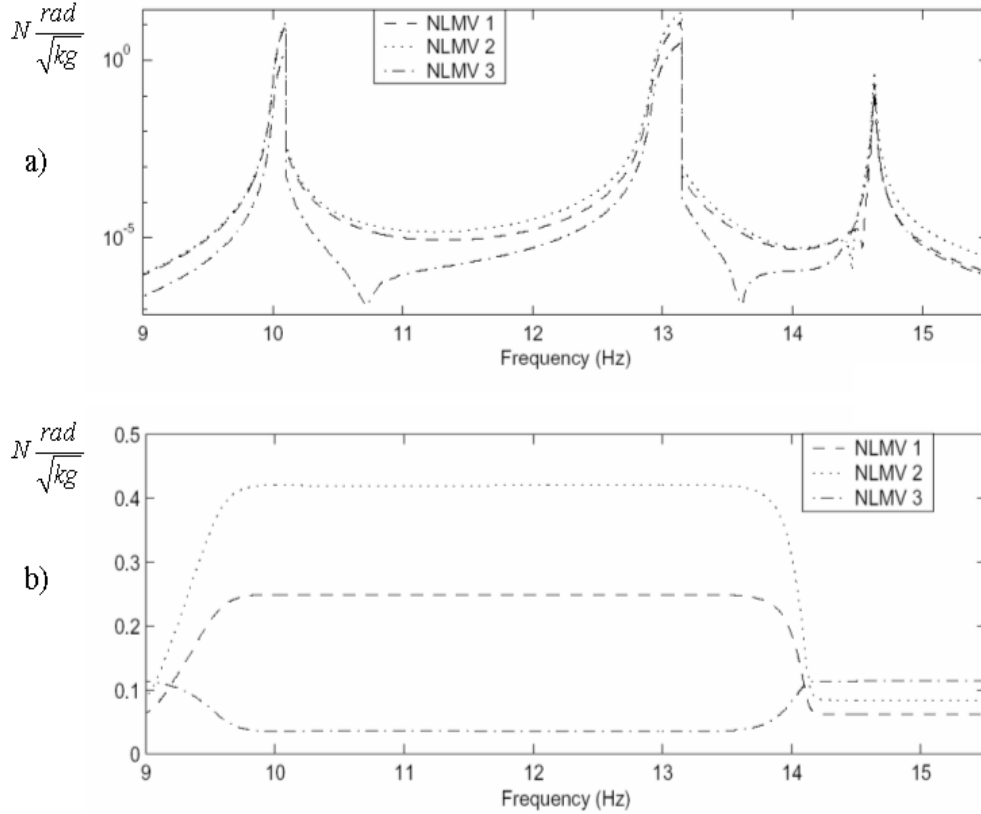
Figure 8.2: (a)-NLMV of a cubic stiffness system. (b)-NLMV of a friction damping system

sign exactly at resonance, providing further evidence of a friction damping mechanism.

Fortunately, both "footprints" exhibit a completely different behaviour from each other, providing a practical detection tool for any system regarding of its size. In later sections, we will use this technique to analyze the NLMV of a large system, applying the aforementioned guidelines.

8.6   Stage IV: degree of nonlinearity in a nonlinear mode

When performing a nonlinear detection, an interesting issue is the quantification of the degree of modal nonlinearity. A legitimate question can be posed:

"How do we know, objectively, if the extracted NLMV is significant to the problem, or even related to the nonlinearities?". An obvious answer might be "It has to be, since the response exhibits significant nonlinear effects". However, this answer pre-assumes that the distortions in the response are due to nonlinearities, thus discarding systematic errors and many other factors, which are all included in the NLMV.

Indeed, the author has not been able to find a practical tool which allows an objective quantification of the degree of nonlinearity in a mode. Instead, loose terms such as "weakly nonlinear", "moderately nonlinear" and "strongly nonlinear" are shamelessly[1] used in the literature. Here, we will present a simple but, hopefully, effective technique to answer this question. Although it is based on experimental observations, it is possible to provide some analytical support, which is given first:

The nonlinear modal space was described by (6.22):

$$\lceil \lambda^2 - \omega^2 \rfloor \left(\mathbf{I} + \mathbf{\Phi^{-1} \Delta \tilde{\Phi}} \right) \{\tilde{P}\} + \{\mathbf{\Phi^T} \tilde{G}\} = \{\mathbf{\Phi^T} F\} \qquad (8.17)$$

and its linear counterpart was described in (6.6)

$$\lceil \lambda^2 - \omega^2 \rfloor \{P\} = \{\mathbf{\Phi^T} F\} \qquad (8.18)$$

In the vicinity of resonance of a given mode, the "nonlinear coupling term" $\mathbf{\Phi^{-1} \Delta \tilde{\Phi}}$ can be neglected, as already argued in Sections 6.3 and 7.2. Thus, by comparing the last two expressions, it can be realized that the introduction of the NLMV $\{\mathbf{\Phi^T} \tilde{G}\}$ solely alters the balance between a linear and a nonlinear normal mode.

In other words, while the linear modal force $\{\mathbf{\Phi^T} F\}$ remains constant in (8.17), the changes introduced by the NLMV $\{\mathbf{\Phi^T} \tilde{G}\}$ are mainly reflected in the

---

[1]The author still uses these terms on a regular basis

transition $\{P\} \to \{\tilde{P}\}$. It follows that, if $\{\mathbf{\Phi^T}\tilde{G}\}$ is significant when compared to the constant value $\{\mathbf{\Phi^T}F\}$, then the transition $\{P\} \to \{\tilde{P}\}$ should be noticeable, in the form of the well-known FRF distortions.

Of course, the transition from linear to nonlinear occurs smoothly for continuous nonlinearities, and it would be equally unfounded to try to establish fixed thresholds to define the degree of nonlinearity. Nonetheless, during the various simulations carried out during this research it was found that thresholds that relate well with the "standard" terminology can be defined as:

$$
\begin{aligned}
0 < \left(\frac{\max\left|(\mathbf{\Phi^T}\tilde{G})\right|}{|\mathbf{\Phi^T}F|} \right)_r &< 1, && \text{weakly nonlinear} \\[2ex]
1 \leq \left(\frac{\max\left|(\mathbf{\Phi^T}\tilde{G})\right|}{|\mathbf{\Phi^T}F|} \right)_r &< 10, && \text{moderately nonlinear} \\[2ex]
10 \leq \left(\frac{\max\left|(\mathbf{\Phi^T}\tilde{G})\right|}{|\mathbf{\Phi^T}F|} \right)_r &, && \text{strongly nonlinear}
\end{aligned}
\tag{8.19}
$$

where $\left(\max\left|(\mathbf{\Phi^T}\tilde{G})\right| \right)_r$ is the peak value found in the NLMV's magnitude, in the vicinity of its own mode r. Most importantly, (8.19) can be used to verify whether the observed distortions in the responses are due to the nonlinearities or not.

Although one could say that the thresholds seem completely arbitrary, they relate well to the frequently-used engineering rule of "10 times greater than" to determine how large/small a dimension is[1]. Extrapolating this rule to the present case yields the following observations: if the linear and NL modal restoring forces are of similar magnitudes, the mode behaves close to linear. If the NL modal force is at least 10 times greater than the linear one, then the mode behaves "strongly nonlinear". Anywhere in between the term "moderately nonlinear" applies well, and this range should be calibrated according to the analyst's experience, or safely assumed as "strongly nonlinear".

Abusing the terminology once more, we can define a single "linear threshold" based in (8.19), above which the nonlinear mode can no longer be approximated

---

[1]For example, the thickness of a thin plate must be at least 10 times smaller than the other two dimensions in order to be considered a "thin plate", according to most engineering manuals.

by its linear counterpart:

$$\boxed{\max \left| (\mathbf{\Phi^T} \tilde{G}) \right|_r \geq \left| \mathbf{\Phi^T} F \right|_r} \tag{8.20}$$

The usability of (8.20) can be illustrated in an enlightening example, provided by Fig. 8.3. This shows the extracted NLMV of a large system. According to the guidelines presented in Section 8.5, it can first be verified that the nonlinear mechanism relates well with a cubic stiffness model (which is the case).
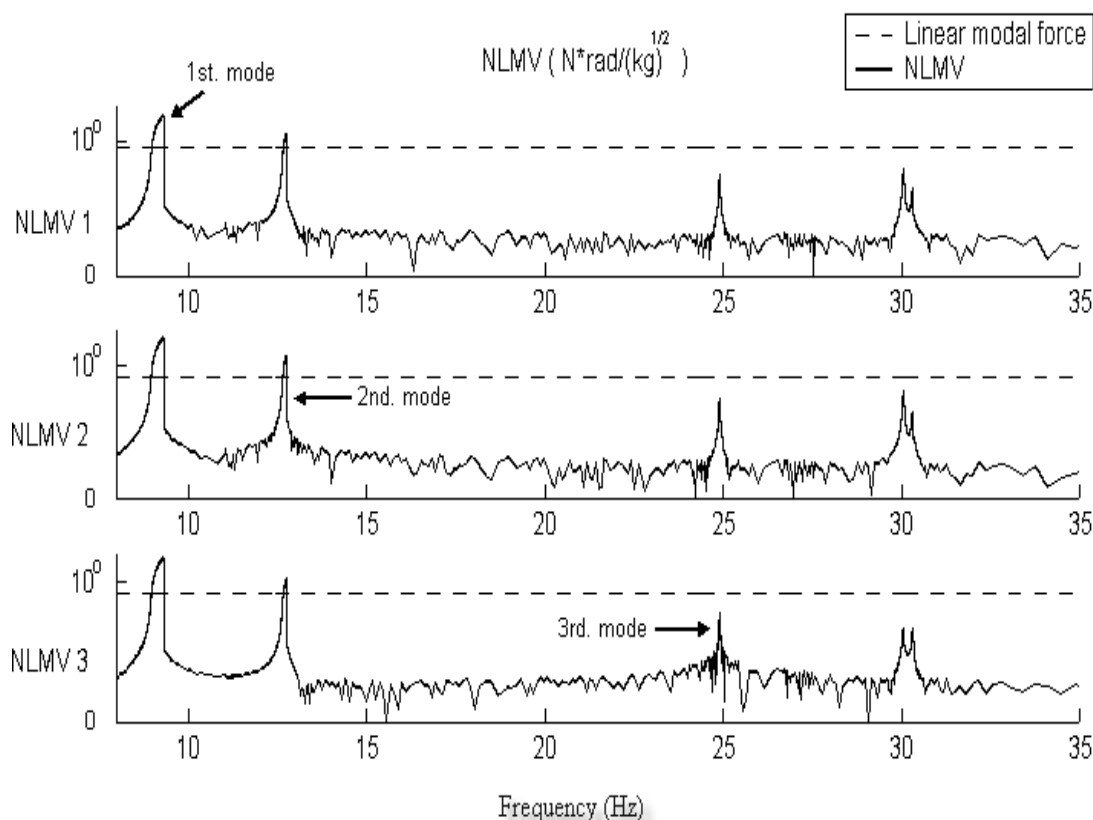

Figure 8.3: NLMV of a large system (solid line), and the "linear threshold" (dashed line) for the first three modes

Fig. 8.3 also shows, in dashed line, the constant linear modal force for each mode. It is immediately obvious that the NLMV of modes 1 and 2 easily exceed their corresponding "linear threshold", confirming that the observed distortions

in the responses are undoubtedly due to nonlinearities. We can also verify that modes 3, 4 and 5 fall way behind their respective threshold, explaining their almost linear behaviour.

By using (8.19), "nonlinear modal grades" can be calculated for all the modes of the previous example. These are listed in Table 8.1.

Mode	Nonlinear modal grade
1	75.56
2	16.52
3	0.07
4	0.1
5	0.025

Table 8.1: "Nonlinear modal grades" for the system of Fig. 8.3

The main purpose of the "nonlinear modal grades" is to provide some degree of automatization for selecting m_{NL}, the nonlinear modes included in the analysis. If the regeneration is calculated by means of a *modal superposition*, the computational cost can be reduced by assuming weakly[1] nonlinear modes as linear. The "linear threshold" can be a-priori calibrated to the analyst's experience, according to (8.19).

This section does not intend to present an exhaustive study of this technique, which is rather a side issue in the context of this work. The concept of a "linear threshold" needs to be supported with experimental data for a large number of experiments and for different systems. Until then, it is just an idea to keep in mind, which performed well in the various simulations run by the author.

8.7 Stage V: transformation to NL modal parameters via the FAT

The following developments represent the LHS path of the flow chart of Fig 8.1, page 152, which assumes that either the nonlinear type was not identified, or the

---

[1] "Nonlinear modal grades" below 1.

NL-DOFs were not included in the measurements. This is representative of the most general case.

An effective method for decoupling the nonlinear information contained in the NLMV into standard nonlinear modal parameters was introduced in Chapter 7, called the *fast approximation technique* (FAT). The transformation provides a bridge between the methodology followed in this research and most works in the field, notably by Chong & Imregun (30). The link allows an otherwise troublesome quantification stage when the input data is significantly incomplete.

The FAT will be extended here to deal with large systems. The introduced modifications are mostly due to the higher-modes residuals and the *measured region* $\Re$. Otherwise, the derivation is similar to that introduced in Chapter 7 for a full model, and will not be repeated. For the sake of completeness, a flow chart with the modified procedure is shown in Fig. 8.4. Also, following are some important remarks relevant to this chart:

- Originally, the input data for the FAT was the *theoretical* NLMV, calculated from the nonlinear response $\{\tilde{Y}\}$ and a complete description of the nonlinearities, $\{\tilde{G}\}$. This time, the input data is the *extracted* NLMV $\{\mathbf{\Phi^T}\tilde{G}\}_m$, which is available as a composite function, although its nonlinear component $\{\tilde{G}\}$ is unknown[1].

- The "$\approx$" symbol in:

$$\Delta\tilde{\lambda}_s^2 \approx \frac{\left(\mathbf{\Phi^T}\tilde{G}\right)_s + \left(\mathbf{\Delta\tilde{\Phi}^T}F\right)_s}{\tilde{P}_s} \qquad (8.21)$$

acknowledges the fact that the "nonlinear coupling term" has been neglected. In Chapter 7, it was proved that this term introduced negligible effects in the resonant mode, and that (8.21) was a close approximation to the nonlinear natural frequency and modal damping, if implemented within a short iterative scheme.

---

[1]This argument finally exposes the value of the FAT method, which is able to calculate the nonlinear modal parameters *analytically*, without previous knowledge about the position or type of the nonlinearities

- The procedure assumes a single excitation force only. Although a multi-excitation system can be considered by applying some simple modifications, these would generate a set of f multi-variable nonlinear equations to solve the eigenvectors only.

- In agreement with the traditional nonlinear modal expansion, it has also been assumed that, in the vicinity of the s_{th} resonance, the effect of the neighbouring nonlinear modes $r = 1 \dots m_{NL}$, $r \neq s$ remains linear. This approximation is valid for fairly well separated modes, although an iterative scheme can account for close modes as well.

8.8 Stage VI: system's quantification via polynomials

Chong & Imregun (30) presented a NLMA method, in which nonlinear modal parameters are extracted from experimental data and expressed as functions of the nonlinear modal amplitude, via a polynomial curve fitting:

$$\tilde{\omega}_r^2 = \tilde{\omega}_r^2(|\tilde{P}_r|), \quad \text{NL natural frequency}$$

$$\tilde{\eta}_r = \tilde{\eta}_r(|\tilde{P}_r|), \quad \text{NL modal damping} \tag{8.22}$$

$$\tilde{\Phi}_r = \sum_{r=1}^{m} \tilde{b}_{ir} \Phi_r, \quad \text{NL eigenvectors, where } \tilde{b}_{ir} = \tilde{b}_{ir}(|\tilde{P}_r|)$$

These functions were found to be *invariant* to the excitation level, able to predict the nonlinear modal parameters at a different excitation and constructing the physical responses via *modal superposition*. The authors obtained successful experimental results for the identification and coupling of engineering structures.

In earlier stages of this research, the aforementioned method was reviewed. It was found to perform very well for a wide range of problems and able to provide a mathematical model even with scarce information. However, it was also observed that the extraction procedure suffers from numerical instabilities for *strongly* nonlinear systems[1] due to a multi-variable nonlinear minimization. This issue restricts the robustness and prediction range of the method.
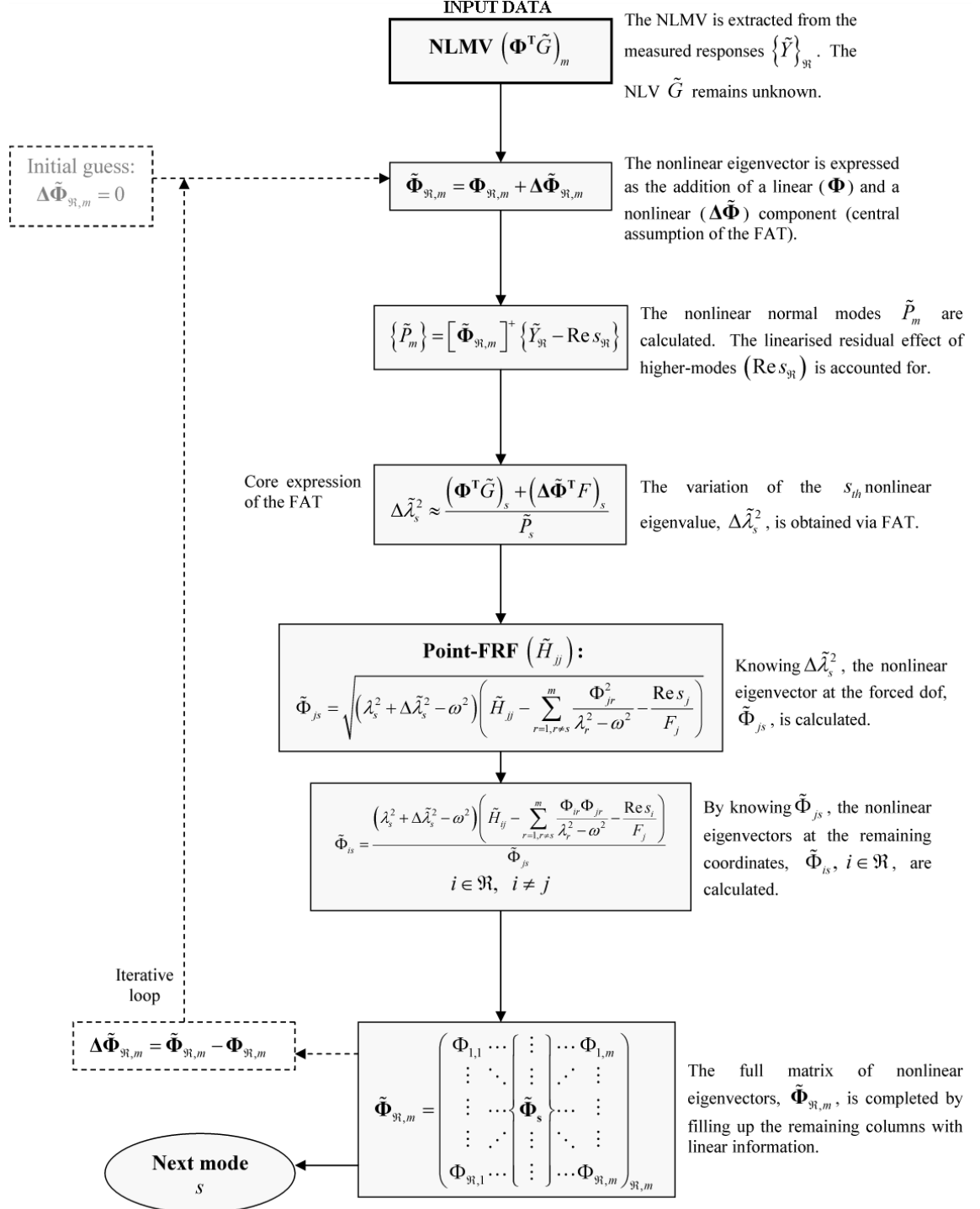
---

[1]Or should we say, for "nonlinear modal grades" above 10?.

Figure 8.4: FAT flow diagram for the calculation of nonlinear eigenvalues and eigenvectors, applied to large systems

In our current research, the nonlinearities are first extracted by a direct calculation, in the form of the NLMV. Next, the nonlinear modal parameters are analytically obtained via the FAT, thus increasing their accuracy and numerical stability. The NL parameters can then be expressed as functions of the nonlinear modal amplitudes, by constructing similar polynomials:

$$
\boxed{
\begin{aligned}
{}_{re}\Delta\tilde{\lambda}_r^2 &= {}_{re}\Delta\tilde{\lambda}_r^2(|\tilde{P}_r|), & {}_{im}\Delta\tilde{\lambda}_r^2 &= {}_{im}\Delta\tilde{\lambda}_r^2(|\tilde{P}_r|), \\
{}_{re}\boldsymbol{\Delta\tilde{\Phi}}_r &= {}_{re}\boldsymbol{\Delta\tilde{\Phi}}_r(|\tilde{P}_r|), & {}_{im}\boldsymbol{\Delta\tilde{\Phi}}_r &= {}_{im}\boldsymbol{\Delta\tilde{\Phi}}_r(|\tilde{P}_r|), \quad r = 1\ldots m_{NL}
\end{aligned}
}
\tag{8.23}
$$

Equation (8.23) contains another subtle, but most important, difference between Chong & Imregun's approach (8.22) and the one implemented here. The original methodology expresses the resonant nonlinear eigenvector as a linear combination of a few neighbouring linear eigenvectors, by means of nonlinear coefficients $\tilde{b}_{ij}$. These nonlinear coefficients are further calculated as nonlinear functions of the modal amplitude. This approach, while effective, has no direct physical meaning, and this introduces certain degree of case sensitivity.

In this work, the nonlinear eigenvectors have been explicitly calculated by the FAT, and can be *directly* expressed as functions of their corresponding modal amplitude, just like the nonlinear eigenvalues. While this path certainly increases the number of polynomials required for the regeneration, it is a small price to pay compared with the increased robustness and physical meaning.

The procedure for the system quantification via the aforementioned approach is explained next:

The traditional nonlinear modal expansion (6.13) expresses the nonlinear normal modes as:

$$
\lceil \tilde{\lambda}^2 - \omega^2 \rfloor \{\tilde{P}\} = \{\boldsymbol{\tilde{\Phi}^T} F\}
\tag{8.24}
$$

According to the methodology introduced in this work, the nonlinear modal parameters can be separated in linear and nonlinear components:

$$
\lceil \lambda^2 + \Delta\tilde{\lambda}^2 - \omega^2 \rfloor \{\tilde{P}\} = \{(\boldsymbol{\Phi} + \boldsymbol{\Delta\tilde{\Phi}})^{\boldsymbol{T}} F\}
\tag{8.25}
$$

Thus, the r_{th} nonlinear normal mode can be expressed as:

$$
\boxed{
\left(\lambda_r^2 + \Delta\tilde{\lambda}_r^2 - \omega^2\right)\tilde{P}_r = \left(\left\{\boldsymbol{\Phi}_r + \boldsymbol{\Delta\tilde{\Phi}}_r\right\}_f^{\boldsymbol{T}} \{F\}_f\right)_r
}
\tag{8.26}
$$

where $\Delta\tilde{\lambda}_r^2, \boldsymbol{\Delta\tilde{\Phi}_r}$, already obtained via FAT, can be expressed as (8.23). The computer implementation of (8.23) is achieved by constructing polynomials of order ρ, linking the nonlinear variables with the magnitude of $\tilde{P}_r$:

$$\boxed{\begin{aligned} \Delta\tilde{\lambda}_r^2 &= a_1\left|\tilde{P}_r\right| + a_2\left|\tilde{P}_r\right|^2 + \ldots + a_\rho\left|\tilde{P}_r\right|^\rho, & r = 1\ldots m_{NL} \\ \boldsymbol{\Delta\tilde{\Phi}_r} &= b_1\left|\tilde{P}_r\right| + b_2\left|\tilde{P}_r\right|^2 + \ldots + b_\rho\left|\tilde{P}_r\right|^\rho, & r = 1\ldots m_{NL} \end{aligned}} \tag{8.27}$$

where a_i and b_i are the numerical coefficients of the polynomials, which can be calculated by a standard curve-fitting algorithm. The eigen-parameters must be split into real and imaginary parts before the process.

Equations (8.26) and (8.27) form a set of single-variable nonlinear equations, in which the only unknown is $\tilde{P}_r$, thus allowing the regeneration of the responses via *modal superposition*. Most importantly, they also allow the prediction of responses at different excitation levels.

In order to regenerate/predict a response at a given DOF i, the following polynomials must be constructed:

1. Polynomials for all the m_{NL} nonlinear natural frequencies and modal damping variables - essential requirement to regenerate any DOF.

2. Polynomials for the f forced nonlinear eigenvectors, for all m_{NL} modes - essential requirement to regenerate any DOF.

3. Polynomials for the i eigenvector, for all m_{NL} modes - only required to regenerate DOF i.

Because separate polynomials must be constructed for the real and imaginary components, the total number required to regenerate a set of n responses is $2m_{NL}(1 + f + n)$.

8.9 Stage VII: regeneration and prediction

Given a set of excitation forces $\{F\}_f$, the nonlinear equations (8.26) and (8.27) are solved for $\tilde{P}_r$ on a mode by mode basis. The nonlinear minimization yields the

new nonlinear normal modes for the system, then *modal superposition* is invoked to obtain the physical responses.

In order to regenerate/predict a given coordinate $\tilde{Y}_i$, the traditional nonlinear modal expansion can be used:

$$\tilde{Y}_i = \underbrace{\left(\sum_{r=m_{NL}} \left(\phi_{ir} + \Delta\tilde{\phi}_{ir} \right) \tilde{P}_r \right)}_{\text{Nonlinear modes}} + \underbrace{\left(\sum_{r=m-m_{NL}} \phi_{ir} P_r + \text{Res}_i \right)}_{\text{Extended linear residual}} \underbrace{\left(\frac{^{2}F}{^{1}F} \right)}_{\substack{\text{Updated} \\ \text{force}}} \quad (8.28)$$

where the m_{NL} nonlinear modes are updated by recalling the newly-found NNMs $\tilde{P}_r$ and the polynomials for $\left\{ \boldsymbol{\Delta\tilde{\Phi}} \right\}_{i,r=1...m_{NL}}$. The linear residual Res is extended to account for the linear modes in m, and ^{1}F and ^{2}F are, respectively, the initial and the updated excitation forces. Note that only the extended linear residual must be updated in order to reflect the excitation change, since the NL modes $\tilde{P}_r$ have been already calculated for ^{2}F.

Two important remarks:

- (8.28) is valid for a single-excitation force. If a multi-excitation system is considered, then a more sophisticated approach (possibly very complex) needs to be implemented in order to update the residual $\{Res\}$. Alternatively, the analyzed frequency range can be extended in such a way that the residual has a minimum impact on the nonlinear modes of interest, thus avoiding the issue ($\{Res\} \approx 0$).

- The force range in which a successful prediction can be achieved will depend on the quality of the fitted polynomials and their behaviour outside the fitted range. To this end, it is better to stick with polynomials of the minimum possible order, to maintain a smooth path beyond the fitted range.

8.10 Stage VIII: detection of the *NL-DOFs*

The procedure described hitherto can be applied in almost any situation, including cases with incomplete data. The model allows the regeneration of the measured responses and the prediction at different levels of excitation, which is the main aim of an identification method.

However, it suffers from some disadvantages. The range of excitation levels for which the response can be regenerated accurately is restricted, depending on the quality and extrapolation characteristics of the fitted polynomials. The number of polynomials needed to regenerate a substantial part of a large system represents a significant burden. Most importantly, the nonlinear component of the system, initially unknown, remains unknown, failing to reveal core issues such as the location of the nonlinear elements.

This section represents the RHS path in the flow chart of Fig. 8.1, page 152, only available when the nonlinear mechanism has been accurately detected. It is also assumed that the *NL-DOFs* n have been included in the *measured region* $\Re$ ($n \in \Re$). The procedure introduced here allows a *full* characterization of the system, by detecting and quantifying the individual nonlinear elements. This, in turn, allows the exact regeneration at any excitation level, plus many other features previously unattainable.

For this section, the concept of a *nonlinear region* Γ needs to be recalled[1]. Γ must be a subspace of the *measured region* $\Re$, enclosing all possible n *NL-DOFs*. These can be mathematically stated as:

$$n \in \Gamma \in \Re, \quad \text{typically } n \ll \Gamma \leq \Re \tag{8.29}$$

In Section 3.4, it was argued that the approximate delimitation of a *nonlinear region* Γ is feasible for most engineering structures. The cautious analyst would rather assume $\Gamma = \Re$, which would only increase the computational burden but *not* the complexity of the calculations, a feature that will be proven soon. Notice that the size of Γ is arbitrary.

The analysis can be carried out once the nonlinear mechanism has been assessed (Section 8.5). First, we decompose the NLMV $\{\mathbf{\Phi^T \tilde{G}}\}$ into m and $(M-m)$ modal components (column-wise), as well as into Γ and $(N-\Gamma)$ coordinates (row-

---

[1]See Section 3.4.

wise):

$$\left\{ \begin{array}{c} \left(\mathbf{\Phi^T}\tilde{G}\right)_m \\ \left(\mathbf{\Phi^T}\tilde{G}\right)_{M-m} \end{array} \right\} = \left[\begin{array}{cc} \mathbf{\Phi}_{N-\Gamma,m} & \mathbf{\Phi}_{N-\Gamma,M-m} \\ \mathbf{\Phi}_{\Gamma,m} & \mathbf{\Phi}_{\Gamma,M-m} \end{array} \right]^T \left\{ \begin{array}{c} \tilde{G}_{N-\Gamma} \\ \tilde{G}_{\Gamma} \end{array} \right\}$$

$$= \left[\begin{array}{cc} \mathbf{\Phi}_{m,N-\Gamma} & \mathbf{\Phi}_{m,\Gamma} \\ \mathbf{\Phi}_{M-m,N-\Gamma} & \mathbf{\Phi}_{M-m,\Gamma} \end{array} \right] \left\{ \begin{array}{c} 0 \\ \tilde{G}_{\Gamma} \end{array} \right\}$$

(8.30)

where the sub-NLV $\{\tilde{G}_{N-\Gamma}\}$ has been assumed to be zero, as all the nonlinearities are contained in the *nonlinear region* Γ. This leads to:

$$\{\mathbf{\Phi^T}\tilde{G}\}_m = [\mathbf{\Phi}_{\Gamma,m}]^T \{\tilde{G}_\Gamma\} \tag{8.31}$$

which proves that the extracted NLMV $\{\mathbf{\Phi^T}\tilde{G}\}_m$ is a function of the Γ DOFs and the m modes only.

Recalling (3.41), the sub-NLV $\{\tilde{G}_\Gamma\}$ can be expressed as a function of the nonlinear matrix (NLM) $[\tilde{\nu}_{\Gamma,\Gamma}]$ and the responses at the Γ coordinates.

$$\{\tilde{G}_\Gamma\} = [\tilde{\nu}_{\Gamma,\Gamma}]\{\tilde{Y}_\Gamma\} \tag{8.32}$$

Introducing (8.32) into (8.31), we have:

$$\{\mathbf{\Phi^T}\tilde{G}\}_m = [\mathbf{\Phi}_{\Gamma,m}]^T [\tilde{\nu}_{\Gamma,\Gamma}] \left\{\tilde{Y}_\Gamma\right\} \tag{8.33}$$

Recalling (3.9) for a cubic stiffness system[1], and taking the coefficients β out of $[\tilde{\nu}_{\Gamma,\Gamma}]$, (8.33) can be transformed to:

$$\{\mathbf{\Phi^T}\tilde{G}\}_m = [\tilde{\tau}_\omega]_{m,\Gamma} \{\beta\}_\Gamma \tag{8.34}$$

where:

$$\tilde{\tau}_\omega = \frac{3}{4} \left[\begin{array}{cccc} \phi_{1,1}\left|\tilde{Y}_1\left(\omega\right)\right|^2 \tilde{Y}_1\left(\omega\right) & \phi_{2,1}\left|\tilde{Y}_2\left(\omega\right)\right|^2 \tilde{Y}_2\left(\omega\right) & \cdots & \phi_{\Gamma,1}\left|\tilde{Y}_\Gamma\left(\omega\right)\right|^2 \tilde{Y}_\Gamma\left(\omega\right) \\ \phi_{1,2}\left|\tilde{Y}_1\left(\omega\right)\right|^2 \tilde{Y}_1\left(\omega\right) & \phi_{2,2}\left|\tilde{Y}_2\left(\omega\right)\right|^2 \tilde{Y}_2\left(\omega\right) & \cdots & \phi_{\Gamma,2}\left|\tilde{Y}_\Gamma\left(\omega\right)\right|^2 \tilde{Y}_\Gamma\left(\omega\right) \\ \vdots & \vdots & \ddots & \vdots \\ \phi_{1,m}\left|\tilde{Y}_1\left(\omega\right)\right|^2 \tilde{Y}_1\left(\omega\right) & \phi_{2,m}\left|\tilde{Y}_2\left(\omega\right)\right|^2 \tilde{Y}_2\left(\omega\right) & \cdots & \phi_{\Gamma,m}\left|\tilde{Y}_\Gamma\left(\omega\right)\right|^2 \tilde{Y}_\Gamma\left(\omega\right) \end{array} \right]_{m,\Gamma}$$

(8.35)

---

[1]The following derivation applies for grounded cubic stiffness nonlinearities only. The extension for a general case with mixed nonlinearities is straightforward, requiring only minor modifications.

and

$$\{\beta_\Gamma\} = \left\{ \begin{array}{cccc} \beta_{11} & \beta_{22} & \cdots & \beta_{\Gamma\Gamma} \end{array} \right\}^T \tag{8.36}$$

Equation 8.34 is valid for a single frequency point ω and also severely under-determined, because typically $m \ll \Gamma$. This is fixed by stacking several versions of (8.34), constructed at q different frequencies, which are valid for the same vector $\{\beta_\Gamma\}$:

$$\left\{ \begin{array}{c} \left\{ \mathbf{\Phi^T}\tilde{G} \right\}_m^{\omega=\omega_1} \\ \left\{ \mathbf{\Phi^T}\tilde{G} \right\}_m^{\omega=\omega_2} \\ \vdots \\ \left\{ \mathbf{\Phi^T}\tilde{G} \right\}_m^{\omega=\omega_q} \end{array} \right\}_{q\cdot m} = \left[\begin{array}{c} \tilde{\tilde{\tau}}_{\omega=\omega_1} \\ \tilde{\tilde{\tau}}_{\omega=\omega_2} \\ \vdots \\ \tilde{\tilde{\tau}}_{\omega=\omega_q} \end{array} \right]_{q\cdot m, \Gamma} \{\beta_\Gamma\} \tag{8.37}$$

Eq. 8.37 represents an over-determined set of linear equations for $q \cdot m \geq \Gamma$, from which the coefficients β can be directly extracted. The solution will implicitly detect the position of the NL elements, given by the non-zero indexes.

(8.37) could suffer from rank deficiency if the selected q frequencies are too close to each other. This will cause two or more rows of (8.35) to be linearly dependent. An effective strategy to solve (8.37) is to split it in its real and imaginary components, halving the number of frequencies needed, then solving a single enlarged problem $[2qm, \Gamma]$. This is best done through a *linear* least squares minimization, applying the constraint $\{\beta\}_\Gamma \geq 0$.

This technique delivers unambiguous results provided that q and m are representative of the nonlinear system under analysis, so that (8.37) is properly constrained.

Once the n *NL-DOFs* have been localized, (8.37) can be solved once more for the reduced set of n DOFs, improving the accuracy of the calculation:

$$\left\{ \begin{array}{c} \left\{ \mathbf{\Phi^T}\tilde{G} \right\}_m^{\omega=\omega_1} \\ \left\{ \mathbf{\Phi^T}\tilde{G} \right\}_m^{\omega=\omega_2} \\ \vdots \\ \left\{ \mathbf{\Phi^T}\tilde{G} \right\}_m^{\omega=\omega_q} \end{array} \right\}_{q\cdot m} = \left[\begin{array}{c} \tilde{\tilde{\tau}}_{\omega=\omega_1} \\ \tilde{\tilde{\tau}}_{\omega=\omega_2} \\ \vdots \\ \tilde{\tilde{\tau}}_{\omega=\omega_q} \end{array} \right]_{q\cdot m, n} \{\beta_n\} \tag{8.38}$$

Some important remarks are as follows:

- The procedure shown here can be applied to any type of nonlinearity, as long as the unknown coefficients β, γ are constant.

- This derivation was done by considering cubic stiffness, grounded nonlinearities only. For the general case of mixed elements, the same principles hold, although slight modifications must be made to matrix $[\tilde{\tau}_\omega]$ and vector $\{\beta_\Gamma\}$.

- The q sample frequencies must be chosen in those regions where the NLMV is significant, evenly distributed over all the modes m. Care must be taken to ensure that Δq, the separation of the selected q frequencies, is large enough to avoid singularity, and that $2qm \geq \Gamma$ to achieve an over-determined set.

- If q frequencies over m modes poorly represent the system, (8.37) can be solved several times, each choosing a different combination of sample frequencies and modes. Then, the detected n DOFs for each solution are gathered, solving a consistent and reduced problem (8.38) for the last time.

8.11   Sample Case #3: pre-processing data (stage I)

The R-HMT method will be applied to the identification of the Sample Case #3, which is thoroughly described in Appendix B. The system represents a large model of a thin plate (Fig. 8.5) in which the following regions are pre-defined:

$N = \{1, 2, \ldots, 150\}$ (Number of active DOFs in the "Y" direction only)
$\Re = \{41, 42, \ldots, 110\}$ (The *measured region*)
$\Gamma = \{51, 52, \ldots, 100\}$ (The *nonlinear region*)
$f = \{67\}, \quad$ single excitation, $F_{67} = 1.5N$
$m = \{1, 2, 3, 4, 5\}, \quad$ for the frequency range $8 - 35\,\mathrm{Hz}$.

$$(8.39)$$

where the symbol "Y" has been dropped from the DOF notation (e.g., "DOF 51Y"), because only vertical motions are considered to be measured. The results for a previous linear modal analysis (LMA) of the measured DOFs are also included in Appendix B.
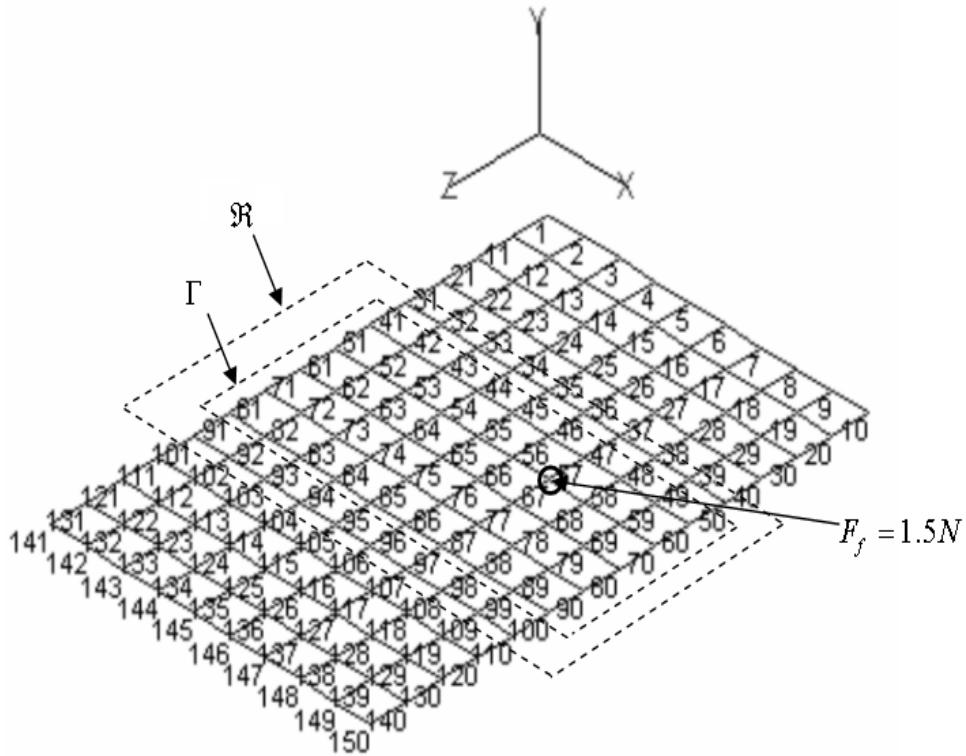
Figure 8.5: The Sample Case #3

8.11.1 Sample Case #3: NLMV extraction (stage II)

The *extended* NLMV $\{\tilde{\chi}_m\}$ can be extracted from the measured responses $\Re$, by applying (8.13) for every frequency point within the measured range:

$$\{\tilde{\chi}_m\} = \lceil \lambda^2 - \omega^2 \rfloor_{m,m} [\mathbf{\Phi}_{\Re,m}]^+ \left\{ \tilde{Y}_\Re - \mathrm{Res}_\Re \right\}$$

The standard NLMV $\left\{ \mathbf{\Phi^T} \tilde{G} \right\}_m$ can be further recovered by (8.15):

$$\left\{ \mathbf{\Phi^T} \tilde{G} \right\}_m = \left\{ \mathbf{\Phi^T} F \right\}_m - \left\{ \tilde{\chi} \right\}_m, \quad \text{where } \left\{ \mathbf{\Phi^T} F \right\}_m = \left[\mathbf{\Phi}_{f,m} \right]^T \left\{ F \right\}_f$$
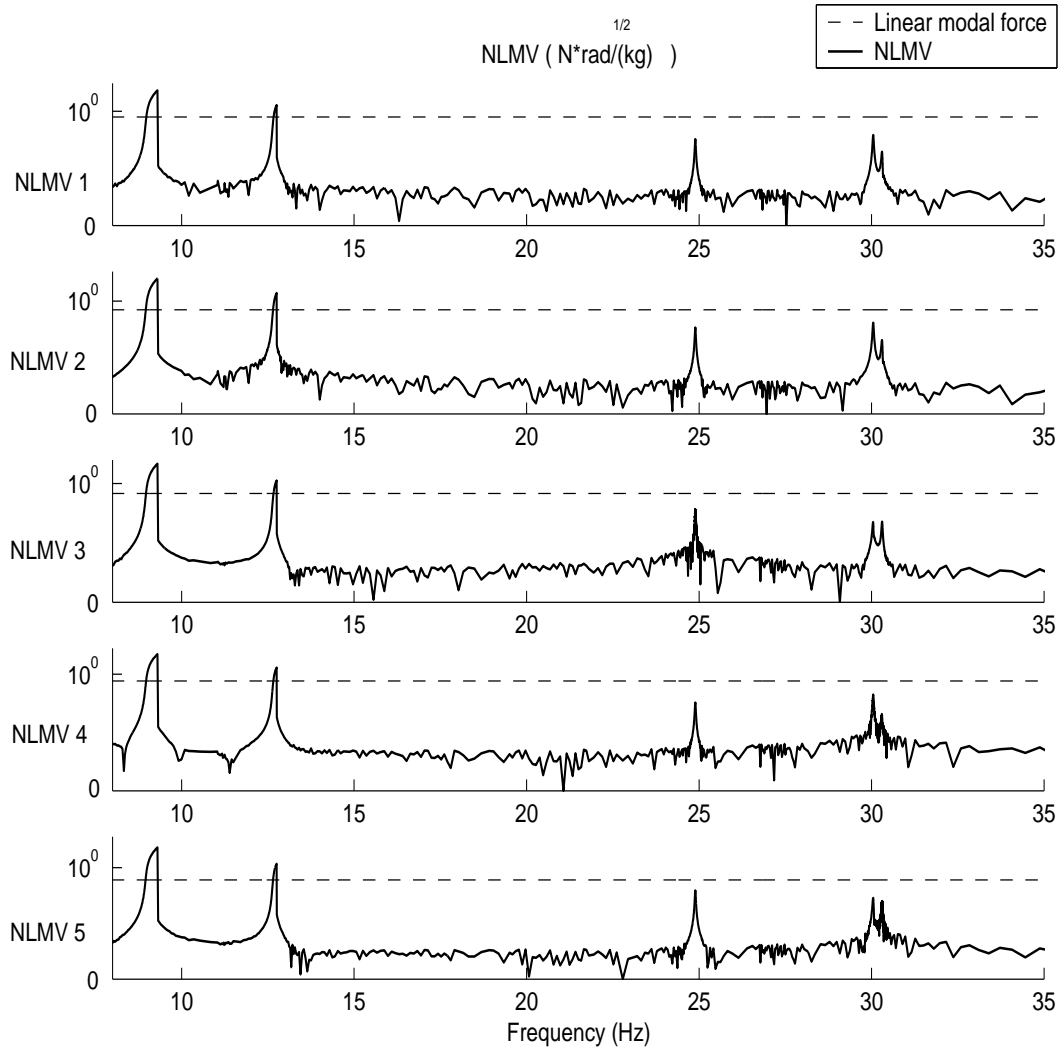
Figure 8.6: The extracted NLMV (solid line) and the correspondent "linear thresholds" (dashed line), for the first five modes of the Sample Case #3

Fig. 8.6 shows the extracted NLMV of the Sample Case #3 for the first five modes (solid line).

8.11.2 Sample Case #3: detection of the nonlinear mechanism (stage III)

The geometric "footprint" of the extracted NLMV (Fig. 8.6) at the first two resonances suggest a cubic stiffness nonlinear type, according to the guidelines presented in Section 8.5. This is correct.

8.11.3 Sample Case #3: degree of nonlinearity in a nonlinear mode (stage IV)

In Fig. 8.6, it can be seen that the extracted NLMV of modes 1 and 2 exhibit high peaks at their own resonances, easily surpassing their respective "linear thresholds". They also exert high coupling effects in the remaining modes. According to (8.19), modes 1 and 2 reach "nonlinear modal grades" of 75.56 and 16.52, respectively. These marks classify them as "strongly nonlinear", in agreement with the observed nonlinear behaviour in the response. Most importantly, the high grades of these modes confirm that the distortions in the response are fully explained by the presence of nonlinearities, rather than more esoteric causes[1].

In comparison, the NLMV of modes 3, 4 and 5 are very small, with "nonlinear modal grades" of 0.078, 0.103 and 0.025, respectively. These marks agree with their almost linear behaviour in the response. In a *nonlinear modal superposition* context, these modes can be regarded as linear.

The selection $m_{NL} = \{1, 2\}$ can be automated on the aforementioned basis.

8.11.4 Sample Case #3: transformation to NL modal parameters via the FAT (stage V)

The extracted NLMV can be transformed to nonlinear natural frequencies and modal damping functions, via the FAT. In agreement with the obtained "nonlinear modal grades", only modes 1 and 2 will be included in the nonlinear analysis. By applying the iterative procedure shown in Fig. 8.4, page 166, the following results are obtained after 10 iterations:

- Fig. 8.7 shows the variation of the nonlinear natural frequencies.

---

[1]Although nonlinearity is still considered an esoteric issue!.

- Fig. 8.8 shows the variation of the nonlinear modal damping. Because of a cubic stiffness nonlinearity, the variation is negligible, almost remaining at the linear value ($\eta = 0.1\%$).

- Fig. 8.9 shows the variation of the nonlinear eigenvector corresponding to the forced DOF (67). Because of a cubic stiffness nonlinearity, the imaginary component is also negligible.

- Fig. 8.10 shows the variation of three randomly chosen nonlinear eigenvectors (real part only), corresponding to DOFs $\{51, 62, 92\}$. The imaginary counterpart is not shown, as it exhibits negligible variation.

8.11.5 Sample Case #3: system's quantification via polynomials (stage VI)

Once the nonlinear modal parameters are known, they can be expressed as functions of the nonlinear modal amplitudes, according to Section 8.8.

The numeric values of $|\tilde{P}_r|$ (for a given nonlinear mode) are first sorted from minimum to maximum and placed in a horizontal axis. Its associated frequencies generate a master index, for which the corresponding nonlinear modal parameters are sorted and plotted in a vertical axis. Finally, the plotted values can be fitted to polynomials of the type (8.27).

The characterization will be confined to modes 1 and 2 only, accounting only for the real part of the nonlinear parameters. Due to negligible variation, the imaginary counterpart was discarded and replaced by the linear value. The results for the Sample Case #3 are shown in Figs. 8.11, 8.12 and 8.13, where the "+" marks represent the extracted nonlinear parameters, and the solid line represents a fitted polynomial of $4^{th.}$ order. The horizontal axis has been extended 1.5 times beyond the last fitted point, to show the extrapolation characteristics of the polynomials. This feature is essential to achieve an accurate prediction at levels further apart from that used for the extraction.
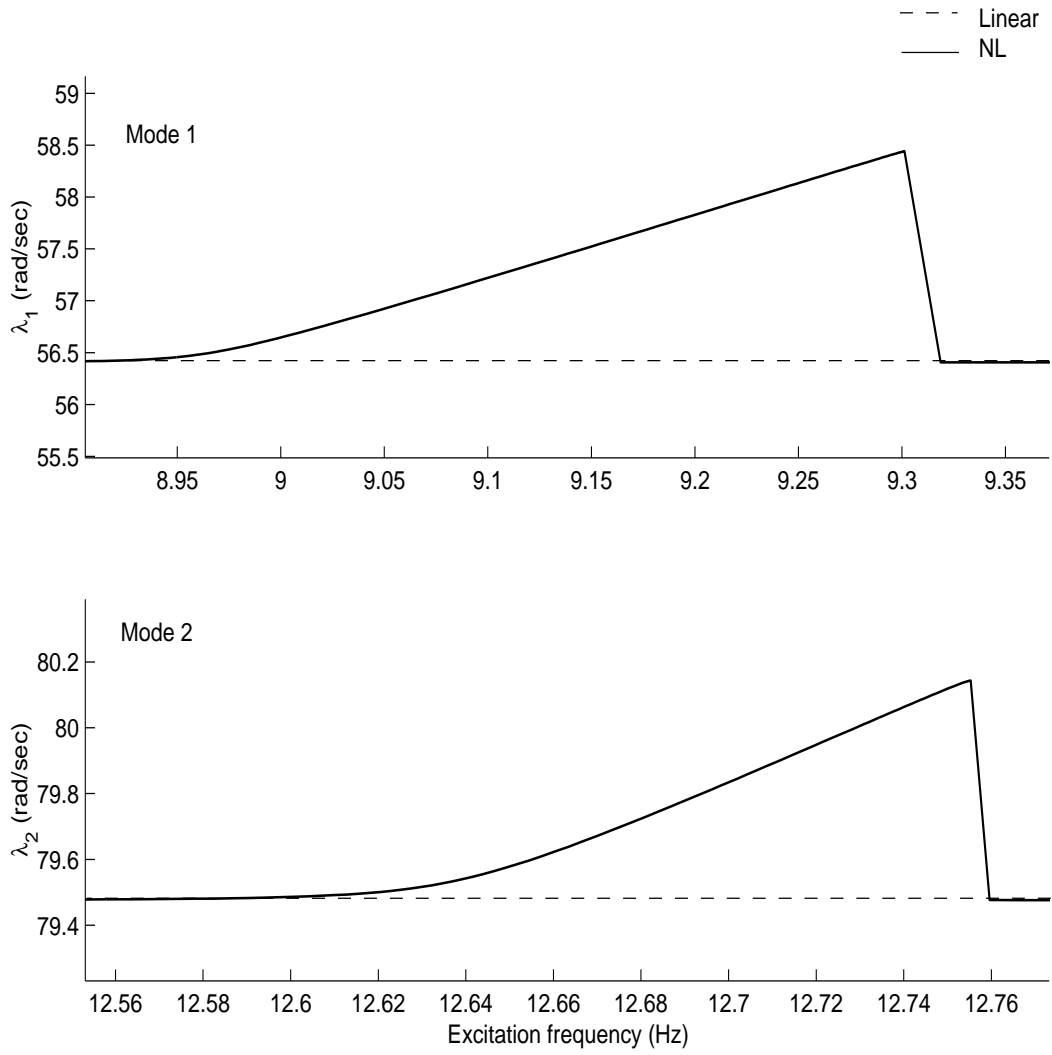
Figure 8.7: Nonlinear natural frequencies ($\tilde{\lambda}_r$) for modes 1 and 2 of the Sample Case #3
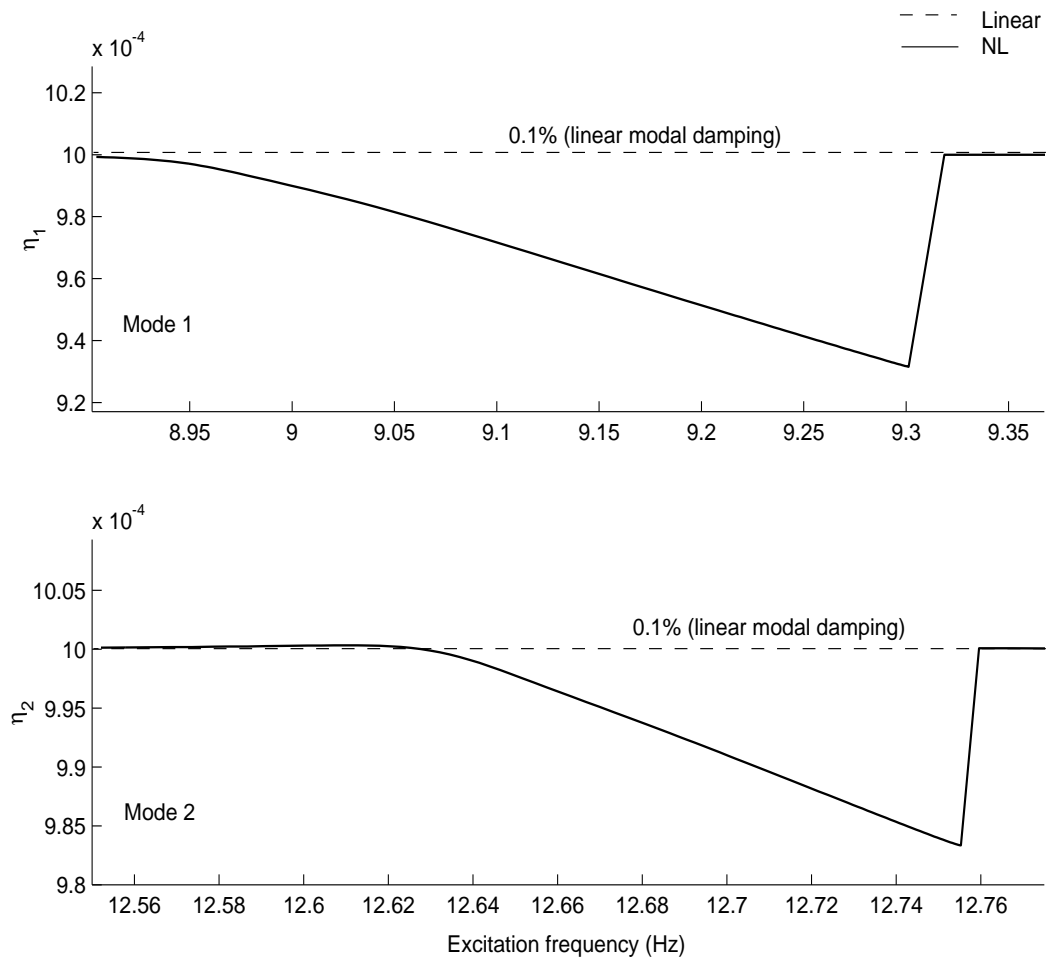
Figure 8.8: Nonlinear modal damping $(\tilde{\eta}_r)$ for modes 1 and 2 of the Sample Case #3
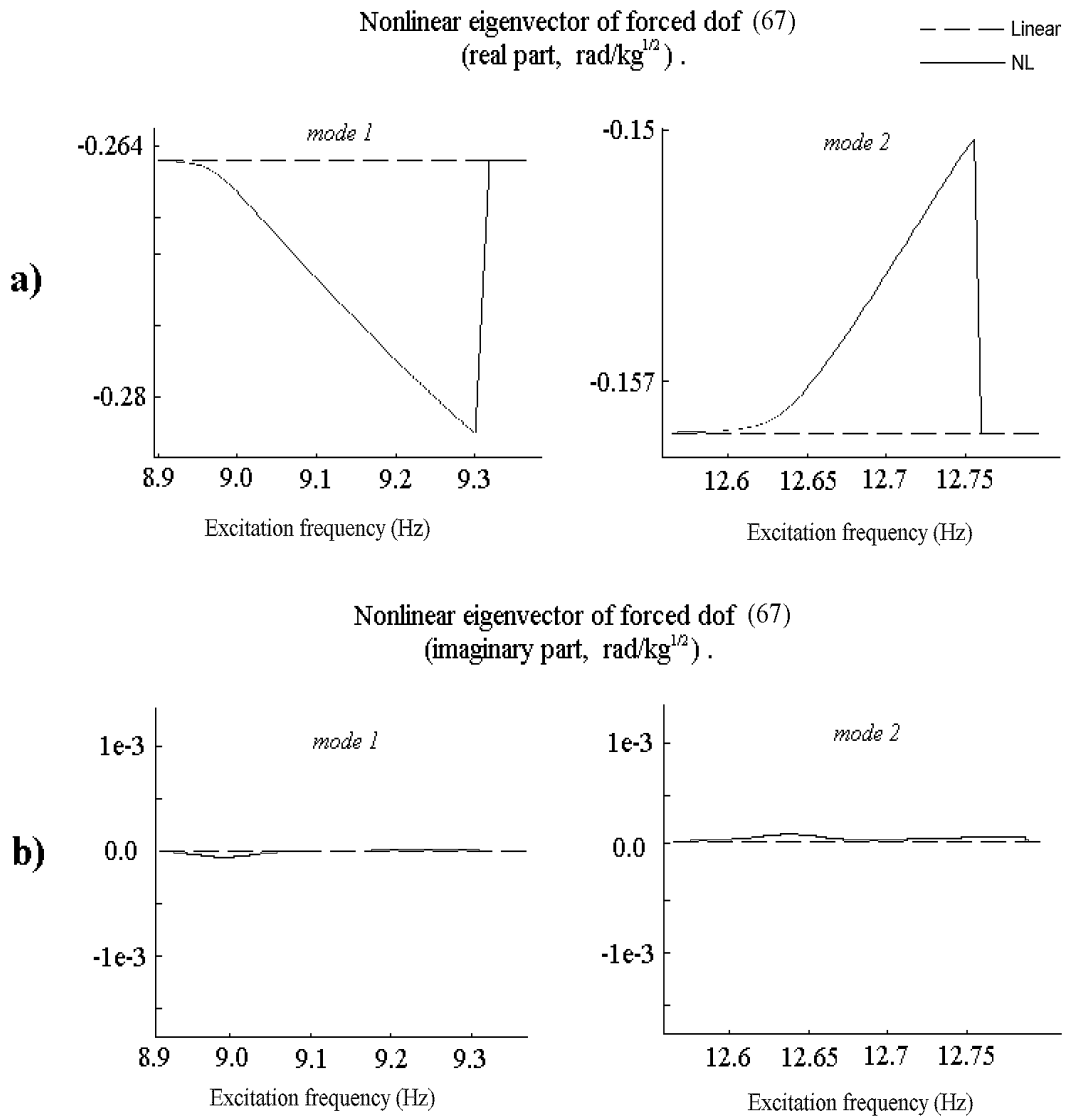
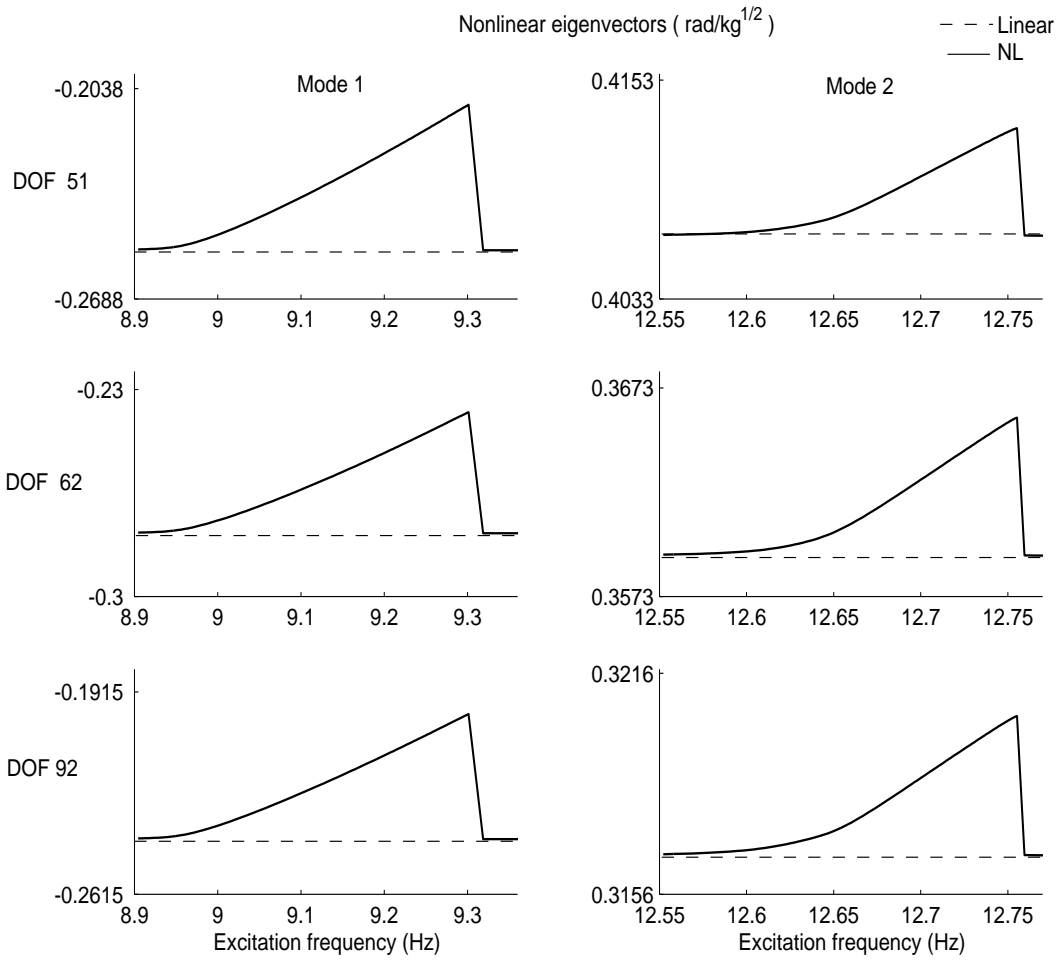Figure 8.9: Nonlinear eigenvectors for the forced DOF 67, for modes 1 and 2 of the Sample Case #3

Figure 8.10: Nonlinear eigenvectors (real part only) for DOFs $\{51, 62, 92\}$, for modes 1 and 2 of the Sample Case #3
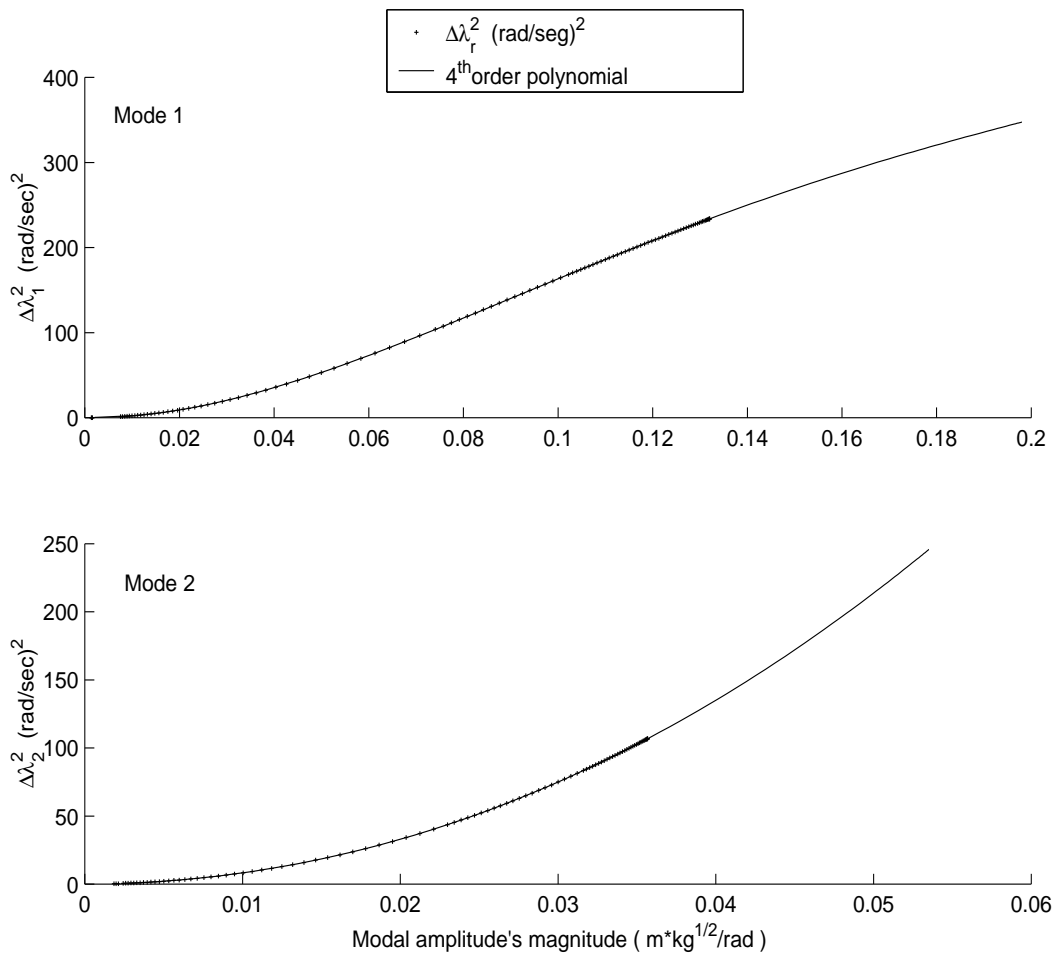
Figure 8.11: Variation of the nonlinear natural frequencies $(\Delta\tilde{\lambda}_r^2)$ against modal amplitude, for the Sample Case #3
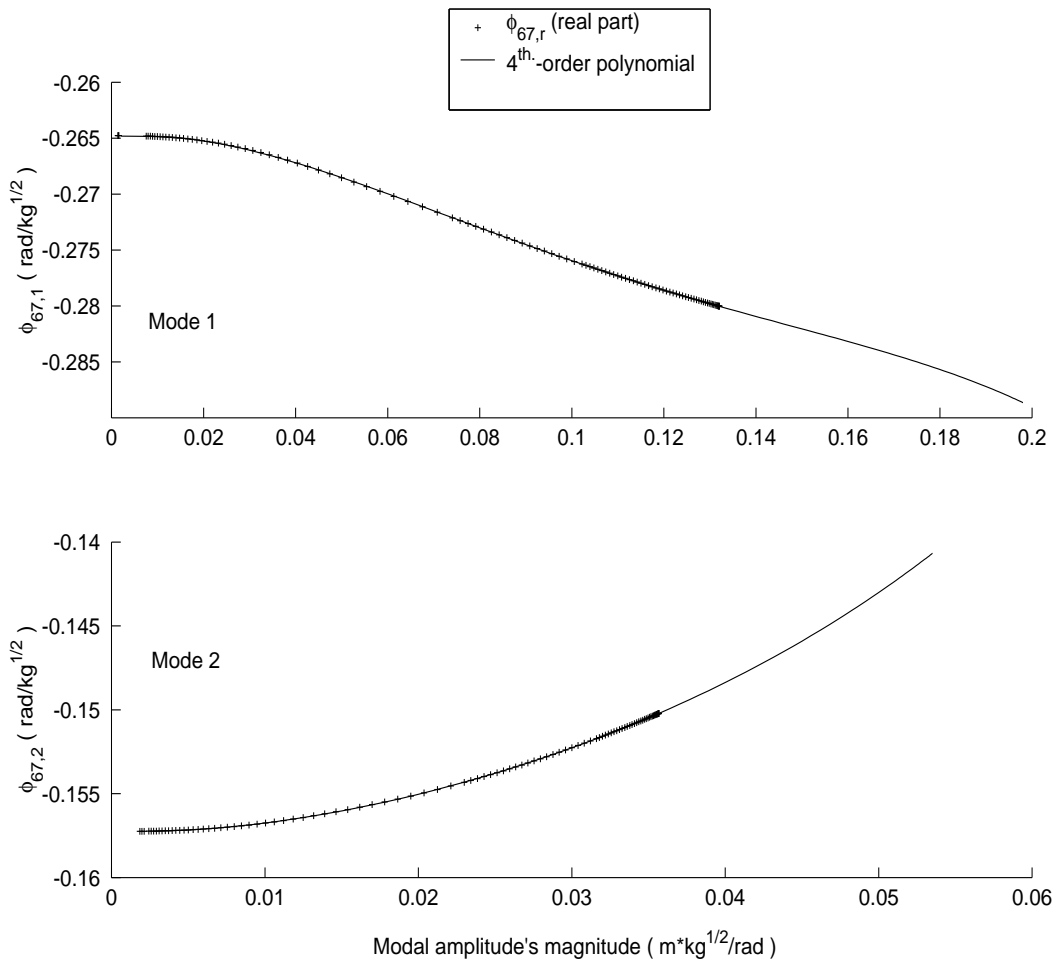
Figure 8.12: Variation of the nonlinear eigenvector 67 (forced DOF, real part only) against modal amplitude, for the Sample Case #3
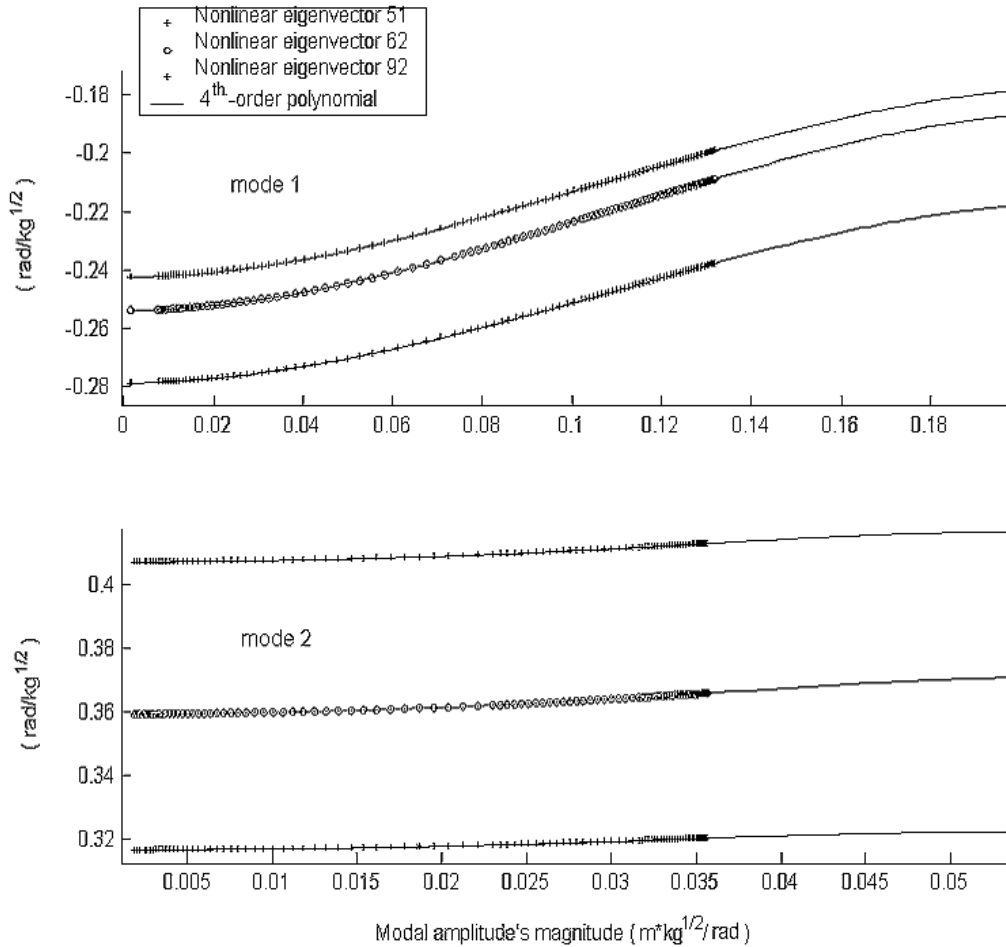
Figure 8.13: Variation of the nonlinear eigenvectors (real part only) of three randomly chosen DOFs ($\{51, 62, 92\}$) against modal amplitude, for the Sample Case #3

8.11.6 Sample Case #3: regeneration and prediction (stage VII)

The regeneration process will be exemplified for the first mode, applying (8.26) and (8.27). The same process must be repeated for all the nonlinear modes, here modes 1 and 2.

Fig. 8.14 shows the first modal amplitude of the Sample Case #3, calculated via our benchmark HBM code. The linear case appears in dashed line, while the results for three different excitation levels, $F = 1N, F = 1.5N$ and $F = 2N$ are shown in solid line. The polynomial-based predictions are displayed in "+" marks, exhibiting remarkable accuracy.

Once the m_{NL} nonlinear modal amplitudes have been separately regenerated, a modal superposition is invoked to obtain the physical responses, via (8.28). The regeneration/prediction for a randomly chosen DOF 52 is shown in Figs. 8.15 and 8.16, focusing on the modes 1 and 2, respectively. It can be appreciated that the regenerated/predicted responses ("+") match very well with the HBM solution.

8.11.7 Sample Case #3: detection of the *NL-DOFs* (stage VIII)

Applying the procedure introduced in Section 8.10, $q = 650$ frequencies were selected, distributed over the first 5 modes in the vicinity of the resonances. Note that, in order to obtain a properly constrained set of equations, the "linear" modes must be also considered, ensuring that they remain so. The following results were obtained:

Fig. 8.17 shows the results of the analysis, clearly establishing that there are three *NL-DOFs* $n = \{51, 62, 92\}$ (which is correct). Fig. 8.18 shows the improved results of the reduced problem (8.38), for the n DOFs only. The improved coefficients are shown in Table 8.2.

Once the nonlinear elements have been localized and quantified, the response for any excitation (not only sinusoidal) can be found, by employing the direct path of the HMT method presented in Chapter 6. The regenerated/predicted responses exhibit no discernible difference from the HBM responses in Figs. 8.15 and 8.16, so there is no need to display them.
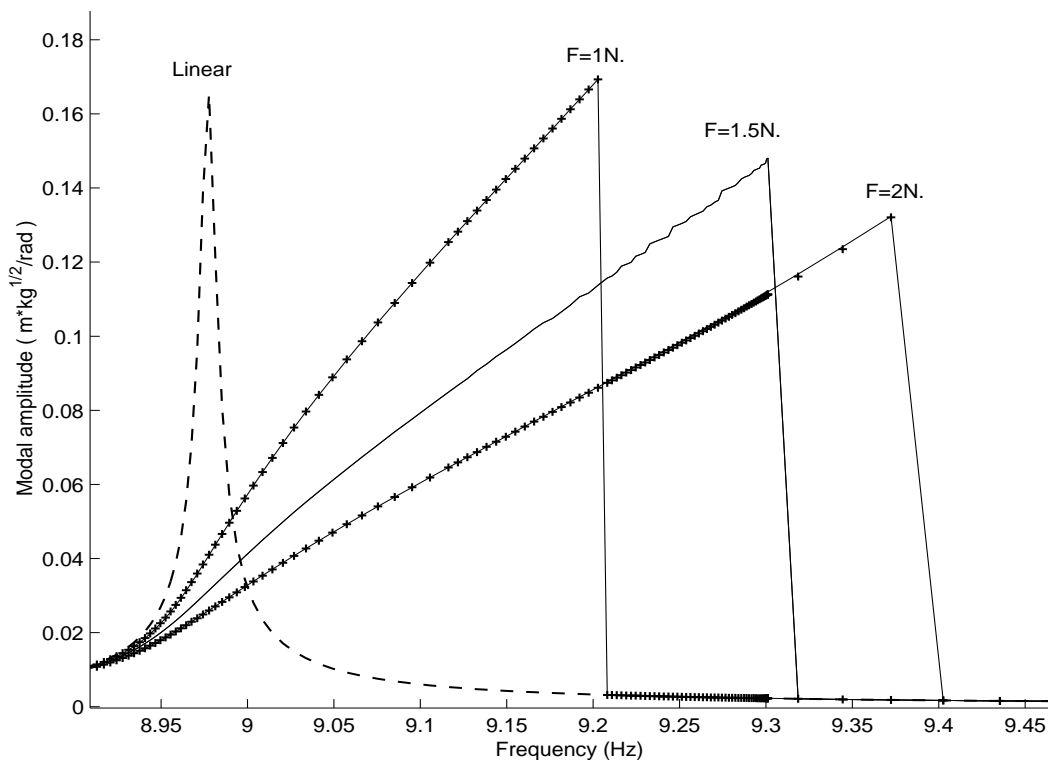
Figure 8.14: HBM results for the first modal amplitude, for three different excitation levels, $F = 1N, F = 1.5N$ and $F = 2N$ (solid line). Also shown in "+" marks, are the polynomial-based predictions

DOF	Identified $\beta(10^6 N/m^3)$	True $\beta(10^6 N/m^3)$	Error %
51	1.5896	1.6	0.65%
62	1.4141	1.5	6.07%
92	7.9885	7.82	2.10%

Table 8.2: Numeric values for the identified coefficients β, as shown in Fig. 8.18
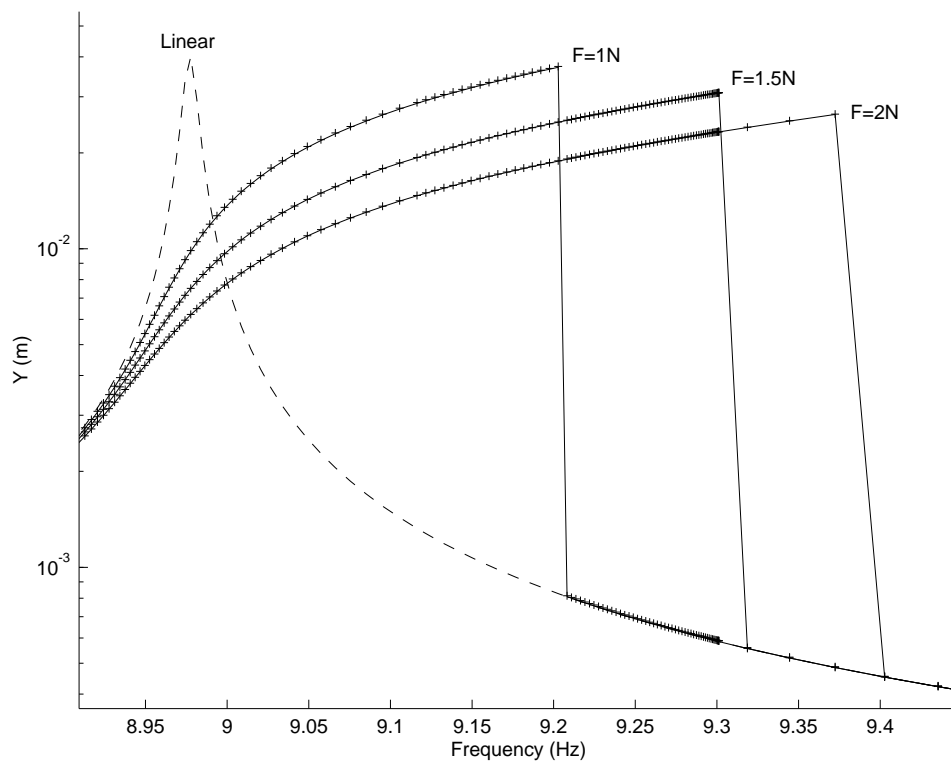
Figure 8.15: Regenerated/predicted physical response ("+") for the first mode of DOF 52, and its HBM counterpart (solid line), for the Sample Case #3
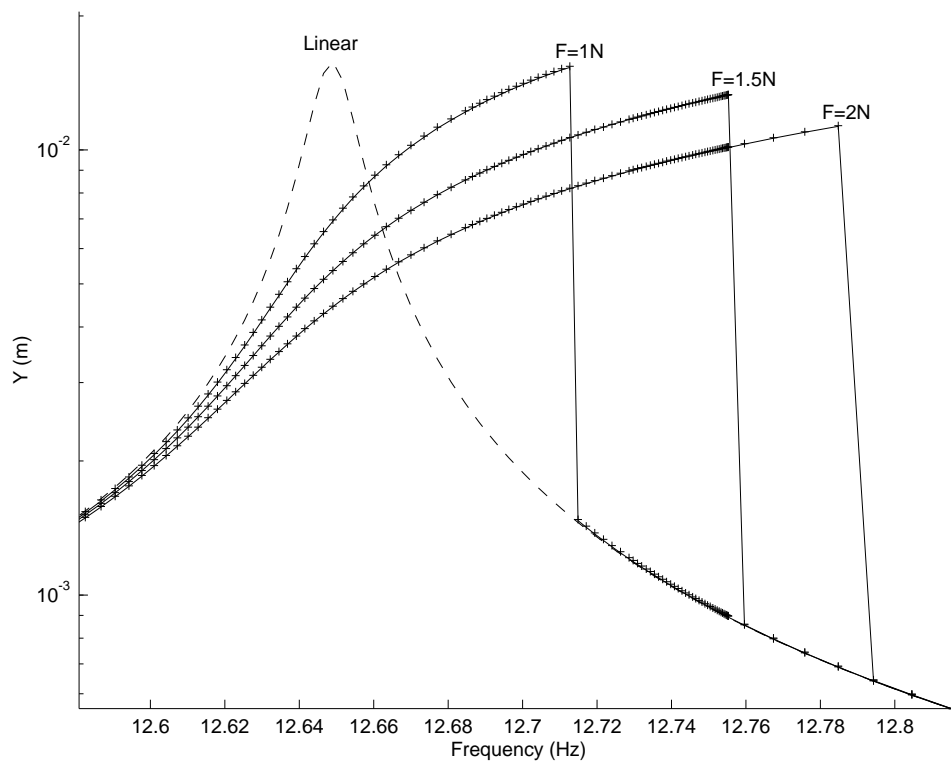
Figure 8.16: Regenerated/predicted physical response ("+") for the second mode of DOF 52, and its HBM counterpart (solid line), for the Sample Case #3
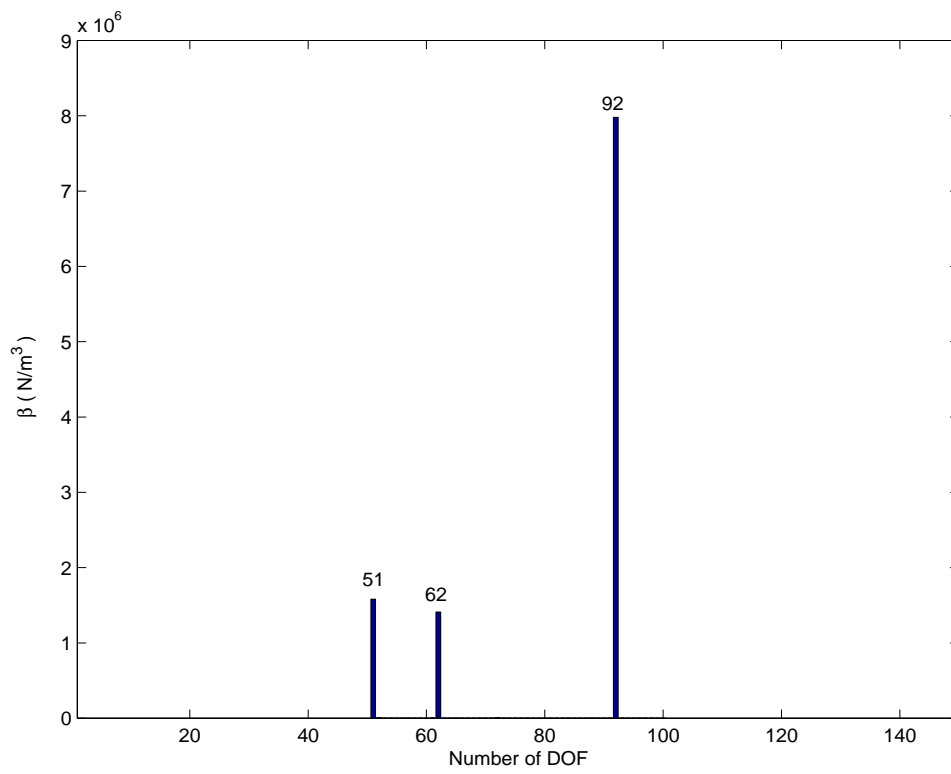
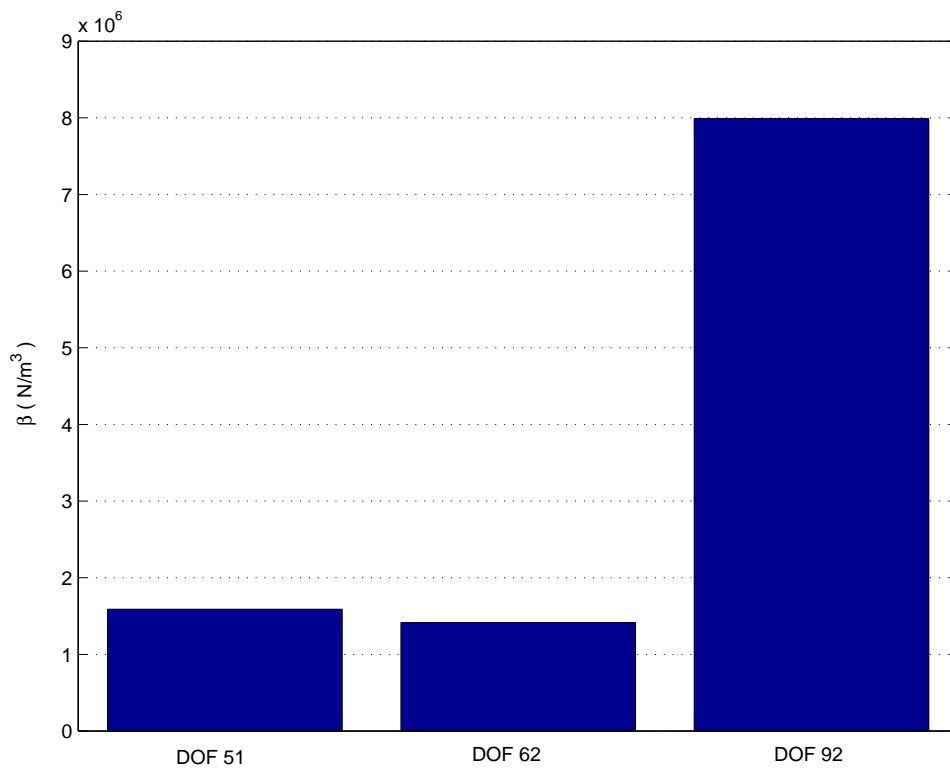Figure 8.17: Detection of the *NL-DOFs* for the Sample Case #3

Figure 8.18: Quantification of the *NL-DOFs* for the Sample Case #3

8.12   Concluding remarks

Right at the beginning of this chapter, we listed some attributes that we would expect from an "ideal" experimental NLMA method. We also said that the introduced method, the R-HMT, might represent a good step forward towards this objective.

So, perhaps the best way to asses the achievements of this chapter is to re-examine this list, in the light of new knowledge:

- Simple to use, so engineers will embrace it. $\sqrt{}$

- Compatible with LMA and standard FE techniques, but does not require a FEM model. $\sqrt{}$

- Relies as little as possible on expert input. $\sqrt{}$

- Size of the model does not matter, within the usual computational restrictions. $\sqrt{}$

- Works with measured data acquired *anywhere* in the system. The availability of more measurements would simply yield higher-quality results. $\sqrt{}$

- Allows a neat separation of the system into linear and nonlinear components, previous to any quantification stage. $\sqrt{}$

- Automatic detection of the nonlinear modes and the type of nonlinearity. $\sqrt{}$

- Automatic and unambiguous localization of the nonlinear elements, provided there are associated measurements. $\sqrt{}$

- If there are no such measurements, the method should still provide a valid mathematical model within a useful range. It should allow, at least, the regeneration/prediction of the response at selected DOFs for different levels of excitation. This is one of the main aims of any method of this kind. $\sqrt{}$

- The method should be numerically stable, relying on proven linear solvers or linear least-squares algorithms. If nonlinear solvers are required, the number of variables should be as small as possible. A good initial guess should be available in such cases. $\sqrt{}$

- The method should not be case sensitive. $\sqrt{}$

Hopefully, the reader will not disagree that the method does indeed go some way to satisfy the above requirements.

Chapter 9

Conclusions and further work

9.1 Conclusions

1. **About the "describing function method" (DFM):**

   - The nonlinear formulation of this research was based on an already well-proved theory, the DFM. This provided the main "engine" of the nonlinear methods developed here. Given the close matching results with the standard "harmonic balance method" (HBM) and experimental measurements, it can be concluded that the DFM is a good choice for modelling nonlinearities.

   - The first-order assumption adopted in this work sufficed to predict the nonlinear behaviour of experimental measurements, with reasonable accuracy. However, this does not represent conclusive evidence for discarding higher-order effects in more complex structures, given the simplicity of the conducted tests.

2. **About the "explicit formulation" (EF):**

   - The EF methodology is conducted entirely in the *physical domain*. This technique manipulates the physical coefficients stored in the system matrices, thus the term "explicit", delivering the nonlinear FRF at a selected DOF as a closed-form expression, regardless of the system's size. Although its derivation is somewhat equivalent to the HBM, the

responses were obtained by a simpler but novel approach involving the ratio of two determinants.

- An *optimized* EF was specially developed for handling large structures. Although the appealing aspect of physical connectivity conservation is lost, the optimization maximises computing economy. This method was validated against real measurements taken from a test rig[1], and the results confirmed that the *optimized* EF can reasonably characterize the behaviour of large structures.

3. **About the "reverse explicit formulation" (REF):**

- A *reverse* path of the "explicit formulation", REF, was implemented as a nonlinear identification tool. In spite of successful results, it was concluded that the computational cost of this approach was too high to gain acceptance in a practical analysis. Still, the method provides a much needed bridge between a full-size theoretical model and the relatively small number of experimental measurements that may be available.

4. **About the "hybrid modal technique" (HMT):**

- The HMT methodology is based on a novel nonlinear modal expansion in the frequency domain, which is analogous to existing nonlinear modal superposition techniques. The underlying linear system is expressed in generalized modal coordinates, while the nonlinearities are kept in the physical domain. The use of hybrid coordinates is a central feature, by which the localization of the nonlinearities is fully addressed.

- The HMT delivers an "exact"[2] representation of a nonlinear FRF. It avoids some common approximations found in other NLMA methods,

---

[1]Described in Appendix C.

[2]Under the first-order assumption of this work. However, higher-harmonics can be included in this formulation, provided that the nonlinear vector $\{\tilde{G}\}$ is a multi-harmonic descriptor.

where the variation of the eigenvectors at the non-resonant modes is often neglected or approximated.

- When compared to traditional NLMA methods, it is believed that the HMT method performs better in an experimental environment. This happens because the nonlinearities are enclosed in a single, thus stronger nonlinear term (the NLMV), whose extraction from measured data is straightforward.

5. **About the "fast approximation technique" (FAT):**

- Although the nonlinear natural frequencies and modal damping are not explicitly needed for identifying the system or regenerating the responses at some other forcing level (by using the HMT), the FAT allowed the *analytical* derivation of these parameters via newly-developed expressions.

- The FAT decouples the nonlinear information contained in the NLMV into single-modal nonlinear parameters, namely, nonlinear eigenvalues and eigenvectors. A further transformation provides a NL model *invariant* to the excitation level, even with scarce measurements.

- The FAT obviates the need of nonlinear optimization techniques for obtaining the nonlinear modal parameters, currently the standard approach. The FAT also provided links with other nonlinear methods, as well as with standard linear modal analysis techniques.

- Based in numerical/experimental observations, Chong & Imregun (30) and others have suggested an invariant relationship between the natural frequencies and the correspondent nonlinear normal modes. The FAT provides mathematical grounds for these works, explicitly determining the analytical relationship.

6. **About the "reverse - hybrid modal technique" (R-HMT):**

- The R-HMT method is aimed at the nonlinear identification of large structures. It operates as a successive application of several "standalone" techniques, also developed here, which can be used indepen-

dently to tackle different aspects of nonlinear modal analysis. When gathered together, the individual techniques provide a robust methodology, able to perform a nonlinear identification within the usual experimental restrictions, while exhibiting high computational efficiency.

- The R-HMT is basically a reverse path of the HMT, expanded to account for the out-of-range modes, also incorporating the FAT methodology. Thanks to a modal approach, the method obviates the need of a FEM model, greatly simplifying an experimental NLMA.

- The localization of the nonlinearities was achieved by a linear least-squares calculation over a predefined *nonlinear region* of arbitrary size. This technique provides an unambiguous localization, provided that the measured frequency range is a fair representation of the system.

- A NLMA technique developed by Chong & Imregun (30) was incorporated into the R-HMT, through the FAT link. This technique adds flexibility to the method, by providing a "black-box" modal identification when the input data is incomplete (e.g., the *NL-DOFs* have not been measured). Although a physical identification is not possible in this case, the addition still allows the regeneration/prediction of the response within a limited range.

7. **About the "nonlinear modal grades":**

- The "nonlinear modal grades" were introduced in Chapter 8, as a mean to quantify the "strength" of the nonlinearities. Thresholds associated with the terms "weakly-", "moderately-" and "strongly-nonlinear" were established, based on observations throughout this research. Also, an absolute "linear threshold" was defined, below which a nonlinear mode can still be considered to behave linearly.

  The practical use of the "nonlinear modal grades" is the automatic selection of the nonlinear modes to be included in the analysis. Currently, this decision relies on the analyst.

8. **About the nonlinear detection techniques:**

- Two nonlinear detection techniques were introduced in this work. These are based in a visual assessment of the geometric shape, or 'footprint", of the NLV and the NLMV. Specifically, it was shown that these techniques are able to discriminate between cubic stiffness and friction damping types.

9.2 Summary of contributions of this thesis

- The EF method, expressing the nonlinear FRF as the ratio of two determinants.

- The REF method, an identification technique aimed to bridge the gap between a full-size theoretical model and the relatively few measurements at specified DOFs.

- The analytical expressions for calculating nonlinear modal parameters, the core of the FAT. They represent, in the author's opinion, the single most important theoretical contribution of this work to the field of NLMA.

- The HMT method, representing an "exact" modal expansion for a first-order nonlinear FRF.

- The R-HMT method, a NLMA technique aimed at the experimental identification of large nonlinear systems. This method represents the most important contribution of this work to the practicing engineer.

- The "nonlinear modal grades", establishing thresholds to quantify the "strength" of the modal nonlinearity.

- The detection of the type of nonlinearity, based in the geometric shape, or "footprint", of both the NLV and the NLMV.

- The localization of the *NL-DOFs* via a linear least-squares calculation, a technique included in the R-HMT method.

9.3 Suggestions for future work

- The nonlinear formulation of this research is based in first-order describing functions. Given that multi-harmonic functions are already available for most nonlinearities, extending the developed methods to account for higher-order terms should be straightforward. Although this approach would enhance the accuracy of the developed methods in a direct-path, the improvement in the identification capabilities is not so clear, given the current difficulties in measuring higher-order FRFs.

- The "explicit formulation" (EF) was expressed as the ratio of two determinants, and it was mentioned that its main drawback is computational cost. Most of this effort is due to the recurrent calculation of a determinant. Special techniques are required to re-calculate a determinant when only a few elements of the matrix (the nonlinear elements) have changed. Solving this issue would dramatically improve the computational efficiency of the EF method, and its identification capabilities.

  Professor J. R. Wright has suggested that the determinant of a large matrix should be calculated from the trace of its eigenvalues. This idea, likely to yield good results, is worth exploring as a first option.

- An exhaustive experimental validation of the "nonlinear modal grades" would be highly valuable, allowing the automatic selection of those modes to be included in a nonlinear analysis, the rest considered as linear.

- Regarding the NL detection technique based on the NLV and NLMV's footprints, further work is needed to incorporate other nonlinearities to this scheme, building a "footprint-library" for the on-line detection of nonlinear types. Also, it is believed that a statistical analysis of the footprint -rather than purely visual- would increase the reliability and automation of the detection.

9.4 Closure

In the grand scheme of things, NLMA is a relatively narrow method in a specialized engineering field. In practice, however, it is a broad and untidy topic. Considering the huge amount of on-going research, things may get worse before improvements are noticed.

This thesis represents just another effort towards the establishment of a general, standard methodology which will settle, for once, the wild variety of existing views and opinions regarding nonlinearities.

While it is fair to recognize that a number of other, more specialized techniques are currently in use to tackle nonlinear issues, it is also true that simple and general approaches often achieve more. The methods developed here are simple and, in principle, general enough to handle most practical problems.

At the end of the day, it is the practicing engineering community who will judge the merits of this work, and the usability of the introduced methods. The author is all aware of the fact that even best theoretical methods do not mean much without a comprehensive experimental validation, which, it should be admitted, this thesis lacks.

Shall we finish by saying that the author will feel rewarded if someone, someday, finds the methods developed in this thesis useful towards the solution of a real engineering problem.

Bibliography

[1] D. J. Ewins, D. Inman, and George R. Goodson. *Structural dynamics 2000: current status and future directions. Full list of questions submitted to SD2000.* Research Studies Press LTD, England, 2001. 1

[2] D. J. Ewins, D. Inman, and George R. Goodson. *Structural dynamics 2000: current status and future directions. Grand challenges for structural dynamics.* Research Studies Press LTD, England, 2001. 1

[3] K. Worden and G. R. Tomlinson. *Non-linearity in structural dynamics: detection, identification and modeling.* Institute of Physics Publishing, Bristol and Philadelphia, Sheffield, 2001. 2, 9, 32, 7.1

[4] D. J. Ewins. *Modal Testing: theory, practice and application.* Research Studies Press LTD, London, 2000. 2, 4.1, 14, 6.2, 8.3, 8.3, 8.3

[5] A. F. Vakakis. Nonlinear normal modes (NNMs) and their applications in vibration theory: an overview. *Mechanical Systems and Signal Processing*, 11(1):3–22, 1997. 2, 6.1

[6] V. Volterra. *Theory of functionals and of integral equations.* Dover Publ., New York, 1959. 1.7

[7] B. Van der Pol. Forced oscillations in a circuit with non-linear resistance. *The London, Edinburgh, and Dublin Philosophical Magazine and Journal of Science*, 3:65–80, 1927. 2.1, 3.2

[8] N. N. Bogoliubov and J. A. Mitropolsky. *Asymptotic methods in the theory of non-linear oscillations.* Hindustan Publishing Company, 1963. 2.1

[9] Y. H. Ku1 and C. F. Chen. A new method for evaluating the describing function of hysteresis-type nonlinearities. *Journal of the Franklin Institute*, 273:226–241, 1962. 2.1

[10] K. Watanabe and H. Sato. A modal analysis approach to nonlinear multi-degrees-of-freedom systems. *ASME Journal of Vibrations, Stress, and Reliability in Design*, 189-3:110–410, 1988. 2.1

[11] H. N. Ozguven. Receptances of non-proportionally and continuously damped plates-reduced dampers method. *Journal of Sound and Vibration*, 85:383–395, 1982. 2.1

[12] H. N. Ozguven. Determination of receptances of locally damped structures. *Proceedings of the Second International Conference on Recent Advances in Structural Dynamics*, 2:887–892, 1984. 2.1

[13] H. N. Ozguven. A new method for harmonic response of non-proportionally damped structures using undamped modal data. *Journal of Sound and Vibration*, 117(2):313–328, 1987. 2.1

[14] H. N. Ozguven. Structural modifications using frequency response functions. *Mechanical Systems and Signal Processing*, 4(1):53–63, 1990. 2.1

[15] E. Budak and H. N. Ozguven. A method for harmonic response of structures with symmetrical non-linearities. *Proceedings of the 15th International Seminar on Modal Analysis, Leuven*, 2:901–915, 1990. 2.1, 3.1

[16] E. Budak and H. N. Ozguven. Harmonic vibration analysis of structures with local non-linearities and validity assessment of some linearization techniques. *Proceedings of the 4th International Conference on Recent Advances in Structural Dynamics*, pages 680–799, 1991. 2.1, 3.1

[17] E. Budak and H. N. Ozguven. Iterative receptance method for determining harmonic response of structures with symmetrical non-linearities. *Mechanical Systems and Signal Processing*, 7:75–87, 1993. 2.1, 3.1

[18] B. Kuran and H. N. Ozguven. A modal superposition method for non-linear structures. *Journal of Sound and Vibration*, 189-3:315–339, 1996. 2.1, 3.1, 3.2

[19] O. Tanrikulu, B. Kuran, H. N. Ozguven, and M. Imregun. Forced harmonic response analysis of non-linear structures. *AIAA Journal (ISSN 0001-1452)*, 31:1313–1320, 1993. 2.1, 2.4, 3.1

[20] A. Besancon-Voda and P. Blaha. Describing function approximation of a two-relay system configuration with application to Coulomb friction identification. *Control Engineering Practice*, 10:655–668, 2002. 2.1

[21] A. Nassirharand and H. Karimib. Input/output characterization of highly nonlinear multivariable systems. *Advances in Engineering Software*, 33:825–830, 2002. 2.1

[22] J. Vaqueiro. *Dynamic response analysis of structures with non-linear components.* PhD thesis, Imperial College London, Department of Mechanical Engineering, Dynamics Section, 1998. 2.1, 3.2, C.1

[23] S. W. Shaw and C. Pierre. Normal modes for nonlinear vibratory systems. *Journal of Sound and Vibration*, 164(1):85–124, 1993. 2.2

[24] S. W. Shaw and C. Pierre. Normal modes of vibration for nonlinear continuous systems. *Journal of Sound and Vibration*, 169(3):319–347, 1994. 2.2, 6.1, 7.2

[25] N. Boivin, C. Pierre, and S. W. Shaw. Nonlinear modal analysis of structural systems featuring internal resonances. *Journal of Sound and Vibration*, 182(2):225–230, 1995. 6

[26] E. Pesheck, N. Boivin, and C. Pierre. Nonlinear modal analysis of structural systems using multi-mode invariant manifolds. *Nonlinear Dynamics*, 25:183–205, 2001. 6

[27] D. Shalev and A. Unger. Nonlinear analysis using a modal-based reduction technique. *Composite structures*, 31:257–263, 1995. 6

[28] P. M. A. Slaats, J. de Jongh, and A. A. H. J. Sauren. Model reduction tools for nonlinear structural dynamics. *Computers & structures*, 54(6):1155–1171, 1995. 6

[29] V. N. Pilipchuk and R. A. Ibrahim. Nonlinear modal interactions in shallow suspended cables. *Journal of Sound and Vibration*, 227(1):1–28, 1999. 7

[30] Y. H. Chong and M. Imregun. Coupling of nonlinear substructures using variable modal parameters. *Mechanical Systems and Signal Processing*, 14(5):731–746, 2000. 7, 7.1, 7.2, 39, 40, 8.7, 8.8, 5, 6

[31] Y. Chong. *Non-linear vibration analysis for multi-degree-of-freedom systems*. PhD thesis, Imperial College London, Department of Mechanical Engineering, Dynamics Section, 1998. 7, 6.1, 7.2, 39

[32] S. F. Masri and T. K. Caughey. A nonparametric identification technique for nonlinear dynamic problems. *Journal of Applied Mechanics*, 46:433–47, 1979. 2.3, 9, 32

[33] E. F. Crawley and A. C. Aubert. Identification of nonlinear structural elements by force-state mapping. *AIAA Journal*, 24:155–162, 1986. 2.3, 32

[34] G. Dimitriadis and J. E. Cooper. A method for identification of nonlinear multi-degree of freedom systems. *Journal of Aerospace Engineering*, 212(4):287–298, 1998. 2.3

[35] R. M. Lin, D. J. Ewins, and M. K. Lim. Identification of nonlinearity from analysis of complex modes. *International Journal of Analytical and Experimental Modal Analysis*, 8(3):290–306, 1993. 2.3

[36] H. J. Rice. Identification of weakly nonlinear systems using equivalent linearization. *Journal of Sound and Vibration*, 185(3):473–481, 1995. 2.3

[37] C. Soize and O. Le Fur. Modal identification of weakly nonlinear, multidimensional dynamical systems using a stochastic linearisation method with random coefficients. *Mechanical Systems and Signal Processing*, 11(1):37–49, 1997. 2.3

[38] C. M. Richards and R. Singh. Identification of MDOF nonlinear systems under random excitations by the "reverse path" spectral method. *Journal of Sound and Vibration*, 213(4):673–708, 1998. 2.3

[39] L. F. Rosa, C. Magluta, and Ney Roitman. Estimation of modal parameters through a nonlinear optimisation technique. *Mechanical Systems and Signal Processing*, 13(4):593–607, 1999. 2.3

[40] M. A. Al-Hadid and J. R. Wright. Developments in the force-state mapping technique for non-linear systems and the extension to the location of non-linear elements in a lumped-parameter system. *Mechanical Systems and Signal Processing*, 3(3):269–290, 1989. 2.3

[41] M. I. McEwan, J. R. Wright, J. E. Cooper, and A. Y. T. Leung. A combined modal/finite element analysis technique for the dynamic response of a nonlinear beam to harmonic excitation. *Journal of Sound and Vibration*, 243(4):601–624, 2001. 8

[42] J. R. Wright, J. E. Cooper, and M. J. Desforges. Normal-mode force appropriation - theory and application. *Mechanical Systems and Signal Processing*, 13(2):217–240, 1999. 8

[43] P. A. Atkins, J. R. Wright, and K. Worden. An extension of force appropriation to the identification of non-linear multi-degree of freedom systems. *Journal of Sound and Vibration*, 237(1):23–43, 2000. 8, 32

[44] J. R. Wright, M. Platten, J. E. Cooper, and M. Sarmast. Identification of non-linear multi-degree of freedom systems using a force appropriation approach. *Proceedings of the International Seminar on Modal Analysis, KU Leuven*, CONF25:439–442, 2001. 8

[45] S. Marchesiello, S. Garibaldi, J. R. Wright, and J. E. Cooper. Applications of the conditioned reverse path method to structures with different types of non-linearities. *Proceedings of the International Seminar on Modal Analysis, KU Leuven*, CONF25:415–422, 2001. 8

[46] M. F. Platten, J. R. Wright, J. E. Cooper, and M. Sarmast. Identification of multi-degree of freedom non-linear simulated and experimental systems. *Proceedings of the International Seminar on Modal Analysis, KU Leuven*, 2002. 8

[47] S. Chen and S. A. Billings. Representations of nonlinear systems: the NAR-MAX model. *Int J. Control*, 49:1013–1032, 1989. 9

[48] J. M. H. Peters. A beginner's guide to the Hilbert transform. *Int. J. Math. Education Sci. Techno.*, 1:89–106, 1995. 9

[49] Y. C. Liang, D. P. Feng, and J. E. Cooper. Identification of restoring forces in non-linear vibration systems using fuzzy adaptive neural networks. *Journal of Sound and Vibration*, 242(1):47–58, 2001. 9

[50] A. A. Ferri and E. H. Dowell. Frequency domain solutions to MDOF, dry friction damped systems. *Journal of Sound and Vibration*, 124(2):207–224, 1987. 2.4

[51] J. H. Wang and W. K. Chen. Investigation of the vibration of a blade with friction damper by HBM. *The American Society of Mechanical Engineers*, 92-GT-8, 1992. 2.4

[52] Y. Ren and C. F. Beards. A new receptance-based perturbative multi-harmonic balance method for the calculation of the steady state response of non-linear systems. *Journal of Sound and Vibration*, 1993. 2.4

[53] S. Hiamang and R. E. Mickens. Harmonic balance: comparison of equation of motion and energy methods. *Journal of Sound and Vibration*, 164(1):179–181, 1993. 2.4

[54] H. J. Rice and K. Q. Xu. A convergent algorithm for harmonic response prediction of general non-linear structures. *Mechanical Systems and Signal Processing*, 10(1):107–112, 1996. 2.4

[55] K. Y. Sanliturk, M. Imregun, and D. J. Ewins. Harmonic balance vibration analysis of turbine blades with friction dampers. *Journal of Vibrations and Acoustics*, 118(001), 1996. 2.4

[56] K. Y. Sanliturk and D. J. Ewins. Modelling two-dimensional friction contact and its application using harmonic balance method. *Journal of Sound and Vibration*, 193(2):511–523, 1996. 2.4

[57] K. Y. Sanliturk, M. Imregun, and D. J. Ewins. Harmonic balance vibration analysis of turbine blades with friction dampers. *ASME Journal of Vibrations and Acoustics*, 119:96–103, 1997. 3.2

[58] K. Y. Sanliturk, M. Imregun, and D. J. Ewins. Friction damper optimization for turbine blades: experimental and theoretical predictions. *In IMechE- Sixth International Conference in Vibrations in Rotating Machinery*, C500/019/96:171–186, 1996. 3.2

[59] N. Maia and J. Silva. *Theoretical and experimental modal analysis*. Research Studies Press LTD, England, 1997. 4.1, 6.2

[60] T. Coleman, M. A. Branch, and A. Grace. *Optimization toolbox for use with MATLAB 5.11*. The MathWorks, Inc., 24 Prime Park Way, Natick, MA 01760-1500, 1999. 13, 1, 6

[61] R. H. Byrd, R. B. Schnabel, and G. A. Shultz. Approximate solution of the trust region problem by minimization over two-dimensional subspaces. *Mathematical Programming*, 40:247–263, 1988. 13, 4.4, 4.4

[62] L. E. Scales. *Introduction to non-linear optimization*. Macmillan Publishers LTD, England, 1985. 13, 4.4, 4.4

[63] J. L. Nazareth. *The Newton-Cauchy framework*. Springer-Verlag, Germany, 1994. 13, 4.4, 4.4

[64] W. L. Ferrar. *Algebra : a text-book of determinants, matrices, and algebraic forms*. Oxford University Press, London, 1941. 14

[65] E. Petrov and D. J. Ewins. Analytical formulation of friction interface elements for analysis of non-linear multi-harmonic vibrations of bladed disks. *Transactions of the ASME*, 125, 2003. 4.5, 6.7, 55

[66] R. M. Rosenberg. On nonlinear vibrations of systems with many degrees of freedom. *Advances in Applied Mechanics*, 9:155–242, 1966. 6.1

[67] R. M. Rosenberg and C. P. Atkinson. On the natural modes and their stability in nonlinear, two degrees of freedom systems. *Journal of Applied Mechanics*, 26-E:377–385, 1959. 6.1

[68] S. Setio, H. D. Setio, and L. Jezequel. A method of nonlinear modal identification from frequency response tests. *Journal of Sound and Vibration*, 3:421–436, 1984. 7.2, 39

[69] S. L. Campbell. *Recent applications of generalized inverses*. Pitman Advanced Pub., London, 1982. 8.3

[70] ICATS users guide. 47 Prince's Gate, Exhibition Road, London SW7 2QA, 2001. B.2

[71] K. Y. Sanliturk. *FINES users guide*. Istanbul Technical University, Istanbul, Turkey, 2000. B.2

[72] Patrick L.M. Chang. Vibration of rectangular plates. Master's thesis, Imperial College London, Department of Mechanical Engineering, 1972. B.2

[73] ProEngineer users guide. PTC, Needham, MA 02494, USA, 2001. C.1

[74] T. J. Royston and R. Singh. Experimental study of a mechanical system containing a local continuous stiffness non-linearity under periodic excitation and a static load. *Journal of Sound and Vibration*, 1908(3):279–298, 1996. C.5

Appendix A

Sample Cases #1 and #2

Sample Cases #1 and #2 are identical in terms of the underlying linear system, but contain different types of nonlinear elements. Sample Case #1 contains purely cubic stiffness NL elements, while Sample Case #2 has friction damping elements.

A.1 Underlying linear data

Fig. A.1 shows a 3-DOF system comprised of 3 masses, whose motion is defined at all times by the response coordinates y_1, y_2 and y_3. Each mass is linked to each other and to the ground by stiffness and damping linear elements, creating fully populated linear matrices. The system is driven by a single harmonic force at mass m_2.

The numerical values for all the coefficients are shown below in matrix format, where a proportional hysteretic damping mechanism has been assumed.

$$\mathbf{M} = \begin{pmatrix} m_1 & 0 & 0 \\ 0 & m_2 & 0 \\ 0 & 0 & m_3 \end{pmatrix} = \begin{pmatrix} 31.590 & 0 & 0 \\ 0 & 55.401 & 0 \\ 0 & 0 & 24.212 \end{pmatrix} kg$$

$$\mathbf{K} = \begin{pmatrix} k_{11} & k_{12} & k_{13} \\ k_{21} & k_{22} & k_{23} \\ k_{31} & k_{31} & k_{33} \end{pmatrix} = \begin{pmatrix} 200491.263 & -64920.980 & -36279.371 \\ -64920.980 & 398118.365 & -17503.205 \\ -36279.371 & -17503.205 & 132578.825 \end{pmatrix} N/m$$
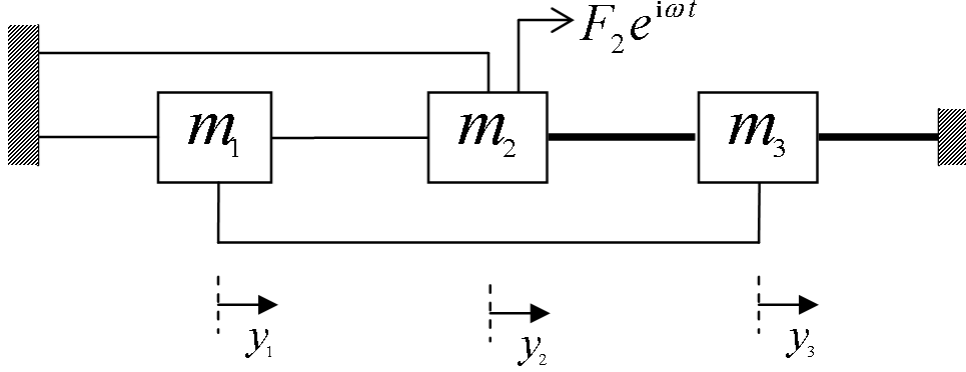
Figure A.1: Diagram for the Sample Cases #1 and #2

$$\mathbf{F} = \left\{ \begin{array}{c} F_1 \\ F_2 \\ F_3 \end{array} \right\} = \left\{ \begin{array}{c} 0 \\ 12 \\ 0 \end{array} \right\} N$$

$\eta = 0.12\%$

Formulating the eigenvalue problem, we have:

$$\left(-\omega^2 \mathbf{M} + \mathbf{K} + i\mathbf{D}\right)\{Y\} = 0$$

from which the linear matrices of eigenvalues and (mass-normalized) eigenvectors are obtained:

$$\lambda^2 = 10^3 \cdot \left(\begin{array}{ccc} 3.9581(1 + 0.0012\mathbf{i}) & 0 & 0 \\ 0 & 6.6045(1 + 0.0012\mathbf{i}) & 0 \\ 0 & 0 & 8.4458(1 + 0.0012\mathbf{i}) \end{array} \right) \frac{rad^2}{sec^2}$$

$$\mathbf{\Phi} = \left(\begin{array}{ccc} 0.1115 & -0.0758 & -0.1160 \\ 0.0537 & -0.0727 & 0.0992 \\ 0.13577 & 0.1472 & 0.0343 \end{array} \right) \frac{rad}{\sqrt{kg}}$$

The corresponding linear response is shown in Fig. A.2, where it can be seen that the three expected resonances occur at approximately 10.01, 12.93 and 14.62 Hz.
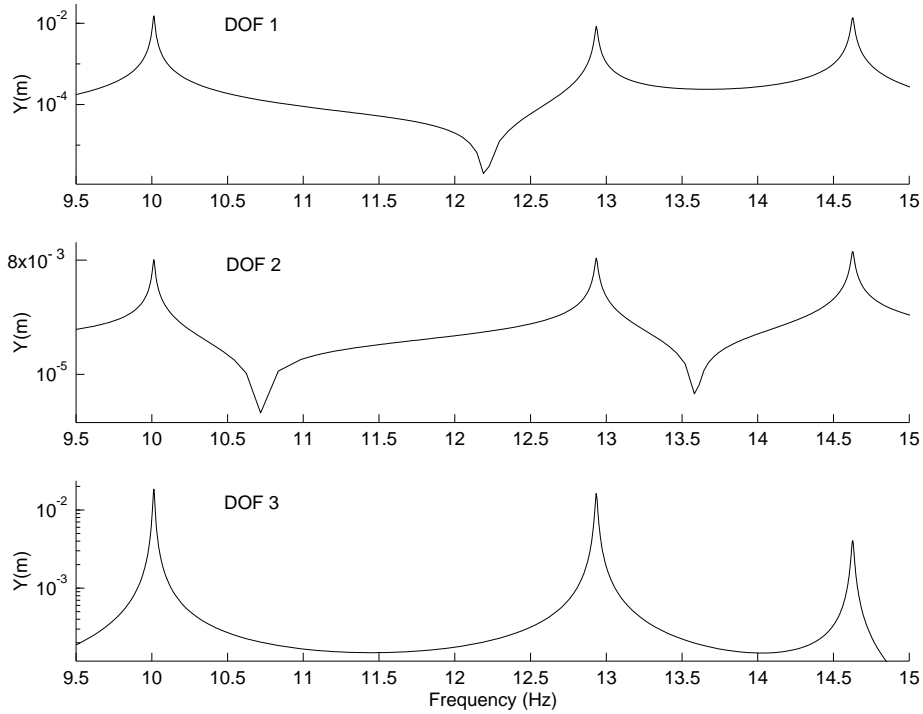
Figure A.2: Sample Cases #1 and #2, linear response

A.2 Nonlinear data

In addition to the linear system, two nonlinear elements have been incorporated, represented by the two thick links in Figure A.1. The numeric values of these coefficients are given in Table A.1, and their correspondent force-displacement curves are shown in Figures A.3 to A.6.

The nonlinear elements were placed as previously described to provide a sufficiently general arrangement considering the size of the system. It has a mixture of grounded and non-grounded NL elements, a "nonlinear region" comprised of DOFs 2 and 3, as well as a "region away from nonlinearities", represented by DOF 1.

DOF	DOF	Sample Case #1 $\beta(N/m^3)$	Sample Case #2 $\gamma(N)$	Type
1	1	—	—	
1	2	—	—	
1	3	—	—	
2	2	—	—	
2	3	7.82E6	1.25	non-grounded
3	3	1.44E7	2.10	grounded

Table A.1: Nonlinear coefficients for the Sample Cases #1 and #2
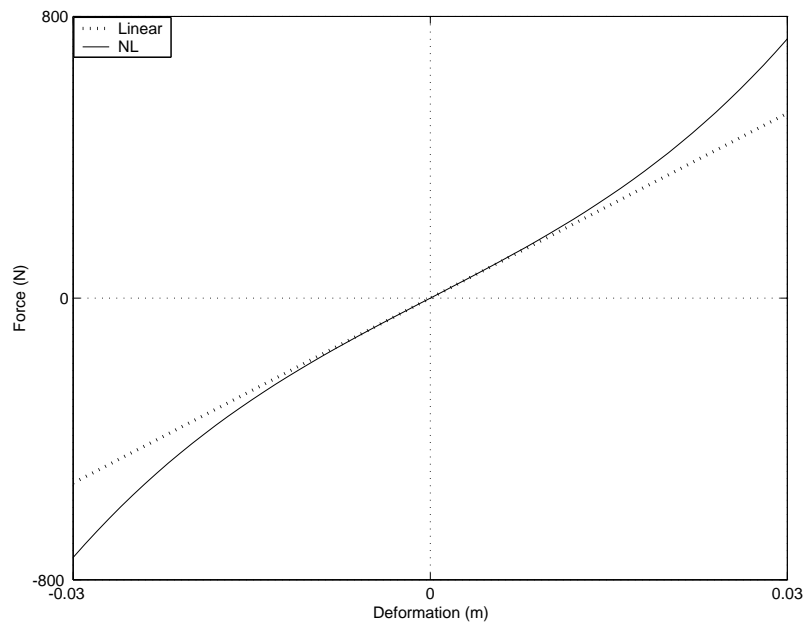
Figure A.3: Sample Case #1, non-grounded cubic stiffness spring
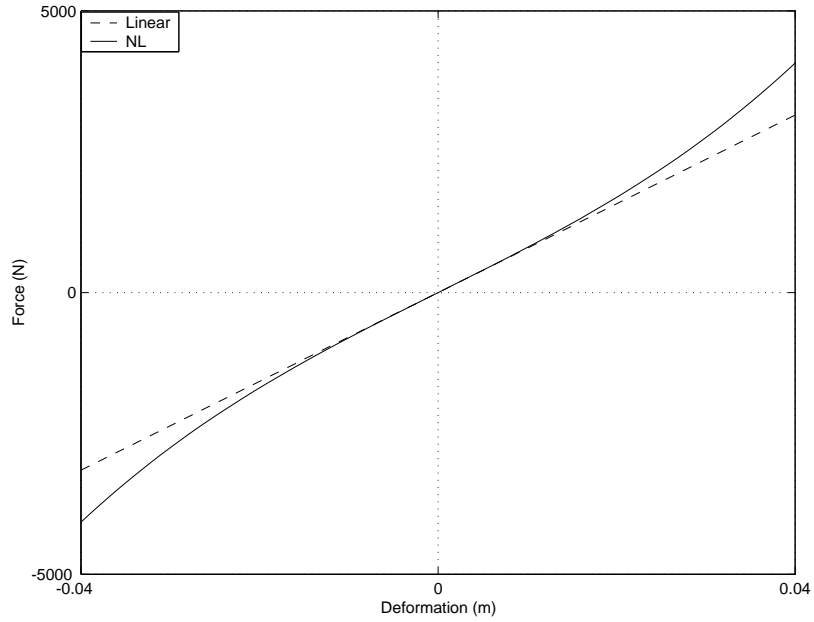
Figure A.4: Sample Case #1, grounded cubic stiffness spring
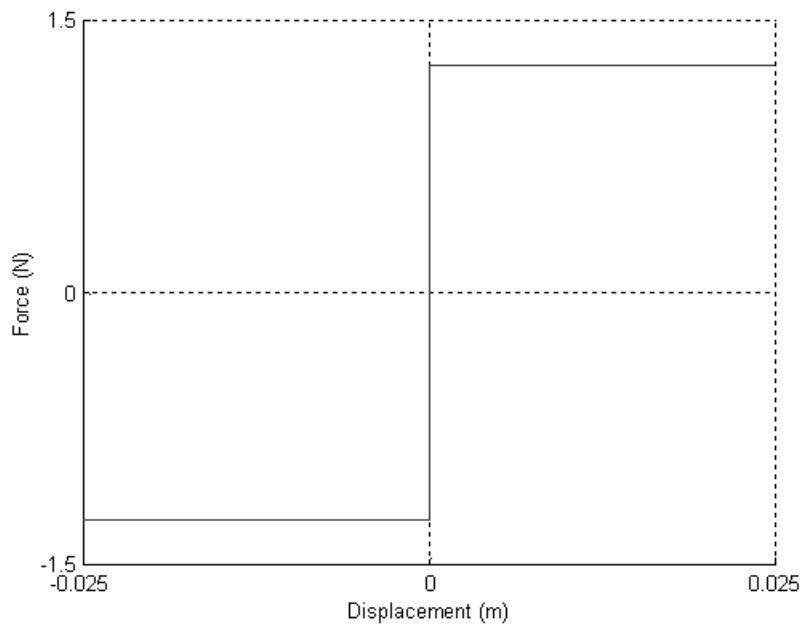
Figure A.5: Sample Case #2, non-grounded friction damping element
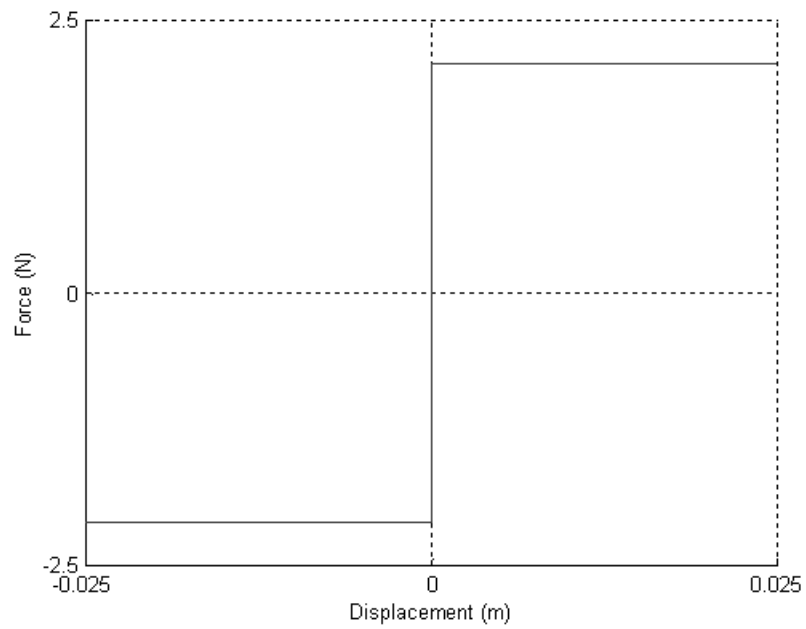
Figure A.6: Sample Case #2, grounded friction damping element

Appendix B

Sample Case #3

A FE model of the Sample Case #3 is shown in Figure B.1, displaying a flat rectangular plate which lies in the "XZ" plane, with its normal aligned in the positive direction of the "Y" axis.

B.1   FEM model

The properties of the FEM model are listed below:

- **Dimensions:** 1m x 0.0032m x 1.4m

- **Material properties:**

  - Material Young's modulus = 207.0E9 N/m^2

  - Poisson's ratio = 0.3

  - Material density = 7800 kg/m^3

  - Material loss factor = 0.1%

- **Computer model:**

  - Number of nodes = 150
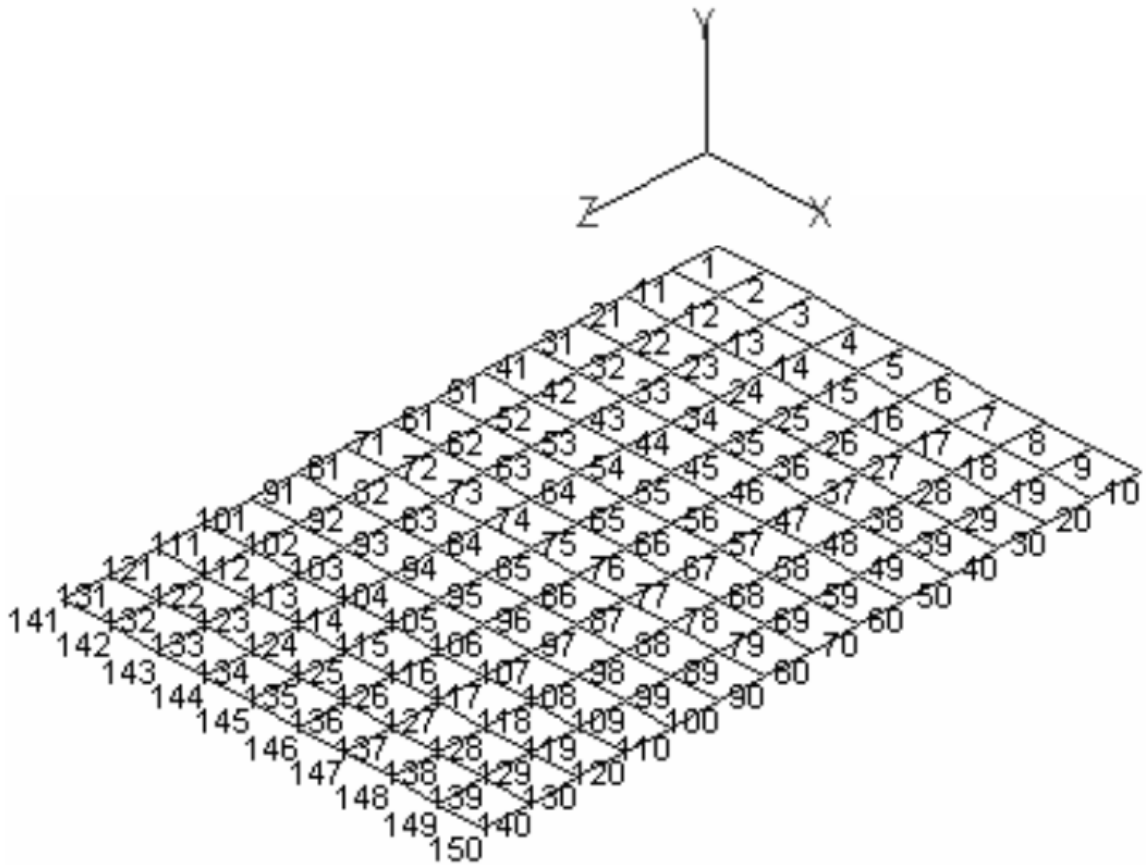
Figure B.1: FEM model of the Sample Case #3

- Number of elements = 126 shell elements with 6 DOFs per node $(x, y, z, \theta_x, \theta_y, \theta_z)$. This type of element has a genuine drilling degree of freedom about its main axis.

- Boundary conditions (BC): clamped at nodes $\{1, 2, .., 10\}$ and $\{141, 142, .., 150\}$.

- Total number of DOFs after applying BC $(N)= 780$

• **Excitation:** $f = \{67Y\}$, a single harmonic force at DOF 67Y (node 67 in the "Y" direction), with a magnitude of 1.5N. See Fig. B.4.

- **Analyzed frequency range:** 8-35 Hz., covering the first five modes of the model. This yields $m = \{1, 2, 3, 4, 5\}$.

- **Measured region** $\Re$**:** DOFs $\{41Y, 42Y, \ldots, 110Y\}$, see Fig. B.4. Outside this region, measurements are not available.

- **Nonlinear region** Γ**:** DOFs $\{51Y, 52Y, \ldots, 100Y\}$, see Fig. B.4. Nonlinearities are assumed to exist only within this region.

- **Nonlinearities:** an unknown number of discrete NL elements, attached between any node within Γ and ground, acting along the "Y" axis.

According to the assumptions surrounding the definition of the various *regions*[1], we have:

$$n \in \Gamma \in \Re \in N, \quad \text{typically} \quad n \ll \Gamma \leq \Re \ll N \tag{B.1}$$

and

$$f \in \Re, \quad \text{typically} \quad f \ll \Re \tag{B.2}$$

B.2   Linear data

The geometry was built using MODENT (70), a modal analysis software developed at Imperial College London, and then exported to FINES (71), a simple but efficient finite element solver. The linear eigenvalue problem was then solved, calculating the first 20 natural frequencies, damping loss factors and translational eigenvectors. The results were sent back to the MODENT suite, allowing the animation of the mode shapes on the computer model.

Figure B.2 shows the first 4 mode shapes of the structure, where it can be verified that the results are in agreement with the theoretical linear predictions (72).

The information obtained so far constitutes the so-called "underlying linear system" and suffices to describe its linear response. As an example, Fig. B.3

---

[1]See Section 3.4.
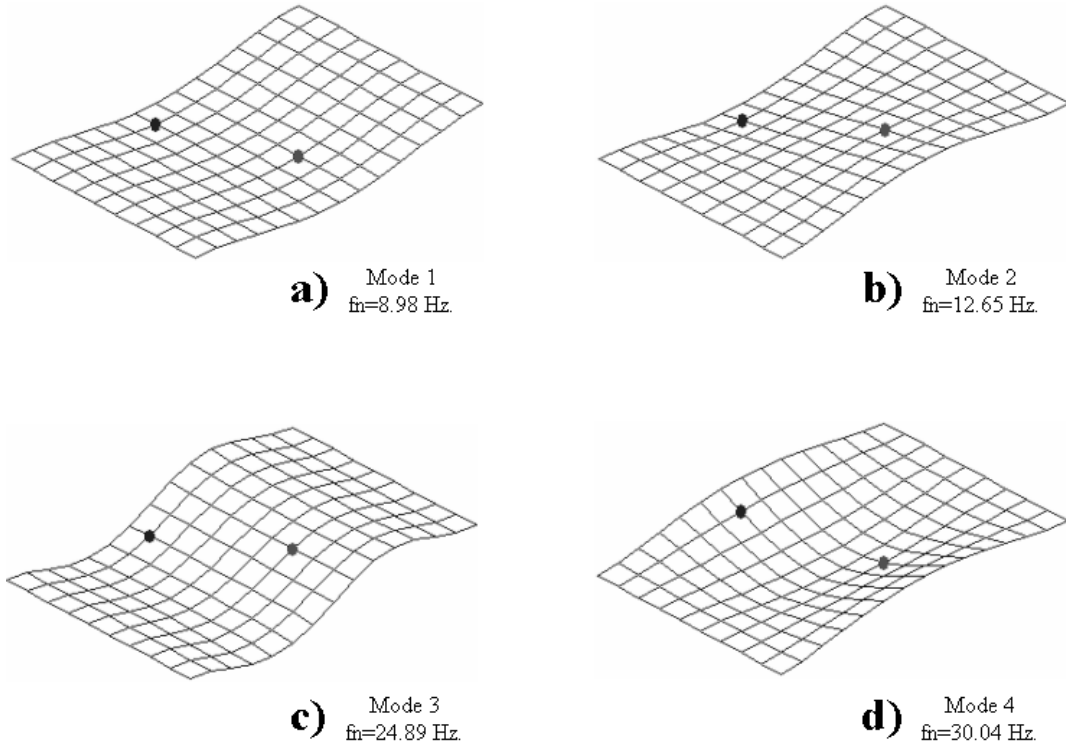
Figure B.2: Visualization of the linear mode shapes on the computer model

shows the linear FRF corresponding to DOF 82Y (node 82 in the "Y" direction). Only the first five modes are shown, as grounded nonlinearities are unlikely to affect higher modes in this type of structure.

Because each node in the FEM model contains 6 DOFs, and because the actual formulation manipulates DOFs instead of nodes, the following convention is handy for translating the node number to its correspondent DOF:

$$\#DOF = (\#node - 1) * 6 + \left\{ \begin{array}{l} 1, \text{ if x direction} \\ 2, \text{ if y direction} \\ 3, \text{ if z direction} \\ 4, \text{ if } \theta_x \text{ direction} \\ 5, \text{ if } \theta_y \text{ direction} \\ 6, \text{ if } \theta_z \text{ direction} \end{array} \right\} - (10 * 6)$$
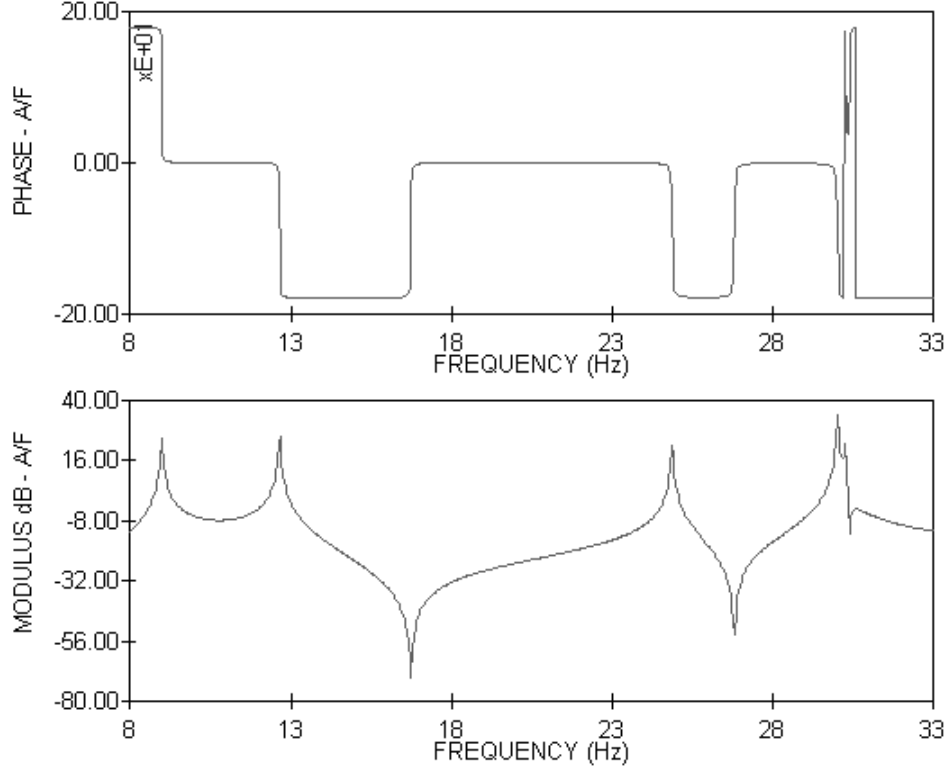
Figure B.3: Linear FRF of the Sample Case #3 corresponding to DOF 82Y

where the included term "$(10*6)$" accounts for the first 10 clamped nodes at $Z = 0$, which are simply dropped from the analysis as their displacement is zero at all times. The clamped nodes at $Z = 1.4$ are also excluded for the same reason, but they play no further role in renumbering the DOFs because they represent the last rows/columns in the system's matrices.

As an example, the DOF in which the excitation has been placed is calculated as follows: the force is acting at node 67, along the "Y" axis, so its corresponding DOF is:

$$F_{DOF} = (67 - 1)*6 + 2 - (10*6)$$
$$F_{DOF} = 338$$

The pre-defined regions for the Sample Case #3, given both in DOF and $nodal$ notation, are:

$$N = \left\{ \underbrace{(1,2,3,4,5,6)}_{11(x,y,z,\theta_x,\theta_y,\theta_z)}, \underbrace{(7,8,9,10,11,12)}_{12(x,y,z,\theta_x,\theta_y,\theta_z)}, \ldots, \underbrace{(775,\ldots,780)}_{140(x,y,z,\theta_x,\theta_y,\theta_z)} \right\} \begin{array}{l} \text{(DOF notation)} \\ \text{\small(node notation)} \end{array}$$

$$\Re = \left\{ \underbrace{182}_{41Y}, \underbrace{188}_{42Y}, \underbrace{194}_{43Y}, \ldots, \underbrace{596}_{110Y} \right\} \begin{array}{l} \text{(DOF notation)} \\ \text{\small(node notation)} \end{array}$$

$$\Gamma = \left\{ \underbrace{236}_{51Y}, \underbrace{242}_{52Y}, \underbrace{248}_{53Y}, \ldots, \underbrace{536}_{100Y} \right\} \begin{array}{l} \text{(DOF notation)} \\ \text{\small(node notation)} \end{array}$$

$$f = \left\{ \underbrace{338}_{67Y} \right\} \begin{array}{l} \text{(DOF notation)} \\ \text{\small(node notation)} \end{array}$$

where $N, \Re, \Gamma$ and f are a-priori defined by the analyst. These regions are shown in Fig. B.4.

B.3 Nonlinear data

The NL-DOFs[1] for the Sample Case #3 are defined as $n = \{51, 62, 92\}$, as shown in Fig. B.4. This vector represents three discrete nonlinear elements attached between each NL-DOF and ground, characterized by cubic stiffness behaviour. According to the restriction posed by the *nonlinear region* Γ, it can be observed that $n \in \Gamma$. The numerical values for the β coefficients[2] are given in Table B.1.

The nonlinear responses were obtained by numerical simulation, with a code based on the "harmonic balance method", which is a recognized benchmark for nonlinear problems. The particular HBM code used in this work was written by Dr. Evgeny Petrov (65) under a long term research program at Imperial College London for the vibration analysis of nonlinear structures with different types of nonlinearities, such as friction damping and cubic stiffness.

Figures B.5 and B.6 show the simulated nonlinear response of three randomly chosen DOFs, within $\Re$. It can be seen that the first two modes exhibit strong nonlinear effects, while the third mode behaves almost linearly. Higher modes are

---

[1] Those DOFs associated with nonlinear elements.

[2] See Chapter 3.

undistinguishable from their linear counterparts. Fig. B.7(a) shows the linear and nonlinear responses of a randomly chosen DOF 92Y, while Fig. B.7(b) shows the corresponding linear residual $Res_{92\mathrm{Y}}$. A suitable choice of nonlinear modes as a subset of m would be $m_{NL} = \{1, 2\}$, as the remaining behave in an almost linear fashion.

DOF	$\beta(10^6 N/m^3)$
51	1.6
62	1.5
92	7.82

Table B.1: Coefficients β for the Sample Case #3
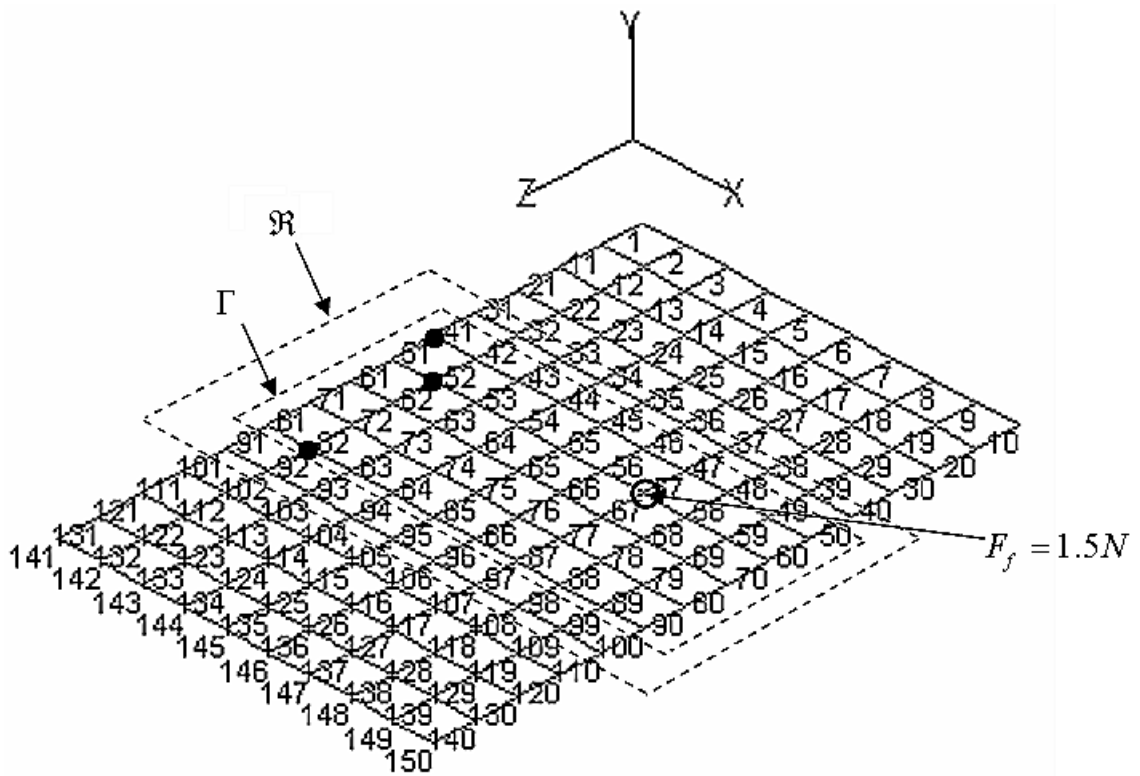
Figure B.4: The *measured region* $\Re$, the *nonlinear region* Γ and the forced DOF f for the Sample Case #3. The NL-DOFs $n = \{51, 62, 92\}$ are marked with black dots.
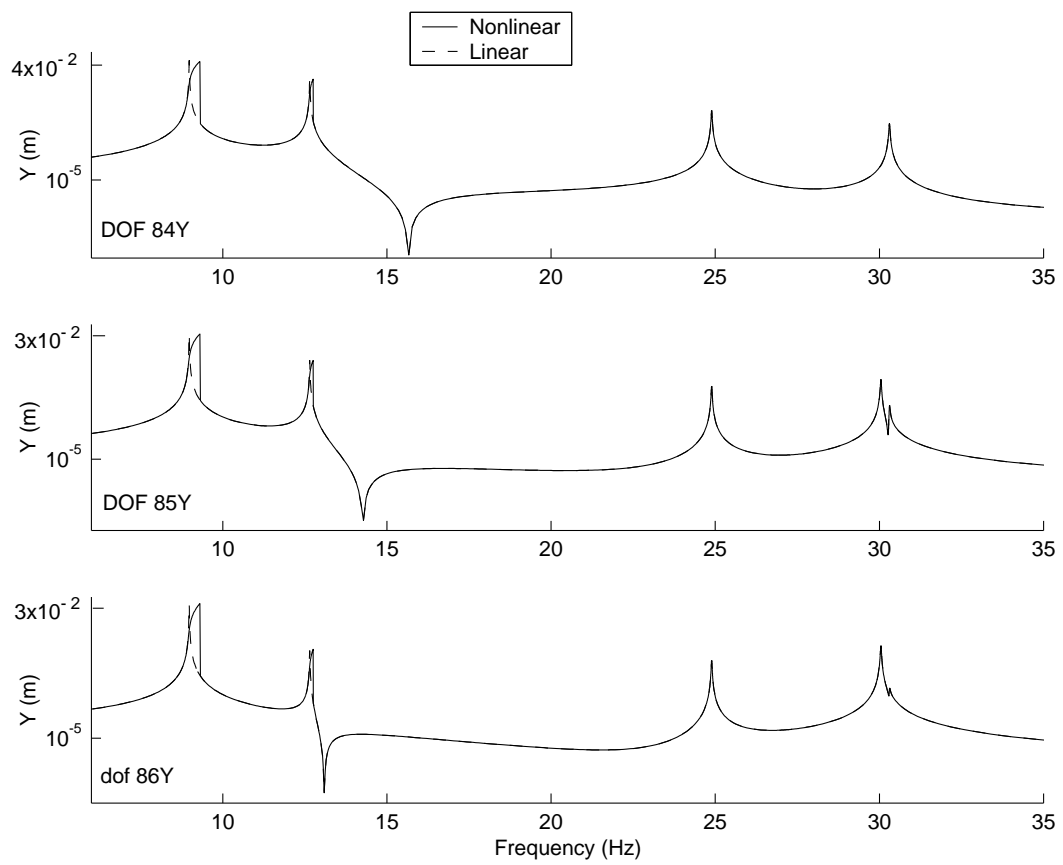
Figure B.5: Nonlinear response of the Sample Case #3, for three randomly chosen DOFs. A Zoom-In of modes 1 and 2 is shown in Fig. B.6
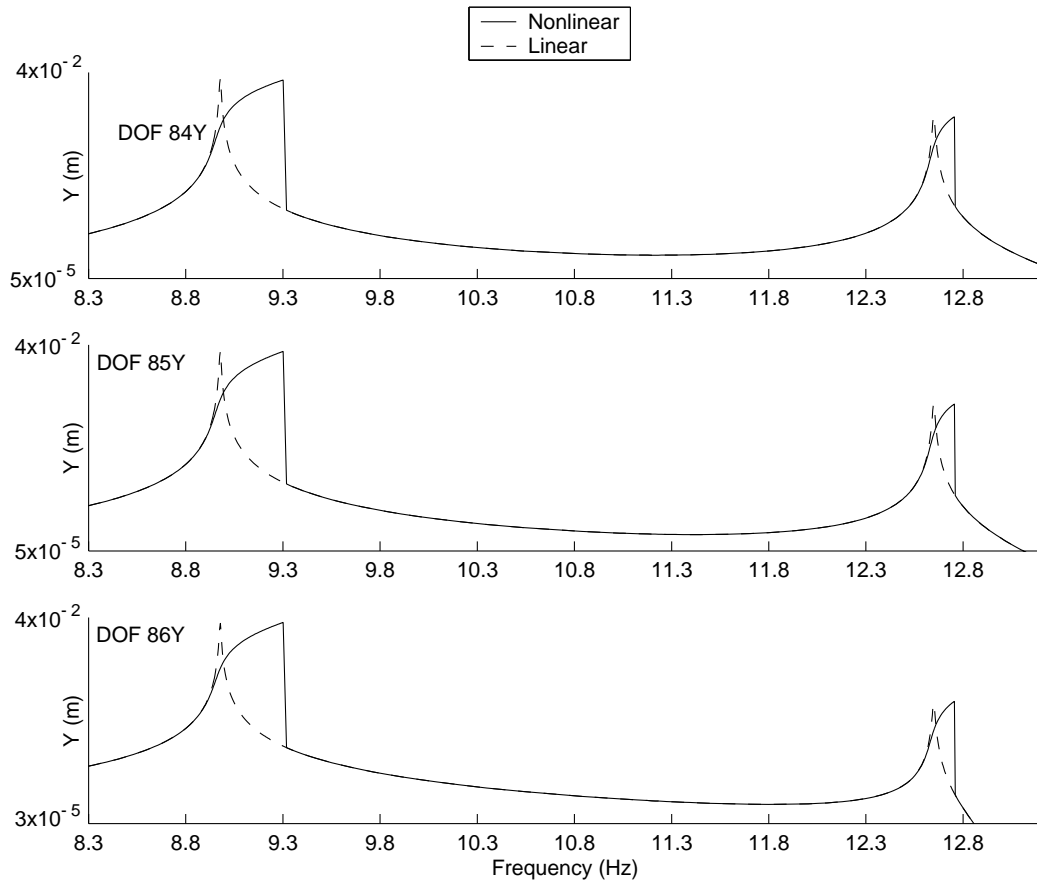
Figure B.6: Zoom-In of the first two modes of Figure B.5
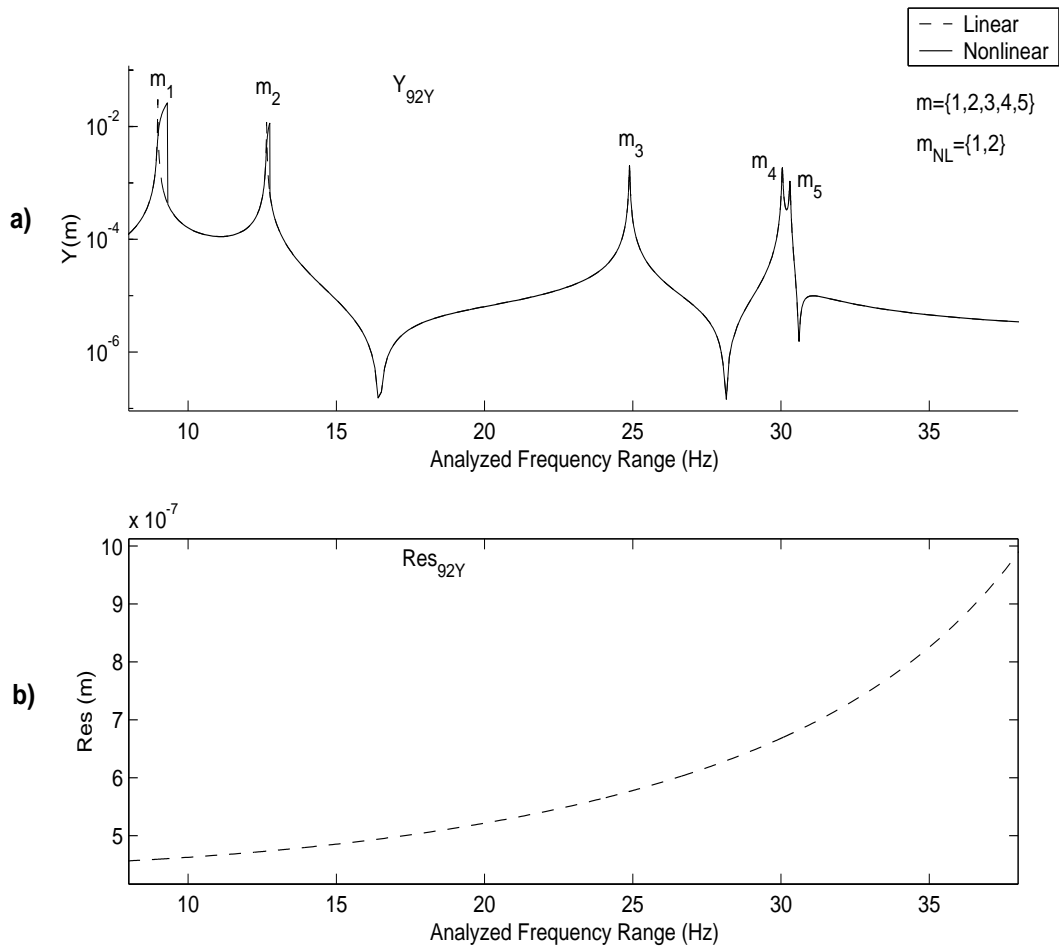
Figure B.7: (a): linear (dashed line) and nonlinear (solid line) responses for DOF 92Y of the Sample Case #3. (b): linear residual for the same DOF

Appendix C

Experimental validation of the explicit formulation (EF)

C.1 Design and construction of the test rig

A test rig was designed and built for the purpose of acquiring nonlinear FRFs. The design is similar to a rig previously made by J. Vaqueiro (22), which was proved to behave nonlinearly. However, the main aim of the current experiment is the validation of the EF method, as it contains the core nonlinear formulation of all the methods developed in this research (EF, REF, HMT, FAT and R-HMT).

The design of the test rig was made in Pro-Engineer (73), a specialized CAD software which allows the representation of mechanical assemblies as well as finished drawings. Figs. C.1 and C.2 show 3D representations of the computer model, while Fig. C.3 specifies its relevant physical dimensions.

As seen in these figures, the test rig consists of a cantilever beam with a rectangular cross-section, representing the linear part of the system. Its free end is supported by a nonlinear spring, in the form of two identical thin beams running transversally to the cantilever, and clamped at both ends. The transversal beams behave nonlinearly even at small displacements, due to their thin rectangular

Figure C.1: Computer model of the test rig

EXPLD STATE: EXP0002
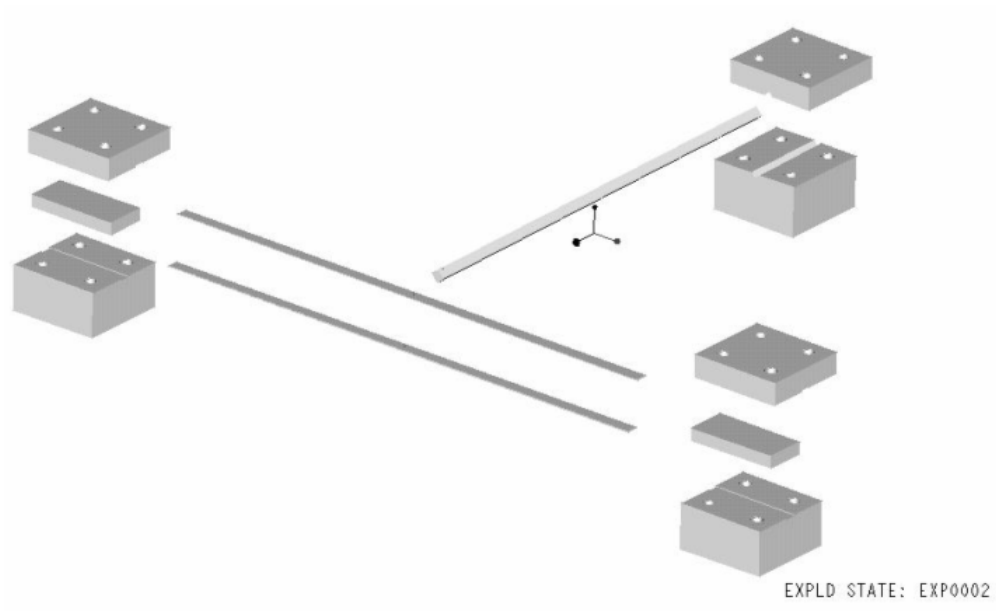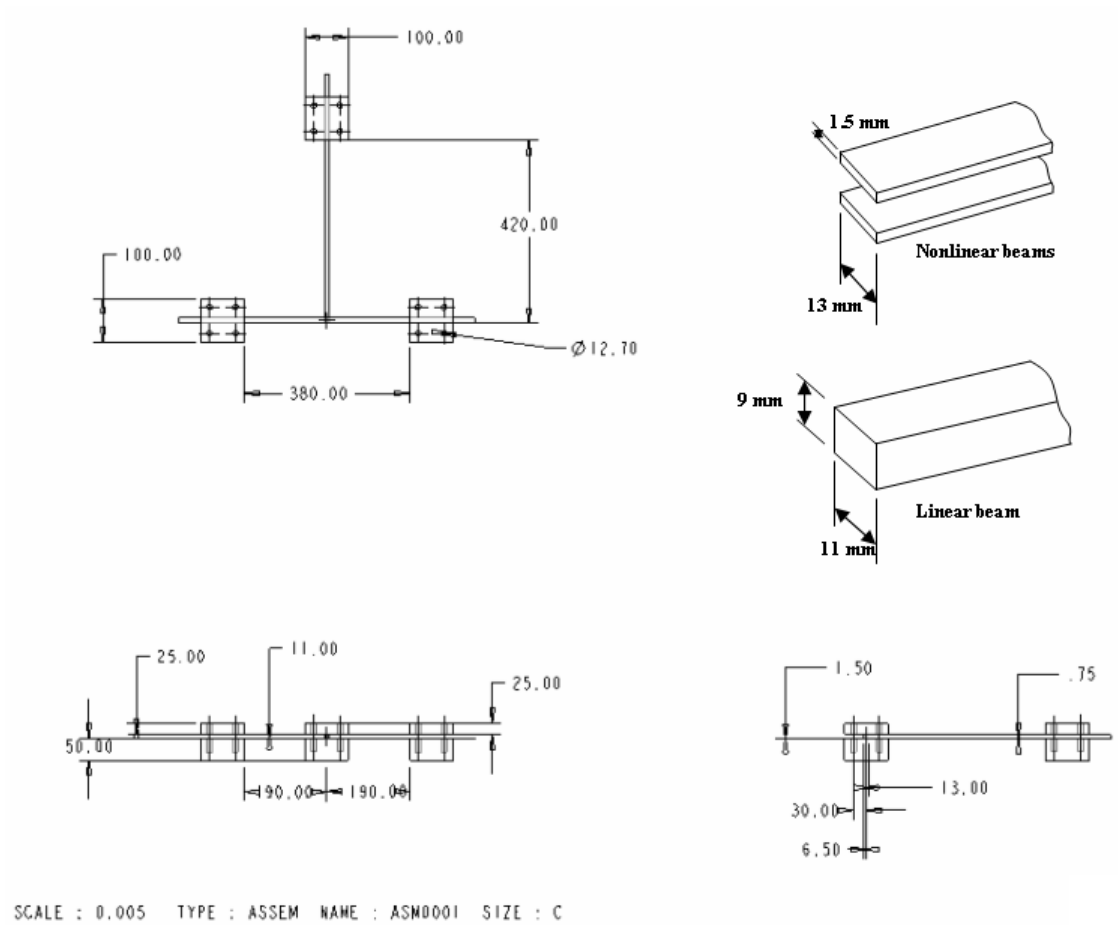
Figure C.2: Exploded view of the computer model

Figure C.3: Physical dimensions (in mm.) of the test rig

cross-section. The assembly is completed by a single bolted-joint, joining the three components in a symmetrical "T" arrangement.

The clamped boundary conditions were provided by 3 massive blocks, which hold the beams' ends in all directions, by means of a bolted fixture. The blocks are further clamped by the same bolts to a common ground (a plate), not shown in the computer model.

The rectangular sections were adjusted in such a way that a displacement of 5mm. at the "T" junction, generates stresses beyond the elastic limit on the nonlinear spring (the transversal beams), according to an earlier FEM analysis. This displacement was chosen because it is considerable less than the maximum displacement allowed by the excitation system in use (1.5cm.).

All the components are made of A40 steel, whose main properties are

- Young's modulus: $E = 207E9 \, N/m^2$.

- Poisson modulus: $\upsilon = 0.3$.

- Density: $\rho = 7800 \, kg/m^3$.

- Hysteretic damping: $\eta = 0.1\%$.

The test rig was built according to the aforementioned specifications, as shown in Fig. C.4.

C.2 FEM analysis

A FEM analysis was carried out to predict the *linear* response of the test rig, previous and after its construction. Several models were built, from extremely simple 3D-beam elements, to more sophisticated ones, conformed of a mixture of 3D-brick, 3D-shell, MPC (multi-point constraint) and discrete spring elements. Fig C.5 show two of these models.

Given that the nonlinearities were expected to arise in the first mode only, it was decided to stick with the simplest possible model which could accurately represent this frequency range. The chosen FEM model is shown in Fig C.6,
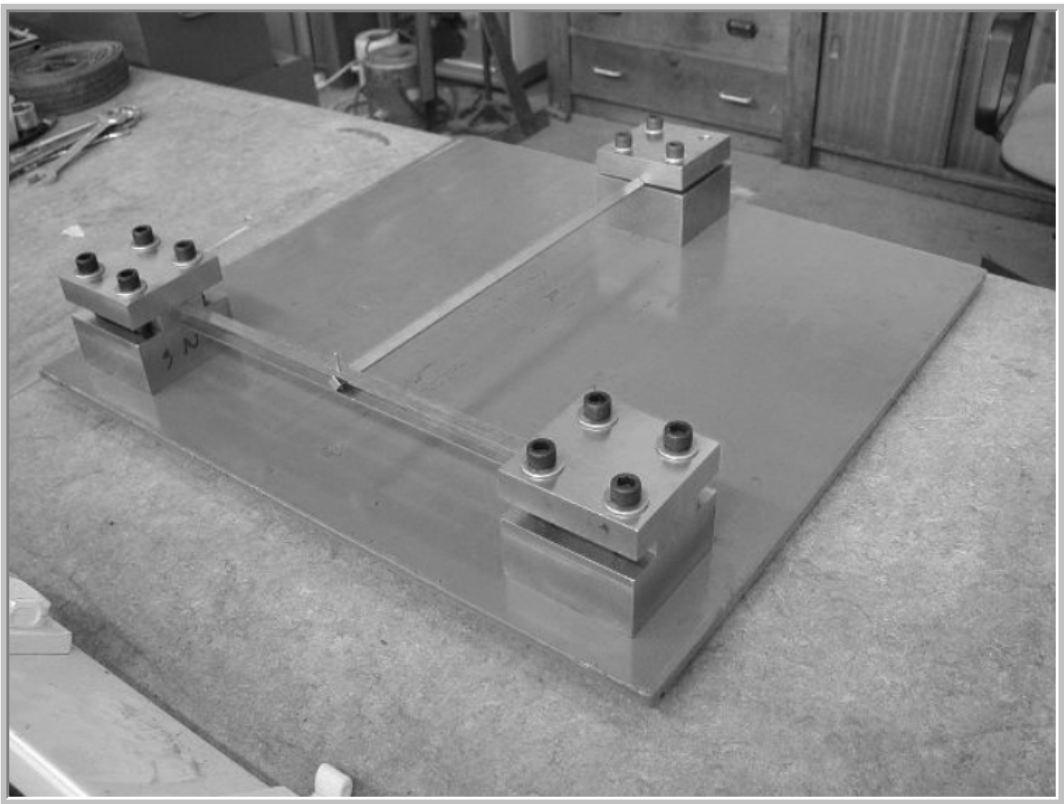
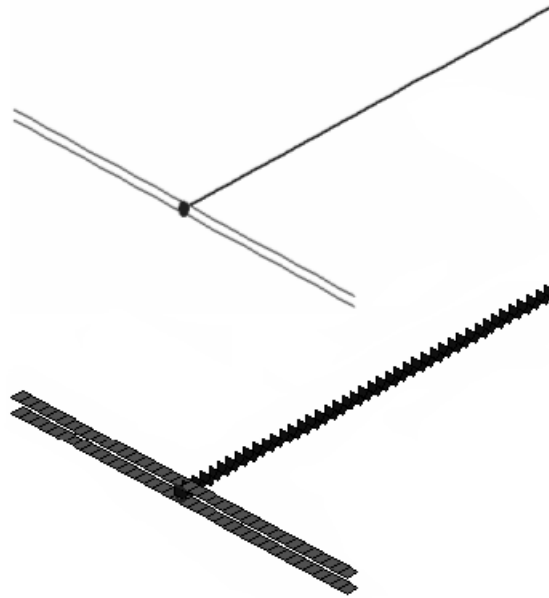Figure C.4: Finished assembly of the test rig

Figure C.5: Two different FEM models for the test rig

which is composed of 66 nodes and 64 beam elements (2-node each), based in Bernoulli's beam theory. The central joint, shown in more detail in Fig C.7 as node #22, was modelled with similar beam elements with a much higher stiffness, to prevent relative motion.

C.3 The static test

A static test was performed prior to the dynamic test, to find out the real force-displacement characteristics of the nonlinear spring. The test was carried out using a load cell and a LVDT (linear variable displacement transducer), previously calibrated against a standard dial gauge and mass.

The results of the static test are shown in Fig. C.8, showing the force-displacement curve of the nonlinear component. A fitted polynomial revealed
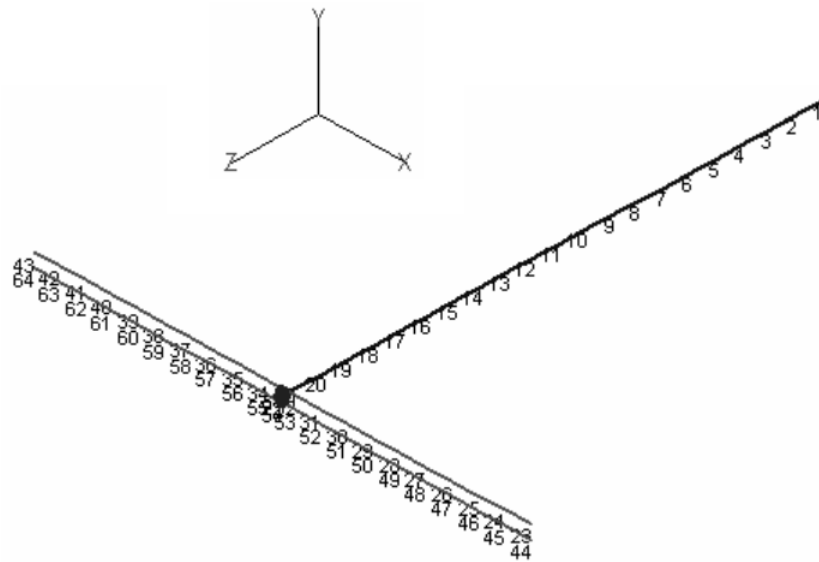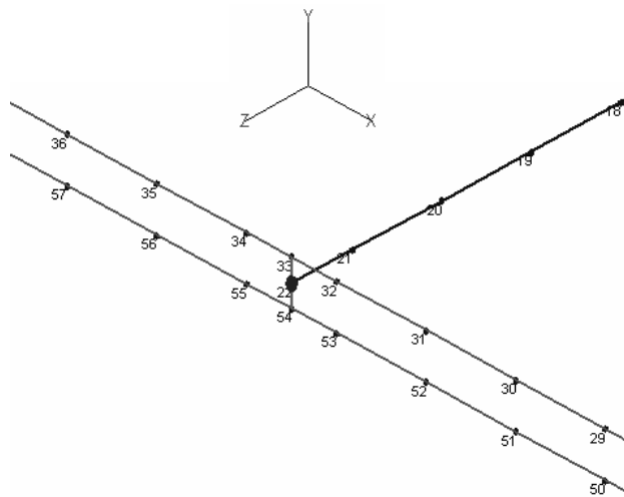
Figure C.6: Chosen FEM model

Figure C.7: Close-up at the central joint (node 22) of the chosen FEM model
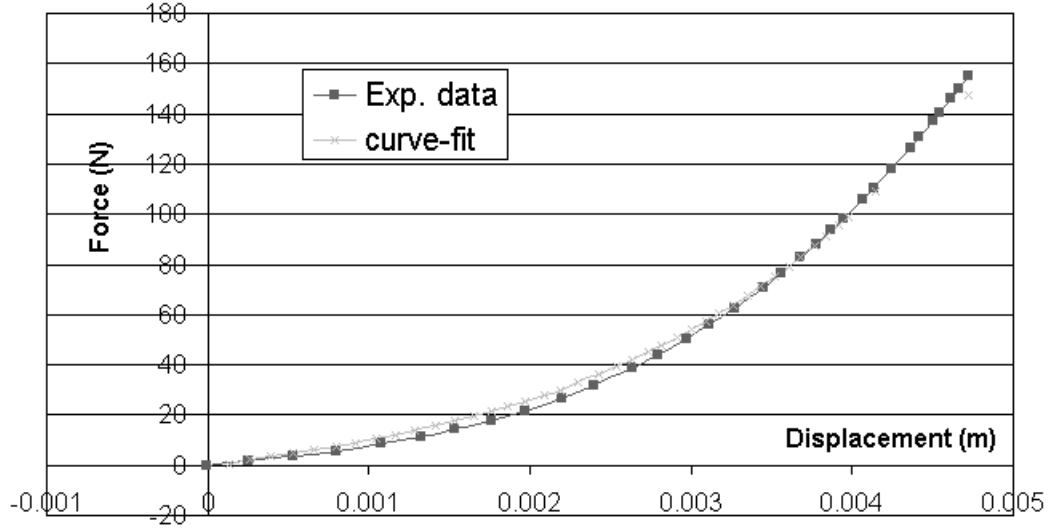
Figure C.8: Static test

a function of the type:

$$F = 6500x + 1.18x10^9 x^3 \qquad \text{(C.1)}$$

which fully characterizes the nonlinear spring.

C.4 The linear test

A hammer test was performed on the structure to approximately localize the linear natural frequencies. A *PCB-309A* accelerometer was fixed at the central joint, while a *PCB-086D20* hammer with a soft tip provided impulses at the 22 nodal points of the linear beam, according to the FEM model of Fig. C.6. The FRF for each impulse was calculated by a *Brüel&Kjær (B&K) 2032 Dual Channel Signal Analyzer*, as shown in Fig. C.9.

These FRFs were further used to validate the linear theoretical results. Fig C.10 verifies that the experimental mode shape of the fundamental response in the range 40-50Hz. corresponds to the first bending mode of the structure.
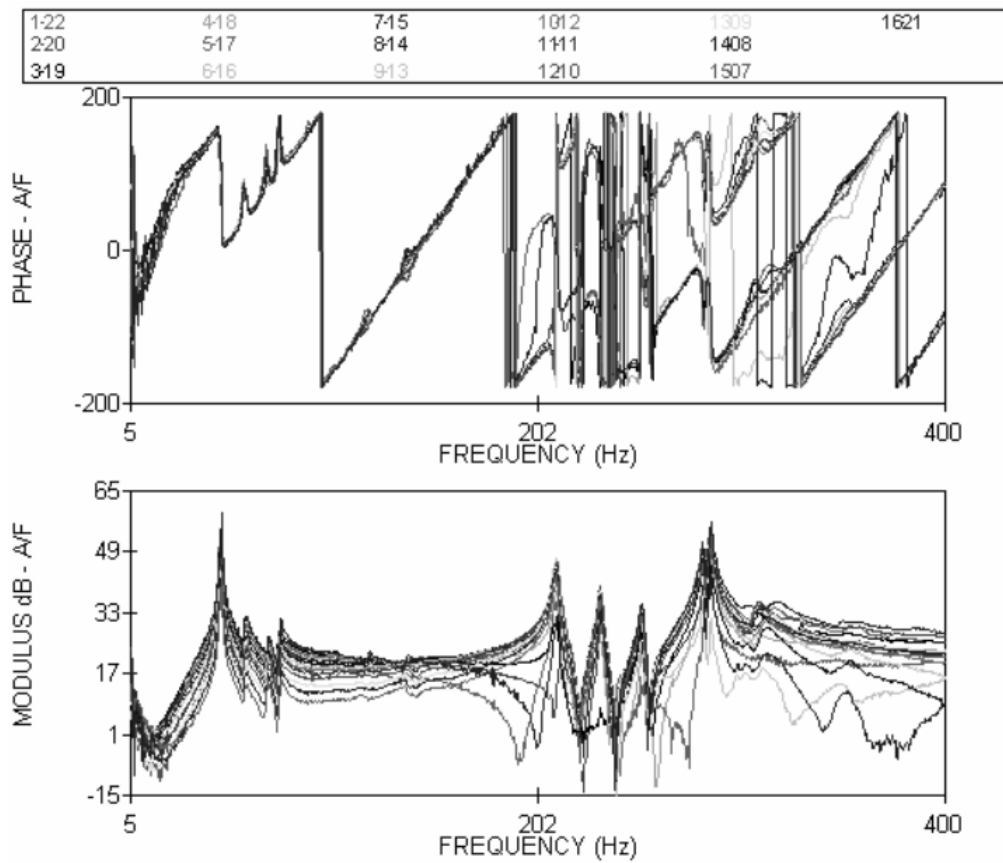
Figure C.9: Results from the hammer test, showing the linear FRFs of some of the tested points
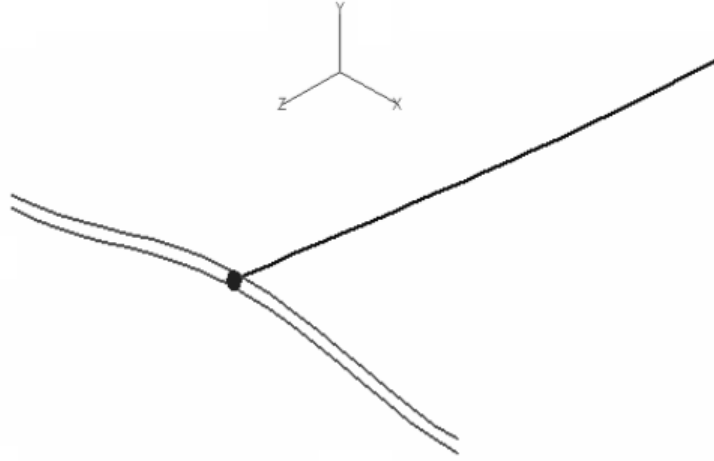
Figure C.10: Experimental mode shape for the first mode of the test rig

The choice of a simple FEM model proved to be sensible because, as found out here, neither model could predict the observed behaviour of the real structure, due to uncertainty in boundary conditions and underestimated damping. Extensive tuning of the FEM model was needed to match the theoretical and observed responses.

The modifications included freeing the θ_x, θ_y DOFs in the otherwise clamped ends of the transversal beams, as well as replacing the fixed θ_x DOF in the clamped end of the linear beam, by a grounded rotational spring and a lumped mass. Finally, a hysteretic damping of $\eta = 0.479\%$ was found to represent more accurately the observed modal damping[1]. Once these modifications were implemented, an almost perfect match was achieved for the first mode. Beyond this frequency range, a close match was not expected due to the simplicity of the chosen model. Fig. C.11 shows an overlay of the predicted and measured point-FRF (node 22). It can be seen that the measured response exhibits a high content of smaller modes between the two first predicted modes. These were verified to be complex motions of the transversal beams, where the linear beam remains almost static. Given that the smaller modes do not introduce strong interaction, they were simply ignored.

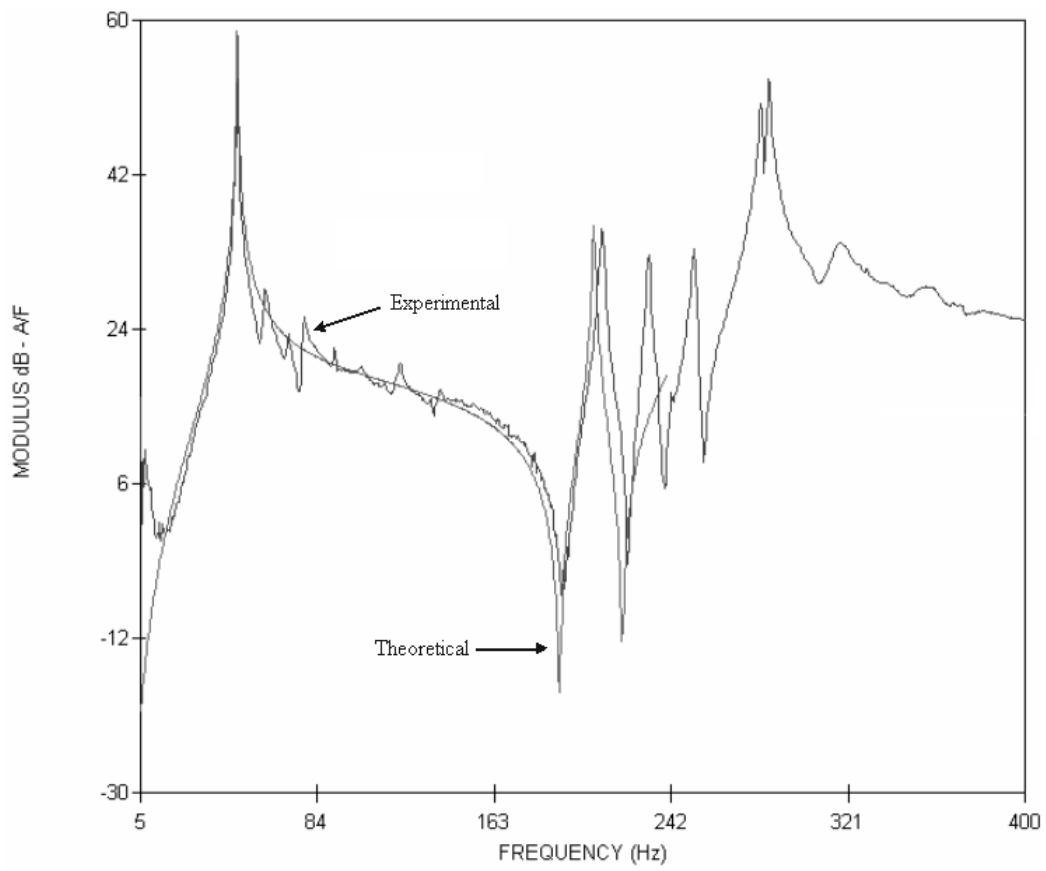[1]During the sinusoidal test, described later

Figure C.11: Experimental and theoretical point-FRFs

C.5 The nonlinear test

A nonlinear test is a far more complex issue, requiring a number of specialized techniques. Among them, we can cite:

- **Type of excitation.** It plays a fundamental role in the suitability of the measurements. Some can generate responses "immune" to nonlinearities, while others are unsuitable for nonlinear identification purposes. For this end, high-quality measurements are needed, and the noise must be kept as low as possible.

- **Force control.** Unlike a linear testing, it must be ensured that the force remains constant during an FRF measurement. This conditions guarantees that the observed deviations are purely due to nonlinear effects.

- **Assembly defects.** At large displacements, construction and assembly defects can have a significant impact. These include gaps, pre-loads, misalignments, etc. As demonstrated in (74), a cubic stiffness structure with a pre-load can behave as an asymmetric *softening* spring[1].

These issues will be discussed in more detail in the following subsections.

C.5.1 The sinusoidal excitation

The dynamic test was carried out using a sinusoidal excitation, selected for a variety of reasons. Among them, we can highlight the excellent signal-to-noise ratio of the obtained FRFs, due to its ability to concentrate all of the input energy in a single frequency only. This, in turn, activates otherwise passive nonlinearities, an essential feature for a successful nonlinear identification.

Another characteristic of a sinusoidal excitation is the greater control regarding the strength (amplitude and power) of the signal. This allows a relatively

[1]This behaviour was clearly observed in our first tests.

236

easy implementation of a feedback control on the input force of the structure, alleviating the well-known *force dropout* phenomenon at resonance[1]. As mentioned before, this feature is also essential for performing a nonlinear identification.

The main drawback of the sinusoidal excitation is the longer measurement time, when compared to other techniques. In order to acquire reliable measurements, the system must be allowed to reach steady state before the next frequency is read. For structures with light damping, this can be very time consuming. In comparison, hammer testing is a popular choice given its low-profile requirements and fast acquisition time. However, its relatively poor signal-to-noise ratio and "immunity" to nonlinearities makes it unsuitable for a nonlinear identification.

C.5.2 The force control

In order to obtain reliable nonlinear data, each FRF must be measured at a constant force level, applied by an electromechanical shaker. However, at resonant conditions occurs a phenomenon called *force dropout*. This is caused, in part, by a back emf interacting with the input voltage in the shaker's armature, which in turn reduces the effective voltage applied to the coil. The overall effect is a sudden drop in the force applied by the shaker.

This condition is exacerbated by the fact that, at large armature displacements, the internal magnetic field becomes nonlinear. The higher harmonics introduced by this condition are unrelated to the structural nonlinearities, thus increasing the noise content of the measurements.

A third source of error is the distortion in the waveform of the applied force, which is meant to be sinusoidal. Due to a high mechanical coupling with the structure, this waveform may scarcely resemble a sine wave, therefore invalidating the FFT[2] assumptions.

A closed-loop control for the input force can alleviate most of these problems. The control tries to keep the applied force (as sensed by a load cell) at a constant level, by boasting or reducing the shaker's input voltage as needed. However, at extreme displacements, the back emf varies rapidly, and the control may not be

---

[1]More on this later.

[2]Fast Fourier Transform.

fast enough to find suitable parameters. If this condition persists for a certain time, the armature can get damaged due to excessive heating.

C.5.3   Procedure for the nonlinear testing

The nonlinear test was carried out according to the diagram shown in Fig. C.12, discussed next:

A sinusoidal signal was generated by a *Beran 402-FRA* (frequency response analyzer) and fed into a *GW* power amplifier. The amplified signal was then applied to a *Derriton-VP4* shaker, which provided the excitation force. A *B&K-8200* load cell, fixed to the central joint of the structure, received the applied force by means of a long and thin stinger.

The stinger is a critical component of the measurement system, since it must transmit all of the axial force, while diluting bending and torsional effects. This is achieved by ensuring a high axial stiffness but relatively low moment of inertia, plus genuine pin-joints at both ends (shaker and force gage).

Three *Endevco-2222c* accelerometers were wax-fixed on the linear beam, coinciding with the nodal positions 8, 15 and 22 (according to Figs. C.6 and C.7). The three signals plus the load cell's signal were fed to four *B&K-2626* chargers, and routed back into the *402-FRA*. A standard oscilloscope was used to monitor the signals going from the chargers to the analyzer.

The analyzer calculates the output-input ratio of each signal respect to the load cell's signal. This delivers the FRF of each measured point, for the actual frequency. Note that the input force, sensed by the load cell, must remain constant during the measuring time. This is achieved by an internal feedback control (also built-in the *402-FRA*), which boosts or reduces the applied voltage to the shaker as required.

The force control of the 402 FRA was found to be rather slow, requiring a few seconds before an adequate voltage was applied to the shaker. Very close to resonance, this condition is troublesome, because the back emf varies rapidly and the control struggles to find adequate parameters. If this condition persists for longer than a user-defined time (30 seconds), the analyzer switches to the next

frequency, creating a spurious measurement. Fig. C.13 shows the nonlinear test being carried out.

C.6 Nonlinear FRF measurements

Nonlinear FRFs were measured for several points along the linear beam, for different force levels within the range $0.5-1.5N$. The same FRFs were numerically obtained by the EF method presented in Chapter 4.

Fig. C.14 shows the results for the point-FRF, for four increasing levels of excitation. The linear FRFs are shown for each case, both numerical (dashed line) and measured ("+" marks). Overlying are the nonlinear counterparts, showing the numerical (solid line) and measured ("x" marks) results. A reasonable agreement is appreciated for the first bending mode of the structure (the fundamental response).

Observe that the numerical excitation level F_{th} needed to match a measurement taken at a level F_{exp} is, in general, lower. This is probably due to a pre-load effect because of a defective assembly, as deduced from the increasing trend. Also, the effect of the slow force control is more evident at higher levels of excitation, as we move closer to resonance. The scattered points in this region are believed to be caused by a force dropout, rather than a true nonlinear behaviour.

In spite of all this, it can be concluded that the EF method can reasonably characterize the nonlinear behaviour of a real nonlinear structure.
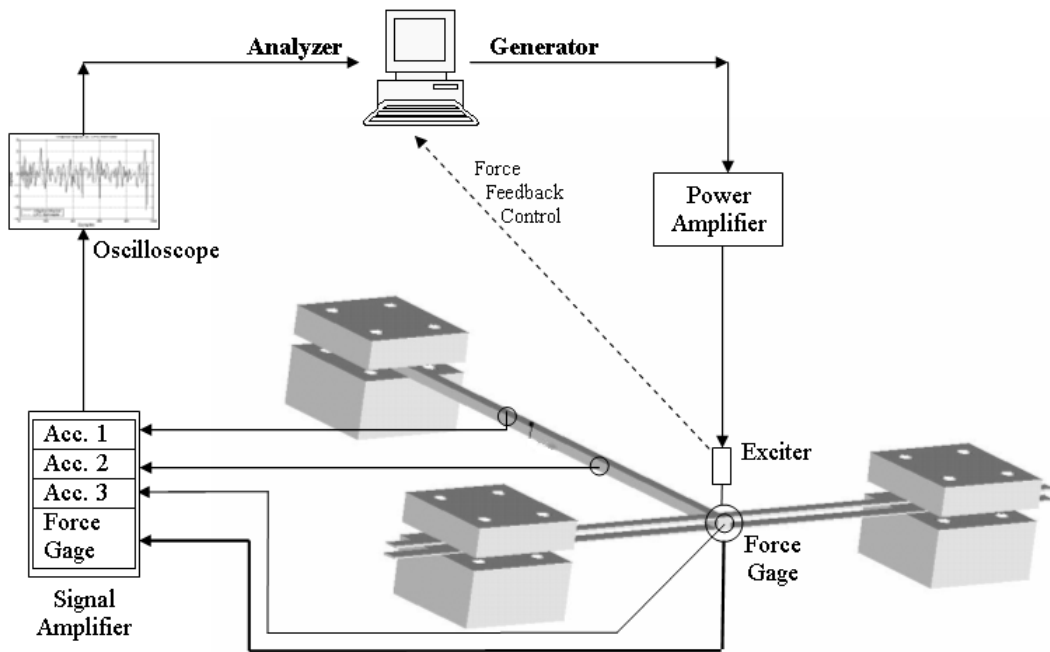
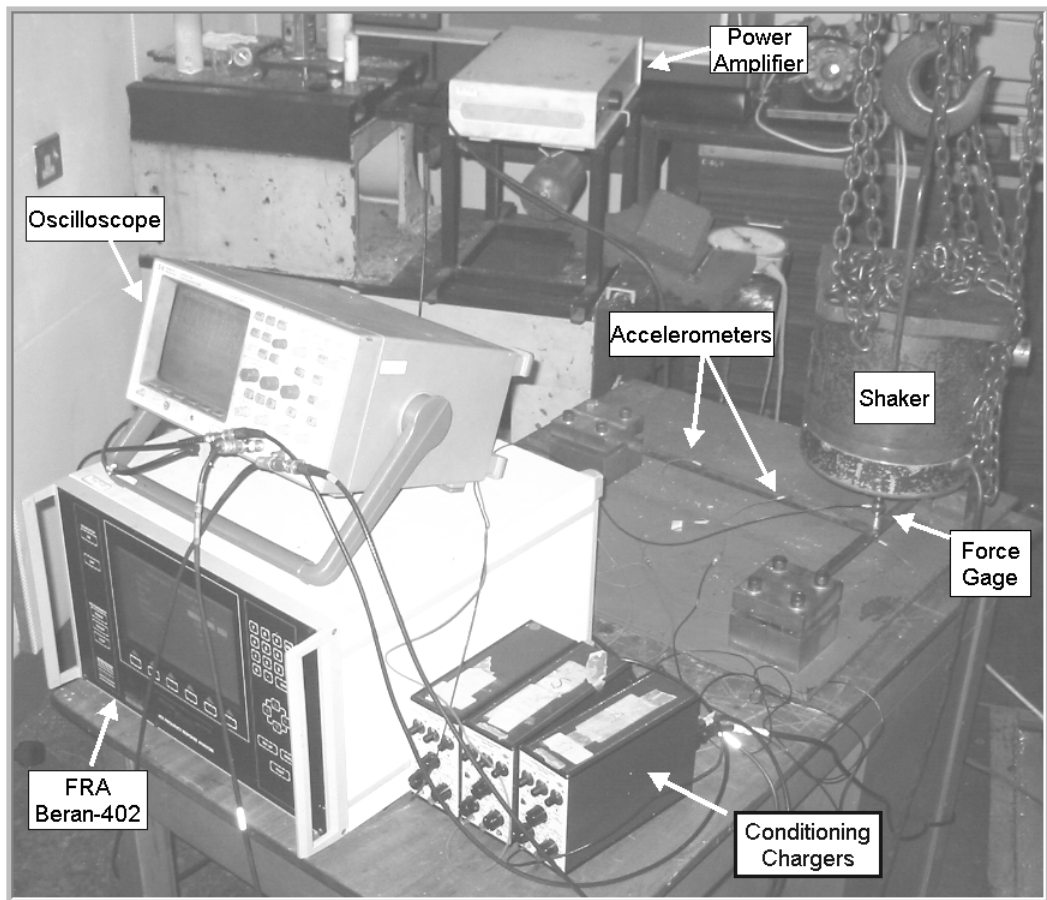Figure C.12: Flow chart of the nonlinear test
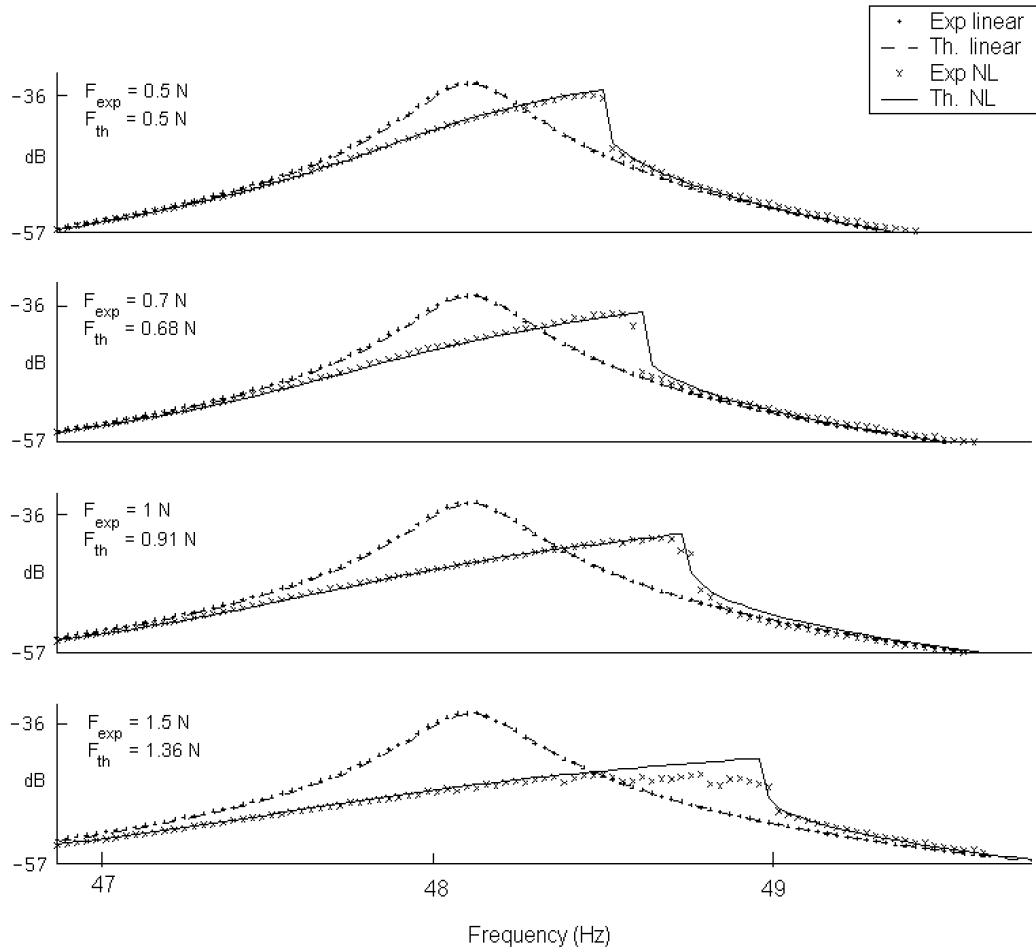
Figure C.13: The nonlinear test

Figure C.14: Experimental and EF-predicted nonlinear point-FRFs (dB) for four increasing levels of excitation, covering the first mode of the test rig